

# The Messenger



No. 123 – March 2006





First Light of the VLT  
Laser Guide Star  
Facility. See article on  
page 16.

# Spain to Join ESO

On 13 February, at a ceremony in Madrid, an agreement was signed by the Spanish Minister of Education and Science, Mrs. María Jesús San Segundo, and the ESO Director General, Dr. Catherine Cesarsky, affirming their commitment to securing Spanish membership of ESO.

Following approval by the Spanish Council of Ministers and the ratification by the Spanish Parliament of the ESO Convention and the associated protocols, Spain will become ESO's twelfth member state on 1 July 2006.

"Since long Spain was aware that entering ESO was a logical decision and it was even necessary for a country like Spain because Spain is ranked eighth in astrophysical research", said Mrs. María Jesús San Segundo. "The large scientific installations are not only necessary for research in different fields but are also partners and customers for high-tech companies, helping to increase the funding of R&D."

"Spanish Astronomy has made tremendous strides forward and we are delighted to welcome Spain as a new member of ESO. We very much look forward to working together with our excellent Spanish colleagues", said Dr. Cesarsky. "For ESO, the Spanish accession means that we can draw on the scientific and technological competences, some of them unique in Europe, that have been developed in Spain and, of course, for Europe the Spanish membership of ESO is an important milestone in the construction of the European Research Area."



The Spanish Minister of Education and Science, Mrs. María Jesús San Segundo, (left) and the ESO Director General, Dr. Catherine Cesarsky (right) signing the agreement.

Indeed, Spain is an important member of the European astronomical community and has developed impressively over the last three decades, reaching maturity with major contributions in virtually all areas of astronomy. In addition, Spain hosts, operates or owns a number of competitive facilities dedicated to foster astronomical research, among which is the Observatorio del Roque de los Muchachos at La Palma, certainly the premier optical/infrared astronomical observing site in Europe and site of the Spanish 10-m GranTeCan telescope now nearing completion.

With the high quality of Spanish astronomical research as well as the technological competence of Spanish industry, it is only fitting that Spain should join ESO. Through ESO Spain will enjoy full access to all of ESO's current facilities and unrestricted participation in the projects that ESO is planning for the future. Spain is already an active partner of the Atacama Large Millimeter Array (ALMA), whose construction and operations are led by ESO on behalf of Europe.

ESO's Council approved the admission of Spain at its 107th meeting held in Garching on 7 and 8 December 2005.

(Based on ESO Press Release 05/06)



# Status of the European ELT

Guy Monnet, Roberto Gilmozzi (ESO)

In December 2004 the ESO Council defined as ESO's highest priority strategic goal the retention of European astronomical leadership and excellence into the era of ELTs, asking that the construction of an ELT on a competitive time scale be addressed by radical strategic planning. Therefore the ESO activities towards the future European ELT underwent a major 'phase transition' during 2005, with the completion of the exploration of the OWL concept and its comprehensive review by an international panel, followed by the start, with an extensive ESO Community involvement, of the iterative process that should lead quickly to the definition of the ELT it needs and wants.

## The OWL conceptual study

Since 1998 ESO has been pursuing a conceptual study for a giant optical-infrared telescope with a primary mirror diameter  $D$  up to 100 metre, dubbed OWL for the eponymous bird keen night vision and for being Overwhelmingly Large. What started at first as a low-key evaluation of the main promises and challenges associated with such a daring endeavour picked up considerable momentum over the last four years. Following the December 2004 Council resolution, it was decided to complete rapidly the study and proceed to a thorough review by an international panel by the end of 2005.

The OWL Study has largely been an ESO internal effort, but with essential feedback from industry and with community involvement in two critical areas. The first of these was the building over the last five years of a thorough science case for a 50–100-m ELT by a large segment of the community under the aegis of the European Commission (EC) FP5 and FP6 OPTICON programme (see its executive summary at: <http://www.astro-opticon.org/>). The second was the preliminary definition and analysis of a potential OWL instrument suite that could cover its science case, and which has been accomplished over the last 12 months through

an ESO-coordinated intense community effort.

Construction of any ELT – especially if up to 100-m diameter – requires securing new enabling technologies through an extensive R&D programme. Early collaboration with industry has led to much progress in a number of crucial telescope design areas such as serial production of (spherical) mirror segments either in glass or SiC, cheap yet high performance position actuators, large deformable mirrors, etc. These developments give a strong basis to break the classical (and potentially lethal)  $D^{2.6}$  cost law. A much more shallow law ( $\sim D^{1.4}$ ) has been established instead, owing in particular to serial production of identical mirror segments, standardised mechanical parts and actuators. The launch four years ago of second-generation VLT instruments has led to the development, largely by the ESO community, of a number of ELT 'pathfinders', in particular KMOS, Planet Finder, MUSE and the VLT Adaptive Optics (AO) Facility (for more information, see <http://www.eso.org/instruments/> and <http://www.eso.org/projects/aot/>). A significant part of the R&D associated with this effort is being conducted through OPTICON.

## The OWL review

The OWL Conceptual Study was completed and its results collated in early October 2005 in the 'Blue Book' report ([http://www.eso.org/projects/owl/Phase\\_A\\_Review.html](http://www.eso.org/projects/owl/Phase_A_Review.html)). A comprehensive review was conducted by an international panel on 2–5 November 2005. Members were: Roger Davies, Oxford University (Chair); Jean-Gabriel Cuby, LAM-Marseille; Brent Ellerbroek, Thirty-Metre Telescope Project Office; Daniel Enard, formerly VIRGO; Reinhard Genzel, MPE-Garching; Jim Oschmann, Ball Aerospace; Roberto Ragazzoni, INAF-Arcetri; Larry Ramsay, Hobby-Eberly Telescope; Stephen Sackett, Carnegie Observatories; and Larry Stepp, Thirty-Metre Telescope Project Office.

The first objective of the review was to assess whether, or to what extent, the proposed technical solutions were reasonable, i.e. judge the strengths and weaknesses of the OWL approach, ana-

lyse feasibility issues, evaluate cost and schedule estimates, and identify the main risks of the project and areas to be further explored. The second was to recommend whether and how to proceed to a next phase of the project.

The panel praised the OWL team for an extensive and largely successful feasibility study for a 100-m ELT. A strong technical point stressed by the panel was the integrated approach chosen for the OWL active/adaptive optics system, with in particular at least one large adaptive mirror as an integral part of the telescope.

Substantial technical risks were however identified, associated with OWL's double segmentation (M1 and M2), the highly aspherical M4 mirror and the telescope size that makes it Laser Guide Star 'unfriendly'. In view of these risks, but also of a consolidated cost ( $\sim 1.2$  G€) larger than the likely available ESO resources in the 2008–2020 time frame, the panel recommended to consider a smaller diameter, less complex and less risky ELT. It emphasised that most of the OWL design effort and virtually all technological developments started so far were directly useful for this new phase. In addition the panel recommended to strongly involve the ESO community in all aspects of the project and to speed up the currently running ELT site selection programme, with additional attention given to starting government level negotiations for site access as soon as possible. The panel concluded recommending "that the project proceed to Phase B, and begin with a new examination of the balance between science return, competitiveness, AO performance, instrumentation, risk and final performance within an affordable cost." It noted that the time to carry out such a re-evaluation was already in the plans proposed in the Blue Book.

## The ELT design study

ELT-related R&D efforts are now accelerating, with a five-year programme started by European astronomical institutes and industries through the ESO-coordinated FP6 ELT design study. With a consolidated 30.5 M€ budget (including 8.4 M€ from the EC), it is aimed at establishing generic technologies critically

required for any ELT through the development of new concepts, advanced components, realistic simulations, breadboards and prototypes.

### Towards the European ELT

Following the review, the already planned two-year consolidation phase towards the final project has started as advocated by the review panel. As it noted, most of the building blocks developed for OWL remain valid for a smaller-size telescope and we expect to develop a basic reference design for what is now the European ELT project by the end of 2006. Our basic goal is to define the best affordable ELT that can be built on a competitive time scale and with acceptable risks. While the project is open to international collaboration, we definitely need to get a baseline design that could be handled within Europe alone, should no other major partner be found.

The process of definition of the E-ELT has been kick-started by mixed community-ESO ELT Working Groups (a.k.a. ELT-WGs) set up by ESO's Director General at the end of December, one for each of main ELT areas, namely (a) its Science case, (b) an Instrument suite, (c) the associated Adaptive Optics systems, (d) the Telescope and Observatory Design and (e) potential Sites evaluation. Their respec-

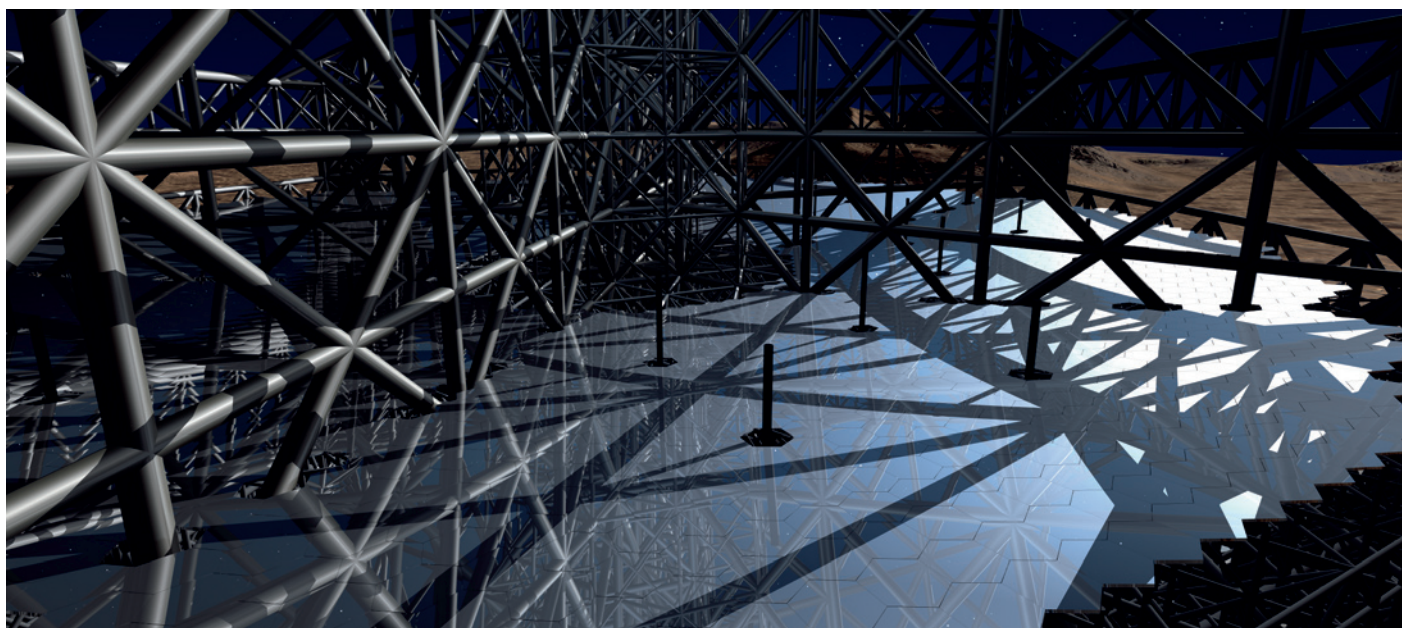
tive chairpersons are: Marijn Franx, Leiden (Science); Colin Cunningham, UKATC (Instrumentation); Gérard Rousset, Observatoire de Paris (Adaptive Optics); Daniel Enard, formerly VIRGO (Telescope Design); and Roland Gredel, Calar Alto (Site). Amazingly – a clear mark of the deep interest and commitment of the community – of the more than 90 WG members (60 % external, 40 % ESO) contacted on 22 December, only two were not able to join at such short notice, due to pressing ESO-related tasks. The brief of the five ELT-WGs called for a two-month burst of activity in January–February 2006 to produce an initial input to the ESO Team in the form of 'toolboxes', synthesising and collating ELT-related present and projected capabilities in their respective topic areas, as well as a first cut at a prioritisation of the requirements. This effort has just ended with all contributions received in time and with the proper content.

Present efforts by the former OWL team – soon to be expanded and restructured as the ELT project office – are primarily focussed at producing the ELT reference design, with as few remaining open options as possible by the end of the year. This involves a multiple iteration process between the main ELT ingredients listed above. Continuing with a strong community involvement during this critical step is essential. To that effect, the ELT Science and Engineering external Work-

ing Group (ESE) suggested by the OWL review panel, or rather a 'core' version of it, has been created to consolidate the reports of the five working groups into a recommendation to ESO (by May 2006). This 'core' ESE is composed of the ELT-WG chairs and co-chairs while the other members of the ELT-WGs will act as ad-hoc experts for ESE until at least the end of 2006. The ESE proper will be set up by STC in the spring to help and advise the ESO ELT project office in the complex iteration loops ahead, hopefully weaving successfully Science, AO, Instruments, Telescope Design and Site requirements to define the basic choices and produce a coherent and powerful ELT project for Europe by the end of the year. To ensure an even wider interaction with the community, the project draft basic reference design will be presented and discussed at a topical workshop in mid-November 2006 in Marseille (France), in time for a final 'loop' before presenting a definite plan to the ESO Council in December 2006.

### Acknowledgements

The OWL study has been the combined effort of many people, both inside and outside ESO, over many years and we want to thank them all. We are also very grateful to the Review Panel members for their timely and highly constructive criticisms. Finally, we thank both the external and internal members of the ELT working groups for agreeing to help at remarkably short notice.



Visualisation: H. Zodet, ESO

# The VLT Adaptive Optics Facility Project: Telescope Systems

Robin Arsenault<sup>1</sup>  
Norbert Hubin<sup>1</sup>  
Stefan Stroebele<sup>1</sup>  
Enrico Fedrigo<sup>1</sup>  
Sylvain Oberti<sup>1</sup>  
Markus Kissler-Patig<sup>1</sup>  
Roland Bacon<sup>6</sup>  
Richard McDermid<sup>7</sup>  
Domenico Bonaccini-Calia<sup>1</sup>  
Roberto Biasi<sup>3</sup>  
Daniele Gallieni<sup>4</sup>  
Armando Riccardi<sup>5</sup>  
Rob Donaldson<sup>1</sup>  
Miska Lelouarn<sup>1</sup>  
Wolfgang Hackenberg<sup>1</sup>  
Ralf Conzelman<sup>1</sup>  
Bernard Delabre<sup>1</sup>  
Remko Stuik<sup>7</sup>  
Jerome Paufigue<sup>1</sup>  
Markus Kasper<sup>1</sup>  
Elise Vernet<sup>1</sup>  
Mark Downing<sup>1</sup>  
Simone Esposito<sup>5</sup>  
Michel Duchateau<sup>1</sup>  
Marijn Franx<sup>7</sup>  
Richard Myers<sup>2</sup>  
Steven Goodsell<sup>2</sup>

- <sup>1</sup> ESO  
<sup>2</sup> University of Durham, United Kingdom  
<sup>3</sup> MicroGate  
<sup>4</sup> ADS International  
<sup>5</sup> INAF – Osservatorio Astrofisico di Arcetri, Italy  
<sup>6</sup> CRAL, Observatoire de Lyon, France  
<sup>7</sup> Leiden University, the Netherlands

The Adaptive Optics Facility is a project to convert UT4 into a specialised Adaptive Telescope. The present secondary mirror (M2) will be replaced by a new M2-Unit hosting a 1170-actuator deformable mirror. The three focal stations will be equipped with instruments adapted to the new capability of this UT. Two instruments have been identified for the two Nasmyth foci: Hawk-I with its AO module GRAAL allowing a Ground Layer Adaptive Optics correction and MUSE with GALACSI for GLAO correction and Laser Tomography Adaptive Optics correction. A future instrument still needs to be defined for the Cassegrain focus. Several guide stars are required for the type of adaptive corrections needed and a Four Laser Guide Star Facility (4LGSF) is being developed in the scope of the AO Facility. Convex mirrors like the VLT M2 represent a major challenge for testing and a substantial effort is dedicated to this. ASSIST, is a test bench that will allow testing of the Deformable Secondary Mirror and both instruments with simulated turbulence. This article focusses on the telescope systems (Adaptive Secondary, Four Laser Guide Star Facility, RTC platform and ASSIST Test Bench). The following article describes the AO Modules GALACSI and GRAAL.

## History of the project

Pioneering efforts were made at the MMT to equip the 6-m telescope with a Deformable Secondary Mirror (DSM). The system was designed and fabricated by an Italian consortium composed of MicroGate, ADS Intl and the Osservatorio Astrofisico di Arcetri. The same consortium is now involved in the development of the two DSM's for the Large Binocular Telescope (Mount Graham). The technology has matured substantially and it seemed appropriate to investigate whether this technology was promising for the VLT.

A feasibility study was launched in June 2004 with MicroGate as the main contractor (including also ADS and OAA). The goal was to demonstrate the feasibility of such a design for one of the VLT 8-m telescopes. The study came to a

positive conclusion in August 2005 and a corresponding data package was delivered covering all main aspects of the design.

In the course of the feasibility study, it became obvious that the scope of the project needed to be broadened in order to answer some basic questions: What are the scientific advantages of such an improvement to the UT? What are the implications on the various systems for the UT and its operation?

A conceptual design review took place in September 2005 to address these questions; it involved several ESO staffs and a few external review board members. The conclusion was positive and it was later endorsed by ESO management as a high priority project and by the STC in October. In December, ESO Council also approved the AOF which is the final approval and gave the green light for the project.

## Strategy rationale

There are fundamental advantages to have one mirror of the telescope train being adaptive. The whole telescope then becomes an adaptive optical system offering fast wavefront correction without the addition of supplementary optics or mechanics. Moreover, with the two Nasmyth and Cassegrain foci this gain is threefold. The system gives better throughput to science instruments, lower emissivity for thermal IR instruments, large field of view accessible to all instruments and less complexity/crowding at the focal planes.

The alternative to a DSM is a 'post-focal' AO system (à la NAOS) which involves an optical train of five to six supplementary warm mirrors at the image focal plane. Table 1 provides a trade-off analysis that justifies the choice of a DSM, although there are other drivers for this choice.

During the elaboration of the AO Facility design it became clear that such a combination of several complex systems raises important questions particularly in term of AIT, commissioning and control strategy. Such questions, typical of

Criterion	DSM	Post-Focal	Comment
Throughput	Optimal	~ 75 % optimal	
Field of View	Full UT FOV (10' for Hawk-I LGS)	Smaller due to relay optics (1' for NAOS)	Post-Focal optical design and the mechanical implementation for relay optics is difficult and provides smaller FOV
Emissivity	Optimal	Larger; exact factor not well known but likely around three	
Cost	€ 1.4 M saving per AO system versus cost of DSM		
FTE	Gain not well defined	Gain not well defined	Possibly a slight advantage to DSM
Spare M2-Unit	Yes	No	The decommissioned Dornier M2-Unit becomes spare for the three other UT's
GRAAL-Hawk-I	OK	Not feasible because large FOV	
GALACSI-MUSE	OK	Very cumbersome mechanical implementation (has been studied)	
Cass. AO + INS	Undefined	Undefined	Great advantage of DSM if instrument exploits Thermal IR
VLT	Piston: 1170 capacitive sensors with 3 nm RMS accuracy	No impact	
Chopping	~ 6" on sky	~ 20" on sky	Reduced chopping of DSM w/r actual M2-Units

Table 1: Technical trade-offs for the AO Facility.

any telescope design including several deformable mirrors (ELTs), and their corresponding answers would benefit tremendously from a hands-on experience gained on a VLT "prototype". In this perspective the AO Facility becomes a highly relevant pathfinder for any ELT design. This argument became an important motivation for ESO management to pursue the AOF concept *with* a DSM. The list below illustrates common issues between AO Facility and an ELT:

- Develop a high-order adaptive telescope at the diffraction limit
- Secure and improve current large DM with 30 mm spacing (~ M6 for OWL)
- Secure manufacturing and handling of large thin shells
- Develop and monitor robust Laser and CCD technologies
- Provide large computing power for AOF ~ 1 kHz (factor 200 w/r NAOS)
- Develop, operate and master Laser Tomography AO and Ground Layer AO systems
- Elaborate and control a detailed error budget to reach the Strehl ratios required
- Master interaction matrix measurement strategies (in-lab and on-sky)
- Manage multiple interlaced control loops and offloading processes
- Develop extensive DSM testing procedures in the laboratory
- Manage efficient commissioning of such a complex facility

### Facility description

The following systems/projects are being conducted in the context of the AO Facility:

- A new-generation M2-Unit hosting a 1170-actuator deformable mirror
- A four-Laser Guide Star Facility using fiber lasers and four Launch Telescopes on the UT centrepiece
- SPARTA: a flexible Real Time Computer Platform to perform the AO correction of the AO modules (and others)
- GRAAL: the AO module allowing wavefront sensing and Ground Layer AO correction for Hawk-I
- GALACSI: the AO module allowing wavefront sensing and GLAO and Laser Tomography correction for MUSE
- ASSIST: a complete test facility allowing complete testing and characterisation of the AO Facility in Europe
- A dedicated effort to address AO calibration issues for the various AO modules

### Second-generation M2-Unit

The concept of thin shell and force actuators is one of the most promising in the field of large deformable mirrors; the largest deformable mirrors have been built/ designed with this technology. A 642 mm diameter convex secondary mirror with 336 actuators has been developed and is being used by the MMT (Mount Hopkins, Arizona), while the two 911 mm diame-

ter and 672 actuators concave secondary mirrors of the LBT (Mount Graham, Arizona) are being integrated. A similar design is envisioned for one of the VLT Unit Telescopes; the deformable secondary design is 1120 mm in diameter and the thin shell is 2 mm 'thin' while offering 1170 actuators for adaptive correction (see Figure 1).

These mirrors are composed of three basic elements: a back-plate, hold, a reference body and the thin shell. The back plate has two functions: holding the voice coil actuators and evacuating heat dissipated by the coils with the help of an integrated cooling fluid circuit. Each voice coil applies a force to a corresponding magnet glued onto the back face of the thin shell. A ring of conductive material is deposited around each magnet and is mirrored on the reference body. These two opposite coatings constitute a capacitance used as gap sensor. The reference body being a calibrated optical surface, an equal spacing for all capacitive sensors insures a relatively good optical quality on the shell.

An internal control loop at 80 kHz insures that the force applied maintains the capacitive sensor to a constant gap. Note also that the derivatives of the capacitive sensor positions provide a measure of the velocity of the shell displacement which in turn is used by the system to define an electronic damping; this feature insures high bandwidth for all mirror modes.

The reference body is a conventional, thick, Zerodur optical component, with the exception of the numerous cylindrical openings allowing passage for the actuators. The VLT design explored a light-weighting scheme (50–60 % light-weighted Zerodur or SiC) to reduce the weight of the complete assembly (realistic without being a huge cost driver). SiC offers the added advantage of being extremely rigid compared to Zerodur. This is important since the rigidity of the reference body insures a reliable shell figure.

The thin shell provides, at rest, the same optical properties as the actual Beryllium mirrors of the VLT M2. The optical surface is thus convex and the optimal shell thickness has been defined as 2 mm thin. To remain within a known field of expertise, the shell is manufactured from a thick Zerodur blank, and is therefore a costly and delicate component. Note that other avenues are explored for thin shell manufacturing in the context of large DM for ELTs (i.e. slumping).

Detailed simulations show that the residual error with all modes corrected is 62.5 nm rms, fulfilling the specifications (see Table 2).

### Calibration requirements

A fundamental limitation of AO systems based on an adaptive secondary mirror like the VLT M2 is that there is no intermediate focus before the deformable mirror. Therefore, it is not possible to install an artificial calibration source, seen by the DM and the Interaction Matrix (IM) measurement in a conventional way is not possible. An extensive program has been initiated at ESO to study this limitation and explore alternatives.

Several solutions are being envisioned for the IM measurement. First, Synthetic (simulated) IM using measured influence functions of the DSM in the laboratory and calibration of the WFS optical path, and second, several different methods of performing on-sky IM measurements.

Even if the synthetic IM is the most seductive solution (noiseless, simplicity, no calibration time required), it still has

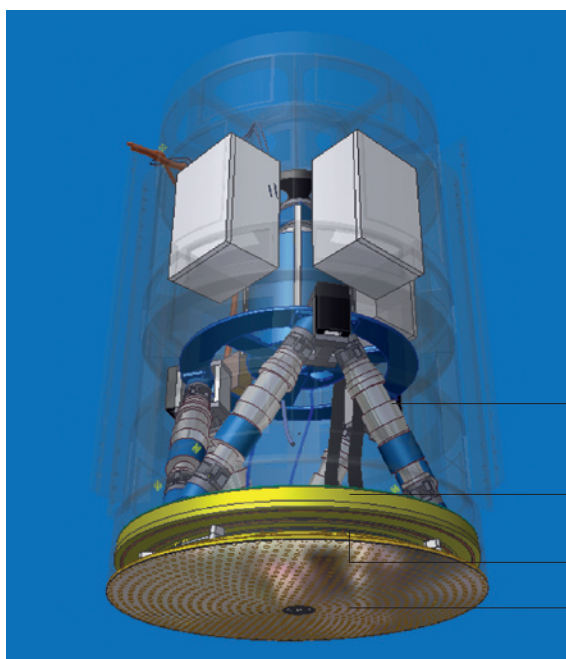


**Figure 1:** Conceptual design for the 1120 mm diameter, 1170 actuator VLT deformable secondary mirror. The M2-Unit contains the electronics (top), Hexapod for centring and focusing (middle) and the deformable thin shell (bottom).

Hexapod for centring and fine focusing

Cold Plate; heat evacuation and actuator attachment

Reference body

Thin shell

Parameter	Value
Median seeing at 30 deg: $r_0$ (0.5 $\mu\text{m}$ )	12.1 cm (0.85" at 500 nm)
Specified fitting error	78 nm rms
Fitting error (all modes) 1170	62.5 nm rms
Zernike modes fitting error	70.0 nm rms
1170 KL modes fitting error	60.2 nm rms
max PTV actuator displacement	13.6 $\mu\text{m}$
max rms actuator displacement	1.66 $\mu\text{m}$ rms
max peak force	0.82 N
max rms actuator force	0.17 N rms
rms force	0.157 N rms

**Table 2:** Summary of the simulation results in the median seeing case. Results of fitting 10 000 uncorrelated wavefronts (this represents the capability of the DSM to fit a turbulent wavefront. It does not take into account the time delay of the AO control loop).

to be demonstrated that the accuracy of the models (DM and WFS) can be high enough to ensure the expected performance. Regarding the experimental estimation of the IM, novel techniques are investigated in order to deal with the new issues that we have to face: There is turbulent noise either because the calibration is performed on sky or because of the telescope internal turbulence. The calibration time might dramatically increase because of the larger number of degrees of freedom. Several methods are being investigated through simulations and laboratory tests as well as on sky tests when possible. The different schemes aim at minimising the noise and bias on the measurement in order to optimise the quality of the reconstructor.

Using various modal bases (zonal, Hadamard, system modes/mirror modes,

Zernike or Karhunen-Loeve), several techniques are foreseen and being compared: (1) Open loop fast DM actuation, which allows freezing the disturbances between modal push and pull and thus minimise turbulent noise as well as any low-frequency effect. (2) Open-loop DM modulation and demodulation by FFT detection. The stimulus power is concentrated on a single frequency beyond the modal atmospheric bandwidth. Low-frequency effects are cancelled out and it allows for multiplexing. This way, several modes can be measured simultaneously, reducing the total calibration time. (3) Closed-loop calibration. Dynamic bias is applied as offset on the WFS signal. The DM command is measured as a response to this bias and therefore the reconstruction matrix (or control matrix) is measured directly.

Furthermore, there is a key issue related to calibration. A pupil offset may have a strong impact on the system performance and must be addressed properly. Indeed, for high-order AO systems such as VLT with DSM, the tolerance is very tight. Dynamical pupil alignment is envisioned to minimise this effect. The several investigated techniques appear promising and have convinced the AO Facility review board of our sound approach.

Therefore, in terms of simplicity and time consumption the most attractive choice is to simulate the IM. A few more aspects of this method need to be secured, and in particular the AO Department will assess the impact of the model errors on the system performance and robustness.

#### Four Laser Guide Star Facility

Four Laser Guide Stars are required for the type of corrections needed; it is envisioned to perform Ground Layer Adaptive Optics for Hawk-I and MUSE involving averaging turbulence measurements in four different directions around the field of view.

The choice of four launch telescopes on the centrepiece is preferred in order to avoid the so-called 'fratricide' effect. This degrades the wavefront sensor measurements when, for instance, four beams are launched from behind M2; inevitably, the beams cross the path of the neighbour sensors and 'pollute' some subapertures increasing the background light level and therefore noise. This effect is reduced if lasers are launched from outside the telescope pupil (centrepiece).

The upgrade of the LGSF to four LGSF takes full advantage of the existing *Laser Clean Room*. As much as possible, the electronics cabinets are in the LCR, the interlock panel and the fibre laser sources are in the LCR, and most of the heating/cooling is confined to this space. The easy access to LCR helps in servicing and maintenance, and the numerous safety issues become more manageable. The existing LCR was already dimensioned to host multiple lasers, in the LGSF project. Moreover, with fibre lasers the power consumption is much reduced. Hence very little modifications

are required to the Laser Clean Room for the upgrade to 4LGSF. Other systems from the existing LGSF are being re-used, such as the Aircraft Avoidance System.

The baseline lasers are 1178 nm fibre Raman lasers, which are frequency doubled to 589 nm. The fibre delivers 20+ W CW at 1178 nm, 1 GHz line-width. The frequency doubling is done via a single pass on PPSLT, a non-linear crystal. The fibre laser is an on-going development at ESO, together with the companies IPF Technology Ltd (UK), Toptica (D) and the Russian branch of the company Volius. ESO has so far reached 2.9 W CW at 589 nm in its lab, aiming to reach full power in the second half of 2006.

The polarisation maintaining single-mode fibre will directly reach the Launch telescopes using a fireproof fibre cable and going through the altitude cable wrap up to the UT4 centrepiece. At each launch telescope, a small box contains the frequency doubling PPSLT crystal, its temperature controller and the frequency feedback control sensor. The frequency doubling unit is located at the Launch Telescope.

The four Launch Telescopes located on the centrepiece (Figure 2) have demanding requirements. The projected laser beam quality has to be diffraction limited to guarantee the minimum LGS angular size, which imposes constraints on the

optical train and calls for the maximum simplification possible. Care has to be applied for optics working at high power densities. This requirement coupled with the flexibility to point the LGS at 0, 60 or 330 arcsec off-axis, as required by MUSE and Hawk-I, has driven the choice of the Launch Telescope optics toward a refractive, single-lens f/5 design, with the fibre laser output at its focal plane. The first Eigenfrequency of the LTS has to be > 60 Hz, in order to avoid LGS wandering and unwanted jitters. This imposes strict choices on the mechanical support structure of the LTS, which is in CFRP to ensure stiffness and reduce weight.

Above the Launch telescope, there is a movable shutter curtain to protect the lens when it is not in use, and a long baffle to avoid as much as possible scattering light in the telescope environment. In operation the diagnostic system can be in or not. A motorised flipper mirror can optionally send the output beam to a Coherent LM-45 calibrated power-metre, to measure the output beam power.

#### ASSIST

A complete testing of the 'AO system' as done for conventional ones (NAOS and such) is not possible without the telescope, or a sophisticated facility reproducing the opto-mechanical interfaces. In the present case there is the additional complexity of testing a large convex optical component.

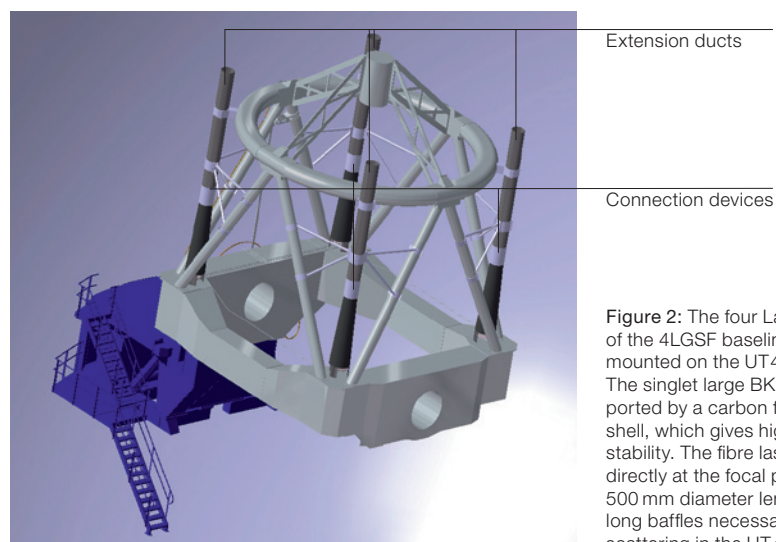


Figure 2: The four Launch telescopes of the 4LGSF baseline design are mounted on the UT4 centrepiece. The singlet large BK7 lenses are supported by a carbon fibre cone-shaped shell, which gives high rigidity and stability. The fibre laser output goes directly at the focal plane of the f/5, 500 mm diameter lens. Note the long baffles necessary to avoid light scattering in the UT4 dome volume.

The Test Facility described below is in itself a complex and relatively costly system; think only of the 1.65 m concave mirror required. However, one must not neglect the usefulness of investing in a versatile and complete test facility in order to characterise and understand these systems. It will allow the designer team to gain sufficient confidence and invaluable experience with the adaptive optics systems before re-assembly and integration on the telescope. In the end this will save valuable telescope time by minimising commissioning time.

This facility will not only allow testing of the DSM itself, but it will also provide a turbulence generator to simulate AO correction in realistic conditions and VLT standard opto-mechanical interfaces to the AO pre-stages GRAAL and GALACSI for the instruments Hawk-I and MUSE respectively.

The opto-mechanical design shown in Figure 3 is composed of two mirrors plus the VLT DSM. The latter is mounted on a vertical structure holding the M2 unit thus providing a support identical to the one of the VLT. The gravity vector is along the M2 optical axis. Two other optical components are required: a main 1.65 m diameter aspheric mirror and a smaller 140 mm diameter aspheric mirror. The asphericity of the former can be handled by conventional polishing techniques while the fabrication of the second would require diamond turning. This setup would offer a 2-arcmin field of view and no pupil distortion.

### Conclusions

ESO is fully dedicated to this major endeavor, requiring some 110 FTE's over the 6-year lifespan. Table 3 shows the major milestones ahead of us. The AO Department of ESO heads the development of the AO Facility, the transformation of one 8-m UT into an adaptive Telescope. This multi-division effort, including also European partners, aims at delivering to the ESO community:

- An 8-m UT4 with a new M2-Unit hosting a 1170 actuators for AO correction
- A 4LGS Facility launching four Na lasers from the telescope centrepiece
- GRAAL: the AO module allowing Ground Layer correction for Hawk-I
- GALACSI: the AO module allowing Ground Layer correction for MUSE Wide Field and Tomographic correction for the MUSE Narrow Field

- ASSIST: a sophisticated test bench allowing complete characterisation of the AOF performance in Europe (this effort is led by the University of Leiden part of the MUSE consortium)

The project passed a Conceptual Design Review last September and Preliminary and Final Design Reviews will be held over in the course of 2007–08. Commissioning activities will be in full swing in the course of 2010–11 and the AOF should be available to the community by 2012.

### Acknowledgements

The work described in this paper is partially funded by the European Commission Sixth Framework Programme under contract No. R1I3-CT-001566.

The authors want to thank in particular Prof. Gerry Gilmore and Dr. John Davies, respectively OPTICON Scientific Coordinator and Project Scientist, for the support provided by OPTICON to this project.

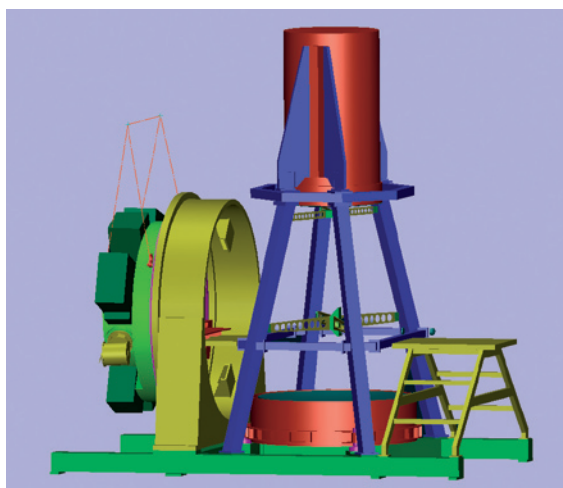


**Figure 3:** Opto-mechanical layout of the VLT DSM test set-up. The image plane is located at the centre of curvature of the three-mirrors system: 1.65-m concave aspheric (bottom red), 1.1-m convex DSM (top red cylinder), and strongly aspheric 140 mm third mirror (just below DSM). A 45° flat mirror and beamsplitters are used to deport the source and image planes at convenient locations on each side of the vertical set-up. The NACO test bench is re-cycled to provide a Nasmyth opto-mechanical interface (left). The 'table' on the right-hand side will support the turbulence generator and source modules.

Milestones	GRAAL	GALACSI	DSM	4LGSF	ASSIST
AOF green light	December 2005				
PDR	January 2007	June 2007	October 2006	June 2007	January 2007
FDR	January 2008	June 2008	August 2007	June 2008	October 2007
End of MAI	October 2009	April 2010	May 2009		October 2008
PAE	February 2011	July 2011	February 2010	July 2010	October 2009
End of Commissioning	December 2011	February 2012	November 2011	February 2011	—

**Table 3:** Milestones for the various systems of the AO Facility.

# The VLT Adaptive Optics Facility Project: Adaptive Optics Modules

Robin Arsenault<sup>1</sup>  
 Norbert Hubin<sup>1</sup>  
 Stefan Stroebele<sup>1</sup>  
 Enrico Fedrigo<sup>1</sup>  
 Sylvain Oberti<sup>1</sup>  
 Markus Kissler-Patig<sup>1</sup>  
 Roland Bacon<sup>6</sup>  
 Richard McDermid<sup>7</sup>  
 Domenico Bonaccini-Calia<sup>1</sup>  
 Roberto Biasi<sup>3</sup>  
 Daniele Gallieni<sup>4</sup>  
 Armando Riccardi<sup>5</sup>  
 Rob Donaldson<sup>1</sup>  
 Miska Lelouarn<sup>1</sup>  
 Wolfgang Hackenberg<sup>1</sup>  
 Ralf Conzelman<sup>1</sup>  
 Bernard Delabre<sup>1</sup>  
 Remko Stuik<sup>7</sup>  
 Jerome Paufigue<sup>1</sup>  
 Markus Kasper<sup>1</sup>  
 Elise Vernet<sup>1</sup>  
 Mark Downing<sup>1</sup>  
 Simone Esposito<sup>5</sup>  
 Michel Duchateau<sup>1</sup>  
 Marijn Franx<sup>7</sup>  
 Richard Myers<sup>2</sup>  
 Steven Goodsell<sup>2</sup>

<sup>1</sup> ESO

<sup>2</sup> University of Durham, United Kingdom

<sup>3</sup> MicroGate

<sup>4</sup> ADS International

<sup>5</sup> INAF – Osservatorio Astrofisico di Arcetri, Italy

<sup>6</sup> CRAL, Observatoire de Lyon, France

<sup>7</sup> Leiden University, the Netherlands

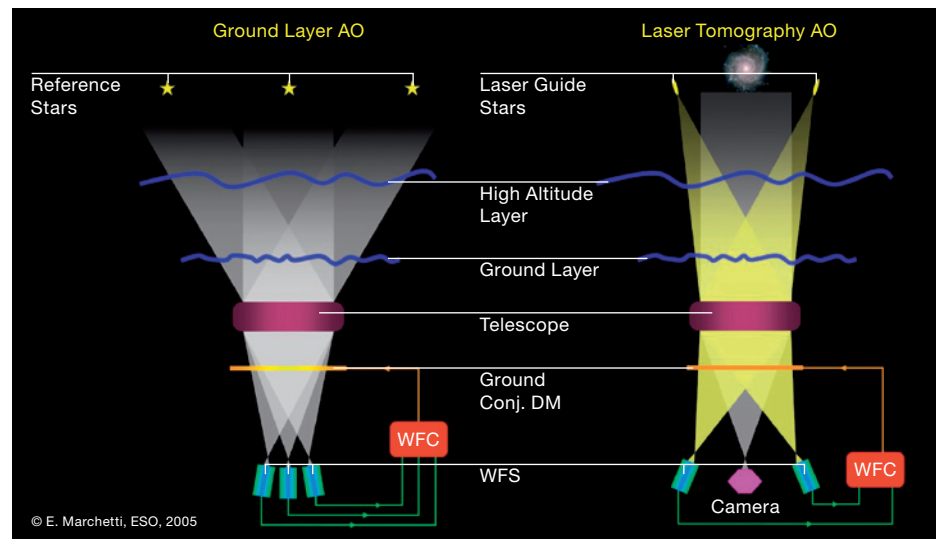
The Adaptive Optics Facility is a project to convert UT4 into a specialised Adaptive Telescope with the help of a Deformable Secondary Mirror (see previous article). The two instruments that have been identified for the two Nasmyth foci are: Hawk-I with its AO module GRAAL allowing a Ground Layer Adaptive Optics correction (GLAO) and MUSE with GALACSI for GLAO correction and Laser Tomography Adaptive Optics correction. This article describes the AO modules GRAAL and GALACSI and their Real-Time Computers based on SPARTA.

## Requirements for the instruments

The three UT focal stations will benefit from the image correction provided by the Deformable Secondary Mirror (DSM). At the time of this writing two instruments are identified: Hawk-I and MUSE on the opposite Nasmyth foci. The corresponding AO modules are GRAAL (GROund layer Adaptive optics Assisted by Lasers) and GALACSI (Ground Atmospheric Layer Adaptive Corrector for Spectroscopic Imaging). The STC has requested ESO to propose options for the future use of the Cassegrain focus; in the meantime SINFONI will remain at this focal station and will be available on the AO Facility.

The AO corrections to be provided are new: Ground Layer Correction (GLAO) and Laser Tomography (LTAO). The former consists in measuring the turbulence in four different directions outside the instrument FOV and to average it in order to provide a homogeneous image improvement across the instrument FOV. The latter compensates for the laser cone effect (not sampling all the turbulence seen on the astronomical target) and optimises high strehl correction on-axis; therefore, the need for four Laser Guide Stars. Figure 1 illustrates these correction modes.

Figure 1: Illustration of the Ground Layer adaptive correction (left) and Laser Tomography (right).



© E. Marchetti, ESO, 2005

The present article details mainly the AO modules for Hawk-I and MUSE and the Real-Time-Computer platform SPARTA. Note that Hawk-I is an ESO-led effort. This instrument completed its Final Design Phase at the end of 2004 and is in the manufacturing stage.

MUSE is an external consortium effort led by the Observatoire de Lyon (CRAL) including the University of Leiden, the Eidgenössische Technische Hochschule Zürich, Astrophysikalisches Institut Potsdam, the Observatoire Midi-Pyrénées (LAOMP), and the Institut für Astrophysik Göttingen.

## Description of the AO Modules

### GRAAL for HAWK-I

#### Concept

The GROund layer Adaptive optics system Assisted by Lasers (GRAAL) is a module designed to provide GLAO correction for the HAWK-I NIR wide-field imager (7.5' x 7.5' FoV with ~0.1" pixels). GRAAL is designed as a module hosting four WFSs for LGS and a tip-tilt sensor for a NGS. The atmospheric turbulence is sampled in four slightly different directions over the instrument field of view to

send an average correction, homogeneous over the scientific field of view, to the DSM. The improvement provided by GRAAL can be summarised in saying that it will allow HAWK-I to work most of the time under better than median seeing conditions (e.g. the FWHM of the PSF will be reduced from 0.94" to 0.73"). Even under most conditions (1" seeing in the visible), the 50% encircled energy diameter will be reduced by 15% in the Y and 30% in the Ks over the entire field of view.

The system will use the Deformable Secondary Mirror (DSM) having enough stroke and degrees of freedom to correct for the atmospheric seeing (up to 2" seeing) including the atmospheric tip-tilt and for VLT field stabilisation. Four Sodium Laser Guide Stars emitted from four 50-cm laser projectors located on the VLT centrepiece will be sensed by four 30 × 30 Wave-Front Sensors (WFS). These wavefront sensors must rotate to compensate for the pupil rotation at the Nasmyth focus and they must acquire and track the focus of the corresponding laser spots.

As baseline a visible tip-tilt sensor has been considered. To avoid obscuration of the HAWK-I FoV the visible NGS will be acquired outside the HAWK-I FoV. As an alternative an IR Natural Guide star could

be used to sense tip-tilt aberrations. The IR NGS will be selected inside the HAWK-I FoV. The sensing would then be performed using the guide mode of the HAWK-I Hawaii2RG infrared detectors: a small window (16 × 16 pixels) around the IR NGS will be read out at high frequency to sense tip-tilt.

Note also that the correction modes of the DSM and SPARTA are not restricted only to GLAO and LTAO. GRAAL contains an on-axis high-order WFS 40<sup>2</sup> subaperture used for the DSM commissioning and maintenance activities. Figure 2 shows the opto-mechanical concept for GRAAL and the performance expected. The relative improvement with respect to no correction can be seen by comparing crosses (GLAO) and diamonds (no correction). The homogeneity of the improvement across the field of view can also be assessed from the plot on the right.

#### Performance improvement for SCIENCE

HAWK-I with GRAAL would constantly reach 1.5 mag fainter on point sources than without correction, for the same integration time. GRAAL will thus emphasise HAWK-I's strengths: very deep imaging at high spatial resolution. But note also that HAWK-I with GRAAL will

reach the same magnitude limit as VISTA 16 times faster, i.e., even with the significantly smaller FoV, HAWK-I with GRAAL would reach 1/2 the survey speed of VISTA but with at least a factor of two improvement in spatial resolution.

HAWK-I prime science cases include deep multi-colour surveys at high  $z$ , stellar population studies in nearby galaxies, and investigations of star-forming regions in our Galaxy. These programmes critically rely on the deepest possible exposures with the highest possible spatial resolution – both of which will be improved by GRAAL. HAWK-I with GRAAL will typically reach 0.5 mag deeper in  $J$ ,  $H$  and  $K$  for a fixed exposure time. For high- $z$  observations, this is equivalent to a gain of 1.26 in distance (adopting a standard cosmology). This translates in turn into ~25% more volume probed by the survey in the same time (surveys will reach  $z \sim 1.2$  instead of  $z = 1$  or  $z \sim 3.6$  instead of  $z \sim 3$ ).

For surveys aiming at studying galaxies at fixed redshift, or stellar populations in a given nearby galaxy, this translates into vastly increased number statistics, as the galaxy luminosity function increases exponentially and the stellar initial mass rises with a power > 2 in the regime of interest. Proposals addressing forefront science often require the

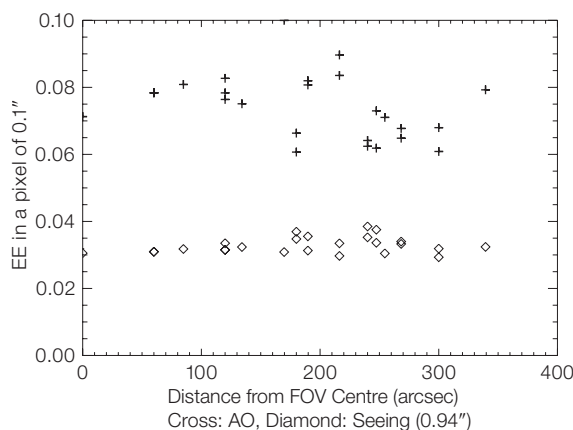
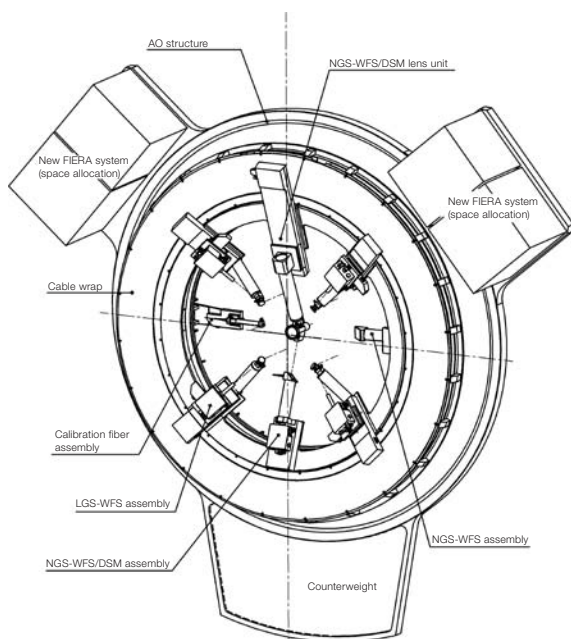
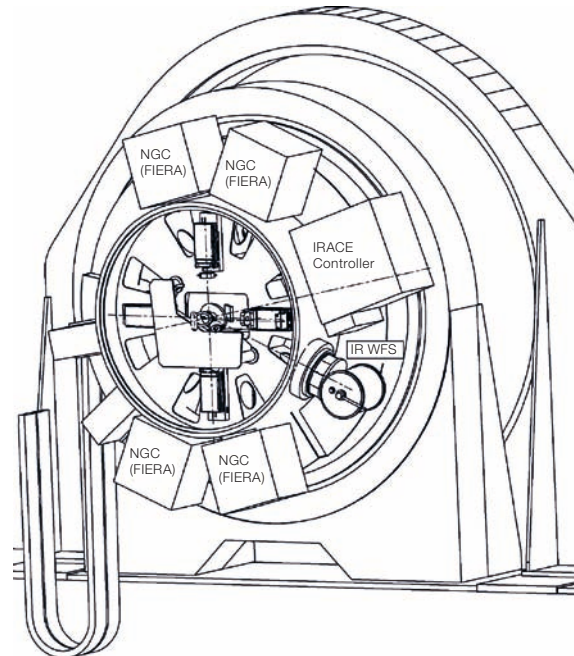
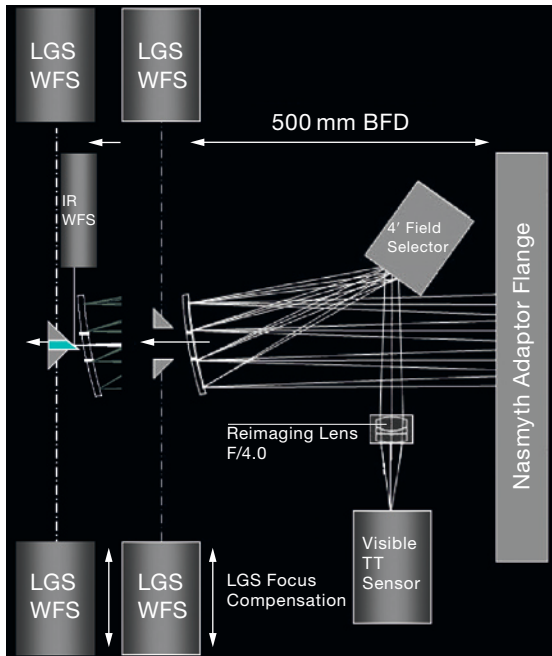


Figure 2: GRAAL opto-mechanical layout. One sees the four LGS wavefront sensors, the visible wavefront sensor and the central natural guide star sensor for the commissioning and maintenance of the DSM. The plot shows the fraction of energy in a 0.1" rectangular pixel K-band; crosses represent GLAO correction and diamonds represent seeing-limited observations.

Figure 3: GALACSI opto-mechanical layout. GALACSI is mounted on the Nasmyth A/R which is used to correct for pupil rotation. This insures that the WFS pattern remains fixed with respect to the DSM actuator geometry.



best seeing conditions. Currently, the natural seeing in the *K*-band is better than 0.4" only 20 % of the time. With GRAAL, an image quality in the *K*-band below 0.4" will be achieved ~ 80 % of the time. GRAAL will provide a fourfold increase in time for the most challenging proposals.

## GALACSI

### Concept

GALACSI is a module very similar to GRAAL. It will include four LGS WFS and one tip-tilt natural star sensor. It will offer a correction mode identical to GRAAL GLAO (laser stars closer since FoV smaller), that is seeing improver, except for a smaller field of view called Wide Field Mode (1 arcmin). Although the field of view is smaller, the gain in ensquared energy gain is similar to GRAAL since the wavelength is shorter (750 nm). The Narrow Field Mode is the real challenge since it aims at a strehl ratio of some 10 % at 650 nm in a 7.5" field of view. Laser Tomography means that the WFS data are used to assess the altitude distribution of turbulence, compensated for the laser cone effect, in order to provide a correction vector to the DSM optimised to allow high strehl ratio on-axis.

It will serve MUSE, a visible spectrograph (0.46–0.93  $\mu\text{m}$ ) sitting on the Nasmyth platform and composed of 24 identical Integral Field Units. MUSE will obtain 90 000 spectra (370  $\times$  106 pixels) with a resolution of 3 000 in a single exposure.

Since the DSM is attached to the telescope structure, its actuator geometry will rotate like the pupil at the Nasmyth focal plane of the VLT. To maintain the matching between the WFS and DSM pattern the WFSs must rotate like the telescope pupil. This corresponds to a co-rotation of the WFSs with the Telescope altitude axis. The same applies for the field position of the LGSs. The rotation is done by co-rotating GALACSI with the Nasmyth rotator. The field de-rotation for MUSE is done inside MUSE.

The visible tip-tilt natural guide star sensor for the Wide Field Mode is expected to have a limiting magnitude around  $M_v \sim 17.5$ . Natural tip-tilt star will be acquired within a 4' technical FOV but outside the 1' square scientific FOV to prevent occultation of the scientific FOV. An IR on-axis tip-tilt natural guide star sensor will be used for the 7.5" Narrow Field Mode. Light separation will be done with a VIS/IR dichroic located after the Adaptive Optics focal plane. Figure 3

shows the optical design and opto-mechanical layout of GALACSI. Figure 4 shows the simulated performance of the WFM and the NFM.

### Science

MUSE and GALACSI will tackle a wide range of astrophysical problems. MUSE has been designed from the start to take great advantage of the combination of IFU spectroscopy and the high spatial resolution provided by AO.

#### 1. Narrow-Field Mode (NFM)

The very high spatial resolution of this mode (0.025 arcsec<sup>2</sup> spatial elements) allows only relatively high surface brightness science targets. The science drivers are therefore quite specific, although still scientifically relevant and totally unique to MUSE. During the operational period of MUSE, the science community may not have access to a space-based (diffraction limited) optical spectrograph, such as the successful STIS long-slit spectrograph onboard HST. Such spatial resolution at optical wavelengths, combined with an 8.2-m aperture, will be at a premium. We give in the following a few examples

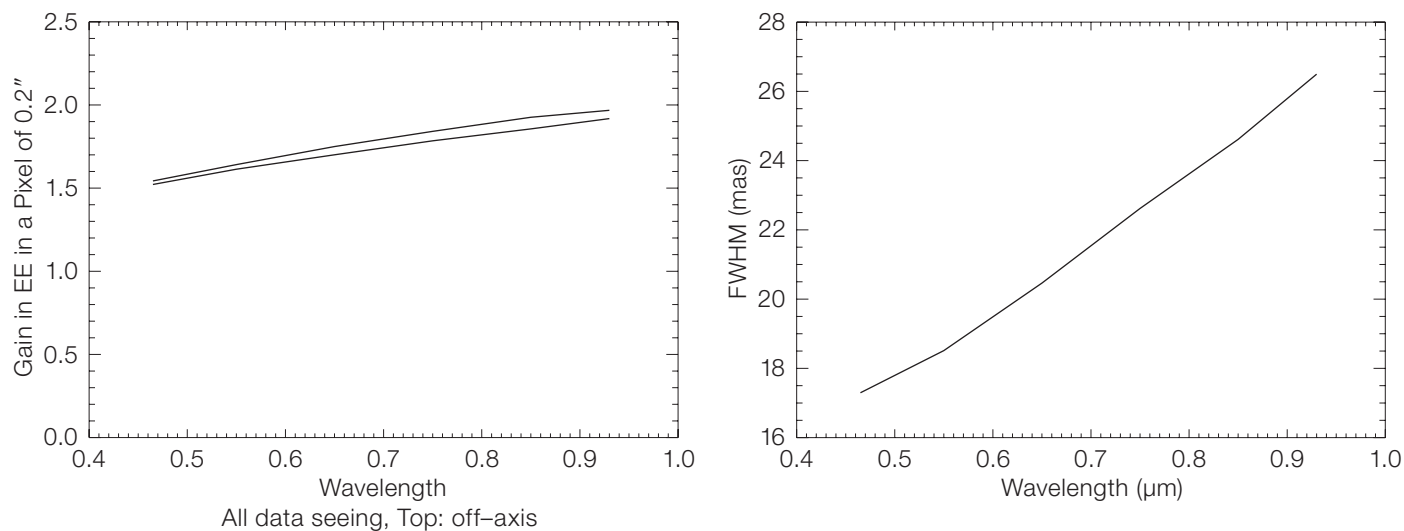


**Figure 4:** Left: Gain in Ensquared Energy (EE) in 0.2'' versus wavelength. These curves were obtained by simulations using recent  $Cn^2$  profiles measured at Paranal and show a gain in EE of about 1.8 at 750 nm. Right: The Narrow Field Mode FWHM performance as a function of wavelength. The instrumental error budget as well as LGS spot elongation and Na height variations have been neglected here.

of scientific questions which could be addressed by MUSE NFM.

In recent years it has become clear that supermassive black holes (SMBHs) are intimately linked with the mass evolution of their host galaxies and are therefore key ingredients of the formation and evolution of galaxies. The SMBHs formation processes should leave signatures in their immediate environment either in terms of stellar orbital structure or chemical enrichment history. These key issues can only be fully addressed with optical IFU observations at near-diffraction-limited resolution.

The MUSE NFM will also provide spectral insight (density, temperature and ionisation) and high spatial resolution over a relatively large field of view of Young Stellar Objects. This will allow the physical processes involved in the formation and structure of the jets to be investigated in details. The MUSE NFM is also ideally suited to the spatially resolved spectroscopy of solar-system bodies. While much more detail can obviously be obtained by space probes, one visit is not the whole story given the significant time evolution of atmospheres and surfaces of most solar-system objects. Monitoring volcanic activity on the Galilean satellites will yield new insights on planetary resurfacing. Other examples include monitoring Titan, Uranus and Neptune atmospheres.

## 2. Wide-Field Mode (WFM)

The main target of the MUSE surveys is to find and study the building blocks of the local, normal galaxies such as our Milky Way, at an epoch when the Universe was typically 1 Gyr old. The observation of such objects will be of great value to clarify the way galaxies form. The benefit of AO correction is obvious since these sources are typically 0.1–0.3'' in size.

Presumably, mass assembly is a long-timescale process that starts early and goes on to the present time. Making the census of large and small objects in the early Universe, when the cosmic age was 1 Gyr, and studying their properties, will set strong constraints on detailed models of hierarchical galaxy formation. In this prospect, the specific questions which one wants to address by studying this population of objects are the following: how did galaxies like our Milky Way assemble from small fragments? What are the stellar and gaseous masses of these fragments? What are the masses of the dark matter haloes they are hosted in? What are their typical star-formation histories?

Intermediate-redshift galaxies at  $z \sim 1$  are well suited to be studied by MUSE-GALACSI WFM since the 0.3'' PSF corresponds to a  $\sim 2$  kpc scale allowing the study of internal variations of stellar population ages, metallicities and gas enrichment. Gas kinematics (2D) allows

exploration of star formation and metal enrichment histories of bulges and discs, of the size, intensity and topology of coherent large-scale starbursts and of the development of galactic structure.

Nearby galaxies will also be prominent targets, especially their central regions containing important information on the fossil record of mass assembly, black-hole formation, star formation requiring resolution of  $\sim 100$  pc spatial scales.

Last but not least, the instrument also has an enormous potential for enabling massive point-source spectroscopy in crowded fields, by using the large contiguous 3D data cubes to deblend and deconvolve sources in the combined spectral and spatial domains. This allows superior performance in dense regions such as the Galactic Bulge and Magellanic Clouds, but also allows extremely dense fields to be observed. At larger distance the investigation of nearby galaxies through detailed spectral analysis of their stellar populations, resolved into individual stars, can provide quantitative templates for the calibration of integrated light studies of higher redshift systems.

## SPARTA

The AO Department has identified the need for a flexible real-time application platform for the new-generation AO systems being developed in the context of

the AO Facility. SPARTA (Standard Platform for Adaptive optics Real Time Applications) is the answer to this need. The RTC's of GRAAL and GALACSI will be based on SPARTA.

SPARTA is a project that starts from the OPTICON/JRA-1 framework to provide a solution to the challenge of building a real-time computer for high-order/high-bandwidth systems but at the same time using mainly Components Off-The-Shelf (COTS). SPARTA goals are to serve all the second-generation VLT instrumentation (AO Facility and the Planet Finder) and to create a basis for growth towards ELT-size AO systems.

The requirements for the new generation of AO systems are beyond the current computational power of single board computers used today. For instance, the requirements for the Planet Finder is 200 times higher than the capacity of the NAOS RTC (plus keeping the latency very low). The latency is the major challenge of SPARTA: the RTC must not only compute the control commands fast enough to cope with the increased loop frequency, but it also has to complete the computation earlier to reduce time-related errors. This is equivalent to a system much faster than the nominal loop frequency. On the other hand, it is clear that the time required to develop an AO system is rather long and the final result consists primarily of infrastructure, data management and interface: the core real time application is a tiny portion of the whole AO RTC system. These are the main reasons to create a common platform to serve all these projects.

The complexity of the control software and the required flexibility would suggest the use of high-end CPUs, programmable with standard programming languages (C/C++) with a relatively fast developing cycle. That was the natural choice for the first SPARTA prototype, based on multi-CPU board connected together to achieve the required throughput. Unfortunately with such architecture the low latency requirements cannot be achieved due to structural problems of the CPU architecture.

To solve this problem one has to change the technology. This is where FPGAs come into play. An FPGA is a chip that provides millions of logical elements that can be connected by means of a programme to create any function that will then execute at the speed of the FPGA core clock. Moreover, many functions can be programmed, until all elements are used. All of these functions run in parallel and this is the great advantage of FPGAs. However FPGA programming is a difficult exercise; it uses the same language as for designing integrated circuits and microprocessors.

Consequently the development cycle of an FPGA application is much slower and the debugging much more difficult. Where the FPGA is unbeatable is the communication infrastructure: being implemented in hardware, there is no additional latency. The perfect application for the FPGA is to manage all the critical communications of SPARTA so that data are routed within the system at the fastest possible speed and the lowest possible latency. Hence the collaboration between ESO and Durham, under the OPTICON/JRA-1 project. Durham is developing an FPGA-based acquisition processor that receives the pixel stream and processes them up to the computation of the gradients. The gradients will then be further processed by a DSP array.

A DSP is fundamentally a CPU, so it shares the same problems if used as a CPU. However a DSP is also equipped with fast communication ports and a big (3 MB) on-chip memory. Using fast I/O and the internal memory a DSP can deliver a high throughput while significantly simplifying the development cycle being a CPU. A DSP can be programmed in C/C++. The market recently made available a board with several DSPs whose link ports are interfaced directly to FPGAs, a good match for our architecture. The I/O is managed by the FPGAs and the DSPs act as an array of co-processors.

The GALACSI SPARTA has four Shack-Hartmann sensors providing four pixel streams coming from the NGCs. They are connected to a switch that converts the optical signals to electrical ones

and routes them to four independent front-end FPGAs, hosted in two boards. Each FPGA will run the Durham module that will produce the gradients. Each FPGA sends the gradient vector to a different DSP board equipped with eight DSPs. Each DSP board will process the related portion of the control matrix and then results are gathered on the back-end FPGA that will complete the processing with the time-domain filter, and finally results are sent to the corrective optics device. This architecture can run at 1 KHz with a latency of about 120  $\mu$ s.

## Conclusions

The AO Department of ESO is heading the development of the AO Facility, the transformation of one 8-m UT (presumably UT4) into an adaptive Telescope. GRAAL and GALACSI, the AO modules for Hawk-I and MUSE respectively, are two major building blocks for this project. The corresponding science cases have convinced the CDR review boards of the scientific competitiveness of the AO Facility. A third instrument and AO module is in the work for the Cassegrain station but has not been yet identified.

The project passed a Conceptual Design Review last September and Preliminary and Final Design Reviews will be completed in the course of 2008. The commissioning activities will be in full swing in the course of 2010–11 and the AOF should be available to the community by 2012.

## Acknowledgements

The work described in this paper is partially funded by the European Commission Sixth Framework Programme under contract No. RII3-CT-001566.

The authors want to thank in particular Prof. Gerry Gilmore and Dr. John Davies, respectively OPTICON Scientific Coordinator and Project Scientist, for the support provided by OPTICON to this project.

## First Light for the VLT Laser Guide Star Facility

On 28 January 2006 a laser beam of several watts was launched from Yepun, the fourth 8.2-m Unit Telescope of the Very Large Telescope, producing an artificial star, 90 km up in the atmosphere. It will enable the VLT's adaptive optics system to measure and correct the atmosphere's blurring effect.

This was the culmination of five years of collaborative work by a team of scientists and engineers from ESO and the Max-Planck Institutes for Extraterrestrial Physics in Garching and for Astronomy in Heidelberg, Germany. After more than a month of integration on-site with the invaluable support of the Paranal Observatory staff, the VLT Laser Guide Star Facility saw First Light and propagated into the sky a 50-cm-wide, vivid, beautifully yellow beam.

"This event tonight marks the beginning of the Laser Guide Star adaptive optics era for ESO's present and future telescopes", said Domenico Bonaccini Calia, Head of the Laser Guide Star group at ESO and LGSF Project Manager.

Normally, the achievable image sharpness of a ground-based telescope is limited by the effect of atmospheric turbulence. This drawback can be surmounted with adaptive optics, allowing the telescope to produce images that are as sharp as if taken from space. This means that finer details in astronomical objects can be studied, and also that fainter objects can be observed. In order to work, adaptive optics needs

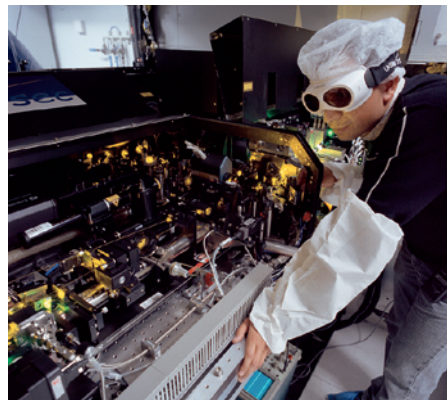
a nearby reference star that has to be relatively bright, thereby limiting the area of the sky that can be surveyed. To overcome this limitation, astronomers use a powerful laser that creates an artificial star, where and when they need it.

The laser beam, shining at a well-defined wavelength, makes the layer of sodium atoms that is present in Earth's atmosphere at an altitude of 90 kilometres glow. The laser is hosted in a dedicated laboratory under the platform of Yepun. A custom-made fibre carries the high-power laser to the launch telescope situated on top of the large Unit Telescope.

Twelve days of tests followed the First Light of the Laser Guide Star (LGS), during which the LGS was used to improve the resolution of astronomical images obtained with the two adaptive optics instruments in use on Yepun: the NAOS-CONICA imager and the SINFONI spectrograph.

In the early hours of 9 February, the LGS was used together with the SINFONI instrument, and in the early morning of 10 February, it was used with the NAOS-CONICA system.

"To have succeeded in such a short time is an outstanding feat and is a tribute to all those who have together worked so hard over the last few years", said Richard Davies, Project Manager for the laser source development at the Max-Planck Institute for Extraterrestrial Physics.



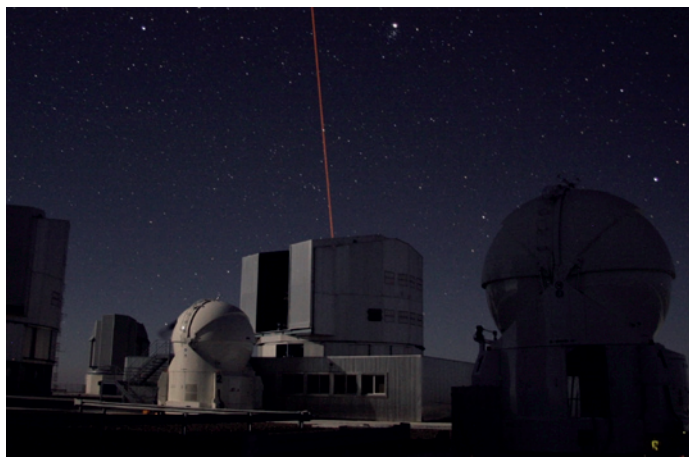
Photos: H. Zodelt (top) and S. Oberti (bottom), ESO

The Laser Guide Star Laboratory.

A second phase of commissioning takes place this spring to optimise the operations and refine the performance. The experience gained with this Laser Guide Star is also a key milestone in the design of a next-generation Extremely Large Telescope in the 30- to 60-metre range now under study by ESO together with the European astronomical community.

The Laser Guide Star Facility is a collaborative project between ESO, the Max-Planck Institute for Extraterrestrial Physics in Garching, Germany (MPE) and the Max-Planck Institute for Astronomy in Heidelberg, Germany (MPIA). The team members are Domenico Bonaccini Calia, Wolfgang Hackenberg, Martin Cullum, Martin Dimmler, Ivan Guidolin, Constanza Araujo Hauck, Erik Allaert, Dan Popovic, Mauro Comin, Marco Quattri, Enzo Brunetto, Franz Koch, Armin Silber, Jose Luis Alvarez, Mario Tapia, Eduardo Bendek, Jutta Quentin, Gerhard Fischer, Massimo Tarengi, Guy Monnet, and Roberto Gilmozzi (ESO), Richard Davies, Sebastian Rabien, Thomas Ott, Reinhard Genzel, Stefan Kellner, Stefan Huber, Wieland Zaglauer, Armin Goldbrunner, and Jianlang Li (MPE), and Stefan Hippler, Udo Neumann, David Butler, Ralf-Rainer Rohloff, and Bernhard Grimm (MPIA). Members of ESO's Adaptive Optics team also participated in First Light: Markus Kasper, Stefan Ströbele, Enrico Fedrigo, Rob Donaldson, Sylvain Oberti, and Christian Sönke.

(Based on ESO Press Release 07/06)



An artificial star above Paranal.

## VLT-UVES Long-Slit Spectroscopy

Swetlana Hubrig, Gerardo Avila, Andreas Kaufer, Sandro D'Odorico, Hans Dekker, Ricardo Schmutzer, Massimiliano Marchesi, Burkhard Wolff, Linda Schmidtbreick (ESO)

In August 2005 we installed eight interference filters in UVES to be used with the red arm in visitor mode. The purpose of these filters is to isolate certain echelle orders to allow the use of a maximum slit length of 30" in UVES.

The UV Visual Echelle Spectrograph UVES (D'Odorico 1997), which has been offered to the astronomical community at the VLT since 2000, is a two-arm cross-dispersed echelle spectrograph covering the wavelength range 300–500 nm in the blue spectral region and 420–1100 nm in the red spectral region with the possibility to use dichroics. The nominal resolution is 40 000 for a 1" slit, and the maximum resolution that can be attained with a narrow slit

or image slicer is 110 000 in the red and 80 000 in the blue with two-pixel sampling.

The scientific aim of the installation of interference filters in UVES is to study faint extended objects, for example planetary nebulae (PNe) or H $\text{II}$  regions which are beyond the limit of a 4-m-class telescope. NTT-EMMI long-slit spectroscopy has been successfully carried out since the beginning of 1996 (e.g. Corradi et al. 1996), with the main goal to study the morphology of PNe. Since PNe are the result of asymptotic giant branch (AGB) mass loss and their birth rate is very likely a function of metallicity, they are important tracers of intermediate-age stellar populations in galaxies. A spectroscopic study of the physical conditions and chemistry of PNe and H $\text{II}$  regions is crucial to understand the metal enrichment during the galaxy lifetime.

PNe are known to display a variety of morphological components, such as multiple shells, extended halos, knots,

bipolar lobes, jets and rings, and the detailed analysis of the structure of these components provides an important insight into the processes governing PNe formation and evolution. The most important parameter to describe the dynamics and various morphological components is the velocity field derived from spatially resolved PNe. Numerous recent studies of PNe are aimed especially at disentangling the full velocity fields by high-resolution spectroscopy. As an example, a study of the structures of faint extended ionised haloes of PNe which are believed to reflect the previous history of heavy mass loss on the AGB, requires the precise knowledge of internal velocity fields. The availability of the high-resolution UVES long-slit mode will give the opportunity to carry out an accurate kinematical analysis of faint halo structures and their puzzling mysterious systems of rings discovered in HST images (e.g., Terzian and Hajian 2000, Corradi et al. 2004). We note that at present, only very few other high-resolution spectrographs at 8–10-m class telescopes in the world

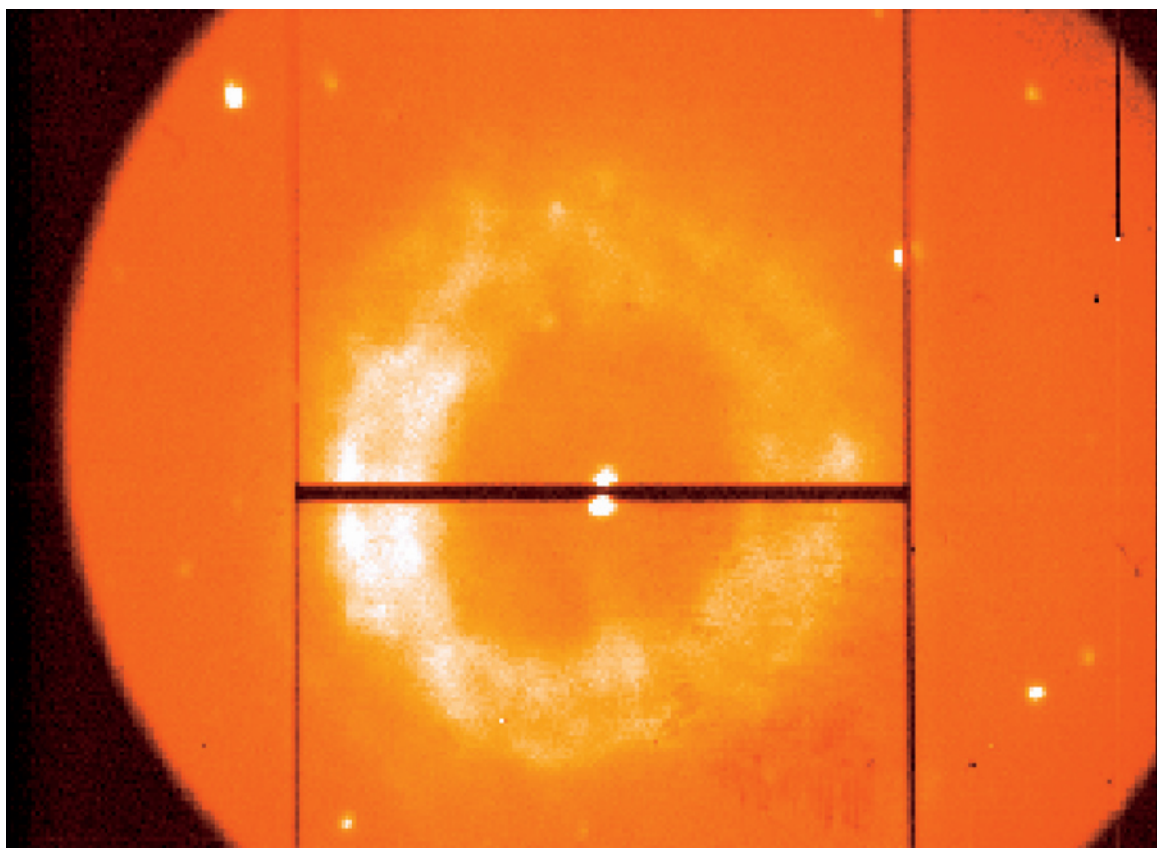


Figure 1: The UVES slit viewer image of the planetary nebula NGC 6369.

have a long-slit capability. Thus, introducing the high-resolution long-slit mode in UVES by adding interference filters to remove the other orders, taking advantage of the full slit length should be of great interest to astronomers working on the kinematics of ionised nebulae and galaxies.

The central wavelengths of the filters were chosen to permit observations of the most important emission lines in extended objects. The order for the filter manufacture was placed to the Andover Corporation in March 2005 and the filters arrived in Garching in June 2005. All eight filters were installed in the UVES red arm filter wheel in August 2005.

The filters and their central wavelengths are: H $\alpha$  (656.6 nm), H $\beta$  (486.1 nm), O $_{III}$  (500.7 nm), O $_{III}$  (436.3 nm), N $_{II}$  (575.5 nm), O $_I$  (630.0 nm), S $_{II}$  (672.4 nm), and He $_{II}$  (468.6 nm). Spectral ranges and peak transmissions are given in Table 1. The FWHM of the H $\alpha$  filter was chosen to allow simultaneous observations of H $\alpha$  with close-by [N $_{II}$ ] lines with wave-

lengths at 654.8 nm and 658.3 nm, respectively, whereas the S $_{II}$  filter allows one to observe simultaneously the [S $_{II}$ ] 671.7/673.1 nm doublet. The transmission curves for all eight filters are available in the UVES components database, accessible through the ETC (<http://www.eso.org/observing/etc/bin/gen/form?INS.NAME=UVES++INS.MODE=spectro>).

A first sky test with the new filters was carried out in the second half of August 2005. The planetary nebula NGC 6369, which has a diameter of 33"0  $\times$  32"7 (Tylenda et al., 2003), was observed with the UVES red arm using CD#3 and a slit width of 0"6 (R  $\sim$  70 000). The slit view image of this nebula is shown in Figure 1. The exposure time for the observations in each filter was 600 s. As at present there is no pipeline support for the reduction of the UVES long-slit mode, the spectra were reduced using both MIDAS-LONG package and the IRAF LONG-SLIT tasks. As an example, we present in Figures 2 and 3 two- and one-dimensional H $\alpha$  and H $\beta$  spectra of NGC 6369.

Our sky tests of the interference filters show that the UVES long-slit mode configuration can be successfully used for observations of extended objects with narrow spectral features.

References

D’Odorico, S., in “The Early Universe with the VLT”, ed. by J. Bergeron, Springer 1997, 54  
 Corradi, R. L. M., Mampaso, A., Perinotto, M. 1996, The Messenger 85, 37  
 Corradi, R. L. M. et al. 2004, A&A 417, 637  
 Terzian, Y., Hajian, A. R., 2000, ASP Conference Series 199, 34  
 Tylenda, R. et al. 2003, A&A 405, 627

Table 1: New Interference Filters.

Name	Spectral range (nm)	Transmission
H $\alpha$	652.8–659.8	92 %
H $\beta$	484.2–488.0	72 %
O $_{III}$ 500.7	498.6–502.7	71 %
O $_{III}$ 436.3	434.8–437.9	69 %
N $_{II}$ 575.5	573.0–578.5	86 %
O $_I$ 630.0	626.9–633.4	90 %
S $_{II}$ 672.4	668.7–676.0	86 %
He $_{II}$ 468.6	466.8–470.3	79 %

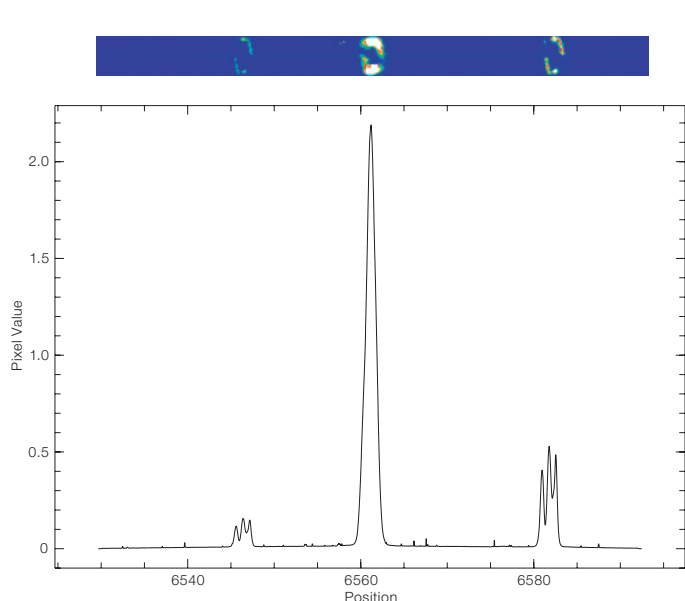


Figure 2: H $\alpha$  and [N $_{II}$ ] spectra of NGC 6369.

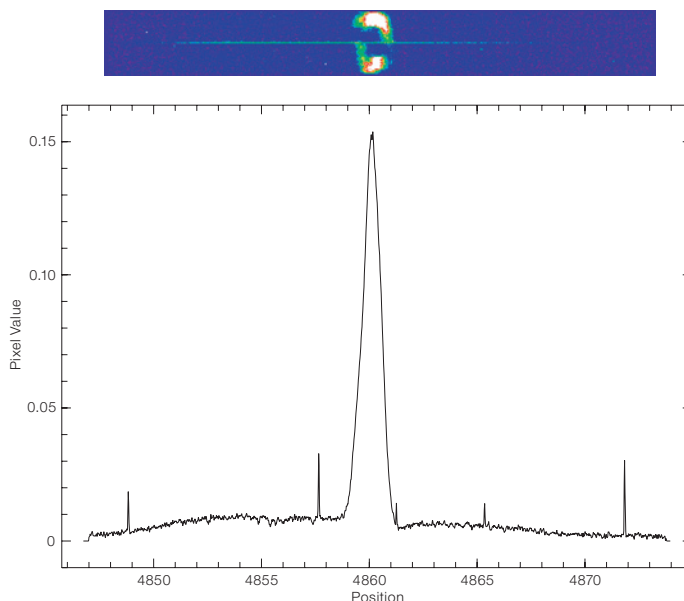


Figure 3: H $\beta$  spectra of NGC 6369.

## ALMA News

Tom Wilson (ESO)

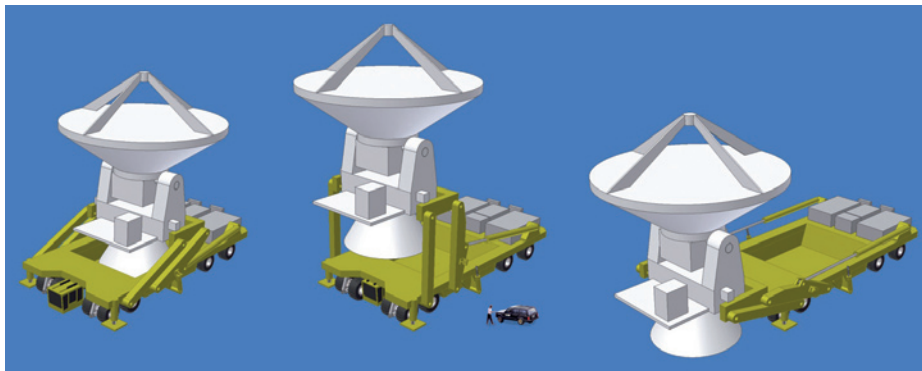
In the last issue of *The Messenger*, there was an article about the signing at ESO of the European part of the ALMA antenna contract. Shortly after this, the contract for the antenna transporters was signed. A short description of the transporters and the contract is given below.

### Antenna transporters

One of the unique features of ALMA is the possibility to move the radio telescopes to well-defined positions around the high-altitude plateau of Chajnantor and to transport antennas from the Operations Support Facility to the observing site. In order to do this, specially designed transporters, meeting all environmental conditions at an altitude of 5 000 metres, need to be designed and manufactured, and delivered to the Atacama desert. ESO has signed a contract with Scheuerle Fahrzeugfabrik GmbH, a world-leader in the design and production of custom-built heavy-duty vehicles, for two antenna transporters.

Given their important functions, the vehicles must satisfy very demanding operational requirements. Each transporter has a mass of 150 tonnes and is able to lift and transport antennas of 110 tonnes. They must be able to place the antennas on the docking pads with millimetre precision. At the same time, they must be powerful enough to climb 2 000 m reliably and safely with their heavy and valuable load, putting extraordinary demands on the 500 kW diesel engines. This means negotiating a 28-km-long high-altitude road with an average slope of 7%. Finally, as they will be operated at an altitude with significantly reduced oxygen levels, a range of redundant safety devices protect both personnel and equipment from possible mishaps or accidents.

The first transporter is scheduled to be delivered in the summer of 2007 to match the delivery of the first antennas to Chajnantor.



An ALMA transporter in action (artist's view).

### News from the ALMA site

Work progresses on the Operations Support Facility (OSF), at an elevation of 3 km. The road connecting the OSF with the Array Operations Site (AOS) is nearly completed. The antennas will be delivered to the OSF. After testing and acceptance, these will be transported on the road to the AOS, where the antennas will be incorporated into the array.



Photos: J. Riquelme, ALMA/INPAO (2)



The state of progress (end of March 2006) on the AOS Technical Building at an altitude of 5 km.

# The ALMA Design Reference Science Plan (DRSP)

Michiel Hogerheijde  
(Leiden University, the Netherlands)

## What is the Design Reference Science Plan?

The ALMA Design Reference Science Plan (DRSP) grew out of the need to have a detailed view of what the first 3–4 years of full ALMA operations will look like. Based on the projects that astronomers will want to carry out with high priority, ALMA's development can be optimised. For example, ALMA's specifications can be tested for realistic scenarios, or plans can be made regarding which configurations or frequency bands to commission with high priority. The DRSP can also be used to determine observing strategies, data rates, and use-cases. Finally, and most crucially, the impact on the science (and ALMA's primary Science Drivers) from any changes in specifications can be quantitatively assessed.

## What the DRSP is not

The DRSP is not a set of observing proposals. Although they look like proposals, they will not form the basis of any kind of ALMA programme, and do not imply any claims on particular observations. The DRSP is also not set in stone. Science priorities will change over time, and

the DRSP is only the current reflection of what the community wants to do with ALMA.

## The current DRSP

In total, by December 2003 128 DRSP projects were submitted for a total of ~ 25 000 hours, distributed over four main science areas: Galaxies and Cosmology (41 % of time), Star and Planet Formation (35 %), Stars and their Evolution (10 %), and Solar System (14 %). These projects were written by more than 75 astronomers, and 'peer reviewed'. The results are collated at a web site (see address below).

From the DRSP, one can, for example, learn that the foreseen use of receiver bands (3/6/7/9 = 20%/30%/37%/13%) is roughly consistent with expected weather statistics. While band 6 is heavily used for spectral-line work, bands 7 and 9 are the most requested for continuum observations, especially for extragalactic targets. Roughly 10% of the proposals employ the total-power capability of the array.

## How to use the DRSP

The DRSP can be accessed at the web site given below. The individual projects can be downloaded together with their review reports. Spreadsheets are also available with overviews of all programme statistics. These have been used, e.g., to get estimates of the calibration requirements, or to assess the impact of various re-baselining decisions. The DRSP is a valuable resource for anyone wishing to get a realistic and detailed view of ALMA's capabilities and foreseen use.

## The DRSP is a living document

The DRSP can only be an accurate reflection of future ALMA use if it is continuously updated. New projects can be added at all times, and existing projects can be augmented as the science questions evolve or instrument specifications change. This evolving aspect of the DRSP is crucial, because planning decisions are based on the DRSP.

The DRSP is being maintained for the ALMA Science IPT by Michiel Hogerheijde, and suggestions for additional DRSP projects can be e-mailed to him at any time ([michiel@strw.leidenuniv.nl](mailto:michiel@strw.leidenuniv.nl)).

For more information, go to <http://www.strw.leidenuniv.nl/~alma/drsp.html>

Photo: H. H. Hever, ESO



A view of Chajnantor and APEX.

# In Search of Terrestrial Planets in the Habitable Zone of M Dwarfs

Martin Kürster<sup>1</sup>  
 Michael Endl<sup>2</sup>  
 Florian Rodler<sup>1</sup>

<sup>1</sup> Max-Planck-Institut für Astronomie,  
 Heidelberg, Germany

<sup>2</sup> McDonald Observatory, University of  
 Texas at Austin, USA

After the availability of UVES at the VLT in 2000, we began a survey of M dwarf stars in order to find low-mass planetary companions. This ongoing survey, which currently enjoys ESO Large Programme status, provides a time baseline of up to six years. It is thus capable of finding planets of just a few Earth masses in close-in orbits that correspond to the habitable zones around these stars.

Measurements of stellar radial velocities at very high precision (a few  $\text{ms}^{-1}$ ) have so far produced the majority of the discoveries of the more than 170 extrasolar planets found during the last ten years. Most of these planets are gas giants comparable to Jupiter, but with increasing measurement precision lower-mass planets have become accessible over time. The current record holder among the low-mass planets discovered by RVs (radial velocities) is the third planet in the Gl876 system found by Rivera et al. (2005). The discoverers estimate its most likely mass to be  $7.5 M_{\oplus}$  (Earth masses) with a minimum mass of  $6 M_{\oplus}$ . This record has been rivalled by a very recent announcement of a planet discovered with the microlensing technique (Beaulieu et al. 2006). The most likely mass of this object is  $5.5 M_{\oplus}$ , but this value has a large uncertainty since the mass of the host star is not known.

Reaching this regime of low-mass planets with RV measurements is possible for close-in planets around low-mass stars due to the stronger associated radial-velocity signal. The low-mass planet in the Gl876 system fulfills both requirements: it is in a short-period orbit with a period of just 1.9 day and it orbits a low-mass star with an estimated mass of  $0.32 M_{\odot}$ . This leads to a semi-amplitude (half of the peak-to-valley variation)

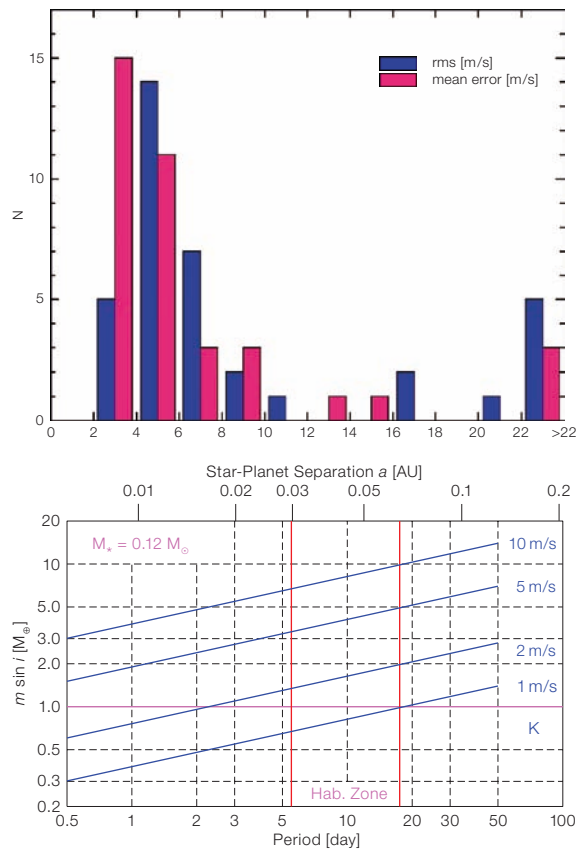


Figure 1: Comparison of the observed rms scatter and the mean error of the RV measurements for our 37 programme stars. In most cases we reach errors in the  $2\text{--}4 \text{ ms}^{-1}$  bin; larger errors either correspond to fainter stars with lower signal-to-noise level or indicate (previously unknown) double-lined spectroscopic binaries such as those in the right-most bin that contains all values exceeding  $22 \text{ ms}^{-1}$ . The rms peaks around  $5 \text{ ms}^{-1}$  indicating the presence of variability either by the star itself or due to possible planets; rms values in the  $> 22 \text{ ms}^{-1}$  bin belong to binaries.

Figure 2: Minimum planet masses  $m \sin i$  for RV signals with different semi-amplitudes  $K$  as a function of orbital period or star-planet separation  $a$  (scale at top). This example is for a star with  $0.12 M_{\odot}$ , e.g. Proxima Centauri. Circular orbits were assumed. The habitable zone is located between the red vertical lines.

of the radial-velocity signal of  $6.5 \text{ ms}^{-1}$ , detectable with state-of-the-art measurement precision.

Studying low-mass planets near the limit of current detection thresholds is the goal of our RV search programme for planets around M dwarf stars using the UVES spectrograph at the VLT-UT2 *Kueyen*. This survey was begun in 2000, when UVES became available, and has recently received ESO Large Programme status for two years, of which the last semester of observations is currently underway. Still the amount of allocated observing time permitted only a moderate sample size, which we have recently increased from originally 20 stars to 37 stars. We selected our stars for moderate levels of stellar activity which could otherwise complicate the measurements.

Using UVES in the self-calibration mode provided by its iodine gas absorption cell we achieve a routine RV measurement precision of about  $2.5 \text{ ms}^{-1}$  for the brighter stars (see Figure 1). This corresponds to spectral displacements of

only about 1/500 of a CCD pixel in UVES, or about 30 nm, reliably recorded over several years. UVES therefore provides us with sufficient precision to find planets of a few Earth masses in close-in orbits around M dwarfs or, in the absence of a detectable RV signal, to exclude the presence of such planets. This can be seen from Figure 2 which, for the example of our nearest neighbour, Proxima Centauri, relates the strength of the observable RV signal (its RV semi-amplitude) to the minimum mass of the planet as a function of orbital period or star-planet separation.

Apart from the better chance of finding low-mass planets with RVs, M dwarfs are interesting for two more reasons. First, they are the most numerous type of star – probably more than 70% of all stars fall into this category. Therefore, any attempt to determine the frequency of planets in the galaxy must include M dwarfs in extrasolar planet searches. A few years ago this was difficult to do with RVs because of the absence of spectrograph/telescope combinations of sufficient efficiency. So early RV surveys

concentrated on spectral types F7V through K7V, i.e. stars with masses greater than  $0.5 M_{\odot}$ . Still today, the bulge of the M dwarfs is still basically out of reach as with decreasing mass this type of star becomes very faint. All stars in our survey are brighter than  $V = 11.7$ , and are on the relatively massive side of the M dwarfs with masses ranging between  $0.2$  and  $0.5 M_{\odot}$ . Exceptions are the two M dwarfs nearest to us, Proxima Centauri and Barnard's star, with masses of just  $0.12 M_{\odot}$  and  $0.16 M_{\odot}$ , respectively.

The second interesting characteristic of M dwarfs is the fact that, due to their small luminosity, the so-called habitable zone is located quite near the star where orbital periods are short and RV signals of terrestrial planets are sufficiently high to be detected (see Figure 2). At this point the terms 'terrestrial planet' and 'habitable zone' should be defined.

### Terrestrial planets and the habitable zone

*Terrestrial planets* are rocky objects that are not dominated by the vast gaseous envelopes that giant planets such as Jupiter, Saturn, Uranus or Neptune possess. Masses of terrestrial planets must be below  $8\text{--}10 M_{\oplus}$ , because more massive planets experience a phase of runaway gas accretion in their formation process. The minimum mass of a terrestrial planet has not yet been well defined.

The *habitable zone* is that region around a star where surface water (a prerequisite for life as we know it) can exist in liquid form on a rocky planet. For this to be really possible, the planetary atmosphere must possess quite a number of suitable properties (Kasting et al. 1991). The location of the thus defined habitable zone depends on the luminosity of the star and therefore on its mass. In a star with  $0.5 M_{\odot}$  the habitable zone is the region separated by about  $0.2\text{--}0.5$  AU

from the star, while for a stellar mass of  $0.1 M_{\odot}$  it ranges from only  $0.02\text{--}0.05$  AU. For circular orbits these separation ranges correspond to periods of  $50\text{--}180$  days for the  $0.5 M_{\odot}$  star and  $3\text{--}13$  days for the  $0.1 M_{\odot}$  star.

The true 'habitability' (i.e. suitability for life) of these zones around M dwarfs has been questioned. One reason is that extreme temperature gradients must exist on most planets in this region where the proximity of the star forces their rotation to synchronise with the orbit via tidal interaction. This means that they always have the same side facing the star, like the Moon to the Earth; see Joshi et al. 1997 for arguments who argue that these planets can still be habitable. Another concern is the high level of X-ray radiation that a close-in planet will receive from its active host star. These issues are still under discussion.

### Known planets around M dwarfs – are Jupiters rare?

The known planets around M dwarf stars are summarised in Table 1. At the time of writing five planets orbiting three different M dwarfs have been found with RV searches. Not included is the recent microlensing announcement with its uncertain mass.

When compared with the total number of more than 165 extrasolar planets discovered by RV searches the number of planets around M dwarfs is quite small. Partially, this can be explained as a selection effect as surveys of faint M dwarfs had to await the advent of efficient instrumentation and therefore do not go as far back in time as surveys of solar-type stars. So the collected data sets are not as rich and have shorter time baselines.

However, some evidence is emerging that this is not the whole story, and that

Jupiter-type planets around M dwarfs are relatively rare, at least for semi-major axes  $< 1$  AU (Endl et al. 2006). Due to small-number statistics this conclusion is not yet 100 % secure, however, and needs to be investigated further.

### Towards Earth-mass planets

Figures 3 and 4 show the time series of our UVES RV data for two of our stars, Barnard's star and GJ1, respectively. Barnard's star is the star with the largest proper motion in the sky ( $10''/\text{yr}$ ), and the motion of GJ1 is also large ( $6''/\text{yr}$ ). This motion changes the direction of the line of sight to the star. Since the radial velocity is the component of the stellar space velocity along the line of sight, its observed value must also change with time. This effect is called the secular acceleration of the RV, and its amount can be predicted using the astrometric data base of the Hipparcos satellite. For Barnard's star and GJ1 the expected RV change is  $4.5 \text{ ms}^{-1}\text{yr}^{-1}$  and  $3.7 \text{ ms}^{-1}\text{yr}^{-1}$ , respectively, in full agreement with our RV measurements and demonstrating the excellent performance of UVES.

In the following we use our particularly rich data set for Barnard's star (data from 70 nights) as an example to illustrate how the data are analysed for the presence of periodic signals that could reveal an orbiting planet. Figure 5 shows our data of Barnard's star, after subtraction of the secular RV change, and displayed together with the best-fit planetary orbit. If interpreted as an orbiting companion, this variation would indicate a terrestrial planet with an orbital period of  $44.9$  d and an RV semi-amplitude of  $3.0 \text{ ms}^{-1}$ , corresponding to an orbital radius of  $0.13$  AU and a minimum mass of  $4.9 M_{\oplus}$ . This would be the lowest-mass planet found so far; it would orbit somewhat outside of the habitable zone. The orbital eccentricity would be small and most likely zero.

Star	Spectral type	Mass [ $M_{\odot}$ ]	V [mag]	$m \sin i$ [ $M_{\text{Jup}}$ ]	$a$ [AU]	$P$ [d]	$e$	Discovered by
GJ876	M4V	0.32	10.17	1.94	0.21	60.94	0.02	Marcy et al. 1998
				0.56	0.13	30.1	0.27	Marcy et al. 2001
				0.02	0.02	1.94	0	Rivera et al. 2005
GJ436	M2.5	0.41	10.68	0.07	0.03	2.64	0.12	Butler et al. 2004
GJ581	M3	0.31	10.33	0.056	0.041	5.366	0	Bonfils et al. 2005

**Table 1:** The five RV-discovered planets around M dwarfs. The columns list name of the star, spectral type, stellar mass, visual magnitude  $V$ , minimum mass  $m \sin i$ , orbital semi-major axis  $a$ , period  $P$ , eccentricity  $e$ , and the discovery paper.

**Figure 3:** RV time series of UVES data for Barnard's star. 'BJD' is the barycentrically corrected Julian date; both the RV and time values are referenced to the barycentre of the solar system in order to take out the movement of the Earth. The red line depicts the expected secular change of the RV of  $4.5 \text{ ms}^{-1}\text{yr}^{-1}$  which agrees well with our measurements.

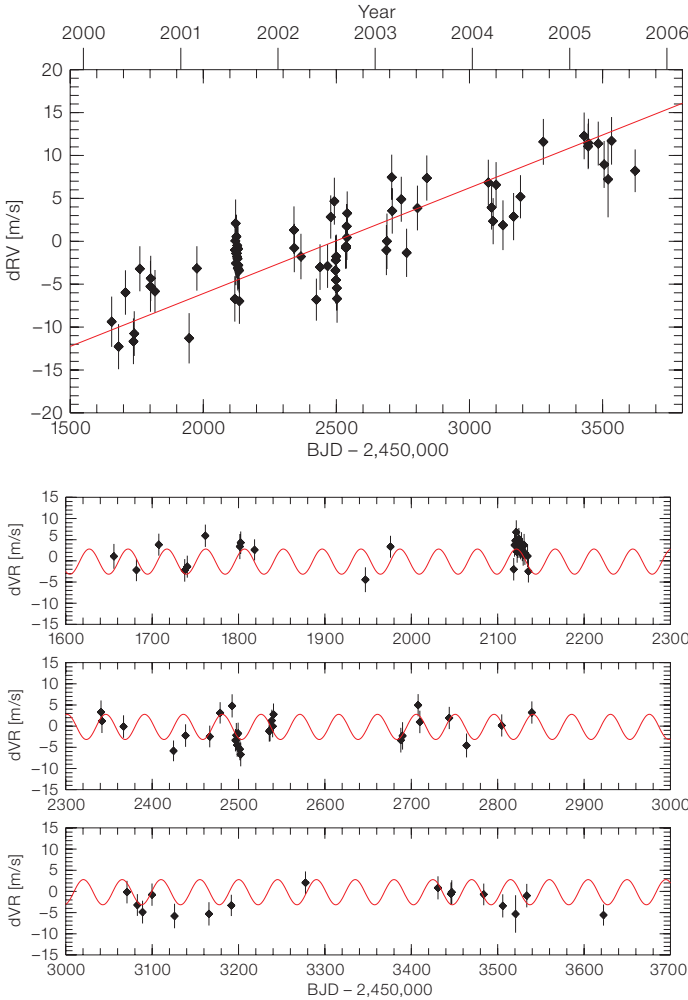


**Figure 5:** RV data for Barnard's star together with the best-fit sinusoidal orbit (red line). For display purposes the time series has been broken into three panels. This variability appears to be largely related to stellar activity rather than a planet.

However, even though this model is formally significant, passes the usual statistical tests, and thus confirms that genuine variability is present, the data appear to show a few systematic deviations from the model, e.g. near BJD 2,452,430 and 2,453,510. It turns out that a two-planet model does not improve the quality of the fit by much. And in fact there is reason to believe that the discovered signal is by itself variable and therefore not due to an orbiting planet.

Further analysis shows the signal to be correlated with the strength of the H $\alpha$  ab-

sorption line (Kürster et al. 2003). This line is an indicator for active regions in the upper stellar atmosphere, the so-called chromosphere. Active region spectra show H $\alpha$  in emission which combines to reduce the strength of the photospheric H $\alpha$  absorption line when active regions come into view. Photospheric star spots associated with these active regions affect the shapes of those absorption lines that are used for RV measurements which become erroneous. Since active regions come and go and reconfigure themselves their influence can be quite irregular, but will to some degree

**Figure 4:** RV time series of UVES data for GJ1. The red line represents the expected secular acceleration of  $3.7 \text{ ms}^{-1}\text{yr}^{-1}$ .

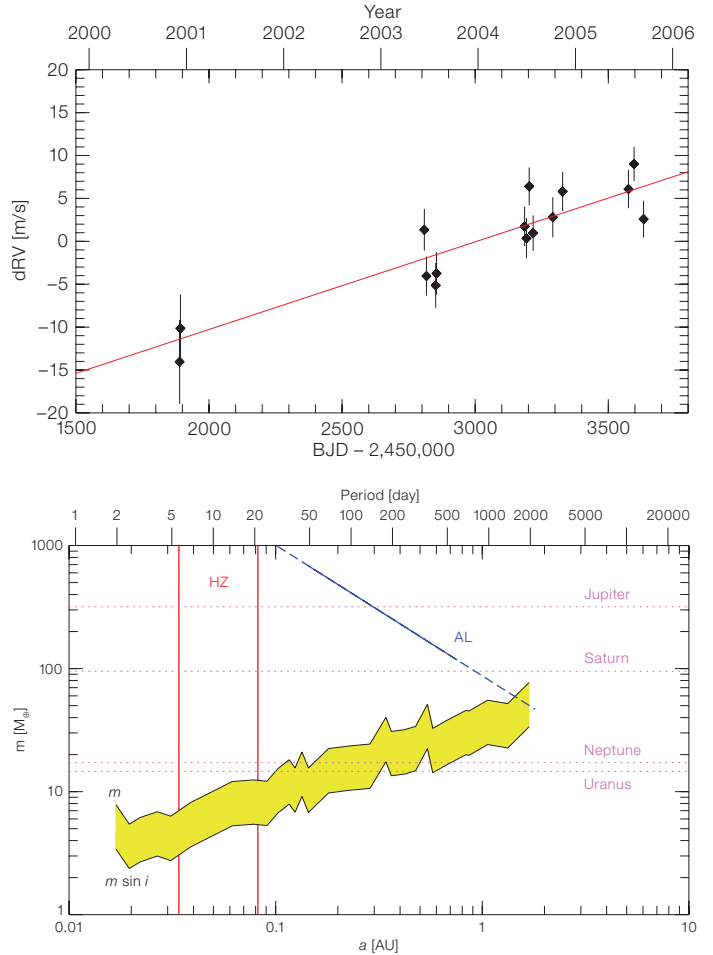


**Figure 6:** Upper limits to companion masses for Barnard's star. The line labelled ' $m \sin i$ ' corresponds to the minimum mass, the line labelled ' $m$ ' is for masses greater by a factor of 2.3, higher true masses are excluded with 90% confidence. The blue line shows astrometric limits from Benedict et al. (1999). Red vertical lines delimit the habitable zone. For comparison, the masses of the Solar System giant planets are indicated.

also show periodic behaviour because of the regular visibility changes caused by stellar rotation.

No clear planetary signal having been found, we can exclude the presence of planets with quite low masses within 1.8 AU around Barnard's star. This is shown as the lower edge of the yellow region in Figure 6 which represents the statistical upper limits for the minimum companion mass as a function of star-planet separation and period (scale on top). Planets with minimum masses larger than this limit would have

produced such a strong RV signal that we would have discovered it, planets below this limit could have gone undetected. The employed statistical method is called bootstrap simulation (details in Kürster et al. 2003). Note that all results relate to the minimum mass of the planet,  $m \sin i$  rather than the true mass, since the inclination  $i$  of the orbit with respect to the plane of the sky is not known. However, one can show that there is a 90 % chance that the true mass is no more than a factor of 2.3 larger (corresponding to the upper edge of the yellow region), and that the minimum mass is the most probable value.

Also shown in Figure 6 are astrometric mass limits (blue line) for Barnard's star from Benedict et al. (1999) based on data from the Fine Guidance Sensor of the Hubble Space Telescope. As astrometry

is more sensitive for larger orbital radii, these limits are complementary to our RV-derived limits. Combining both types of limits we can exclude the presence of any Saturn-mass planet with high confidence.

In short-period (few days) orbits planets of just a few Earth masses would have been discovered. In the habitable zone planets with minimum masses greater than about  $5 M_{\oplus}$  are excluded and the true mass of any undiscovered planet should be below the mass of Uranus. Continued monitoring of Barnard's star will lower these limits over time enabling us to search for planets of increasingly lower mass.

**Acknowledgements**

Thanks are due to quite a number of people who helped to make this survey happen. We are spe-

cially grateful for the assistance of Andreas Kaufer, Stéphane Brilliant, and all the ESO staff who supported this project by carrying out service-mode observations and by securing the high quality of the instrument and data. Artie Hatzes created the title of the programme. Sebastian Els, Frédéric Rouesnel, and William Cochran helped in the early phase of the project.

**References**

Beaulieu, J.-P. et al. 2006, Nature 439, 473  
 Benedict, G. F. et al. 1999, AJ 118, 1086  
 Bonfils, X. et al. 2005, A&A 443, L15  
 Butler, R. P. et al. 2004, ApJ 617, 580  
 Endl, M. et al. 2006, ApJ, submitted  
 Joshi, M. M., Haberle, R. M., Reynolds, R. T. 1997, Icarus 129, 450  
 Kasting, J. F., Whitmire, D. P., Reynolds, R. T. 1991, Icarus 101, 108  
 Kürster M. et al. 2003, A&A 403, 1077  
 Marcy, G. W. et al. 1998, ApJ 505, L147  
 Marcy, G. W. et al. 2001, ApJ 556, 296  
 Rivera, E. J. et al. 2005, ApJ 634, 625

## Low-Mass Exoplanet Found Using Microlensing

Using a network of telescopes scattered across the globe, including the Danish 1.54-m telescope at ESO La Silla, astronomers have discovered a new extrasolar planet which is only about five times as massive as the Earth, and circles its parent star in about 10 years. It is the least massive exoplanet around an ordinary star detected so far and also the coolest. The planet most likely has a rocky/icy surface. Its discovery marks a ground-breaking result in the search for planets that may support life.

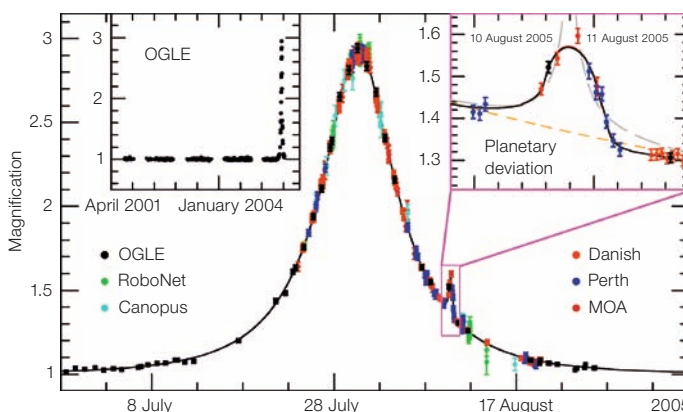
The microlensing technique is based on the temporary apparent brightening of a background star by the gravity of an intervening massive object (star or planet) passing in front. An intervening star causes a characteristic brightening that lasts about a month. Any planets orbiting this star can produce an additional signal, lasting days for giant planets down to hours for Earth-mass planets.

In order to be able to catch and characterise these planets, nearly-continuous round-the-clock high-precision monitoring of ongoing microlensing events is required, once the beginning of an event has been reported. The present case was discovered on 11 July 2005, and observed until well into August, when the planetary deviation was noticed.

The new planet orbits a red star five times less massive than the Sun, located at a distance of about 20 000 light years, not far from the centre of our Milky Way Galaxy. Its relatively cool parent star and large orbit implies that the likely surface temperature of the planet is  $-220^{\circ}\text{C}$ , too cold for liquid water. It is likely to have a thin atmosphere, like the Earth, but its rocky surface is probably deeply buried beneath frozen oceans. It may therefore more closely resemble a more massive version of Pluto, rather than the rocky inner planets like Earth and Venus.

A full report has been published by Jean Philippe Beaulieu et al. in Nature 439, 437 (2006). This result is a joint effort of three independent microlensing campaigns: PLANET/RoboNet, OGLE, and MOA, involving a total of 73 collaborators affiliated with 32 institutions in 12 countries (France, United Kingdom, Poland, Denmark, Germany, Austria, Chile, Australia, New Zealand, United States of America, South Africa, and Japan).

(Based on ESO Press Release 03/06)



Light Curve of OGLE-2005-BLG-390.

# Direct Imaging of Sub-Stellar Companions around Young Stars – Special Case: GQ Lup A + b

Ralph Neuhäuser<sup>1</sup>  
 Markus Mugrauer<sup>1</sup>  
 Eike Guenther<sup>2</sup>

<sup>1</sup> Astrophysical Institute and University Observatory (AIU), Jena, Germany  
<sup>2</sup> Thüringer Landessternwarte (TLS), Tautenburg, Germany

In several years of direct imaging searches of sub-stellar companions around young nearby stars, first with plain and speckle imaging, now with Adaptive Optics (AO), we have found several brown dwarf companions – and most recently also an object with a mass estimate well below 13 Jupiter masses, so that it is probably a giant planet imaged directly, GQ Lup b. We were able to confirm all these companion candidates by common proper motion and spectroscopy showing a cool spectral type of late-M or early-L. They are only a few million years old and allow us to study the formation of planets and brown dwarfs observationally.

Objects below the hydrogen-burning mass limit of  $\sim 0.078 M_{\odot}$  are called *sub-stellar objects*, which include brown dwarfs and planets. The definitions of *brown dwarfs* and *planets* and their distinction are still under dispute. Can the mass ranges of those two types of sub-stellar objects overlap? May only objects orbiting normal stars be called planets? The working definition of the IAU for planets accepts objects below the deuterium-burning mass limit of  $\sim 13$  Jupiter masses orbiting around normal stars.

The formation mechanism of sub-stellar objects is also not yet clear. Do brown dwarfs form just like stars, or always as companions to normal stars, so that all free-floating, isolated brown dwarfs are ejected stellar embryos? Do planets form fast by direct gravitational collapse in a massive circumstellar disc or by a slow build-up of a solid core? Such questions can be studied observationally, just by observing young sub-stellar objects, in particular as companions to young stars. E.g., the youngest star found to be or-

bited by a planet gives the lower limit for the planet formation timescale. Migration of planets in a circumstellar disc can also be studied by comparing young planetary systems with old ones.

However, imaging detection of sub-stellar companions is difficult due to the problem of dynamic range: Sub-stellar objects are too faint and too close to much brighter stars. After a brief phase of deuterium burning, a few million years only, brown dwarfs cool down and fade away. Planets also get fainter as they age.

In 1993, it became clear that young sub-stellar objects are hotter and brighter than old sub-stellar objects by several orders of magnitude: young sub-stellar objects, still contracting and possibly even accreting, gain gravitational energy and become self-luminous in the infrared (Burrows et al. 1993). The magnitude difference between a sub-stellar companion of a given mass and its stellar primary gets worse as they age, because the stellar primary will reach stable hydrogen burning, i.e. constant luminosity, while the sub-stellar companion gets fainter. Hence, direct imaging of sub-stellar companions should be less difficult around young stars.

For a direct imaging detection of a faint companion next to a bright star, one also needs high angular resolution, i.e. nearby young stars. Without AO, we set our distance limit to roughly 70 to 100 pc. However, around the mid-1990s, basically no pre-main-sequence stars were known within 100 pc. All the well-known star-forming regions like Taurus, Lupus, Corona Australis, Chamaeleon are at roughly 140 pc. Hence, the first step should be a search for stars which are both *young* and *nearby*. That is what we did in the 1990s with optical follow-up observations of unidentified ROSAT X-ray sources, using mostly the B&C spectrograph at the ESO 1.5-m telescope, and Caspec at the 3.6-m for high-resolution spectra of good candidates (Neuhäuser 1997).

In the course of this survey, many new pre-main sequence stars were found, both within and around the star forming clouds. If some of them are tens of degrees, i.e. tens of pc, off the clouds, then

they should partly be tens of pc closer than the clouds, but no parallaxes were available. Towards the end of the 1990s, newly available Hipparcos data gave the distances of many of those and previously known young stars, showing that some of them were indeed located within 100 pc (Neuhäuser and Brandner 1998), e.g. TW Hya and the stars of the group now called TW Hya Association (TWA) and many more. Hence, we could now start our direct imaging survey, namely deep, high angular resolution images of pre-main-sequence stars within 100 pc. For the southern sky, we used the MPE speckle camera SHARP at the ESO 3.5-m NTT.

Sub-stellar companions show up as faint objects close to the primary target star. Faint dots next to bright stars are not always companions, they are mostly background. However, they can all be regarded as companion candidates. To confirm such a candidate as a real companion, one has to check for common proper motion and take a spectrum of the companion, which should be as cool as expected from the magnitude difference between primary and companion candidates, given the age and distance of the target. Given the known proper motion of the primary stars, the pixel scale of the detector used, and the actual astrometric precision achieved (primary sometimes saturated or in the non-linear regime, companion very faint with low S/N), one has to wait one to a few years before second-epoch images can be taken.

Once common proper motion is shown and the spectral type and, hence, temperature of the companion is determined, one can place primary and companion together in the H-R diagram to check whether they appear to be coeval, and to measure the mass of the companion from theoretical evolutionary tracks. Here, it becomes clear whether we are dealing with a low-mass stellar companion or, e.g., a brown dwarf.

Since brown dwarfs are both brighter than planets and may also be at larger separations, we first found a few brown dwarfs: Within our project, we found and/or confirmed three brown dwarfs as companions to young nearby stars within 100 pc by both common proper motion

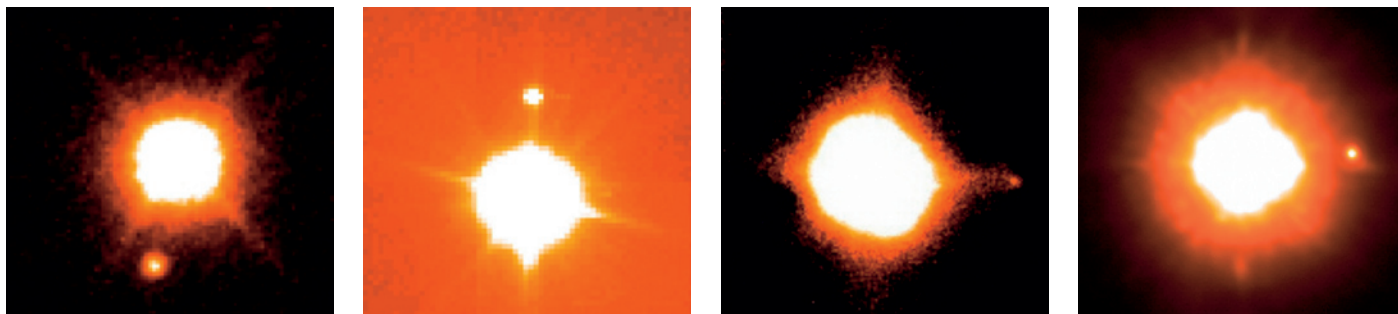


Figure 1: These three images show the three brown dwarf companions found so far by us around young nearby stars: HR 7329 B (left, VLT/ISAAC), TWA-5 B (middle, VLT/FORS1), and GSC 8047 B (right, NTT/Sharp). They show common proper motion with their primary star and a cool spectral type of M7-9, so that they have 15 to 40 Jupiter masses.

and spectroscopy (Figure 1). These were the first three brown dwarfs found and confirmed as companions to young stars.

With the advent of NACO, i.e. AO at the VLT, we (and other groups) were able to extend the sample of young stars to those in the nearby star forming regions at 140 pc including Lupus, and also reobserve those within 100 pc including TWA and other associations. We could now hope for both closer and fainter companions, i.e. giant planets.

About one year ago, we announced the detection of a sub-stellar companion to GQ Lup (Neuhäuser et al. 2005), which could well be a planet imaged directly. The direct evidence presented included the common proper motion (high significance after five year epoch difference), a cool spectral type (M9–L4), and apparently low gravity ( $\log g = 2$  to 3), however from a low-resolution NACO spectrum only. Given the location in the H-R diagram, the companion to GQ Lup could have a mass of 3 to 42 Jupiter masses according to calculations from the Tucson and Lyon groups (Neuhäuser et al. 2005), which do not take into account the formation of the objects, so that they are not valid in the first few million years, but only a few Jupiter masses according to more recent formation models (Wuchterl 2005).

Figure 2 shows our deepest image of GQ Lup so far, after shift-and-add of three NACO observations from June

2004 to August 2005. The dynamic range obtained is then shown in Figure 3. We can exclude all other companions outside of 0.2 arcsec (28 AU at 140 pc) with at least the mass of GQ Lup b.

Our NACO *K*-band spectrum of GQ Lup b shows a spectral type of M9 to L4, consistently obtained from comparison to standards and from spectral indices. Note in particular the water-steam absorption band in the blue part (Figure 4) of both GQ Lup b and the L2 dwarf, which is not present in the M8 brown dwarf, which is hotter. The spectral slope was corrected with both the GQ Lup primary (in the same slit) and a telluric standard (Neuhäuser et al. 2005).

From the *K*-band magnitude ( $\sim 13.1$  mag), the flux observed at  $\sim 140$  pc (distance towards the Lupus clouds), and the best-fit temperature of  $\sim 2000$  K, we obtain a radius of one to two Jupiter radii. With the gravity  $\log g = 2$  to 3, this results in  $\sim 0.5$  to 6 Jupiter masses (Neuhäuser et al. 2005), so that GQ Lup b may very well be an object with mass below the deuterium-burning limit (13 Jupiter masses), i.e. a planet. Our mass determinations are model-dependent, not yet from orbital dynamics.

The companion to GQ Lup is younger in age and later in spectral type than the previously found brown dwarf companions to young stars, so that GQ Lup b is lower in mass. GQ Lup b is also cooler than the two components of the eclipsing double-lined spectroscopic brown dwarf – brown dwarf binary found in Orion (Stassun et al. 2005), and at about the same age, so that GQ Lup is lower in mass than those two brown dwarfs (Guenther 2006), which are 30-Jupiter-mass objects determined dynamically (Stassun et al. 2005).

Figure 2: Deep, high S/N, high angular resolution VLT/NACO image of GQ Lup A (bright star in the centre) and b (0.7 arc sec west of it) after shift-and-add of three deep observations of  $\sim 20$  to 30 min each (June 2004, May and August 2005). The FWHM is 68 mas, the field size shown is 2.2 arcsec  $\times$  2.2 arcsec, east is left, north is up.

Comparing the images obtained over the last few years, including the new observations from 2005, shows that the separation remains constant, no orbital motion is detected so far. Orbital motion would be detectable as a slight deviation from a constant separation (or position angle), but within about  $\pm 5$  mas/yr, the expected maximal orbital motion. We would have to wait at least until the detection of curvature in the orbit before we could determine the mass dynamically. This may take tens to hundreds of years.

GQ Lup b has a projected separation of  $\sim 100$  AU (732 milliarcsec at 140 pc), which is three times further out than the outermost gaseous planet in the solar system. It could have formed further inwards, but got onto an highly eccentric orbit by a close encounter with another protoplanet (Debes and Sigurdsson 2006) or another star. For the time being, its formation remains unclear.

By now, we and other groups have observed roughly 100 young nearby stars, and two planet candidates were found, GQ Lupi b and 2M1207 b in the TWA group (Chauvin et al. 2005). For the latter case, it is not yet shown that the remaining motion between the two components is significantly smaller than the expected escape velocity for the companion, given the smaller epoch difference and/or the small total mass. In the case of GQ Lup A + b, this has been shown: The remaining motion seen be-

tween the two objects is  $1.4 \pm 2.2$  mas/yr, the maximum orbital motion could be  $3.7 \pm 1.5$  mas/yr, and the estimated escape velocity would be  $5.2 \pm 2.1$  mas/yr.

Being located close to a star, common proper motion and a cool spectrum are not sufficient for an object to be considered a bound companion, however. The binding energy (total mass for the given separation) also needs to be large enough for the pair to remain bound and stable long-term. Figure 5 shows the total mass of stellar and brown dwarf binaries versus their separations: Binaries to the upper left of the line(s) should be long-term stable against encounters with other stars and clouds in the Galaxy. There are no old wide brown dwarf – brown dwarf pairs known, because they are probably not long-term stable. There is not even a young wide brown dwarf – brown dwarf pair with common proper motion known or observed.

While GQ Lup b (100 AU away from a 0.7 solar-mass star) seems to be long-term stable, 2M1207 (55 to 70 AU from a brown dwarf primary) might not be long-term stable (Mugrauer and Neuhäuser 2005). The 2M1207 system may be an interesting case, where we see two brown dwarfs formed together as a pair, but possibly separating from each other right now. Whether systems like GQ Lup and 2M1207 are rare or frequent, is still to be investigated. Many more young nearby stars can and should be observed with NACO.

### References

Burrows A. et al. 1993, ApJ 406, 158  
 Chauvin G. et al. 2005, A&A 438, L25  
 Debes J. H. and Sigurdsson S. 2006, A&A, submitted, astro-ph/0512450  
 Guenther E. W. 2006, in: Reviews in Modern Astronomy 19 (ed. S. Röser), in press  
 Mugrauer M. and Neuhäuser R. 2005, AN 326, 701, astro-ph/0509162  
 Neuhäuser R. 1997, Science 276, 1363  
 Neuhäuser R. and Brandner W. 1998, A&A 330, L29  
 Neuhäuser R. et al. 2005, A&A 435, L13  
 Stassun K. G. et al. 2005, Protostars & Planets V, abstract  
 Wuchterl G. 2005, AN 326, 633

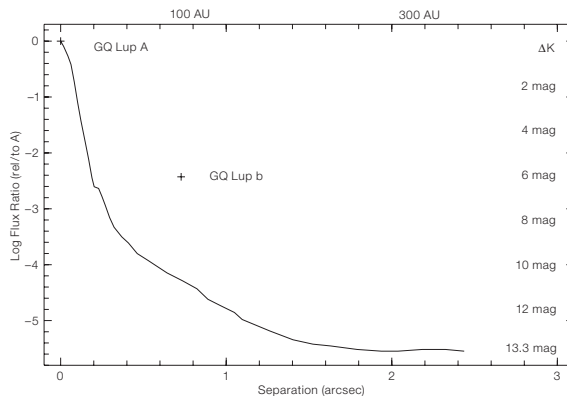


**Figure 3:** Dynamic range obtained from Figure 2 as flux ratio between background noise and primary GQ Lup A (at 0,0) versus separation. GQ Lup b is shown at 6.1 mag difference at 0.7325 arcsec separation. Projected separation at 140 pc is indicated at the top, magnitude difference in K at the right. Achieved dynamic range is  $\Delta K = 13.3$  mag outside of 2 arcsec, 12 mag at 1 arcsec, 10 mag at 0.5 arcsec, and 7 mag at 0.2 arcsec. No other companions are detected so far. We can exclude other companions with at least the mass of GQ Lup b outside 0.2 arcsec (28 AU).

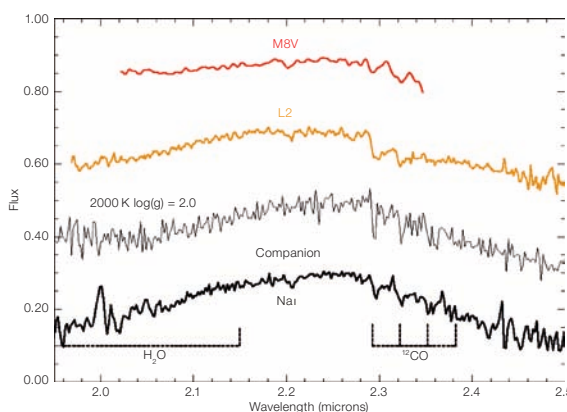


**Figure 4:** Our low-resolution K-band spectrum of GQ Lup b taken with NACO (bottom) compared to M8 (top), L2 (second from top), and a GAIA-Dusty template spectrum (Hauschildt et al., in preparation) for 2000 K and  $\log g = 2$ , which compares well with the companion (Neuhäuser et al. 2005). One can see water-steam bands and CO absorption, possibly also Na.

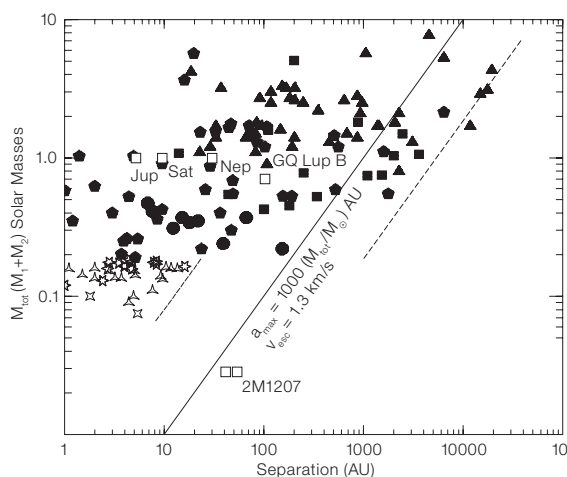


**Figure 5:** The total mass of binaries (binding energy) versus separation with very low-mass binaries as open stars and normal stellar binaries as filled symbols. There are no low-mass common proper-motion systems with separations larger than 16 AU. The solid line gives the stability limit: Bound in the upper left, unbound in the lower right. The companions of 2M1207 and GQ Lup and the giant planets in our Solar System are shown. The GQ Lup system seems bound and long-term stable (100 AU), 2M1207 does not (Mugrauer and Neuhäuser 2005), distance and, hence, projected separation are not well known for 2M1207, hence two symbols for 53 and 70 pc).

# The Formation and Early Evolution of Massive Stars

Thomas Henning<sup>1</sup>  
 Markus Feldt<sup>1</sup>  
 Hendrik Linz<sup>1</sup>  
 Elena Puga Antolin<sup>2</sup>  
 Bringfried Stecklum<sup>3</sup>

<sup>1</sup> Max-Planck-Institut für Astronomie,  
 Heidelberg, Germany

<sup>2</sup> Instituut voor Sterrenkunde Leuven,  
 Belgium

<sup>3</sup> Thüringer Landessternwarte Tautenburg,  
 Germany

**The enormous influence exerted by massive stars on their environment can affect the evolution of entire galaxies. It manifests itself most strongly during their formation in molecular clouds and their deaths as supernovae. We give examples for current observational results that shed light on the formation of these fascinating objects. We examine how this knowledge has been achieved and how it can be extended with the help of the latest observational methods.**

The birth and death of high-mass stars play a major role in shaping the morphological, dynamical, and chemical structure of many galaxies. How dramatic the effects of the formation of massive stars can be is best seen in starburst galaxies, whose structure is entirely determined by the almost explosive formation of OB stars. From which mass upwards is a star called massive? The lower mass limit can be set quite well to be 8–10  $M_{\odot}$ . Only stars at least that massive are capable of producing enough UV photons to ionise the surrounding gas and to form HII regions, to create supersonic winds, and finally to explode as supernovae. Moreover, it is known that the accretion phase is longer than the contraction period for stars exceeding roughly 8  $M_{\odot}$ . Thus, newly forming massive stars are still deeply embedded in their parental molecular cloud. Therefore, no optically visible massive pre-main-sequence stars are observed. This is in strong contrast to the low- and intermediate-mass pre-main-sequence stars – the so-called T Tauri and Herbig-Ae/Be stars. It is obvious that especially this fact has a large impact on observational strategies; to

overcome the large extinction one has to go to longer wavelengths, mainly the near- and thermal infrared. For the earliest phases even this is not sufficient, and new knowledge has to be extracted from far-infrared and (sub-)millimetre observations.

The formation of massive stars represents one of the major astrophysical problems which is still unsolved despite the crucial role these stars play in the evolution of galaxies (see the proceedings of the recent IAU Symposium 227, Cesaroni et al. 2005). The single key question is how these stars manage to accumulate that much matter during their birth process. Even during the main accretion phase, they already exhibit very high luminosities. This is a severe problem since the immense radiation pressure on dust grains counteracts the accretion, and the growing ionisation further pushes the gas to expand. It is not clear whether spherical accretion on the one hand can compete against the strong radiation, and on the other hand can cope with the vastly growing ionising flux of the forming star in order to quench an HII region for many dynamical times. The formation of massive stars by spherically symmetric mass infall therefore seems rather unlikely.

However, if the material is accumulated from a circumstellar disc the problem *may* disappear. The reason is that due to the presence of a disc, a highly anisotropic radiation field is produced, with different energy flows parallel and perpendicular to the disc's axis. First evidence for such accretion discs was thought to be found in the bipolar morphologies of the ionised regions around some well-known massive young stars or by the existence of very energetic and massive molecular outflows. We now have accumulating evidence that at least early B and late O stars (up to probably 20  $M_{\odot}$ ) form via disc-accretion processes similar to their low-mass counterparts. The characterisation of massive accretion discs is often considered as the missing link in the understanding of massive star formation.

An alternative theory to explain the formation of massive stars is based on the merging of lower-mass stars. The 'coa-

lescence' scenario implies that tidal friction in close binary systems and dense clusters 'melt' a number of lower-mass stars into one high-mass star. In its originally proposed form, this scenario implied a broken mass distribution function in the cluster (due to missing lower-mass stars that already underwent merging), which is not observed in 'normal' clusters. The concept of coalescence may still play a role in very dense clusters especially in starburst regions, but observational indications such as the omnipresent outflows and even more collimated jets cannot be easily explained in this scenario and thus are in favour of a more conventional accretion scenario for more typical galactic environments.

A related issue is the question of what the observational characteristics of the earliest stages of massive stars are. Do they always form in clusters? What is the initial mass function (IMF) in these clusters? How important is competitive accretion? When do the outflows start? What are the spectral properties of the very young massive stars? Answers to these questions can only be obtained by disentangling the complex structure of massive star-forming regions, using near-infrared adaptive optics and long-baseline infrared interferometry, sensitive thermal infrared observations, and interferometry at millimetre and radio wavelengths. In this article, we will give examples of such observations and concentrate on recent results where ESO instrumentation has provided important contributions.

## The early stages of evolution

The earliest stage of star formation is the collapse and fragmentation of a molecular cloud to (a) protostellar object(s). These objects are rather cold and usually not detected at near- or mid-infrared wavelengths. The search for massive and cold (pre-)protostellar cores only recently led to the detection of the first good candidates.

The best tool to find such cold and massive molecular cloud cores is an unbiased, large survey at far-infrared and sub-millimetre wavelengths. With more than 15% sky coverage, the ISO/PHOT 170  $\mu\text{m}$  Serendipity Survey (ISOSS) is cur-

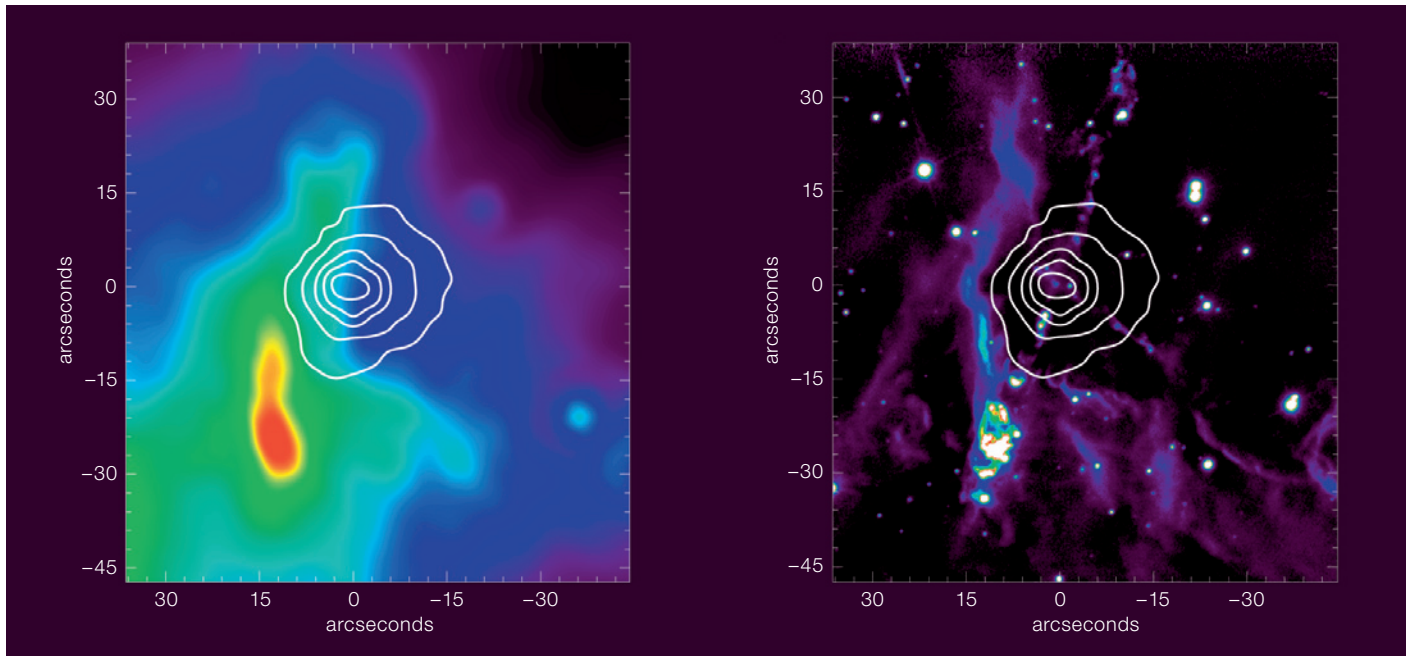


**Figure 1:** The cold core UYSO1 detected at the edge of the molecular cloud near IRAS 07029-1215. (Reference position R.A.  $07^{\text{h}}05^{\text{m}}10^{\text{s}}.80$  Dec  $-12^{\circ}18'56''.8$  (J2000).) **Left:** Spitzer  $24\ \mu\text{m}$  image of the region with superimposed SCUBA  $450\ \mu\text{m}$  contours tracing the actual young core. **Right:** VLT ISAAC near-infrared image of the same field in the  $\text{H}_2(1-0)\text{S}1$  narrow-band filter before continuum

subtraction (from Forbrich, Stanke et al. in preparation). In particular, it features two crossed arms of near-infrared  $\text{H}_2$  emission whose intersection point (close to the reference position) is compellingly near to the peak of the  $450\ \mu\text{m}$  emission. Note that the near-infrared emission visible at the respective core centre is not a continuum source but an  $\text{H}_2$  knot.

rently still the largest survey performed beyond the IRAS  $100\ \mu\text{m}$  band at medium spatial resolution. It provided very good candidates for massive cold cores (e.g., Birkmann et al. 2006) which we are presently investigating with millimetre and Spitzer observations. Another related class of objects are the so-called infrared dark clouds which appear as dark regions even at mid-infrared wavelengths and were first detected with the MSX satellite and in the ISOGAL survey.

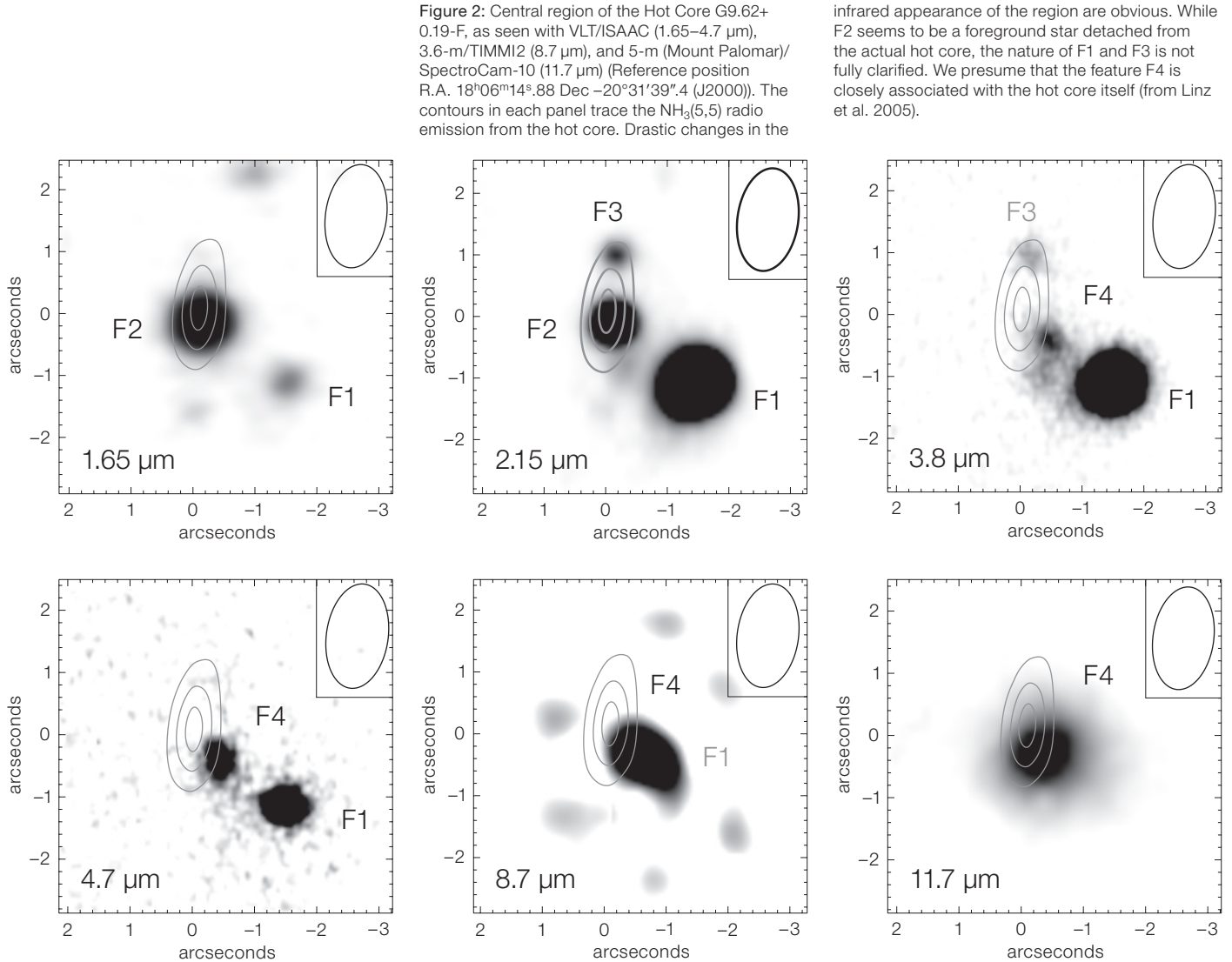
We performed another survey for massive protostellar cores and protoclusters in the outer Galaxy using SCUBA and IRAM bolometers (Klein et al. 2005). These (sub-)millimetre observations yielded the detection of a particularly interesting object (Figure 1): near to IRAS 07029-1215, which itself is an object with a luminosity of  $1700\ L_{\odot}$ , located at a distance of 1 kpc, a deeply embedded object ('UYSO1') was discovered. This object appears to be in a particularly early evolutionary stage, since it has no detectable continuum counterpart in the

near- or thermal infrared. Yet, it is already driving a high-velocity bipolar CO outflow with a total mass of  $M_{\text{outflow}} = 5.4\ M_{\odot}$ . Mass estimates and subsequent empirical relations as well as considerations of the spectral energy distribution (SED) point to the object being an early B star surrounded by an envelope of  $30\text{--}40\ M_{\odot}$  (Forbrich et al. 2004). To investigate the content of this core, we subsequently utilised the Spitzer MIPS camera. As can be seen in Figure 1, no  $24\ \mu\text{m}$  point source associated with the core is detected. This is a rare finding among the presently known objects of this class since the vast majority of cores from the surveys mentioned above apparently already exhibit such localised  $24\ \mu\text{m}$  emission. The near-infrared data for the UYSO1 region, taken recently with the VLT (see Figure 1 right), show an intensity gradient towards the cold core similar to the  $24\ \mu\text{m}$  data. In addition, they reveal the presence of two crossed  $\text{H}_2$  jets which both more or less intersect the cold core. The orientation of the north-south arm is very similar to the one of the

previously revealed CO outflow. Thus, one can speculate that UYSO1 is associated with at least one of these jet features. This means in turn that star formation has already turned on in the core. A next step will be high spatial resolution interferometric observations at (sub-)millimetre wavelengths which can be achieved with the Plateau de Bure Interferometer and with the SMA. Furthermore, UYSO1 is certainly a good candidate for ALMA observations for the future in order to pinpoint the mass distribution in the interior of the core and to sort out whether additional low-mass sources are present that introduce independent jet activity.

#### The hot core phase

The next stage in the evolution of a massive star towards the main sequence is the so-called hot-core stage. Here, massive stars are located within dense molecular cloud cores and – because of the high extinction – are neither visible in the



optical nor in the near-infrared, but in the mid-infrared spectral region. These cores are heated by the embedded or neighbouring massive stars to temperatures between 100 and 300 Kelvin, forming ‘hot cores’ about 0.1 pc across, which have a density of molecular hydrogen of about  $10^7$  particles per  $\text{cm}^3$ . Typically, in this stage the objects are not yet surrounded by larger amounts of ionised hydrogen. The formation of H<sub>II</sub> regions is possibly suppressed by the high rate of mass infall. This also means that the youngest massive stars are only observable in the thermal infrared and the (sub-)millimetre range, whereas they are not strong centimetre radio continuum sources. The particularly interesting case of the G9.62+0.19-F Hot Core is shown in Figure 2, for which we conducted a multi-wavelength study with ISAAC at the VLT and with TIMMI2 at the ESO 3.6-m telescope (Linz et al. 2005). From classical spherically sym-

metric models it is *not* expected that hot cores themselves could be detected with ISAAC (wavelength range 1–5  $\mu\text{m}$ ) due to hundreds of magnitudes of visual extinction. However, we previously showed that the G9.62 hot core drives a massive molecular outflow roughly oriented along the line-of-sight (Hofner et al. 2001) which might severely disturb the spherical symmetry. Indeed, our ISAAC 3.8  $\mu\text{m}$  and 4.7  $\mu\text{m}$  observations reveal the presence of a feature (F4) not seen at shorter wavelengths which eventually dominates the emission at longer wavelengths (Figure 2). This leads to a scenario where the outflow has a ‘clearing effect’ so that thermal infrared radiation from the inner interior of the hot core can more easily escape through the outflow cone directed towards us. This finding clearly demonstrates the deviation from spherical symmetry which has to be taken into account in detailed radiative transfer models. Here we should

note that accurate astrometry, especially between the thermal infrared images and the radio interferometry data is an important requirement to prevent misidentifications. Together with existing millimetre interferometer data, our new sub-arc-second thermal infrared data facilitate an order-of-magnitude assessment for the luminosity of this hot core (without disturbing contributions from other sources); we estimate it to be around  $1.9 \times 10^4 L_{\odot}$ . This is a clear indication that the G9.62 hot core harbours a young massive star. However, caution is advisable, as we see in the case of the Orion Hot Core, where on a much smaller scale than in our case several infrared sources can be distinguished. (G9.62+0.19 is more than 12 times farther away from our Sun than the Orion Hot Core.) Thus, diffraction-limited *L*- and *M*-band observations with NACO (yielding a spatial resolution of ca. 0.1”) will be a logical step to trace potential substructures in this hot core.

### Ultracompact HII regions

During the next evolutionary phase of massive stars – now in or very close to the zero-age main sequence – ‘ultra-compact HII regions’ (UCHIIs) form around the young stars. In these ionised regions of about 0.1 pc diameter with electron densities of about  $10^5$  per  $\text{cm}^3$ , electrons decelerating in the plasma emit strongly at radio wavelengths (free-free emission). Thus, these objects can be best found by radio continuum surveys. These very compact objects have lifetimes of about one million years. Eventually the regions of ionised hydrogen expand, forming ‘compact HII regions’ of 0.5 pc diameter and electron densities up to 1000 electrons per  $\text{cm}^3$ . These then evolve into ‘diffuse HII regions’ which are well known to us in the form of the Orion Nebula.

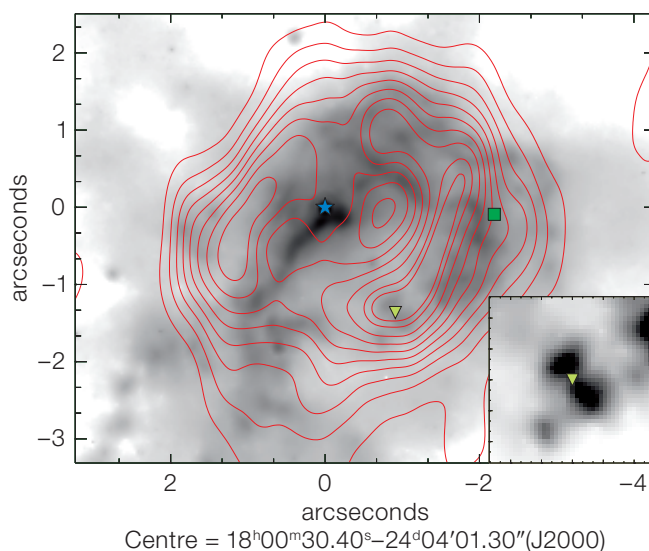
A particularly interesting source in the context of ultra-compact HII regions is G5.89-0.39. Classified by Wood and Churchwell (1989) as a shell-type UCHII, it seemed to agree with models of a classical Strömberg sphere expansion additionally driven by the wind of a single massive star. The object is also the source of one of the most massive outflows within our Galaxy. The outflow has been studied at a variety of wavelengths and resolutions. Interestingly, also different outflow orientations and outflow velocities were derived by different groups: the east-west direction from various CO line observations, the north-south direction from the expansion of the radio shell ( $8 \pm 2$  AU/yr) and from CS and H<sub>2</sub>O maser observations. Yet another orientation was introduced by tracing outflow motions in SiO which led to the conclusion of an NE-SW outflow. Recently, Sollins et al. (2004) confirmed this latter direction by means of SiO observations with the SMA. They also found a 1.3-mm continuum source which they proposed to be the driver of the outflow.

The driving source of ‘the outflow’ was always assumed to be the ionising source of the shell. A direct detection of the central ionising source was first claimed by Feldt et al. (2003), who detected a star slightly off-centre inside the shell in NACO *K* and *L*-band images. From the

position in the colour-magnitude diagram, its spectral type was estimated to be O5V.

Follow-up spectroscopy of the central source is presented in Puga et al. (2006). In the long-slit *K*-band spectrum, the only remarkable line showing up at the location of the detected star is HeI; this indicates that the source is hotter than 40 000 K which corresponds to a spectral type earlier than O7V. Moreover, Puga et al. (2006) present Fabry-Perot spectroscopy with the Adaptive Optics instruments ADONIS/GraF (at the 3.6-m telescope) and NACO (at the VLT UT4) as well as long-slit spectroscopy of the H<sub>2</sub> emission around the shell. Two prominent bow-shock-like features are detected north and south of the UCHII region equidistant from the star seen in *K* and *L*. The study of the ratio between several ro-vibrational H<sub>2</sub> lines confirms the shocked nature at least of the southern region. The Fabry-Perot data of this southern H<sub>2</sub> feature show its velocity structure to be entirely consistent with a deceleration from about  $100 \text{ km s}^{-1}$  to the ambient velocity. It appears pretty clear now that these H<sub>2</sub> features indeed represent terminating bow-shocks of a jet originating from G5.89-0.39. With the connecting line passing the detected O5V star at less than  $0.3''$ , it seems reasonable to assume that this star is indeed the driving source. Also, the axis

**Figure 3:** *L*-band image of G5.89-0.39 taken with NACO. The contours represent 2-cm emission from Wood and Churchwell (1989), the star, the triangle, and the square show the locations of the ionising star candidate found by Feldt et al. (2003), the 1.3-mm source found by Sollins et al. (2004), and the centre of a possible newly identified outflow, respectively (from Puga et al. 2006).



passes through the disruptions in the shell apparent in Wood and Churchwell’s (1989) 2-cm image, and coincides with the direction of preferred shell expansion. The data show the power of combining high spatial resolution provided by Adaptive Optics and high spectral resolution.

But what about the other outflows? The *L*-band image in Figure 3 shows a bipolar feature at the location where Sollins et al. (2004) report their mm continuum source. The feature is elongated at a position angle matching that of the Sollins’ outflow and resembles the structure of reflection lobes above and below a circumstellar disc seen edge-on (see inset in Figure 3). We concluded in Puga et al. (2006) that the *L*-band structure is the small-scale counterpart of the SiO outflow that is driven by the 1.3-mm continuum source. We also mapped the shell in the Br $\gamma$  line with Fabry-Perot observations (see Figure 4). This resulting velocity map implies that another bipolar structure exists and that the shell is not as ‘puzzlingly symmetric and undisrupted by massive outflows’ as described earlier by Ed Churchwell. The feature might be connected to an outflow in NW-SE direction – about the only direction not quoted before for an outflow from G5.89. The possible driving source would naturally be assumed to be situated between the two parabolas in Figure 4, with no detected counterpart at any wavelength yet.

What do we learn from all this? First of all, it again appears that massive star formation is always more complex than you thought. In G5.89 everything appeared clear and matching a very simple model until a few years ago. Now we have a number of outflows confirmed in all possible directions, and we have two quite robust detections of driving sources and evidence for a third one inside a volume not larger than the shell with its diameter of about 0.05 pc. In the general notion, G5.89 has turned from a single star with an ionised shell into yet another young, massive cluster with complex interactions between the stars, the outflows, and the radiation fields and the produced HII region. This demonstrates how important it is to carefully determine and characterise the complete stellar content of any site of massive star formation, before trying to draw conclusions on the formation mechanism from integrated data like overall luminosities or outflow energies. It is also another example of massive star formation taking place at stellar densities of more than  $10^4 \text{ pc}^{-3}$ , confirming that massive stars prefer to form in very dense clusters.

### Outlook

Infrared and millimetre observations of very young massive stars in the stage of cold and hot cores now complement detailed observations of slightly later stages, in particular ultra-compact HII regions. Here, the identification of the ionising and illuminating sources and the detailed study of the interaction between them and nearby molecular cloud structures have opened the way for much better modelling of these important and abundant objects.

It is clear that the riddle of massive star formation is not yet solved. However, our observational methods are getting closer to the very early stages of formation and the very immediate surroundings of young massive stars. New 3D radiative transfer models will help interpreting the data measured by interferometers, aided by input from 8-m telescope diffraction-limited observations between  $1 \mu\text{m}$  and  $20 \mu\text{m}$  wavelength. With these methods, we can hope to determine the mechan-

isms and timescales of the early evolutionary stages of massive stars within the next few years.

The currently operating Spitzer IR satellite produces a wealth of new data covering the mid- and far-infrared regime. In terms of sensitivity, it provides a major improvement with regard to its predecessors IRAS, MSX, and ISO and is of course superior to present-day ground-based observations. However, even at the smallest operating wavelength of 3.5 microns, Spitzer does not provide sub-arcsecond spatial resolution, a prerequisite to disentangle the usually crowded central regions of high-mass star formation. Hence, ground-based thermal infrared observations conducted at 8-m-class telescopes (for instance, ISAAC, VISIR, NACO, and soon CRIRES at the VLT) can contribute important knowledge about the intricate details of massive star-forming regions. Furthermore, in a few years from now, the synergy between space-based exploratory studies, especially Herschel-satellite

far-infrared observations, and ground-based follow-up observations with ALMA will become a growing field of research.

### Acknowledgements

We thank our collaborators and former/present students Dániel Apai, Carlos Alvarez, Esteban Araya, Henrik Beuther, Stephan Birkmann, Wolfgang Brandner, Jan Forbrich, Peter Hofner, Randolph Klein, Oliver Krause, Ilaria Pascucci, Bettina Posselt, Katharina Schreyer, and Thomas Stanke in joining the adventure to investigate how massive stars form.

### References

- Birkmann, S. M., Krause, O., and Lemke, D. 2006, ApJ, in press  
 Cesaroni, R. et al. 2005, Proceedings of the IAUS 227, Cambridge University Press  
 Feldt, M. et al. 2003, ApJL 599, L91  
 Forbrich, J. et al. 2004, ApJ 602, 843  
 Hofner, P., Wiesemeyer, H., and Henning, T. 2001, ApJ 549, 425  
 Klein, R. et al. 2005, ApJS 161, 361  
 Linz, H. et al. 2005, A&A 429, 903  
 Puga, E. et al. 2006, ApJ, in press  
 Sollins, P. K. et al. 2004, ApJL 616, L35  
 Wood, D. O. S., and Churchwell, E. 1989, ApJS, 69, 831

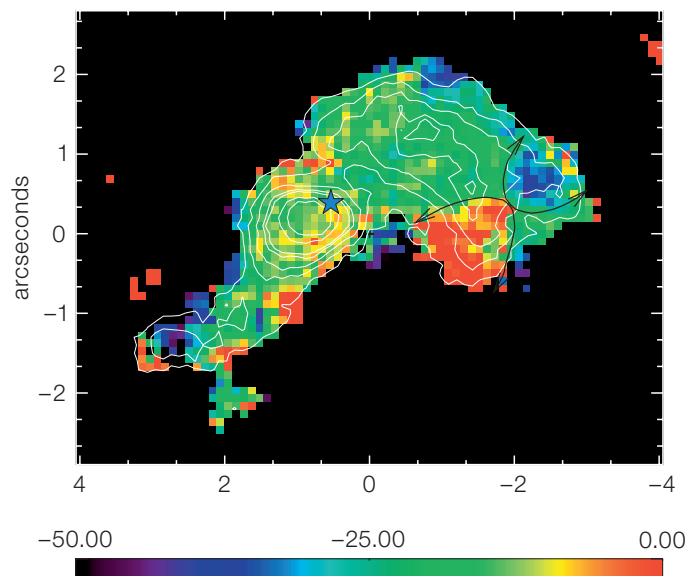


Figure 4: Peak velocities in Br $\gamma$  in the upper half of G5.89's shell. The colour bar indicates the velocity range in km/s. The blue star symbol again shows the location of the ionising star candidate (see Figure 3). The overlaid thin white contours mark the velocity-integrated Br $\gamma$  intensity. In the western half, a bipolar velocity structure (also indicated by the arrows) is clearly visible and recognised here for the first time (from Puga et al. 2006).

# The Dwarf galaxy Abundances and Radial-velocities Team (DART) Large Programme – A Close Look at Nearby Galaxies

Eline Tolstoy<sup>1</sup>  
 Vanessa Hill<sup>2</sup>  
 Mike Irwin<sup>3</sup>  
 Amina Helmi<sup>1</sup>  
 Giuseppina Battaglia<sup>1</sup>  
 Bruno Letarte<sup>1</sup>  
 Kim Venn<sup>4</sup>  
 Pascale Jablonka<sup>5,6</sup>  
 Matthew Shetrone<sup>7</sup>  
 Nobuo Arimoto<sup>8</sup>  
 Tom Abel<sup>9</sup>  
 Francesca Primas<sup>10</sup>  
 Andreas Kaufer<sup>10</sup>  
 Thomas Szeifert<sup>10</sup>  
 Patrick Francois<sup>2</sup>  
 Kozo Sadakane<sup>11</sup>

<sup>1</sup> Kapteyn Institute, University of Groningen, the Netherlands

<sup>2</sup> Observatoire de Paris, France

<sup>3</sup> Institute of Astronomy, University of Cambridge, United Kingdom

<sup>4</sup> Department of Physics and Astronomy, University of Victoria, Canada

<sup>5</sup> Observatoire de Genève, Laboratoire d'Astrophysique, Ecole Polytechnique Fédérale de Lausanne, Switzerland

<sup>6</sup> on leave from Observatoire de Paris, France

<sup>7</sup> University of Texas, McDonald Observatory, Fort Davis, Texas, USA

<sup>8</sup> National Astronomical Observatory, Tokyo, Japan

<sup>9</sup> KIPAC, Stanford University, Menlo Park, California, USA

<sup>10</sup> ESO

<sup>11</sup> Astronomical Institute, Osaka Kyoiku University, Japan

We review the progress of ESO/WFI imaging and VLT/FLAMES spectroscopy of large numbers of individual stars in nearby dwarf spheroidal galaxies by the Dwarf galaxy Abundances and Radial-velocities Team (DART). These observations have allowed us to show that neither the kinematics nor the abundances nor the spatial distributions are easy to explain in a straightforward manner for these smallest galaxies. The main result is that dwarf galaxies show complex and highly specific evolutionary and metal-enrichment processes, especially at ancient times. This conclusively proves that these small galaxies are not the building blocks of the larger galaxies in the Local Group.

The dwarf galaxies we have studied are the lowest-luminosity (and mass) galaxies that have ever been found. It is likely that these low-mass dwarfs are the most common type of galaxy in the Universe, but because of their extremely low surface brightness our ability to detect them diminishes rapidly with increasing distance. The only place where we can be reasonably sure to detect a large fraction of these objects is in the Local Group, and even here, 'complete samples' are added to each year. Within 250 kpc of our Galaxy there are nine low-mass galaxies (seven observable from the southern hemisphere), including Sagittarius which is in the process of merging with our Galaxy. We will show that only the closest galaxies can be observed in detail, even with an 8-m telescope.

The lowest-mass galaxies are dwarf irregular (dI) and dwarf spheroidal (dSph) type galaxies. The only difference between these low-mass dSphs and dIs seems to be the presence of gas and current star formation in dIs. It has already been noted that dSphs predominantly lie close to our Galaxy (< 250 kpc away), and dIs predominantly further away (> 400 kpc away). This suggests that the proximity of dSph to our Galaxy played a role in the removal of gas from these systems. However, the range of properties found in dSph and dI galaxies does not allow a straightforward explanation, particularly not the large variations in star-formation histories and chemical-evolution paths that have now been observed in different systems (e.g., Dolphin et al. 2005).

It is perhaps not a surprise that there is apparently a lower limit to the mass of an object which is able to form more than one generation of stars, which is related to the limit below which one supernova will completely destroy a galaxy. Numerical and analytic models tell us that this must be around a few  $\times 10^6 M_{\odot}$ . Globular clusters typically have much lower masses than this limit.

## Observations

VLT/FLAMES with fibre-feeds to the Giraffe and UVES spectrographs has made a revolution possible in spectroscopic studies of resolved stellar populations in

nearby galaxies. The modes of operation, the sensitivity and the field of view are an almost perfect match to requirements for the study of Galactic dSph galaxies. For example, it is now possible to measure the abundance of numerous elements in nearby galaxies for more than 100 stars over a 25'-diameter field of view in one shot. A vast improvement on previous laborious (but valiant) efforts with single-slit spectrographs to observe a handful of stars per galaxy (e.g., Tolstoy et al. 2003; Shetrone et al. 2003; Geisler et al. 2005).

The DART Large Programme has measured abundances and velocities for several hundred individual stars in a sample of four nearby dSph galaxies: Sculptor, Fornax, Sextans and Carina. We have used the VLT/FLAMES facility in the low-resolution mode (LR 8, R ~ 8000) to obtain CaII triplet metallicity estimates as well as accurate radial-velocity measurements over large areas in Sculptor, Fornax and Sextans out to the tidal radius (Tolstoy et al. 2004; Battaglia et al. 2006, in prep.), see Figure 1 for the example of Sculptor. In Figure 1 we show the area on the sky around the Sculptor dSph galaxy. The large ellipse is the tidal radius of Sculptor as determined by Irwin and Hatzidimitriou (1995). The positions observed with VLT/FLAMES are marked as circles, where the solid circles represent the 10 individual FLAMES pointings analysed so far, and the dashed-line circles are the positions of five additional fields that were observed in November 2005. Also plotted for the analysed fields are the positions of the stars that are probable members (small red squares) and the non-members (black crosses). Each of the four galaxies has been observed at high resolution (Giraffe settings HR 10, 13 and 14) in the central region to obtain detailed abundances for a range of interesting elements such as Mg, Ca, O, Ti, Na, Eu to name a few (Hill et al. 2006 in prep.; Letarte et al. 2006a in prep.) for about 100 stars. During the Giraffe HR observations we were also able to use the fibre feed to the UVES spectrograph to obtain greater wavelength coverage and higher resolution for a sample of seven to 14 stars per galaxy (e.g., Venn et al. 2006 in prep.; Shetrone et al. 2006 in prep.). The comparison we can make between results from UVES spectroscopy (R ~ 40000) and Giraffe spectroscopy

( $R \sim 20000$ ) for the same stars is very useful in convincing ourselves, and others, that we are able to obtain reliable results with lower resolution spectra than was previously thought possible or advisable. This lower-resolution is less of a problem at lower metallicity (e.g., Sculptor) than at higher metallicity (e.g., Fornax).

Colour-magnitude diagrams

The first step in a detailed analysis of the resolved stellar population of a galaxy is an accurate colour-magnitude diagram (e.g., Figure 2), ideally down to the oldest main-sequence turnoffs ( $M_V \sim +3.5$ ). In Figure 2 is plotted the colour-magnitude diagram of the Sculptor dSph from ESO/WFI imaging out to the tidal radius. The coloured symbols are the stars we observed with VLT/FLAMES. The probable members of Sculptor are shown as purple circles and the non-members are shown as green stars. A careful analysis leads to the star-formation history all the way back to the first star formation in the Galaxy. This approach is the most accurate for intermediate-age populations, but for stars older than about 10 Gyr the time resolution gets quite poor (and the stars are getting very faint), and it becomes hard to distinguish a 12-Gyr-old star from a 10-Gyr-old star. Here it becomes useful to consider the Horizontal Branch stars ( $M_V \sim 0$ ) which are the bright He-burning phase of low-mass stars  $> 10$  Gyr old. The ratio of red to blue horizontal-branch stars (see Figure 2) tells us about the age and metallicity variation. In Figure 2 regions used to define the Blue Horizontal Branch (BHB), the Red Horizontal Branch (RHB) and foreground comparison (FG) stellar populations in Sculptor are outlined in blue boxes. The spatial distribution of red and blue horizontal-branch stars in Sculptor is shown in Figure 3. In this Figure the outline of the extent of the ESO/WFI imaging is shown, as is the tidal radius of Sculptor.

We can also consider the much brighter Red Giant Branch (RGB,  $-3 < M_V < 0$ ) stars which have ages  $> 1$  Gyr old, back to the oldest stars in the Galaxy, however, the interpretation of the RGB using only photometry is plagued by the age-metallicity degeneracy (graphically illustrated

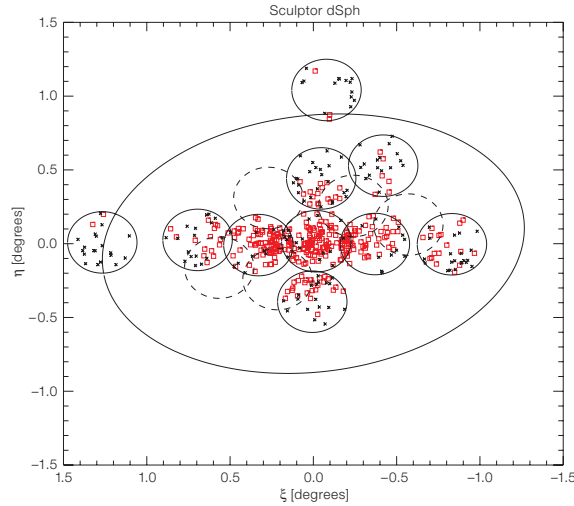


Figure 1: The area on the sky around the Sculptor dSph galaxy. The positions observed with VLT/FLAMES are marked as circles. Also plotted are the positions of the stars that are probable members (red squares) and the non-members (black crosses).

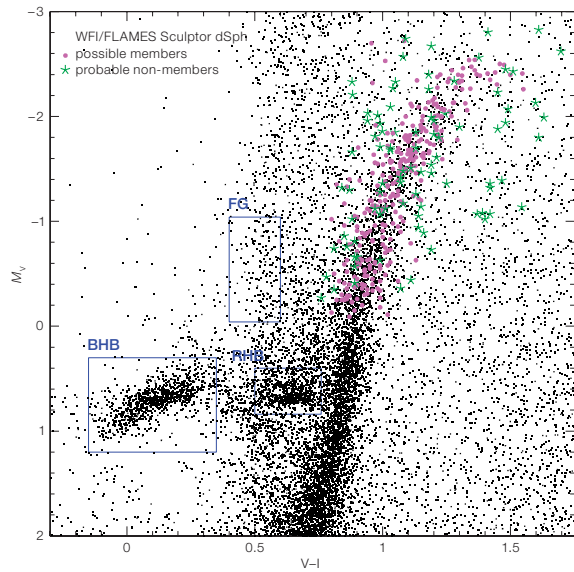


Figure 2: Colour-magnitude diagram of the Sculptor dSph from ESO/WFI imaging. The coloured symbols are the stars observed with VLT/FLAMES. The probable members of Sculptor are shown as purple circles and the non-members are shown as green stars. Also shown outlined in blue are the regions used to define the Blue Horizontal Branch (BHB), the Red Horizontal Branch (RHB) and foreground comparison (FG) stellar populations.

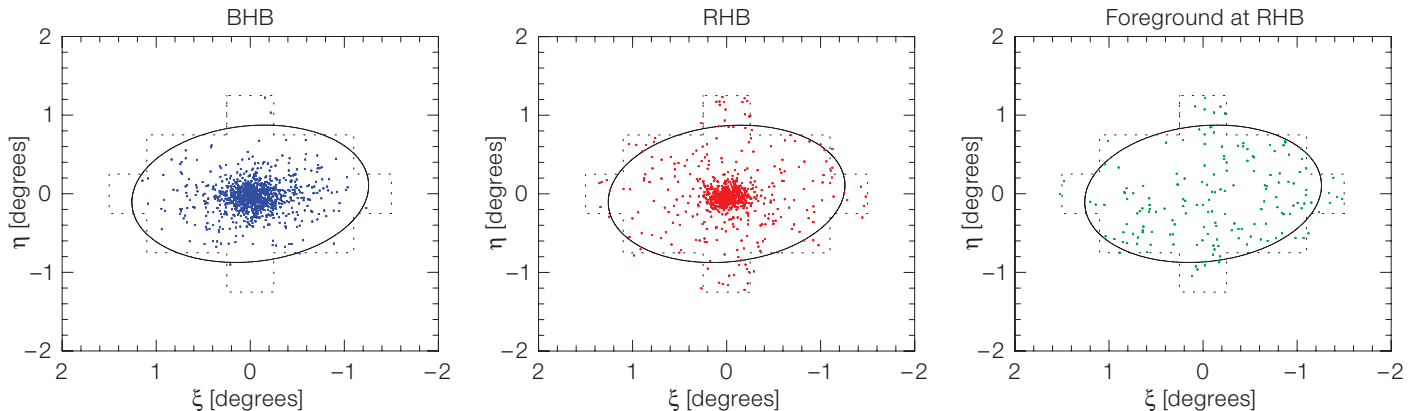
by Cole et al. 2005; their Figure 8). The observed magnitude and colour (e.g.,  $M_V$ ,  $V-I$ ) of a star combined with a measured  $[Fe/H]$ , allows us to effectively remove the age-metallicity degeneracy and determine the age of an RGB star from an isochrone, and thus to trace the enrichment patterns of as many elements as we can measure with time.

Detailed abundance analysis

In the majority of RGB stars it is believed that the atmosphere of the star remains an unpolluted sample of the interstellar medium out of which it was formed. This means we have small

pockets of interstellar medium of different ages (enriched by different numbers of processes) conveniently covering the nuclear burning core of stars. This hot stellar core provides a useful bright background source to be absorbed in the stellar atmosphere allowing very detailed studies of the elemental abundances in these ancient gas samples. Thus, a spectroscopic analysis of the variation of the abundances of different elements seen in absorption in atmospheres of different age stars allows us to trace the detailed chemical enrichment history of a galaxy with time. Different elements are created in different circumstances and if we are able to determine the abundance of elements known to be created in a particular

**Figure 3:** The distribution of horizontal-branch stars from ESO/WFI imaging of the Sculptor dSph selected as shown in Figure 2.



set of physical conditions, we can assess the importance and frequency of these conditions during the history of star formation in a galaxy.

For example, the abundances of light elements (e.g., O, Na, Mg, Al) are considered to be tracers of ‘deep mixing’ patterns which are found only in globular-cluster environments, which gives a limit to the number of dissolved globular clusters which can exist in a stellar population. These typical (Galactic) globular cluster abundance patterns have also been recently found in the globular clusters of Fornax dSph (Letarte et al. 2006b in prep.), but not (so far) in the field star populations (e.g., Shetrone et al. 2003).

The creation of  $\alpha$ -elements (e.g., O, Mg, Si, Ca, Ti) occurs predominately in supernovae type II explosions, i.e. the explosion of massive stars a few  $10^6$ – $10^7$  yrs after their formation. The abundance of the different  $\alpha$ -elements is quite sensitive to the mass of the SNII progenitor so the  $\alpha$ /Fe ratio traces the mass function of the stars which contributed to the creation of the  $\alpha$ -elements, and ratios of different  $\alpha$ -elements themselves can put limits on the highest-mass star which has enriched a galaxy and also the typical mass range (e.g., McWilliam 1997).

Heavy Elements ( $Z > 30$ ) are a mix of  $r$ - and  $s$ -process elements. That is to say elements which were produced by rapid or slow neutron capture which tells us about the environment in which enrichment occurred. Rapid capture ( $r$ -process) is assumed to occur in high-energy circumstances, such as supernovae explosions. For example Eu is considered to

be an element produced almost exclusively by the  $r$ -process. The slow capture ( $s$ -process) is thought to be created by more quiescent processes such as the stellar winds common in AGB type stars of intermediate age (and mass). Typical elements which are thought to be created by the  $s$ -process are Ba and La. The ratio between  $r$ - and  $s$ -process element abundances gives an indication of the relative importance of these different enrichment processes during the history of star formation in a galaxy. Dwarf spheroidal galaxies are found to have a strong evolution from  $r$ -process domination to  $s$ -process domination as a function of the metallicity of the stars. This may indicate that supernovae products are typically lost to a shallow potential well, or that the slow star formation rate means that massive stars are not very common (e.g., Tolstoy et al. 2003; Venn et al. 2004).

Our latest results for the  $\alpha$ -elements are shown in Figure 4. The  $\alpha$ -element abundance is an average of Ca, Mg and Ti abundances from high-resolution spectroscopy for stars in Sculptor and Fornax dSphs. The VLT/FLAMES measurements of 92 stars in the centre of Sculptor are shown in the upper panel as purple crosses (Hill et al. 2006 in prep.) and the preliminary measurements for 55 stars observed in Fornax are shown as green crosses in the lower panel (Letarte et al. 2006a, in prep.). The open blue squares, five in Scl and three in Fnx are UVES measurements of individual stars (Shetrone et al. 2003). The four open red squares are Geisler et al. (2005) measurements of Scl, and the 10 open green squares are FLAMES fibre fed UVES spectra of Scl, taken at the same

time as the Giraffe spectra (Venn et al. 2006, in prep.). A representative error bar is also given in the bottom left hand of each panel. The Fornax VLT/FLAMES results are preliminary, as the problems with the appropriate stellar models for such cool stars as are found in Fornax have not yet been fully resolved. We can compare the detailed abundance patterns that we see in dSph galaxies, with other galaxies such as the Milky Way. This is shown in Figure 4, where the Galactic stars shown in both panels as black dots come from various literature sources (see Venn et al. 2004 for references), and the disc and halo component are also labelled. This can also be done for Sagittarius and the Magellanic Clouds (e.g., Venn et al. 2004). These comparisons show that enrichment patterns differ strongly between different types of galaxy, making it hard to build one type of galaxy out of another once they have formed a significant number of stars.

### The CaII triplet and kinematics

The ideal is to be able to obtain high-resolution spectra for individual stars in nearby dSph over a large wavelength range, and make a detailed analysis of a range of different elements along with accurate velocities. However, this is quite time consuming both in telescope time (even with VLT/FLAMES) and in analysis. One of the most simple ways to get an estimate of the metallicity of RGB stars is with the CaII triplet. This is a basic metallicity indicator requiring only low or intermediate spectral resolution, based on three lines around 8500 Å which have been empirically calibrated from obser-

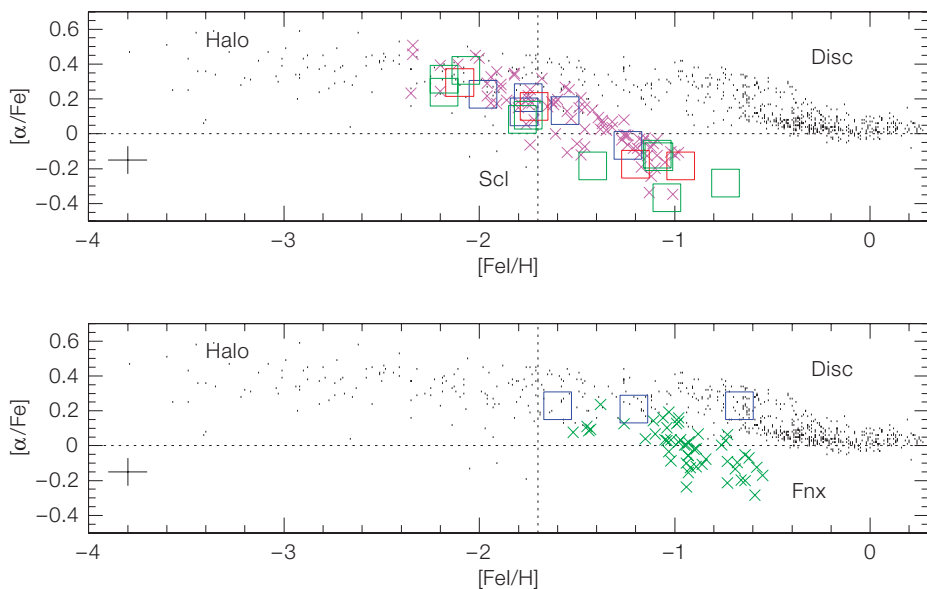


**Figure 4:** The  $\alpha$ -element abundances from high-resolution spectroscopy for stars in the Sculptor dSph (upper panel, Hill et al. 2006 in prep) and also preliminary results for the Fornax dSph (lower panel, Letarte et al. 2006a, in prep.). The open squares are UVES measurements of individual stars

(Shetrone et al. 2003; Geisler et al. 2005; Venn et al. 2006, in prep.). Galactic stars coming from various literature sources (see Venn et al. 2004 for references) are shown for comparison in both panels as black dots and labelled as disc and halo components.

measurements of stars in globular clusters with high-resolution abundances. Assuming sufficient signal-to-noise spectra ( $S/N > 10$ ) it provides  $[Fe/H]$  within typical (internal) errors of  $\pm 0.1$  dex, and also the radial velocity of each star with  $\pm 2$  km/s accuracy. These accuracies are well suited for ‘quick look’ surveys of the resolved stellar population of a galaxy. In the DART project these  $CaII$  triplet measurements are complementary to the high-resolution observations made in the centre of each dSph. In the low-resolution observations a much larger area is surveyed and we can assess how representative the detailed study is of the whole galaxy.

Our first VLT/FLAMES results (Tolstoy et al. 2004), were based upon  $CaII$  triplet measurements, which clearly showed that Sculptor dSph contains two distinct stellar components with different spatial, kinematic and abundance properties (see Figure 5). The upper panel shows the VLT/FLAMES spectroscopic measurements of  $[Fe/H]$  for 307 probable velocity members of Sculptor (with  $S/N > 10$ ). We see a clear trend of metallicity with radius. The lower panel shows  $v_{hel}$  as a function of elliptical radius for all stars

satisfying  $S/N > 10$ . Likely Sculptor members are clearly seen clustered around the systemic velocity of 110 km/s. The stars which are potential members are plotted as red stars ( $[Fe/H] > -1.7$ ) and blue circles ( $[Fe/H] < -1.7$ ), while the green crosses are assumed to be non-members. There appears to be a metal-rich,  $-0.9 > [Fe/H] > -1.7$ , and a metal-poor,  $-1.7 > [Fe/H] > -2.8$ , component. The metal-rich component is more centrally concentrated than the metal-poor, and on average appears to have a lower velocity dispersion,  $\sigma_{metal-rich} = 7 \pm 1$  km/s, whereas  $\sigma_{metal-poor} = 11 \pm 1$  km/s. A similar effect is seen in Fornax, where the metal-rich stars are centrally concentrated, and the metal-poor stars appear more uniformly and diffusely distributed.

It is clear from the histogram of  $[Fe/H]$  measurements that both Sculptor and Fornax lack a low metallicity tail (see Figure 6). In Figure 6 are plotted in the left-hand histogram distributions of  $[Fe/H]$  for Sculptor dSph: the 91 stars within the central,  $r < 0.2$  degree region (solid black line); and the 216 stars beyond  $r > 0.2$  degrees (dashed red line). In Figure 6 in the right-hand histogram is the  $[Fe/H]$  distribution for the Fornax dSph: the 332 stars

within the central,  $r < 0.5$  degree region (solid black line); and the 229 stars beyond  $r > 0.5$  (dashed red line). Clearly the distributions are very different. Most noticeably Fornax has a substantial ‘metal-rich’ population. The lowest metallicity star in our combined sample of more than 850 stars for both galaxies is  $[Fe/H] = -2.7$ . We find a similar lack of low-metallicity stars in Sextans and Carina. Although it is difficult to make an accurate comparison with the Galactic surveys, where the completeness can be hard to quantify, there appears to be a significantly different distribution between all the dSph and the (metal-poor) halo of the Milky Way. It can be seen that there is a clear difference in the distribution of the metal-rich and metal-poor stars in both Fornax and Sculptor.

#### Future work

There are indications that the presence of two distinct populations is a common feature of dSph galaxies. Our preliminary analysis of Horizontal Branch stars,  $v_{hel}$  and  $[Fe/H]$  measurements in the other galaxies in our sample (Fornax and Sextans dSph; Battaglia et al. 2006, in prep.) also show similar characteristics to Sculptor, especially in the most metal-poor component. Pure radial-velocity studies (e.g., Wilkinson et al. 2004) have also considered the possibility that kinematically distinct components exist in Ursa Minor, Draco and Sextans dSph galaxies. Interestingly, the Carina dSph appears to go counter to this trend, and another VLT/FLAMES study finds no obvious evidence for more than one component, or even a gradient within Carina dSph (Koch et al. 2006).

What mechanism could create two or more distinct ancient stellar components in a small dwarf spheroidal galaxy? A simple possibility is that the formation of these dSph galaxies began with an initial burst of star formation, resulting in a stellar population with a mean  $[Fe/H] \leq -2$ . Subsequent supernova explosions from this initial episode could have been sufficient to cause gas (and metal) loss such that star formation was inhibited until the remaining gas could sink deeper into the centre. Thus the subsequent generation(s) of stars would form in a region

closer to the centre of the galaxy, and have a higher average metallicity and different kinematics. Another possible cause are external influences, such as minor mergers, accretion of additional gas or the kinematic stirring by our Galaxy. It might also be that events surrounding the epoch of reionisation influenced the evolution of these small galaxies and resulted in the stripping or photo-evaporation of the outer layers of gas in the dSph, meaning that subsequent more metal-enhanced star formation occurred only in the central regions.

#### Acknowledgements

Eline Tolstoy gratefully acknowledges support from a fellowship of the Royal Netherlands Academy of Arts and Sciences. The data presented here were collected under ESO Large Programme 171.B-0588 and GTO programme 71.B-0641.

#### References

Cole A. A. et al. 2005, AJ 129, 1465  
 Dolphin A. E. et al. 2005, Resolved Stellar Populations, eds. D. Valls-Gabaud and M. Chavez (astro-ph/0506430)  
 Geisler, D. et al. 2005, AJ 129, 1428  
 Irwin M. and Hatzidimitriou D. 1995, MNRAS 277, 1354  
 Koch A. et al. 2006, AJ, in press (astro-ph/0511087)  
 McWilliam A. 1997, ARA&A 35, 503  
 Shetrone M. D. et al. 2003, AJ 125, 684  
 Tolstoy E. et al. 2003, AJ 125, 707  
 Tolstoy E. et al. 2004, ApJL 617, 119  
 Venn K. et al. 2004, AJ 128, 1177  
 Wilkinson M. et al. 2004, ApJL 611, 21

**Figure 6:** In the left panel is the histogram distribution of  $[Fe/H]$  measurements for the Sculptor dSph: inner region, solid black line outer region dashed red line. In the right panel is the same for the Fornax dSph.

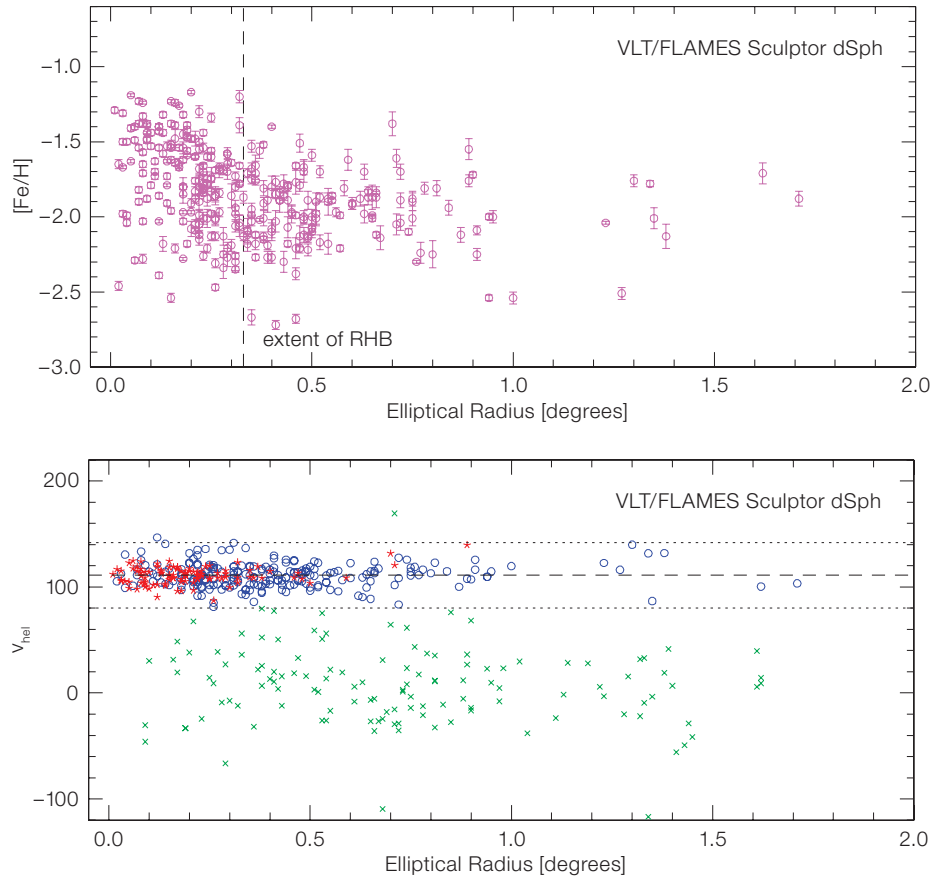
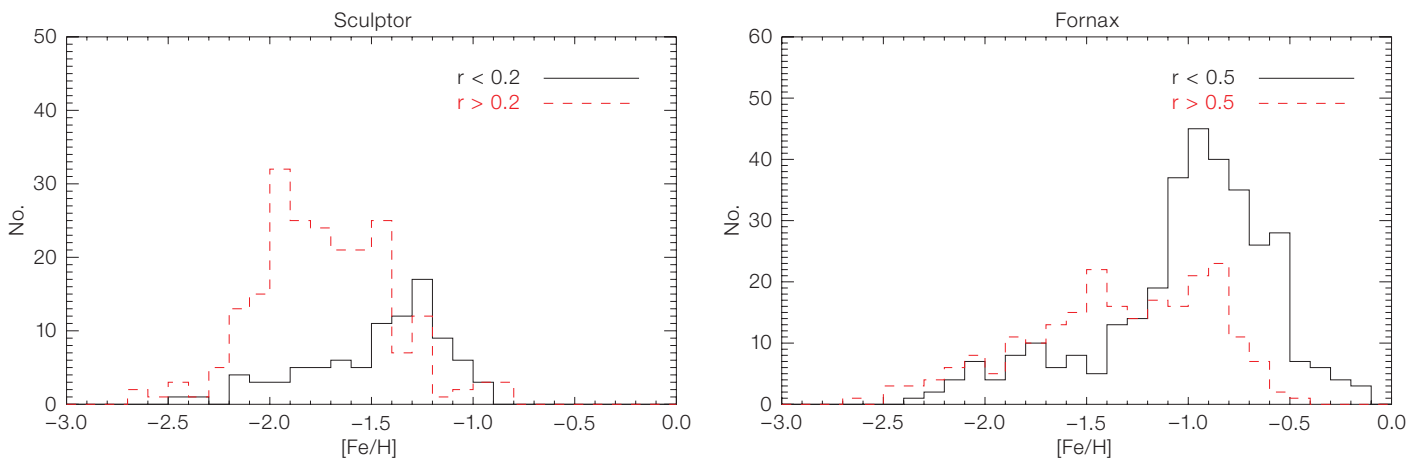


**Figure 5:** The upper panel shows the VLT/FLAMES spectroscopic measurements of  $[Fe/H]$  for 307 Red Giant branch stars in Sculptor plotted as a function of distance from the centre of the galaxy. The lower panel shows  $v_{hel}$  as a function of elliptical

radius. The stars that are probable members are plotted as red stars ( $[Fe/H] > -1.7$ ) and blue circles ( $[Fe/H] < -1.7$ ), showing metal-rich and metal-poor stars respectively. The 128 green crosses are unlikely to be members of Sculptor.

# The Age-Metallicity Degeneracy in the Dwarf Spheroidal Carina as Seen by FLAMES

Andreas Koch<sup>1</sup>  
 Eva K. Grebel<sup>1</sup>  
 Rosemary F. G. Wyse<sup>2</sup>  
 Jan T. Kley<sup>3</sup>  
 Mark I. Wilkinson<sup>4</sup>  
 Daniel R. Harbeck<sup>5</sup>  
 Gerard F. Gilmore<sup>4</sup>  
 N. Wyn Evans<sup>4</sup>

<sup>1</sup> Astronomical Institute of the University of Basel, Department of Physics and Astronomy, Binningen, Switzerland

<sup>2</sup> The Johns Hopkins University, Baltimore, USA

<sup>3</sup> Institute for Astronomy, Honolulu, USA

<sup>4</sup> Institute of Astronomy, Cambridge University, United Kingdom

<sup>5</sup> Department of Astronomy, University of Wisconsin, Madison, USA

The Carina dwarf spheroidal galaxy is the only one of this type to show clearly episodic star formation separated by long pauses. Still its Red Giant Branch is remarkably narrow. Our medium-resolution spectroscopy of 437 Red Giants in this galactic satellite with FLAMES reveals a full range of metallicities from  $\sim -3.0$  up to  $\sim 0.0$  dex. There also appears to be a mild radial gradient in that more metal-rich populations are more centrally concentrated, matching a similar trend in ages with an increasing fraction of intermediate-age stars in the centre (Harbeck et al. 2001). Complemented by the colours of the more metal-rich stars, this suggests that Carina exhibits an age-metallicity relation. We address the star formation in this intriguing galaxy by also pursuing its age-metallicity degeneracy, resulting in a narrow Red Giant Branch despite the considerable spread in metallicity and wide range of ages, and applying basic models of chemical evolution.

Dwarf spheroidal galaxies (dSphs) are the least luminous, least massive galaxies known. Most of them are found within 300 kpc around more massive galaxies. DSphs are gas-deficient and are typically dominated by old ( $> 10$  Gyrs) or intermediate-age populations (1–10 Gyrs). All dSphs studied in sufficient detail have been found to contain ancient populations that are indistinguishable in age from

the oldest populations in the Milky Way (Grebel and Gallagher 2004). While their detailed star-formation histories (SFHs) vary from galaxy to galaxy, dSphs exhibit a trend of increasing luminosity with increasing mean metallicity (e.g., Grebel, Gallagher, and Harbeck 2003). DSphs usually show fairly continuous star formation (SF) with some amplitude variations. Younger and/or more metal-rich populations are more centrally concentrated, indicating longer-lasting SF episodes in the centres of the dSphs' shallow potential wells (Harbeck et al. 2001).

DSphs are enigmatic objects. Their past extended SF histories contrast with their present, puzzling lack of gas. It is still under debate whether they are dark matter dominated and how much dark matter they contain. While they clearly interact with more massive galaxies, their importance as cosmological building blocks remains unclear. Not only do cosmological models predict two orders of magnitude more 'dark matter halos' than the observed number of low-mass dSphs (e.g., Moore et al. 1999), but also the element abundance ratios in the galactic halo differ from those measured in dSphs (e.g., Shetrone, Côté, and Sargent 2001).

Our current knowledge of the detailed evolutionary history of nearby dwarf galaxies is mainly based on photometry, occasionally supplemented by rather sparse spectroscopic information. But spectroscopy is of paramount importance since it permits us to break the age-metallicity degeneracy that plagues purely photometric colour-magnitude-diagram analyses. The information from independent spectroscopic metallicity determinations for individual stars removes this ambiguity from subsequent photometric determinations of the SF history.

In the gas-deficient dSphs, our primary sources of metallicity information are Red Giants, which are now easily accessible for ground-based 8- to 10-m-class telescopes. Thus, we may ultimately be able to derive detailed evolutionary histories by using the VLT with its powerful multi-object spectroscopy facility FLAMES. Moreover, velocities can be extracted from such spectra, permitting membership and kinematic analyses.

Our VLT Large Programme (171.B-0520, PI: Gilmore) aims at doing just that: We wish to (1) constrain the chemical evolution of dSphs and to (2) measure the size and extent of the dark-matter halos of dSphs. One of our prime targets is the galactic dSph companion Carina at a distance of about 94 kpc from the Milky Way. Here we present first results of our abundance analysis of Carina (see also Koch et al. 2006). A detailed kinematic analysis is in preparation (Wilkinson et al. 2006).

## The dwarf galaxy Carina

Carina stands out among the dSphs in the Local Group because of its unusual, episodic star-formation history (e.g., Smecker-Hane et al. 1994). In no other dSph has clear evidence for well-separated episodes of star formation been found. Carina may have experienced at least four episodes of star formation, one possibly as recently as 0.6 Gyr ago (Monelli et al. 2003). The dominant episodes occurred approximately 2, 3 to 6, and 11 to 13 Gyrs ago. Their distinct main-sequence turn-offs all connect to the same narrow Red Giant Branch with an estimated mean metallicity of  $[\text{Fe}/\text{H}] \sim -1.99$  dex and a spread of about 0.08 dex (Smecker-Hane et al. 1999). Smecker-Hane et al. (1999) argue that the narrow Red Giant Branch of Carina results from an age-metallicity conspiracy in the sense that more metal-rich, but younger stars come to lie at the same location in the colour-magnitude plane as older, metal-poor stars. Based on a photometric study, Rizzi et al. (2003) suggest that the narrow Red Giant Branch is a consequence of the contribution of the dominant intermediate-age star-formation episode, while the contribution of the ancient episode is almost negligible, which cannot be rejected as a plausible cause, unless reliable spectroscopic age estimates are available.

These findings underline the highly complex star-formation history of Carina. There is not yet a satisfactory explanation of why Carina would have experienced episodic SF, and why its evolution was so different from that of other dSphs. Was Carina's SF activity triggered by interactions? Did this dSph manage to repeat-

edly accrete potentially unenriched gas?  
Did feedback halt its SF periodically?

### Red Giant spectroscopy

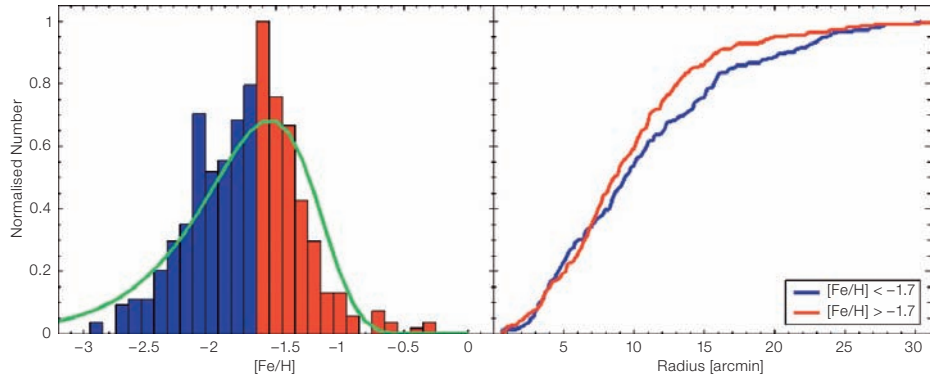
Determinations of accurate spectroscopic abundances require a well-calibrated and widely applicable reference scale. The infrared lines of the singly ionised calcium ion at 849.8, 854.2, 866.2 nm have become one of the spectral features of choice, since these Ca triplet (CaT) lines can be relatively easily distinguished as the strongest absorption lines in the near infrared regime of Red Giant Branch (RGB) spectra, where true Fe absorption features become increasingly weaker at intermediate resolution. Cole et al. (2004) extended the CaT calibration to ages as young as 2.5 Gyrs, providing a good match to the expected dominant populations in Carina.

We observed these three lines in 1257 Red Giant candidates in Carina in the framework of our ESO Large Programme. Our targets are distributed across five fields in the galaxy to cover most of Carina's area, but also reach beyond its nominal tidal radius. The observations were carried out in 22 nights spread over two semesters in 2003 and 2004 using FLAMES/GIRAFFE in MEDUSA 'low-resolution' mode ( $R = 6500$ ) and centred at the near-infrared CaT ( $\sim 850$  nm).

In addition, more than 80 Red Giant candidates in four calibration globular clusters were observed in order to permit us to place our CaT measurements on a scale of known reference metallicities (Rutledge et al. 1997; Carretta and Gratton 1997). These clusters range in metallicity from approximately  $-1.1$  dex to  $-2$  dex in  $[\text{Fe}/\text{H}]$ .

We selected our targets covering three magnitudes in brightness from the tip of the RGB downward. Since we selected stars across the full width of the RGB (approximately 0.2 mag in B-V), we circumvented any bias with respect to metallicity or age, and still could ensure the inclusion of potential extremely metal-poor and metal-rich giants. Our radial-velocity measurements led to the rejection of about 60% of the targeted stars as Galactic foreground contamination, leaving

**Figure 1:** Left Panel: Metallicity distribution of Red Giants derived from CaT spectroscopy in Carina, where the colour-shading illustrates the separation used in the right panel. The green line illustrates a best-fit closed-box model. The right panel displays



us with a total number of 437 Red Giants around Carina's systemic velocity of  $223.9 \text{ km s}^{-1}$ .

### Carina's wide metallicity range

The distribution of the metallicities derived from our CaT spectroscopy is shown in Figure 1 (left). This metallicity distribution function (MDF) is peaked at a mean metallicity of  $-1.72 \pm 0.01$  dex, slightly higher than the previously derived mean spectroscopic metallicity of  $-1.99 \pm 0.08$  dex from a CaT sample of 52 RGB stars (Smecker-Hane et al. 1999). These former results are in reasonable agreement with our data if the quoted uncertainties and the widths of the distributions are taken into account.

The MDF appears remarkably broad. The entire distribution's *formal* full width at half maximum is 0.92 dex ( $1 \sigma$ -width of 0.39 dex). The *full* metallicity range, on the other hand, covers approximately 3.0 dex, reflected in the extreme tails of the MDF, where we find stars with metallicities approaching  $-3$  dex and near-solar metallicity, respectively, when extrapolating our calibration. Follow-up spectroscopy of these stars would be desirable to disclose the detailed chemical properties of these stars, which appear to be in part as metal-poor as the most metal-poor Red Giants found in other nearby dwarf galaxies (e.g., Shetrone et al. 2001). At the metal-rich end, a handful of them would be as metal-rich as the metal-rich population in the Sgr dSph (Bonifacio et al. 2004).

While part of the spread may be attributed to the usual measurement uncer-

cumulative spatial distributions of the metal-poor (blue) and metal-rich (red) components. The metal-rich stars clearly tend to concentrate towards the galaxy's centre.

tainties, to star-to-star variations in the actual Ca abundance (up to 0.2 dex), and calibration uncertainties, the spread in the metallicities seems to be influenced by the occurrence of several subpopulations with different peak metallicities.

Any MDF, as derived here, is rather insensitive to the details of the star-formation history. However, we have calibrated our CaT *metallicities* onto *iron* which in systems with extended star formation can have a significant contribution from long-lived stars through type Ia supernovae. Hence, one can have enrichment in Fe *without* accompanying SF. In the case of a SF history that consists of several SF episodes with long pauses in between, the Fe distribution can show 'gaps'. A Gaussian decomposition results in four underlying populations, which are preferred over a one-population model at the 98.1% level. However, one has to keep in mind that such a decomposition is a purely formal procedure, since SF events do not naturally produce Gaussian metallicity distributions.

Comparing our MDFs to simple chemical evolution models such as a closed-box model (see the green overplotted curve in the left panel of Figure 1) reveals a G dwarf problem at low metallicities: This model overpredicts the number of metal-poor stars. Also the pronounced metallicity peak of the MDF is not reproduced. Better fits may be obtained through the inclusion of infalling, pre-enriched gas and accounting for important outflows (Lanfranchi and Matteucci 2004). In this vein, one possible reason for the repeated cessation and onset of the SF episodes in Carina is the re-accretion of previously blown-out material. More de-

tailed chemical modeling to quantify the dominant processes is in preparation (Wyse et al., in prep.).

### An age-metallicity relation?

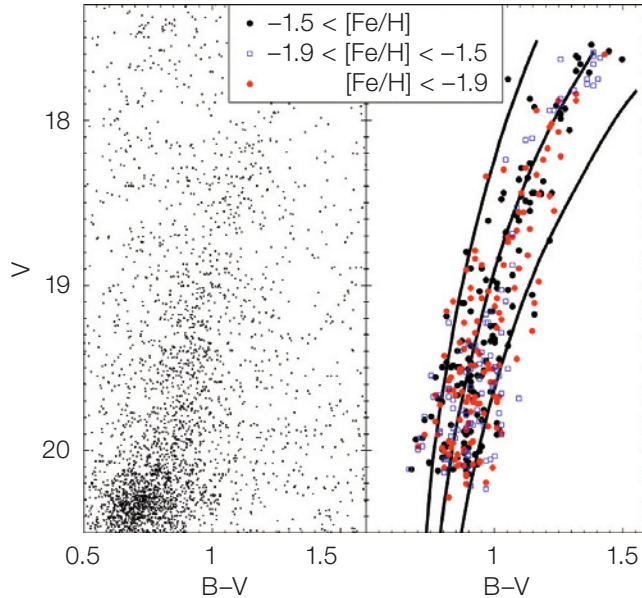
The (lack of a) relation between the colour of our targets and their metallicity is demonstrated in Figure 2 (right panel). In a population with little age spread, metal-poor stars would have blue colours and metal-rich ones would appear redder. This is indicated by three isochrones with metallicities, which span a similar range to those found in Carina and an age of its oldest population. In fact, there is no clear correlation with the data points. Obviously one cannot derive the metallicity of an individual star from its colour and magnitude on the RGB when dealing with mixed-age populations as in Carina. Our data thus confirm earlier suggestions that Carina shows an age-metallicity degeneracy in the sense that higher metallicities counteract the effects of younger ages. This conspiracy in turn leads to the observed narrow RGB.

Note that there are also quite a number of metal-poor stars ( $[\text{Fe}/\text{H}] < -1.9$ ) present redwards of the most metal-rich isochrone. Each of the physical systems, for which such isochrones apply, have a Red Giant Branch of a finite width, despite the underlying ‘fixed’ metallicity. This becomes more pronounced towards the lower part of the RGB, where the different isochrones will lie closer together, and lead to a progressive overlap of the respective branches. That is, for any star of a given metallicity and age, one will inevitably end up with a large spread in colours. Bearing this in mind and accounting for photometric uncertainties, these effects will have a larger impact than the uncertainties in metallicities, and can account for the increased scatter in the colour-magnitude diagrams.

We also found a higher concentration of metal-rich, presumably intermediate-age stars towards the inner regions of the galaxy as compared to more metal-poor stars – indicated in the cumulative plot of the stars’ galactocentric radii (Figure 1, right). Metal-poor stars are, however, detected throughout the entire galaxy. This trend matches the observed population

Figure 2: Left panel: Carina’s narrow Red Giant branch (from EIS photometry). Also visible at the lower left is the prominent intermediate-age red clump. The right panel shows confirmed member stars, colour coded by their metallicity. Also

shown (black lines) are sets of Yonsei-Yale isochrones with an age of 12.6 Gyrs and (left to right)  $[\text{Fe}/\text{H}] = -2.3$ ,  $[\text{Fe}/\text{H}] = -1.7$  and  $[\text{Fe}/\text{H}] = -1.3$ , which illustrate the effects of Carina’s prominent age-metallicity degeneracy.



gradient in terms of a central concentration of intermediate-age stars in Carina (Harbeck et al. 2001). This supports the idea that the more metal-rich stars are also the younger ones. A possible reason for such a gradient can be stronger dissipation of the more metal-enriched gas. It may as well indicate that the material at disposal for SF is more easily retained at the centre of the galaxy’s shallow potential well.

### Outlook

Carina is the only dSph known to have undergone distinct, well-separated episodic star formation. The dominant episodes of star formation took place at intermediate ages. It is not yet understood what caused the repeated cessation and delayed re-start of star formation in this enigmatic dSph.

We have compiled a large spectroscopic sample of CaT metallicities in Carina, which exceeds the previously largest published data set (Smecker-Hane et al. 1999) by more than a factor of eight. This will help us to disentangle its pronounced age-metallicity degeneracy and the galaxy’s age structure, since we can now in principle derive age estimates for our stars of known metallicity from finding the best-matched isochrone at that metallicity. Ultimate age distributions and

age-metallicity relations can additionally be well derived from turn-off stars, provided that the photometry is at a sufficient level of accuracy. Such an analysis, complemented by high-resolution spectroscopy, is currently in progress. A second article, giving an overview of the whole project, will be published in the June issue of *The Messenger*.

### References

- Bonifacio, P. et al. 2004, *A&A* 414, 503
- Carretta, E. and Gratton, R. 1997, *A&AS* 121, 95
- Cole, A. et al. 2004, *MNRAS*, 347, 367
- Grebel, E. K., Gallagher, J. S., and Harbeck, D. 2003, *AJ* 125, 1926
- Grebel, E. K. and Gallagher, J. S. 2004, *ApJ* 610, L89
- Harbeck, D. et al. 2001, *AJ* 122, 3092
- Koch, A. et al. 2005, *AJ* 131, 895
- Lanfranchi, G. A. and Matteucci, F. 2004, *MNRAS* 351, 1338
- Monelli, M. et al. 2005, *AJ* 126, 218
- Moore, B. et al. 1999, *ApJ* 542, L19
- Rizzi, L. et al. 2003, *ApJ* 589, L85
- Rutledge, G., Hesser, J. E., and Stetson, P. B. 1997, *PASP* 109, 907
- Shetrone, M. D., Côté, P., and Sargent, W. L. W. 2001, *ApJ* 548, 592
- Smecker-Hane, T. A. et al. 1994, *AJ* 108, 507
- Smecker-Hane, T. A. et al. 1999, *ASP Conf. Ser.* 192, 159

# The Formation of Intermediate-Mass Galaxies over the Last 8 Gyrs

François Hammer<sup>1</sup>  
 Matthew Lehnert<sup>2</sup>  
 Mathieu Puech<sup>1</sup>  
 Hector Flores<sup>1</sup>  
 Yan-Chun Liang<sup>3</sup>

<sup>1</sup> Laboratoire Galaxies, Etoiles, Physique et Instrumentation, Observatoire de Paris, France

<sup>2</sup> Max-Planck-Institut für Extraterrestrische Physik, Garching, Germany

<sup>3</sup> National Astronomical Observatories, Chinese Academy of Sciences, China

The physical processes driving the growth of galaxies can be robustly investigated all the way to  $z = 1$ , i.e. when the Universe was only about 40 % of its current age. The advantage of restricting ourselves to this redshift range is that the total stellar mass, extinction, star-formation rate, gas-phase metal abundance, and galaxy kinematics can be recovered with reasonable accuracy. Moreover, half of the stars in spirals were formed less than 8 Gyrs ago. More practically, as we shall show, the current generation of instruments at the ESO VLT allows us to study galaxies up to  $z = 1$  at approximately the same level of detail as what has been done for nearby galaxies. Here we present the first results of the properties of galaxies out to this redshift based on a moderately large sample of  $0.4 < z < 1$  galaxies using VLT/FORS, ISAAC and GIRAFFE. This study has allowed us to investigate the important physical processes that shaped galaxies including merging, gas accretion, and feedback from intense star formation.

[Measuring stellar masses, star-formation rates and oxygen abundances: the importance of extinction](#)

To investigate the physical processes shaping galaxies at 40 % of the age of the Universe, we have gathered a sample of 200 galaxies selected from the Canada France Redshift Survey ( $I_{AB} < 22.5$ ,  $0.4 < z < 1$ ). These galaxies have stellar masses ranging from  $3 \times 10^{10}$  to  $3 \times 10^{11} M_{\odot}$ , i.e., dominated by intermediate-mass galaxies. Almost all of them have been imaged by the Hubble

Space Telescope and several have been observed using the combination of FORS2 and ISAAC in order to recover their physical characteristics and to compare them to local galaxies in the same mass range.

But before reviewing our findings, we believe it necessary to be precise in the definition of the words ‘massive’ and ‘dwarfs’ when these terms are applied to galaxies. The physical characteristics of local galaxies seem to suggest that massive galaxies have  $M_{\text{star}} > 3 \times 10^{11} M_{\odot}$  (i.e., approximately the Milky Way and more massive), and that dwarfs are defined by  $M_{\text{star}} < 3 \times 10^{10} M_{\odot}$ . At this dividing point, the massive galaxies are dominated by older populations, high surface mass densities, and are dominated by the morphological type, E/S0. Spiral and irregular galaxies with lower surface densities and younger populations dominate the intermediate and dwarf mass regime respectively (Kauffman et al. 2003).

Studies of the ‘star-formation history’ of the Universe suggest that the star-formation rate density has declined significantly from  $z \approx 1$  to the current epoch. Massive E/S0s and dwarfs are apparently not the main contributors to this decline, because the early-type galaxies were mostly in place at  $z = 1$ , and dwarf galaxies contribute marginally to the global stellar mass or metal content. Therefore to understand how galaxies grew, we focus, in the following, on the population of intermediate-mass galaxies. Intermediate-mass galaxies populate the ‘knee’ of the luminosity function and comprise at least 2/3 of the current stellar mass density (Brinchman and Ellis 2000; Heavens et al. 2004). Locally, according to the morphological classified luminosity function from the Sloan Survey (see Nakamura et al. 2004), 53 % of galaxies are early-type spirals (earlier than Sbc), 27 % are E/S0, 17 % are late-type spirals, and only few (3 %) are classified as irregulars.

The near-IR luminosity of galaxies seems to correlate well with their stellar masses. This is intriguing because most of the near-IR light is not coming from the main-sequence stars that make up most of the galaxy mass. One may justifiably suspect that mass estimates based on near-infrared photometry must have large un-

certainties and whether this method can apply equally to starbursts and early-type evolved galaxies. Bell et al. (2003) have ingeniously circumvented these difficulties, by applying an empirical correction depending on the  $B-V$  colour of the galaxies (the bluer galaxies have lower stellar masses at a given  $K$  luminosity which is contaminated by red supergiant stars). Nevertheless the systematic uncertainty related to stellar-mass estimates could be as high as a factor of 2–3, by, for example, ignoring the effects or range of possible choices for the stellar initial mass function (IMF). Since dynamical mass estimates are sensitive to different systematic effects, only through the comparison of dynamical and photometric mass estimates can we overcome problems related to, e.g., the choice of plausible IMFs, the amount and distribution of the extinction, and our ignorance of the star-formation history of individual galaxies.

Estimates of star-formation rates (SFRs) for individual galaxies are usually believed to be very uncertain. A significant uncertainty is the IMF: most (all?) tracers used to estimate SFRs are proportional to the number of massive (e.g., IR) or very massive, ionising, stars (e.g.,  $H\alpha$ ). In a critical examination of the literature, Kennicutt (1998) has provided us with some useful tools to derive SFRs based on various indicators and all assuming the same IMF. Similarly, it is also important to be consistent when comparing SFR with stellar mass by using a common IMF. For observational reasons, UV continuum or  $[OII]\lambda 3727$  fluxes have been frequently used to estimate the SFR, since these wavelengths are redshifted into the visible window at moderate or high redshifts. Unfortunately, these estimates are strongly affected by dust, its distribution and amount, and thus underestimate the true SFR of individual galaxies by very large factors (see Figure 1). Indeed, actively star-forming galaxies, starbursts, especially the dust-enshrouded ones, the luminous infrared galaxies with bolometric luminosities about  $10^{11} L_{\odot}$ , LIRGs, are so numerous at  $z > 0.4$ , that the only viable tracers of the star-formation rate at those redshifts are only those which account for the light reprocessed by dust (IR), or those that can be properly corrected for extinction (e.g.,  $H\alpha$  after using  $H\alpha/H\beta$  to estimate the extinction). For a given

IMF, mid-IR and extinction-corrected  $H\alpha$  fluxes can be used to estimate the SFR with an uncertainty  $< 0.3$  dex (Flores et al. 2004).

The strong evolution of the number density of luminous IR galaxies means that extinction must be properly accounted for when estimating SFRs or metal abundances. A commonly used method to estimate the gas-phase metal abundance of a galaxy is  $R_{23} = ([OII]\lambda 3727 + [OIII]\lambda 4959, 5007) / H\beta$ .  $R_{23}$  is sensitive to the extinction through the ratio of  $[OII]\lambda 3727$  to  $H\beta$ . Further, one needs a sufficient spectral resolution ( $R > 1000$ ) and signal-to-noise ratio ( $S/N > 10$ ) to properly correct the underlying stellar absorption, especially for measurements of  $H\gamma$  and  $H\beta$  lines. Another difficulty is due to the fact that, at  $z > 0.5$ , the  $H\alpha$  line is redshifted to the near-IR, and the  $H\alpha/H\beta$  ratio has to be estimated using two different instruments. A way to circumvent the difficulty (and the cost of near-IR spectroscopy), is to use the ratio  $H\gamma/H\beta$ , although the  $H\gamma$  line is often faint. The most exhaustive study has been made by Liang et al. (2006), by comparing the extinction from  $H\gamma/H\beta$  to that from the ratio of IR to  $H\beta$  emission (Figure 2). The typical uncertainty in this case is 0.2–0.3 dex when oxygen abundance is derived from  $R_{23}$ .

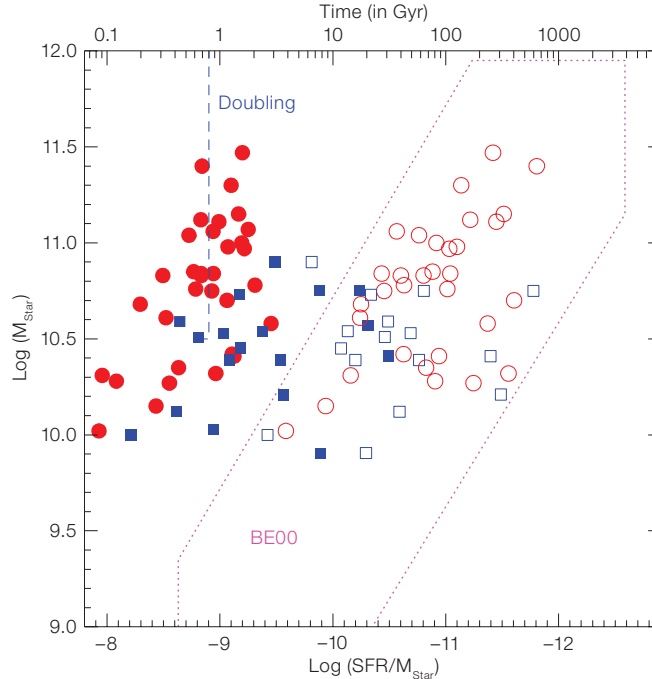
The uncertainties in the estimates of stellar masses, SFR, and oxygen abundance for intermediate-redshift galaxies can appear very high, even if derived with great care. However, what we need is to compare the properties of intermediate-mass galaxies at high and low redshift. By adopting exactly the same method at both redshifts, it is very likely that the residual relative error is much smaller than a few tenths of a dex.

#### Measuring kinematics of $z = 0.6$ galaxies: the need for 3D spectroscopy

The Tully-Fisher (T-F) relation is an important correlation linking stellar mass to the maximal rotational velocity in disc galaxies. The evolution of this relation at intermediate redshift is currently a matter of intense debate (e.g., Conselice et al. 2005). Conselice et al. (2005) has obtained the first T-F relation in  $K$ -band up to  $z \sim 1.2$ , using slit spectroscopy at

**Figure 1:** Stellar mass versus specific star-formation rate (red full dots: LIRGs, full blue squares: starbursts). The star-formation rates have been estimated from the IR luminosity or extinction-corrected  $H\alpha$  luminosity. Open symbols represent the same objects, but for which the SFR has been estimated using the  $[OII]\lambda 3727$  luminosity, not corrected for extinction by dust (see Brinchmann and Ellis 2000,

BE2000). The difference in the star-formation rates illustrates the danger in making such estimates on the sole basis of UV line or continuum emission. The LIRGs observed at  $z > 0.4$  can easily double their stellar masses if their star formation was sustained at the observed rate for  $\sim 800$  Myrs. This figure is reproduced from Hammer et al. (2005).



Keck. Compared to the local relation, the distant relation does not seem to have evolved in slope or zero point but shows a significantly larger scatter. In fact, the scatter is so large, that one can even wonder if the T-F is still a valid relation at all for intermediate-redshift spiral galaxies (see Figure 3).

We made use of the unique opportunity afforded by the 15 deployable integral field units of the 3D spectrograph GIRAFFE, as part of the FLAMES facility on UT2. With GIRAFFE, in its IFU mode, we are able to recover the kinematics of almost all the emission-line galaxies with  $I_{AB} < 22.5$  (Flores et al. 2006). We obtained, during the GIRAFFE GTO, the kinematics of a sample of 32 galaxies (selected in the CFRS and Hubble Deep Field South) at  $z \sim 0.6$  using the  $[OII]$  doublet. At first sight, the T-F relation obtained from GIRAFFE IFU data is very similar to the one obtained by Conselice et al. (2005).

We then constructed a classification scheme that took advantage of both maps of the kinematics of each galaxy (velocity field and velocity dispersion maps) and optical morphologies from high-resolution images taken with the HST. This classification scheme aims to identify rotating discs, relying on the

fact that given the spatial resolution of the GIRAFFE IFU ( $0.52 \text{ arcsec pixel}^{-1}$ ), most of the velocity gradient of the rotation curve in rotating discs falls into only one IFU pixel. The measured dispersion within this pixel is then dominated by large-scale motions (i.e., the rotation) rather than by random motions at smaller scales resulting in a peak in their velocity dispersion map located at their dynamical centre of their large scale kinematics. Using such prescriptions, we find that only 34 % of galaxies in our sample are rotating discs; 22 % were classified as ‘perturbed rotation’ because a rotation is seen in their velocity field but the peak in their velocity dispersion map is off-centred and thus cannot be attributed to rotation; the remaining 44 % of galaxies have very complex dynamics with quite chaotic velocity fields, and are similar to what is expected for merging or strongly interacting galaxies. A few of the galaxies show a rotation-like pattern in their velocity fields with a dynamical axis significantly rotated from the optical main axis: complex kinematics like this are possibly a sign of strong feedback from the star formation within these galaxies. Translated into the whole intermediate-mass population (including E/S0 and spirals with low star-formation activity), we were led to the astonishing conclusion that only 60 % of these galaxies

are in a relaxed dynamical state such as a rotating disc!

Given these results, a more critical examination of the GIRAFFE T-F relation (Figure 3) and its scatter is very instructive: most (all?) of the scatter of the T-F relation is related to galaxies whose kinematics were classified as perturbed rotations or complex, i.e., precisely those that likely have not yet reached dynamical equilibrium. This illustrates that only 3D spectroscopy can be used to study the evolution of the T-F relation, because slit spectroscopy does not sample the whole kinematics of the galaxies, and it is simply unable to correctly identify galaxies with complex, not yet relaxed dynamics. Keeping only those galaxies with securely identified rotating discs, the distant T-F relation becomes very similar to the local one, even with similar scatter.

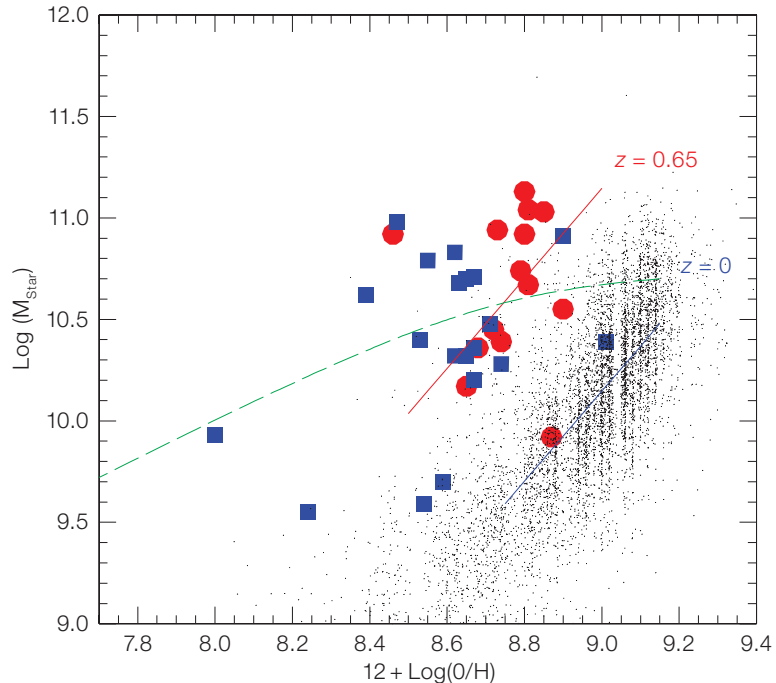
### Growth of spirals: secular or driven by mergers?

Intermediate mass galaxies in the local Universe are predominantly spirals (70 %) and E/S0 (27 %). They show small or negligible specific star-formation rates, the star-formation rate per unit stellar mass,  $SFR/M_{\text{stars}}$  (e.g.,  $10^{-11} \text{ yr}^{-1}$  for the Milky Way) and very few are LIRGs (0.5 %). Local intermediate-mass galaxies form a well-defined mass-metallicity sequence with O/H abundance increasing with stellar mass. Six to seven billion year ago, intermediate-mass galaxies showed very different properties (Figures 1, 2 and 3). A significantly higher fraction of galaxies in this mass range are LIRGs (15 %), and, at their observed instantaneous star-formation rates, they can easily double their stellar mass within  $\sim 800$  Myrs. On average their O/H abundances are half the local value at a given stellar mass. One fourth of them show complex kinematics implying that they are neither rotating discs nor ellipsoids supported by dispersion. This fraction is similar to that of galaxies with peculiar morphologies seen in deep HST surveys.

The integrated star formation related to the numerous LIRGs at  $z < 1$  suffices by itself to account for the formation of about 40 % of the stellar mass in present-day intermediate-mass galaxies. The

**Figure 2:** Evolution of the mass-metallicity relation at  $z = 0.6$  (red dots: LIRGs, blue points: starbursts; small black dots: local galaxies selected from the Sloan Digital Sky Survey). At  $z = 0.65$ , the gas phase metal abundance of oxygen is about half that of present-day galaxies. Assuming a 'close-box model'

of chemical evolution, meaning that we do not account for in-falling or out-flowing gas, this increase in metallicity can be related to a decrease in the gas content of 30 % to 10 % from  $z = 0.6$  to 0 (green dashed line). This figure is reproduced from Liang et al. (2006).



evolution of stellar mass since  $z = 1$  independently confirms this. The luminous IR galaxies show a large variety of morphologies and kinematics, including those of rotating discs, mergers, compact galaxies or merger remnants. Which present-day galaxies have experienced such strong star-formation events less than eight billion years ago? Which galaxies in the local Universe had peculiar morphologies or complex kinematics several billion years ago? What physical mechanism is responsible for the strong decline in the star-formation density since  $z = 1$ ? The complexity and the variety of the physical phenomena do not demand a unique scenario for every galaxy. Let us however investigate if one scenario is able to explain most of the observations (see Figure 3). One could be tempted to associate complex kinematics with an early collapse of what will become a normal centrifugally supported disc. This is, however, very unlikely since a significant fraction of stars in all  $z = 0.5-1$  galaxies have ages larger than several billion years. So mechanisms which are related to galaxy environment or internal characteristics must be investigated.

Six to seven billion years ago, galaxies themselves and their environments were much more gas-rich than today. This is expected from both the star-formation

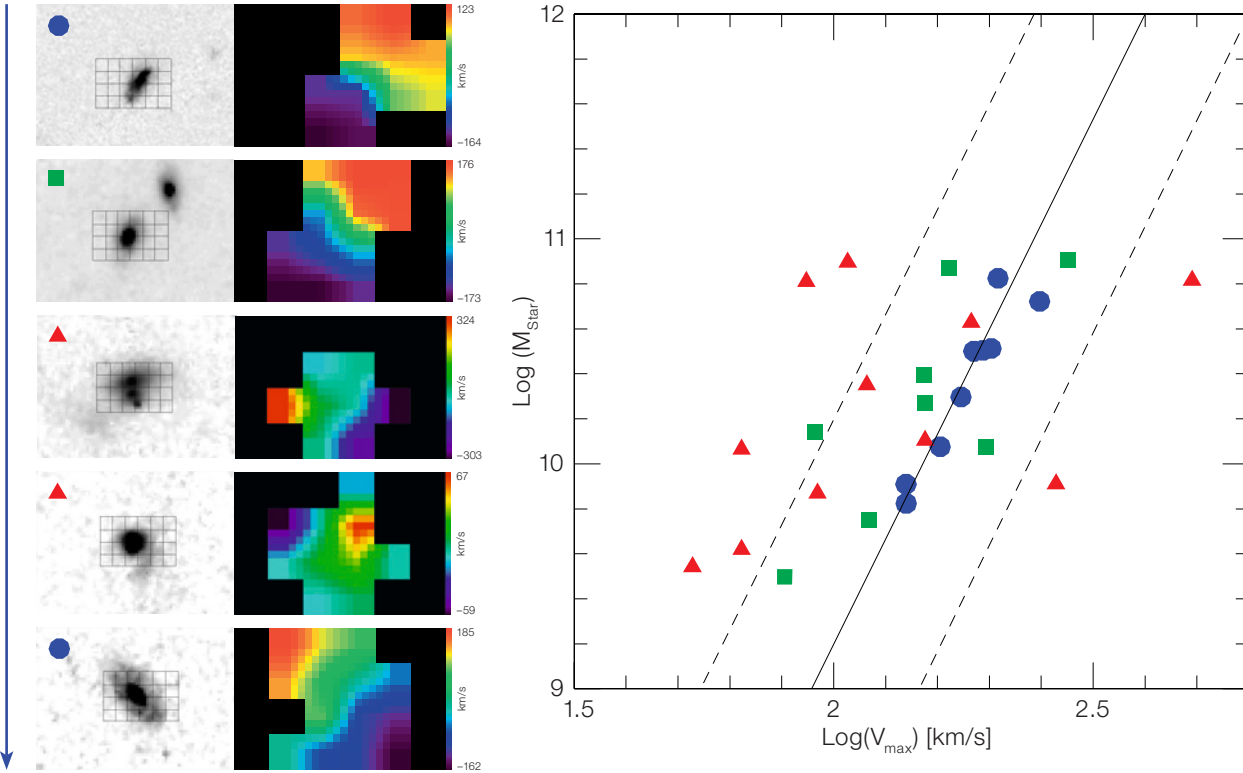
history of the Universe and the metal abundance evolution of galaxies (Figure 2). Even if the gas density on large scales was twice what it is today, accretion of gas in the intergalactic medium gas cannot account for the high frequency of LIRGs. For example the Milky Way is located in a filament, is near a super-cluster, and forms stars at about  $1 M_{\odot} \text{ yr}^{-1}$ . This is compared to more than  $20 M_{\odot} \text{ yr}^{-1}$  for a LIRG. The complex kinematics and peculiar morphologies of a third of distant galaxies also belies such 'secular evolution'. Merging is broadly recognised both observationally and theoretically to be the most efficient way to produce intense and rapid star formation. Accretion of satellites is widely believed to explain most evolutionary features of galaxies and has strong support in the observations of the halo of the Milky Way and other nearby galaxies. It is unclear from modelling if the accretion of gas from the IGM and small satellites is enough to explain the high specific star-formation rates of LIRGs, and most models of this type indeed fail to explain the dramatic evolution in the number of strong infrared emitters. Moreover these models cannot explain the complex kinematics observed with GIRAFFE (Figure 3).

Major mergers, however, are extremely efficient at producing stars, at maintain-

**Figure 3:** (right) Tully-Fisher relation for 32 intermediate-mass galaxies at  $z \sim 0.6$ , as produced using data taken with the GIRAFFE IFUs (Flores et al. 2006). The full line represents the  $z = 0$  Tully-Fisher relation (and the dotted lines its 3-sigma scatter). Blue dots represent rotating discs, green squares represent perturbed rotating discs (as by a minor merger or by a galaxy-galaxy interaction) and red triangles rep-

resent galaxies with complex kinematics (expected from major mergers). This is illustrated on the left by a few inserts which include HST images and velocity fields (increasing velocity from blue to red). These have been organised either to follow a major merger event which can produce either an elliptical, an S0, or a new spiral (see text).

Major merger evolution



ing or even increasing the high values of specific angular momentum observed in local spiral galaxies, and at generating the complex kinematics and morphologies often observed in these galaxies. A scenario whereby major mergers destroy and rebuild discs, the so-called ‘spiral rebuilding scenario’, is indeed able to account for all the evolutionary trends discussed above (see Hammer et al. 2005). This is not however a proof of the validity of this idea: it is generally believed that the end product of a major merger is an ellipsoidal galaxy, not a disc galaxy. Only complex mechanisms related to strong feedback such as that associated with supermassive black holes would be enough to efficiently expel sufficient amounts of gas, a fraction of which with high angular momentum being available to collapse to form a new disc. It could be also argued that the spiral rebuilding scenario is not necessary. For example, one can imagine that all galaxies with complex kinematics (or peculiar morphologies) are progenitors of early-type galaxies, E/S0. However at  $z \sim 0.6$  peculiar/complex galaxies are as numerous as E/S0, and early-type galaxies

seem to be largely in place at  $z \approx 1$ , so it is difficult to believe that this hypothesis could be a realistic alternative.

We have presented here preliminary results showing the evolution of star-formation rate, specific star-formation rate, O/H gas-phase abundance, and circular velocity, all as a function of stellar mass. The fact that rotating discs defined a tight sequence relating their stellar mass and rotation velocity (Tully-Fisher relation) supports the robustness of our estimates based on the dynamics of galaxies at intermediate redshifts. We obviously need better statistics, over a broader range of galaxy types and masses. More robust answers to the questions we have raised here are likely to come from the ESO VLT Large Programme, IMAGES, the ‘Intermediate Mass Galaxies Evolution Sequence’. This study, with GIRAFFE IFU and FORS2 MXU mode, will yield the spatially-resolved dynamics and velocity dispersions of  $\sim 400$  disc/early-type, mass-selected galaxies from redshifts of  $z = 0.4-1$ . Only GIRAFFE with its multi-IFU mode is able to recover properly the Tully-Fisher relation at moderate redshifts.

Equally important are the studies of nearby galaxies such as M31, which may be an example of a disc rebuilt after a major merger at  $z \sim 0.6$ . Beyond more observations, comparisons with simulations including all of the complex physics associated with gas in-fall, gas out-flow, feedback and formation of supermassive black holes, major and minor merging, etc. will be important for understanding and interpreting the dynamics and properties of high-redshift galaxies, especially those numerous galaxies at intermediate/high redshifts without relaxed kinematics.

References

Bell, E. F. et al. 2003, *ApJ* S. S. 149, 289  
 Brinchmann, J. and Ellis, R. S. 2000, *ApJ* 536, L77  
 Conselice C. et al. 2005, *ApJ* 628, 160  
 Flores, H. et al. 2004, *A&A* 415, 885  
 Flores, H. et al. 2006, *A&A*, accepted  
 Hammer F. et al. 2005, *A&A* 430, 115  
 Kauffmann, G. et al. 2003, *MNRAS* 341, 33  
 Heavens, A. et al. 2004, *Nature* 428, 625  
 Kennicutt R. 1998, *ApJ* 498, 541  
 Liang Y., Hammer F. and Flores H. 2006, *A&A* 447, 113  
 Nakamura, O. et al. 2004, *AJ* 127, 2511

# Masses and Mass-to-Light Ratios of Early-Type Galaxies at High Redshift – The Impact of Ultradeep FORS2 Spectroscopy

Arjen van der Wel<sup>1,2</sup>  
 Marijn Franx<sup>2</sup>  
 Pieter G. van Dokkum<sup>3</sup>  
 Hans-Walter Rix<sup>4</sup>  
 Garth D. Illingworth<sup>5</sup>  
 Jiasheng Huang<sup>6</sup>  
 Bradford P. Holden<sup>5</sup>  
 Piero Rosati<sup>7</sup>

<sup>1</sup> Johns Hopkins University, Baltimore, USA

<sup>2</sup> Leiden Observatory, the Netherlands

<sup>3</sup> Yale University, New Haven, USA

<sup>4</sup> Max-Planck-Institut für Astronomie Heidelberg, Germany

<sup>5</sup> University of California, Santa Cruz, USA

<sup>6</sup> Harvard-Smithsonian CfA, Cambridge, USA

<sup>7</sup> ESO

With FORS2 on the VLT we obtained ultradeep spectra of a sample of early-type galaxies at  $z \sim 1$ , which, together with high-resolution imaging from HST, provide dynamical masses. We study the evolution of the multi-wavelength photometric Fundamental Plane, including the rest-frame near-infrared, which places strong constraints on the formation and evolution of early-type galaxies as a function of mass and environment. Most prominently, we find that massive early-type galaxies formed early (at  $z > 2$ ), independent of their large-scale environment.

Spectroscopy of distant galaxies is a major focus of today's large telescopes. For  $z \approx 1$  or less, the exposure time to obtain a redshift measurement is typically less than an hour. Hence, with the currently available instruments, it is possible to measure redshifts of thousands of galaxies in order to determine galaxy number densities, luminosity functions and clustering properties, and the evolution thereof with cosmic time. Although redshift is a useful piece of information, it is insufficient to infer the physical properties of an individual galaxy. Arguably, the single most important quantity is mass, or mass-to-light ratio (M/L), which provides direct insight into the build-up of the galaxy mass-function over cosmic time. Mass-related quantities can be un-

ambiguously compared with model predictions, contrary to luminosities and colours. In order to measure galaxy masses, high signal-to-noise ratio (S/N) spectra are required: from the spatial and dynamical structure of spectral features, information about the galaxies' gravitational potential can be inferred. This requires the selection of relatively bright galaxies at moderate redshifts ( $z \approx 1$ ) and long integration times.

In this article we describe an observational programme at the VLT which was used to obtain 8–24-hour deep spectroscopic observations of early-type galaxies up to  $z = 1.3$ . These long integrations enabled us to obtain two new results. We measured the rate of luminosity evolution of early-type galaxies out to  $z = 1.3$ , constraining their formation epoch. We describe how this depends on environment and galaxy mass, and how this compares to model predictions. Second, we compared the evolution of optical colours and M/L with the evolution in the rest-frame near-infrared, derived from observations from the Spitzer Space Telescope. This provides insight into the applicability of IR light as a mass indicator and a test for stellar population models.

## The Fundamental Plane at $z = 1$

The Fundamental Plane (FP) is a relation between size, surface brightness and

stellar velocity dispersion for early-type galaxies (see Figure 1). From the virial theorem it can be seen that this scaling relation in fact represents an underlying relation between M and M/L. The evolution of M/L (or L) with redshift can therefore be traced by measuring the offsets of distant galaxies from the local FP. Since the scatter in the FP is relatively small, the offset can be determined accurately. For massive early-types in dense environments (i.e., clusters) it has been known for several years that they have decreased in luminosity since  $z = 1$  by a little over 1 magnitude in the optical. Assuming that such galaxies have evolved passively between the epoch of observation and the present, this rate of luminosity evolution implies that their stars must have formed at rather high redshifts ( $z > 2$ ).

An important issue is whether the epoch of early-type galaxy formation depends on large-scale environment, or whether it is driven by the intrinsic properties of the galaxies themselves and their immediate neighbourhood. Up to several years ago, galaxy formation models very generally suggested that early-type galaxies in low-density environments (the field) form their stars at later times than early-types in clusters. More recent models, on the other hand, indicate that the mass of a galaxy itself is a crucial parameter in describing its evolution and that no large differences between massive field and cluster galaxies are to be expected.

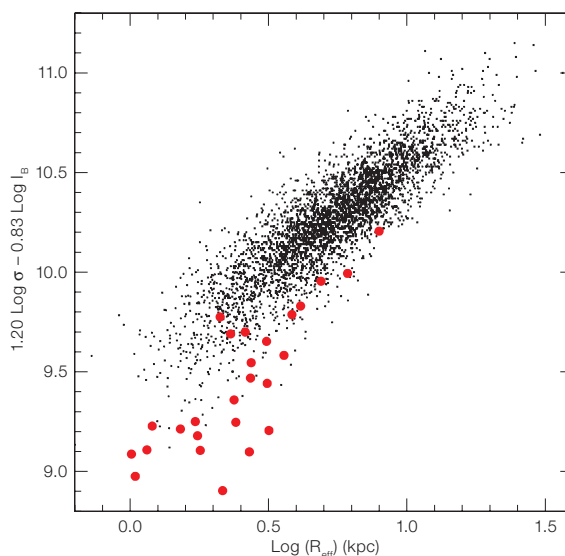


Figure 1: The edge-on projection of the FP of low-redshift early-type galaxies from SDSS (small black dots) and our sample of  $z \sim 1$  early-types (large red dots). There is a clear offset between the two samples, indicating that there is significant luminosity evolution between  $z = 1$  and the present.

A crucial test is to measure the rate of luminosity evolution for galaxies in different environments, as age differences manifest themselves in differential evolution. Before our observing programme was undertaken, it was unclear whether or not the luminosities of galaxies in the field evolve differently from the luminosities of galaxies in clusters. Our programme mainly aimed at measuring masses of field early-type galaxies at  $z = 1$ , because the field samples thus far had been of lesser quality (smaller numbers, lower data quality and lower redshift) than the cluster samples.

With FORS2 we targeted the Chandra Deep Field-South (CDF-S), which has been imaged by the Advanced Camera for Surveys (ACS) on board the Hubble Space Telescope (HST). These imaging data are essential for selecting  $z \sim 1$  galaxies with early-type morphologies, and to determine their sizes and surface brightnesses (two of the FP parameters). Besides the CDF-S, we also targeted a field containing the high-redshift ( $z = 1.24$ ) cluster RDCS 1252.9-2927 (hereafter, CL1252). This field has been imaged by ACS as well.

The spectroscopic observations were carried out between September 2002 and October 2003, in a series of five runs. Since the spectral features suitable for our analysis are situated in the rest-frame optical, and we target galaxies up to  $z = 1.24$ , we needed to measure the spectra as far toward the red as possible, at wavelengths of about 850 nm, where FORS2 is very sensitive.

The obtained spectra are of outstanding quality. In particular, the S/N of the spectra of the CL1252 cluster members is unprecedented after 24 hours of integration with a typical seeing of 0.65". The integration times for the galaxies in the CDF-S are typically 10 hours, with a typical seeing of 0.9". In Figure 2 we show four examples of VLT spectra and HST images of  $z \sim 1$  field early-type galaxies. The spectra clearly show that the stellar populations of these galaxies are several billion years old, although there are age differences among these galaxies: the  $z = 1.09$  galaxy is the youngest, which can be seen from the strong high-order Balmer lines. For the other three galaxies,

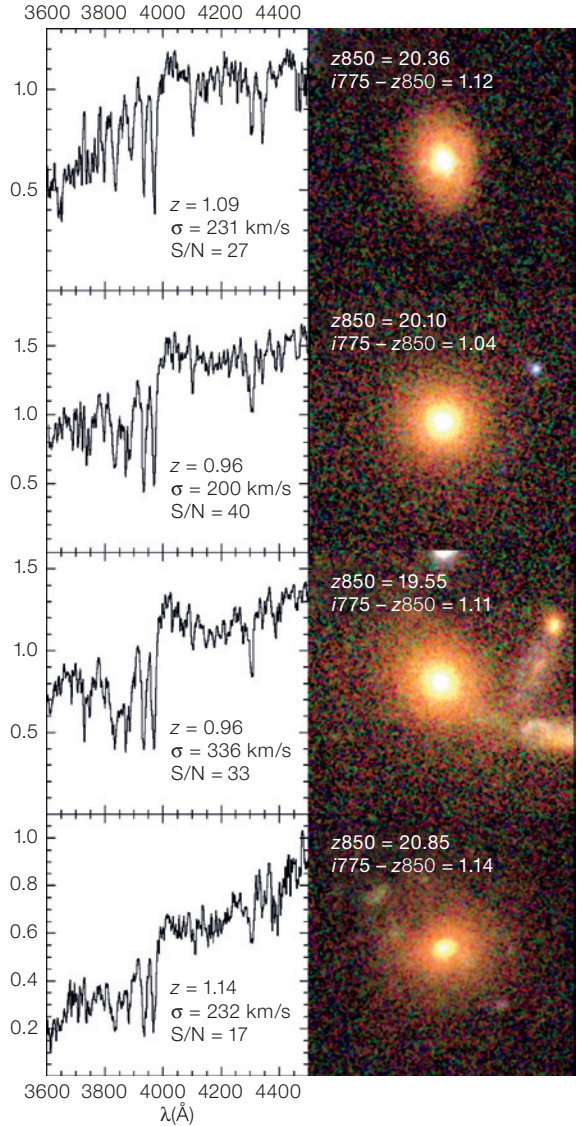


Figure 2: VLT/FORS2 spectra and HST/ACS colour images of four field early-type galaxies at  $z \sim 1$ . The images, which are 5.4" (43 kpc at  $z = 1$ ) on a side, are a combination of F606W, F775W, and F850LP ACS images.

there is a clearer 4000 Å break, indicative of evolved stellar populations without significant star formation for at least a billion years before the epoch of observation. The smooth, concentrated morphologies of the images indicate that these are genuine early-type galaxies. A de Vaucouleur model fits best to the surface-brightness profiles. These deep spectra are used to compare the widths of absorption features with those in stellar spectra in order to obtain velocity dispersions of the stars in the galaxies, measuring the third FP parameter. We measured 42 velocity dispersions of galaxies in the redshift range  $0.62 < z < 1.25$ . Four of these are cluster early-type galaxies at

$z = 1.24$ , (Holden et al. 2005) and 20 are field early-type galaxies at  $0.95 < z < 1.15$  (van der Wel et al. 2004, 2005).

Our field sample is of similar size and quality as the cluster samples, such that we can properly compare the evolution of field and cluster early-types. The offset of  $z \sim 1$  field early-type galaxies from the local Fundamental Plane is shown in Figure 1. We find that this offset of the  $z \sim 1$  field early-types corresponds to a luminosity evolution of almost 2 magnitudes in the  $B$ -band. This is significantly larger than for cluster early-types, which are about 1.4 magnitudes brighter at  $z = 1$  than at  $z = 0$ . This apparently agrees with

the model prediction that field early-types are younger than cluster early-types. However, the galaxies in the field sample are on average less massive than those in the cluster samples. If only massive galaxies (with  $M > 2 \times 10^{12} M_{\odot}$ ) are selected, there is no difference between the field and cluster samples: the luminosity evolution amounts to about 1.3 magnitudes, implying high formation redshifts ( $z > 2$ ) for massive early-type galaxies in either environment, falsifying the prediction by some models that there is a large age difference between field and cluster galaxies.

As was suggested above, there is a difference in luminosity evolution between high- and low-mass early-types. Indeed, galaxies with masses  $M < 2 \times 10^{12} M_{\odot}$  are 2.1 magnitudes brighter at  $z = 1$  than at  $z = 0$ , which is much more than the 1.3 magnitudes brightening inferred for massive galaxies. This is illustrated in Figure 3, where we show that high-mass galaxies have higher M/L than low-mass galaxies, and that the observed relation between M and M/L for the  $z \sim 1$  field galaxies clearly differs from the equivalent relation at  $z = 0$ . Other workers in this field have, independently, also found such a strong relation (Treu et al. 2005; Di Serego Alighieri et al. 2005). This change in slope might indicate that the mass of an individual galaxy determines its formation redshift. The idea that massive galaxies form earlier than low-mass galaxies is referred to as down-sizing and is supported by other observational evidence besides the FP results described here, and can be reproduced by recent theoretical models.

However, selection effects severely hamper data sets such as these. Our magnitude-limited sample, at a given galaxy mass, is biased towards galaxies with low M/L, i.e., young stellar populations. Obviously, this effect is strongest for low-mass/faint galaxies. We show the luminosity limit of our survey in Figure 3 by the red line. It is clear that the galaxies with the lowest M/L are likely not representative of all early-type galaxies with such masses. Considering the distribution of luminosities and M/L of the galaxies in our sample and the magnitude limit of the survey, we conclude that the described bias is the main cause of the

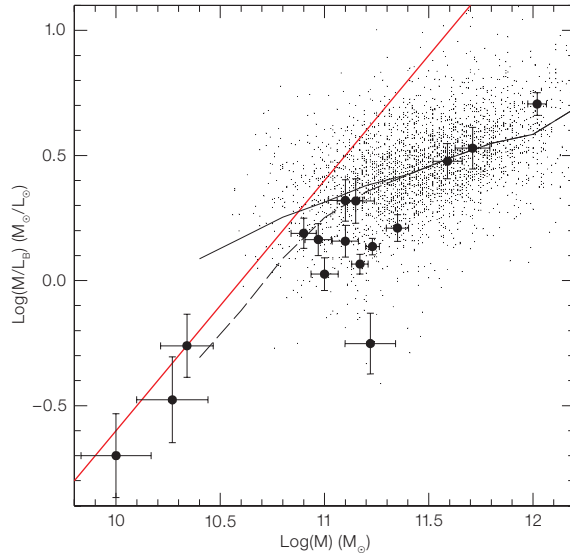


**Figure 3:** M versus M/L for the  $z \sim 1$  field galaxies (large circles) and local galaxies from SDSS corrected for luminosity-evolution to  $z = 1$  (small dots). The red line indicates the luminosity limit of our survey. The solid black line shows the relation between M and  $M/L_B$  for the SDSS galaxies. The dashed black line indicates the same relation for the SDSS galaxies, but only including those that are brighter than the  $z = 1$  luminosity limit.

observed differential evolution of galaxies with different masses. But even if this selection effect is taken into account, we still find a mass-dependent evolution in M/L, although it is reduced to a very subtle effect (see also Figure 3).

Di Serego Alighieri et al. (2005) use a *K*-band selected sample, and also find a steep relation between M and M/L. This shows that selecting galaxies by their *K*-band luminosity is very different from selecting by stellar mass (see also the next section). We note that Treu et al. (2005) claim that selection effects cannot account for the steep observed slope and  $z = 1$ , and that the strongly mass-dependent evolution of M/L is largely intrinsic. Remarkably, they find an equally steep slope for all redshifts  $z > 0.3$ , implying a sudden steepening between  $z = 0.3$  and the present, and no evolution after that. We conclude that even deeper surveys, probing the early-type galaxy population to lower masses, are needed to determine, in a model-independent way, whether the FP slope has or has not evolved strongly over the past 7 Gyrs.

#### The evolution of the rest-frame near-IR properties of early-type galaxies

As is clear from the above, obtaining masses of high- $z$  galaxies dynamically is observationally extremely expensive. It is therefore not feasible to obtain masses of very large samples in order to measure

the evolution of quantities such as the total mass density of the galaxy population. Such measurements necessarily rely on mass estimates based on photometric properties. These estimates are derived from stellar population models that predict how colours and M/L depend on each other. To verify the robustness and accuracy of this method, the correspondence between models and observations of the evolution of colours and M/L needs to be tested. With our dynamically determined M/L we are in a position to perform such a test.

First, it is important to note that there is a strong correlation between the dynamically obtained M/L and the rest-frame optical colours of the galaxies in the  $z \sim 1$  sample presented above (van der Wel et al. 2005). Furthermore, in Figure 4 we show that the evolution in the rest-frame *B-I* colour generally agrees well with the predictions of stellar population models: assuming a single stellar population with solar metallicity and a Salpeter IMF, the evolution in  $M/L_B$  implies a certain amount of evolution in *B-I*. The expected  $z = 1$  colours are indicated for three different models in Figure 4 by the coloured squares. This indicates that the methodology of converting colours into M/L is viable.

Next, it is especially interesting to include the near-infrared (NIR) in the analysis, as this is much less sensitive to extinction by dust, and probably less affected by

recent and ongoing star-formation. In other words, NIR light is thought to be more representative of stellar mass than optical light. It should be noted, however, that various results in the literature have already indicated that the NIR photometric properties of galaxies are rather poor indicators of their ages and M/L, contrary to their optical colours. To investigate this matter, we use Spitzer/Infrared Array Camera (IRAC) images at  $3.6\ \mu\text{m}$  and  $4.5\ \mu\text{m}$  to determine the optical-to-NIR colours of our  $z = 1$  galaxies. We compare those with the rest-frame colours of local early-types. In Figure 5 we show that the evolution in the rest-frame  $B-K$  colour is about 0.3 magnitudes between  $z = 1$  and  $z = 0$  (van der Wel et al. 2006). In Figure 5 we make a similar comparison as in Figure 4. First, it is very remarkable that the predictions differ by much from each other. Second, the most widely used model, that of Bruzual and Charlot (2003), predicts much faster evolution of  $B-K$  than observed. The Vazdekis (1996) and Maraston (2005) models provide better agreement.

We have tested whether our result can be reconciled with the Bruzual-Charlot model by adopting different metal contents, stellar initial mass functions and more complex star-formation histories, but it turns out that the discrepancy persists. Large quantities of dust in the high- $z$  sample may affect the  $B-K$  colours such that slow evolution of  $B-K$  is mimicked. Spitzer/MIPS photometry at  $24\ \mu\text{m}$  will be a useful test to constrain the dust content. However, the red colours are most likely intrinsic to the stellar populations of the galaxies.

We conclude very generally that estimating galaxy masses from rest-frame NIR photometry is not very robust. First, the M/L in the NIR evolves at a comparable rate as the optical M/L, which means that the NIR magnitude of a galaxy is not a better indicator of its M/L than its optical magnitude (this is at least true for dust-poor galaxies). Second, the disagreement among the models indicates that there is a systematic uncertainty in the M/L as derived from NIR photometry of at least a factor of two for this type of galaxy. More specifically, the systematic difference between the observations and the Bruzual-Charlot model implies that

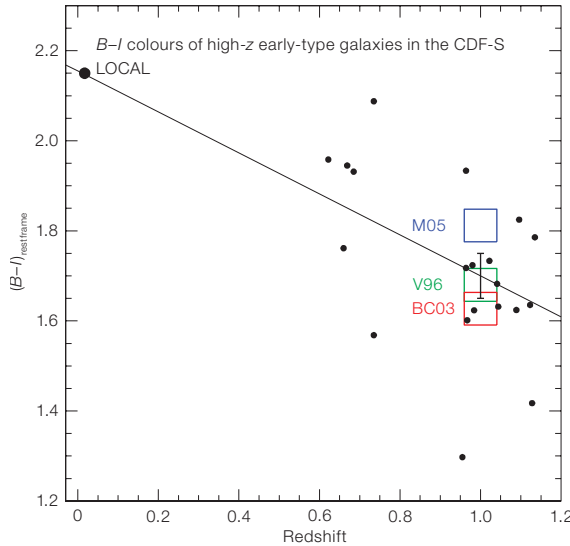


**Figure 4:** Evolution of the rest-frame  $B-I$  colour of early-type galaxies. The observed evolution is about 0.45 mag. The error-bar shows the uncertainty in the measured evolution. The coloured squares are model predictions for  $B-I$  at  $z = 1$ . The three different colours indicate different stellar population models. From top to bottom: Maraston (2005), Vazdekis (1996), and Bruzual & Charlot (2003). These models are for single stellar populations with a Salpeter IMF and solar metallicity.

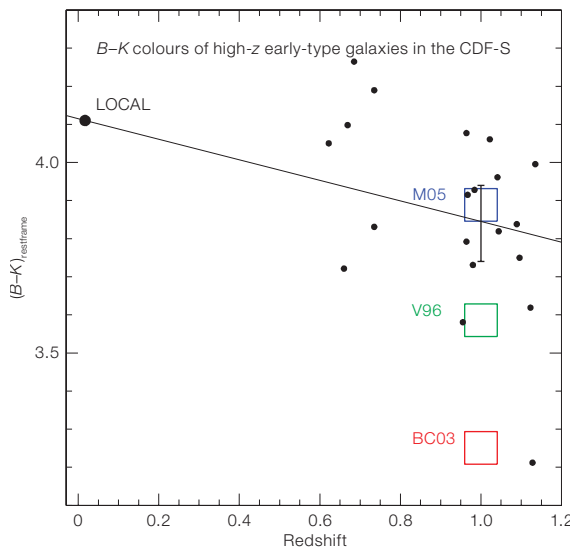


**Figure 5:** Evolution in the rest-frame  $B-K$  colour of early-type galaxies. The observed evolution is about 0.3 mag. The error-bar shows the uncertainty in the measured evolution of the sample. The coloured squares are model predictions for  $B-K$  at  $z = 1$  (see Figure 4).

M/L as derived from NIR photometry and this model are a factor of  $\approx 2$  too high. This is a severe problem. For example, the evolution in the mass density of early-type galaxies is about the same factor of two between  $z = 1$  and the present. The agreement among the models and between the models and the observations are much better in the optical, which should therefore be preferred over the NIR to estimate M/L. Before we can take advantage of the full potential of rest-frame NIR observations, the models need to converge to similar predictions that can stand empirical tests such as described here.

References

Bruzual, G. and Charlot, S. 2003, MNRAS 344, 1000  
 Di Serego Alighieri, S. et al. 2005, A&A 442, 125  
 Holden, B. P. et al. 2005, ApJ 620, L83  
 Maraston, C. 2005, MNRAS 362, 799  
 Treu, T. et al. 2005, ApJ 633, 174  
 van der Wel, A. et al. 2004, ApJ 601, L5  
 van der Wel, A. et al. 2005, ApJ 631, 145  
 van der Wel, A. et al. 2006, ApJ 636, L21  
 Vazdekis, A. et al. 1996, ApJS 106, 307

# Unveiling the Structure of Galaxy Clusters with Combined ESO-VLT, WFI, and XMM-Newton Observations

Hans Böhringer<sup>1</sup>  
 Filiberto Braglia<sup>1</sup>  
 Daniele Pierini<sup>1</sup>  
 Andrea Biviano<sup>2</sup>  
 Peter Schuecker<sup>1</sup>  
 Yu-Ying Zhang<sup>1</sup>  
 Alexis Finoguenov<sup>1</sup>  
 Gabriel W. Pratt<sup>1</sup>  
 Hernan Quintana<sup>3</sup>  
 Paul D. Lynam<sup>4</sup>

<sup>1</sup> Max-Planck-Institut für Extraterrestrische Physik, Garching, Germany

<sup>2</sup> INAF-Osservatorio Astronomico di Trieste, Trieste, Italy

<sup>3</sup> Pontificia Universidad Católica de Chile, Santiago, Chile

<sup>4</sup> ESO

Understanding the dynamical structure and matter content of galaxy clusters is crucial for many cosmological and astrophysical applications. While optical studies provide information on the distribution and dynamics of the galaxies, allowing for a tentative reconstruction of the cluster mass distribution, X-ray observations provide complementary details through the study of the hot, X-ray luminous intracluster plasma which is confined by the cluster's gravitational potential well. To exploit the advantage of such a combined approach we have been conducting observations with VIMOS at the ESO-VLT, the Wide Field Imager at the 2.2-m MPG/ESO telescope at La Silla, and ESA's XMM-Newton X-ray observatory. In this article we illustrate the power of the combination of these instruments for galaxy cluster studies.

Galaxy clusters are important astrophysical laboratories and test objects for cosmological research. The key for this application of galaxy cluster research is the knowledge of the cluster mass and dynamical structure. For instance, the cluster abundance and the statistics of the cluster spatial distribution provide the basis for tests of cosmological models (Böhringer et al. 1998; Schuecker et al. 2003). Among many possible applications, the use of galaxy clusters as laboratories involves (i) the determination of the baryon-to-dark matter ratio, where-

by the clusters provide a representative sample of matter of our Universe, and (ii) the determination of the mass-to-light ratio, which is a measure of the efficiency of galaxy formation. It is obvious that the determination of the cluster mass and internal mass distribution is an essential prerequisite in such studies.

Cluster-mass measurements have so far preferentially been performed on presumably relaxed, regular systems. For general cosmological applications we need to know the mass of clusters of any type. To take one crucial example: the mass function of galaxy clusters provides important information on the statistics of the cosmic large-scale structure. It has been suggested on the basis of some simulations that the X-ray luminosity, the X-ray temperature, and the galaxy velocity dispersion, all three important indicators of the cluster mass, may be boosted to high values during major mergers of galaxy clusters. Thus, in many important surveys, where these measures of cluster mass have been used without this precaution, the high end of the mass function could be seriously distorted, thereby leading to incorrect implications. This and other important applications, which rely on a precise knowledge of cluster structure and mass, have led us to embark on a systematic study of cluster structure for representative cluster samples using detailed observations at X-ray and optical wavelengths.

While deep X-ray images, which show the distribution of the hot intracluster medium (ICM) tracing the gravitational potential of the cluster, reveal much of the cluster structure as projected onto the sky, the galaxy redshift distribution provides a complementary view of the cluster dynamics projected onto the line-of-sight. Thus, a major aim of the project is to employ the combined X-ray/optical information for the reconstruction of the dynamical state of the cluster, to search for the best strategy for the mass estimate for each case, and to test the consistency of the optical and X-ray mass estimates. For this research Europe currently offers two superb instruments. The XMM-Newton X-ray observatory with its high throughput, good spatial resolution (8 arcsec), and simultaneous imaging and spectroscopic capabilities is by far

the best instrument to study the density, temperature, pressure and entropy structure of the ICM. This provides a very good basis for mass estimates as well as an understanding of the formation and thermal history of the cluster and its ICM. The VIMOS multiplexing spectrograph at the ESO-VLT is the most efficient instrument (apart from IMACS at Magellan) to collect sufficient numbers of redshifts for a dynamical analysis. In addition the Wide Field Imager (WFI) allows us to map the optical emission from the cluster galaxies on large scales. Further goals of this programme involve the study of the galaxy population and the star-formation activity as a function of environment in and around the cluster, the relation of the heavy element abundances in the ICM with the properties of the galaxy population, and the connection between the thermal structure of the ICM and the galaxy distribution and dynamics (which can provide clues on the accretion history of the cluster).

While we have already collected interesting results on the X-ray and optical properties of the clusters in this project, the overall data assessment and interpretation are still in progress. Here we would therefore like to give an illustration of the diagnostic power of the combined use of VLT-VIMOS and XMM-Newton observations, in particular, and to describe our observational approach.

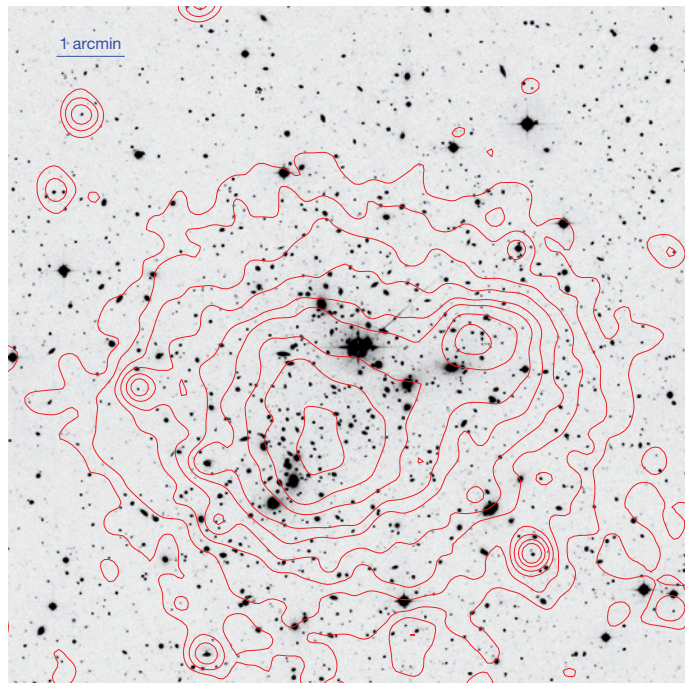
## X-ray morphology

As an example of this diagnostic power we choose the case of the massive cluster RXCJ 0014.3-3023 (Abell 2744), reproduced in a composite colour WFI image in Figure 1. This cluster is taken from our complete sample of massive galaxy clusters (with X-ray luminosity above  $2 \cdot 10^{45} h_{50}^{-1} \text{ erg s}^{-1}$  for 0.1–2.4 keV) in the redshift range from  $z = 0.27$  to 0.31 in the southern sky, as identified in our ROSAT Sky Survey-based REFLEX Cluster Survey (Böhringer et al. 1998, 2004). The X-ray-determined mass of the cluster is about  $7.4 \cdot 10^{14} h_{70}^{-1} M_{\odot}$  inside a radius  $1.24 h_{70}^{-1} \text{ Mpc}$  (i.e. half of the virial radius), excluding substructure (Zhang et al. 2006). This cluster is also known as a gravitational lens (Smail et al. 1991). An overlay of the X-ray contours (Figure 2)

**Figure 1:** Colour composite image of the cluster RXCJ 0014.3-3023 (A2744) obtained from *B*- (blue, 4800 s exposure), *V*- (green, 3600 s), and *R*-band (red, 3600 s) imaging with the Wide Field Imager at the 2.2-m MPG/ESO telescope at La Silla. The angular size of the field shown is  $10'$  on a side ( $2.7 h_{70}^{-1}$  Mpc for the 'concordance' cosmological model). East is to the left and North up.



**Figure 2:** X-ray contour plot of the 0.5 to 2.0 keV XMM-Newton image superposed on the *R*-band WFI image for RXCJ 0014.3-3023. We clearly see two X-ray maxima tracing the gravitational potential minima of the main cluster (to the SE) and a subcluster (to the NW), both also marked by slightly offset concentrations of massive galaxies.



reveals two X-ray maxima belonging to the main cluster to the South-East (SE) and a considerable subcluster to the North-West (NW), which are in the process of merging.

Two signatures indicate that the NW subcluster is still on its infalling track. Namely: (1) the galaxies are preceding the intra-cluster plasma of the subcluster, which is stopped by the interaction with the main cluster's ICM, and (2) a detailed Chandra X-ray image shows signs of a bow shock in front (i.e. to the SE) of the infalling subcluster (Kempner and David 2004). The latter signature is consistent with an entropy enhancement in the region between the two maxima discovered from our XMM-Newton observations (Figure 3, Finoguenov et al. 2005).

### Galaxy population

To study the galaxy population we covered the region of RXCJ 0014.3-3023 with three VIMOS fields, overlapping at the cluster centre, aligned in the EW direction. For each field (but one), we designed one multi-object spectroscopy (MOS) mask for a few bright galaxies and one MOS mask for many faint galaxies. The total exposure time was about

one hour per field including all overheads. With the VIMOS Low-Resolution Blue grism and a conservative 3 arcsec-wide sky strip per slit, we obtained in total 871 spectra including 134 confirmed cluster members. The targets were selected from an *I*-band image with no colour selection to obtain an unbiased view of the galaxy population as a function of star-formation activity. The MOS masks cover the entire cluster slightly beyond the virial radius ( $\sim 2.5 h_{70}^{-1}$  Mpc), where the cluster galaxy density becomes low. Thus, the investment for covering this important outer region is a reduction in the overall efficiency.

Figure 4 shows typical galaxy spectra. At the dispersion given by the coupling of the low-resolution grism (a price paid for the high multiplexing power of VIMOS) with the 1-arcsec-wide slits adopted, the galaxy velocities have relatively large uncertainties (of the order of  $300 \text{ km s}^{-1}$ ) and the sensitivity for the detection of emission lines is reduced with respect to higher-resolution spectroscopy. However, as we show below, we still obtain much useful information. The sensitivity limit for the detection of emission lines still corresponds to about  $10 \text{ \AA}$  in equivalent width. Since one of our goals is the study of the nature of the galaxy population

as a function of environment, we show in Figure 5 (left hand) as an example the cumulative ratio of emission-line galaxies versus galaxies with spectra typical of passive stellar populations. We clearly see an increase in star-formation activity at larger cluster radii which has been seen before (e.g. Kodama et al. 2001) and in the Sloan Digital Sky Survey in nearby clusters (Gomez et al. 2003). There is a very clear signature that star formation is quenched inside the cluster and this quenching sets in far outside the virial radius. This implies that the interaction with the hot cluster ICM (e.g. by interstellar gas stripping effects) is not the only mechanism that leads to a suppression of star formation in cluster galaxies. Quenching effects must already be operative in the infall region. The actual projected distributions of star-forming and non-star-forming galaxies in the cluster are shown in Figure 5 (right hand). There is no obvious correlation between the distribution of emission-line galaxies and the merger structure of the cluster. Also, we note that most of the emission-line galaxies are found at large radii, except for a striking compact group of three emission-line objects near the cluster centre, which could well lay off-centre along the line-of-sight.

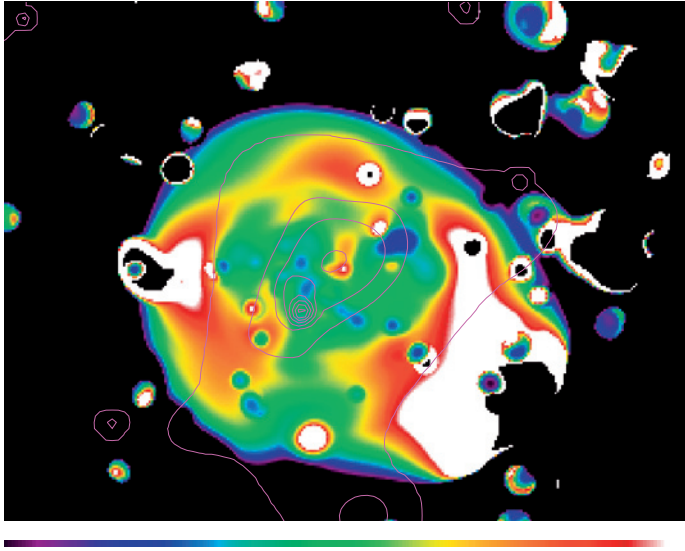


Figure 3 (above): Entropy structure of the ICM in RXCJ 0014.3-3023 seen in projection as derived from the XMM-Newton spectro-imaging (Finoguenov et al. 2005). While we expect the entropy to steadily increase with radius in a relaxed cluster, we here observe low entropy gas (in blue) marking the two subcomponent centres, whereas the high entropy (in yellow/red) in the region in-between implies energy dissipation due to the merger shock. Another interesting feature is the low-entropy channel connecting the main cluster centre with the southern edge (in green). The overplotted contours show the galaxy distribution (see Figure 7).

Figure 5 (below): Left: Radial distribution of the cumulative ratio of galaxies with and without emission lines in their spectra. The central peak in the blue line (all galaxies) is due to only three galaxies (see right hand), which are excised in the red curve. Right: Projected distribution of the galaxies with spectroscopic observations. Different colours mark the redshift regions (blue:  $\Delta v < -1321$  km s<sup>-1</sup>, green:  $-1321 < \Delta v < 0$  km s<sup>-1</sup>, yellow:  $0 < \Delta v < 1321$  km s<sup>-1</sup>, red:  $\Delta v > 1321$  km s<sup>-1</sup>) and the asterisk symbol indicates ongoing star formation activity. The cluster centre is marked by a cross.

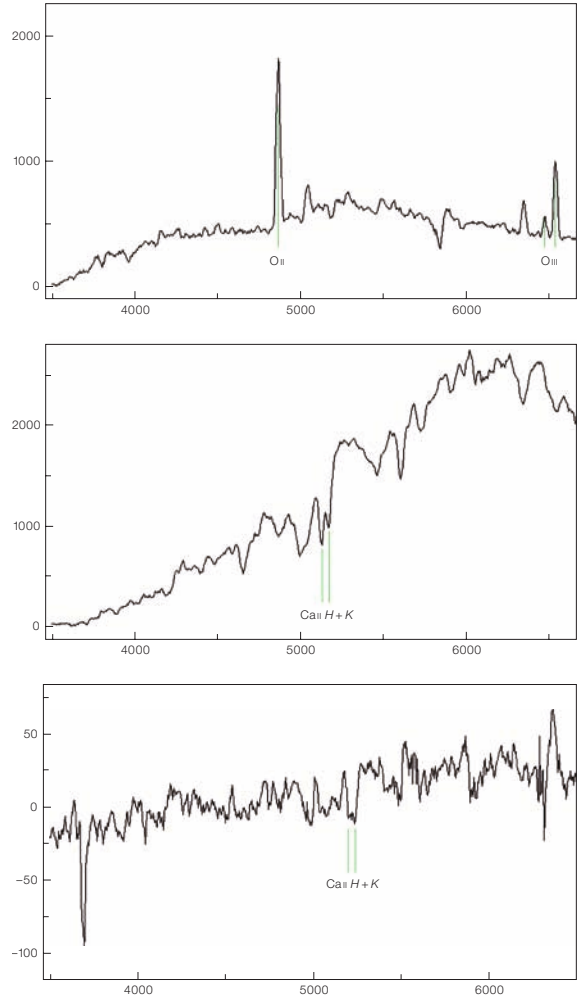
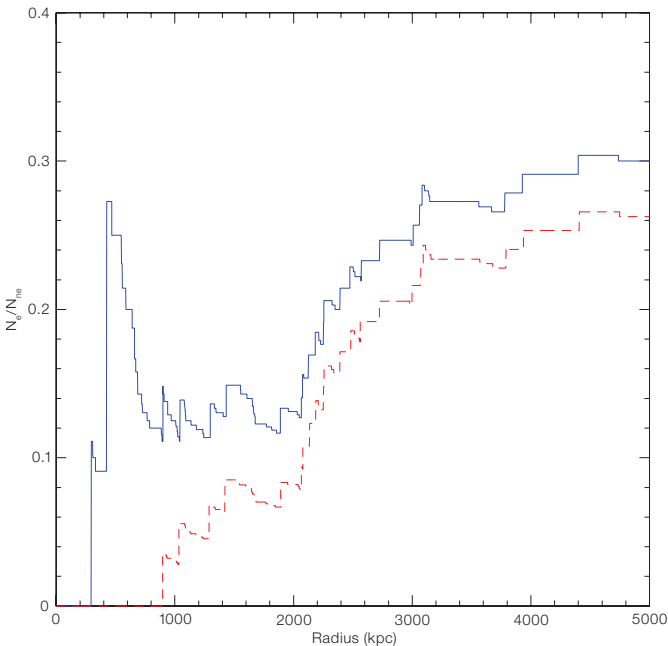
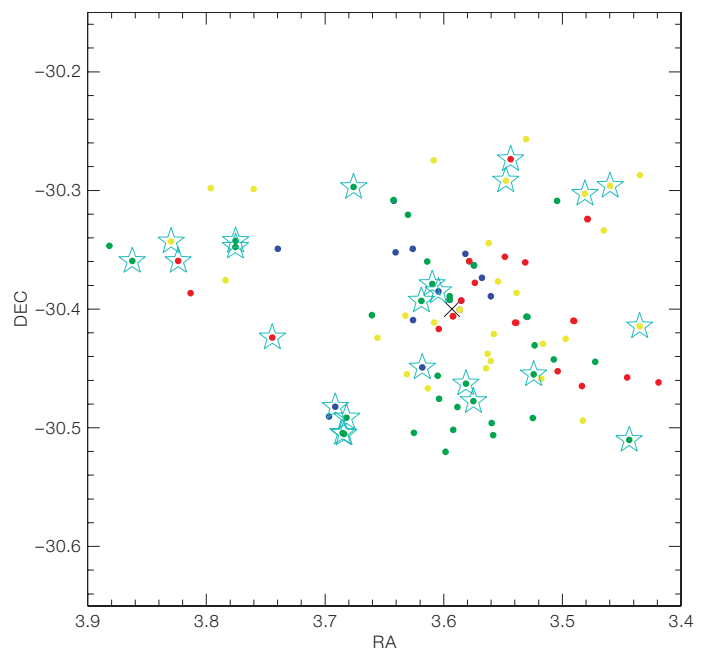


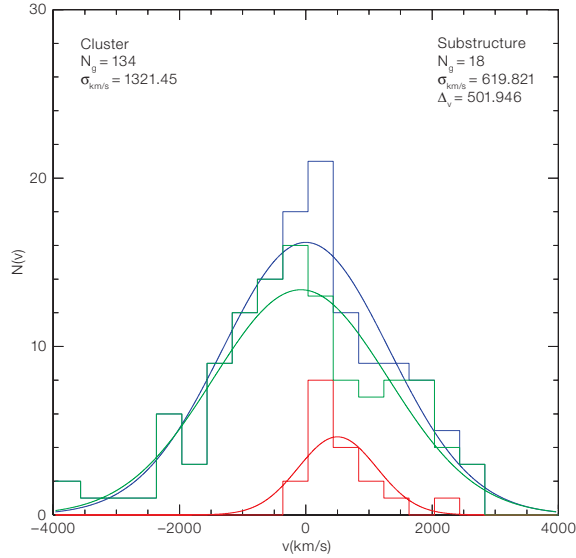
Figure 4: Examples of VIMOS spectra (observed-frame wavelength in Å) of three cluster galaxies, including a star-forming emission-line galaxy (top) and two galaxies dominated by old, passively evolving stellar populations (middle and bottom). While the upper two examples include two bright galaxies, a galaxy near the detection limit of 22.5 I-mag is shown at the bottom.



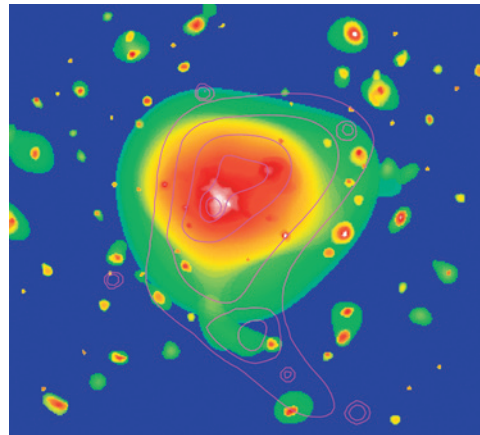
### The structure of the cluster merger

Figure 6 shows the (rest-frame) velocity distribution of the galaxies in the cluster. The overall velocity dispersion is very large, with  $\sigma_v = 1321 \text{ km s}^{-1}$ . Since there is a clear signature of an infalling subcluster in X-rays, we can use this information to search for a velocity difference between the two subcomponents. Therefore Figure 6 also shows the velocity distribution of the galaxies in the region to the right and above a point intermediate to the two X-ray maxima. This section nicely separates the infalling subcluster from the main cluster. We note a clear shift to higher velocities for the infalling subcluster, with a mean velocity difference of about  $500 \text{ km s}^{-1}$ . Since we see clear signatures in X-rays that the two subcomponents are interacting (e.g. a high entropy region in the X-ray emitting plasma between the two X-ray maxima, see Figure 3), we interpret the higher redshift of the subcluster as indicating that this subcomponent is infalling from the front. We can further speculate that the mutual attraction of the two subcomponents with a combined mass of about  $10^{15} h_{70}^{-1} M_\odot$  allows a maximum approach velocity at a separation of about 1 Mpc (equivalent to a separation of about  $800 h_{70}^{-1} \text{ kpc}$  in projection) of about  $2200 \text{ km s}^{-1}$ . The low observed line-of-sight velocity thus implies that the merger axis is near the plane of the sky with an angle of the order of about 15 degrees. The signature of a bow shock seen in the Chandra data (Kempner and David 2004) supports this picture of a motion almost perpendicular to the line-of-sight. A more detailed analysis of this merger structure is in progress, and we also plan to support our investigation by comparison to tailored simulations.

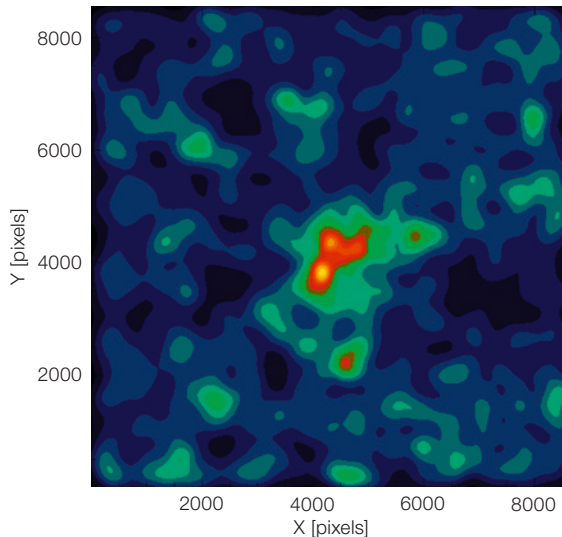
The strategy we then adopted for the mass analysis of the cluster is to use the undisturbed sector of the main cluster (see Zhang et al. 2006). Both the spectroscopic dynamical analysis and the X-ray analysis were then performed excluding the substructure. Our assumption of a relatively undisturbed sector of the cluster is supported by the fact that we observe a gently falling velocity dispersion profile in this sector, as expected for a regular cluster. Preliminary results based on the sky and velocity distribution of the galax-



**Figure 6:** Histogram and Gaussian fit of the RXCJ 0014.3-3023 galaxy velocity distribution from the VIMOS spectroscopic observations. The blue curves show the overall distribution, while the red curves give the distribution of galaxies in the sector covered by the infalling subcluster, showing a higher recession velocity by about  $500 \text{ km s}^{-1}$ . The green curves show the velocity distribution of the remaining galaxies.



**Figure 7:** Projected distribution of galaxies with  $R \leq 22 \text{ mag}$  (without z-cut) in the cluster RXCJ 0014.3-3023 and its surroundings. **Top:** The X-ray surface brightness map with the galaxy number density superposed as a contour plot. Colours from white to green correspond to decreasing X-ray surface brightnesses. The maximum of the galaxy distribution clearly marks the centre of the main cluster. In the outer contours we recognise extensions to the NW and to the S. **Bottom:** The galaxy distribution on scale that is twice as large (entire WFI field-of-view) and to lower overdensity thresholds (decreasing from yellow to black). The extensions of the top panel now find their continuation in possible filaments of galaxy overdensities leading further away from the cluster.



ies give a value for the mass of the main cluster that is in agreement with the X-ray estimate.

### The surroundings

The large field-of-view of the WFI camera ( $34' \times 33'$ ) allows us to image the whole cluster together with its infall region. Figure 7 (top) shows a contour plot of the projected galaxy density distribution down to  $R \sim 22$  mag (no  $z$ -cut being applied) superposed on the X-ray image, and (bottom) a large-scale map of the galaxy distribution extending even outside the virial radius of RXCJ 0014.3-3023. The maximum of the galaxy density distribution is centred on the main cluster. The extensions in the galaxy distribution and the X-ray surface brightness distribution to the NW and to the South (S) in Figure 7 (top) find their continuation in a possible large-scale filamentary structure in the bottom panel of this figure, where the galaxy distribution is reproduced with a lower threshold for the density contours. There is a very interesting correspondence between the filaments and the internal structure of the cluster, although a spectroscopic confirmation is needed. The main subcluster is falling into the system from the NW. The extension to the S is connected to a low entropy channel linking the possible filament with the cluster centre (Figure 3). We have seen analogous features in other clusters of our sample and we inter-

pret them as the signature of a previous infall of galaxy groups, with a low entropy intergroup medium, from the surrounding large-scale filamentary structure. Thus we are obtaining a glimpse of the accretion history of this cluster. The fact that RXCJ 0014.3-3023 exhibits a giant radio halo (see Kempner and David 2004), which was most probably formed by cosmic-ray acceleration in a previous merger shock, is a further confirmation that this cluster has recently suffered from other mergers in addition to the one observed here.

### Outlook

Similar results to those shown here have been obtained in the past from deep optical and X-ray studies. The point here is that the power of XMM-Newton and VLT-VIMOS makes such observations a routine enterprise which can be applied to a larger, representative sample of galaxy clusters. We are currently exploiting these two facilities to study two representative cluster samples, one comprised of the most massive, southern galaxy clusters in the redshift range from  $z = 0.27$  to  $0.31$ , all observed with XMM-Newton, from which the above example was taken, and for more than half of which we have recently collected VIMOS data. The other sample, covering the whole mass range of clusters in a homogeneous way, was designed from the REFLEX sample in the redshift range from  $z = 0.055$  to  $0.2$ .

For all 33 clusters of this sample deep XMM-Newton observations have been conducted, and now we inspect a wide spectrum of cluster morphologies. So far only few optical data are available but systematic observations are planned. As spectroscopy at medium redshift and low resolution on a wide field is time-demanding, complements to VIMOS will be considered at no loss of efficiency or science throughput. Both samples are becoming benchmark samples, for which observations based on the Sunyaev Zel'dovich effect are scheduled, and lensing studies are planned. With this rich information on cluster structure we will significantly improve our calibration of cluster mass measurements, as these first results illustrate.

### Acknowledgements

The X-ray data used here are based on observations with XMM-Newton, an ESA science mission with instruments and contributions directly funded by ESA member states and NASA.

### References

- Böhringer, H. et al. 1998, *The Messenger* 94, 21
- Böhringer, H. et al. 2004, *A&A* 425, 367
- Finoguenov, A., Böhringer, H., Zhang, Y.-Y. 2005, *A&A* 442, 827
- Gomez, P. L. et al. 2003, *ApJ* 584, 210
- Kempner, J. C., David, L. P. 2004, *MNRAS* 349, 385
- Kodama, T. et al. 2001, *ApJ* 562, L9
- Schuecker, P., et al. 2003, *A&A* 398, 867
- Smail, I. et al. 1991, *MNRAS*, 252, 19
- Zhang, Y.-Y. et al. 2006, *A&A*, submitted



The centre of the globular cluster Messier 12 as observed with the FORS1 multi-mode instrument on ESO's Very Large Telescope. The picture covers a region of about 3.5 arcmin on a side, corresponding to about 23 light years at the distance of Messier 12. It is based on data in five different filters:  $U$ ,  $B$ ,  $V$ ,  $R$  and  $H\alpha$ . The observations were obtained with very good conditions, the image quality ('seeing') being around 0.6 arcsec. (ESO PR Photo 04/06)

# Gamma-Ray Bursts: Learning about the Birth of Black Holes and Opening new Frontiers for Cosmology

Guido Chincarini<sup>1,2</sup>  
 Fabrizio Fiore<sup>3</sup>  
 Massimo Della Valle<sup>4</sup>  
 Angelo Antonelli<sup>3</sup>  
 Sergio Campana<sup>2</sup>  
 Stefano Covino<sup>2</sup>  
 Giancarlo Cusumano<sup>5</sup>  
 Paolo Giommi<sup>6</sup>  
 Daniele Malesani<sup>7</sup>  
 Felix Mirabel<sup>8</sup>  
 Alberto Moretti<sup>2,9</sup>  
 Patrizia Romano<sup>2,9</sup>  
 Luigi Stella<sup>3</sup>  
 Gianpiero Tagliaferri<sup>2</sup>

<sup>1</sup> Università degli Studi di Milano-Bicocca, Italy

<sup>2</sup> INAF – Osservatorio Astronomico di Brera, Italy

<sup>3</sup> INAF – Osservatorio Astronomico di Roma, Italy

<sup>4</sup> INAF – Osservatorio Astrofisico di Arcetri, Italy

<sup>5</sup> INAF/IASF Palermo, Italy

<sup>6</sup> ASI Science Data Center

<sup>7</sup> International School for Advanced Studies (SISSA), Trieste, Italy

<sup>8</sup> ESO

<sup>9</sup> Supported by the Italian Space Agency (ASI)

Swift, a satellite devoted to the study of cosmic gamma-ray bursts (GRBs), is now fully operational and detects about 100 GRBs per year, as the first year of operation demonstrated. Since its launch (20 November 2004), Swift has monitored with the narrow-field X-Ray Telescope (XRT) 75 afterglows (out of 97 GRBs), starting just a few minutes after the GRB onset. Together with the events detected by HETE-II and INTEGRAL, Swift gives us a unique position to unveil the details of these enigmatic events, which likely identify the birth of black holes. GRBs are also useful cosmological tools, and can be used as powerful, distant beacons to trace the history and evolution of the early Universe. All of this can be accomplished by the use of Swift, coupled to large ground-based telescopes. In this article we describe some of the fresh, exciting results obtained in the field.

Zwicky used to say that Nature manifests itself in any form we may think of and has far more ways than we can possibly imagine. Indeed every time we increase the sensitivity of our instruments or develop the technology to open a new window in the electromagnetic spectrum, we discover new phenomena that in most cases were not predicted or even expected.

The Swift mission is no exception, its strength being the mission concept itself based on: multi-wavelength coverage with the on-board instrumentation, fast pointing capabilities of the satellite, tight international collaboration with team members permanently on duty, and worldwide networks with robotic and very large telescopes ready to respond in a matter of minutes. Facilities like the VLT, Keck, Gemini, Subaru, and many others, play a fundamental role with their fast response and high sensitivity. The fundamental discoveries made in the past year were made possible by the excellent level of coordination between Swift team members, ground-based telescopes and the GRB community at large. The key elements in this scientific enterprise, i.e. speed and coordination, were discussed and carefully planned over the years; they are now working very efficiently.

Back in 1963 Hoyle and Fowler pointed out that the energy source of a quasar or AGN could arise from a collapsed object or black hole. A flow chart originally due to Martin Rees illustrates different channels possibly leading to the formation of black holes, on a variety of scale lengths, always with gravity as the main player. We do not know the quantitative aspect of various processes but we are making important theoretical progress in the field. The energy that black holes irradiate can be produced in different ways, for instance via extraction of black hole rotational energy through the Blandford and Znajek mechanism, or via the more generally accepted mechanism involving the release of gravitational energy from matter inflowing through an accretion disc. Both mechanisms can be made to work on a sufficiently short time and with high enough efficiency to power GRBs, provided that nuclear density matter, possibly in the form of a torus, surrounds the

innermost regions around the event horizon of the black hole.

The collapse of a massive star towards a black hole occurs in a very short time and releases a very large amount of energy. Woosley, Paczyński and coworkers proposed the collapsar/hypernova model: the fast rotating iron core of a very massive star collapses and forms a rotating black hole surrounded by a very high-density accretion ring. This scenario was illustrated by the simulations of Zhang, Woosley and MacFadyen. Powerful relativistic jets along the polar axis are formed by extracting the potential energy and rotational energy via neutrinos or magnetic fields. Contrary to ordinary core-collapse supernovae (SNe), a collapsar/hypernova is also expected to expel matter at relativistic speed. This model envisages that long GRBs should go off mainly in star forming regions.

The coalescence of two relativistic stars (double neutron star or black hole/neutron star binary mergers) is the end result of 0.1–1 Gyr of orbital decay caused by the emission of gravitational waves. This paroxysmal event should also give rise to a black hole surrounded by a torus of matter at nuclear densities, possibly producing relativistic jets that are less energetic and shorter lived than those of collapsars and originating short GRBs. These merger events should, in general, be associated with galaxies having an older stellar population and take place, in a fraction of the cases, in the outskirts of (or even outside) the galaxy.

These are the two main models invoked to explain the two flavours in which GRBs manifest themselves: long and short. Gathering evidence in favour of this overall scenario is certainly among main results so far obtained by Swift, in conjunction with large ground-based telescopes, the ESO VLT facility in particular, where, thanks to the MISTICI and GRACE collaborations, most of the bursts visible from the southern hemisphere have been monitored. The deep significance of the ongoing research is not only that of putting together a complicated mosaic, but also trying to match at an unprecedented level the observational results with the predictions of the models. This

is what Swift can do in conjunction with ground-based telescopes: witnessing the birth of black holes surrounded by very dense matter, and extracting crucial new information from these events.

In the following we will refer in particular to the data obtained with the X-ray telescope onboard Swift and to the fast follow-up observations carried out especially with the ESO VLT. These are indeed the two facilities that allowed us to gather most of the information. Needless to say, none of this would have been possible without the Burst Alert Telescope (BAT) on board Swift, the instrument that detects the bursts. The sequence of events is led by the Swift satellite so that in this paper we will follow the same outline dictated by the Swift observations.

### X-ray light curves and optical observations

Thanks to the remarkable theoretical progress achieved in recent years, we now have a reasonably good understanding of the afterglow light curves observed in the soft X-ray band by Swift (Figure 1). Most of them are characterised by a steep early decline, followed by a milder one after a few hundred seconds, which breaks again to a faster decline generally in less than 10 000 seconds. The spectral shape does not change much in time, even in correspondence of the light curve breaks. The first break seems to mark the transition between the GRB tail and the long-lasting afterglow emission, which is continuously energised by the central engine (thus the decay is slow). The end of this energy input is marked by the second break. A further break is often visible due to the collimation of the ejecta. Such a break has been observed in long GRBs, while it has not yet been detected unambiguously in short bursts (a low significance indication has been reported by Fox and co-authors in GRB 050709). A minority of bursts do not display the early steep decline. The afterglow emission is produced by the so-called ‘forward shock’, produced in the impact between the GRB ejecta and the surrounding medium. There is additional emission from the ‘reverse shock’, produced inside the shocked ejecta themselves. This emission lasts for a rather short time and

**Figure 1:** Rest frame 0.2–10 keV light curves of GRB 050126 (light blue), GRB 050315 (blue), GRB 050318 (violet), GRB 050319 (red), GRB 050401 (green), GRB 050408 (dark green), GRB 050505 (dark blue). The dot-dashed line is a mean curve of the type-I (steep, shallow, steep) light curve. The squares on the top left of the figures represent the

mean luminosity of the prompt emission detected by BAT and converted to the XRT band pass. The inset shows four representative light curves, combining BAT and XRT data. There is a clear continuity between the two instruments. The light curve of GRB 050401 does not show the steep early decay.

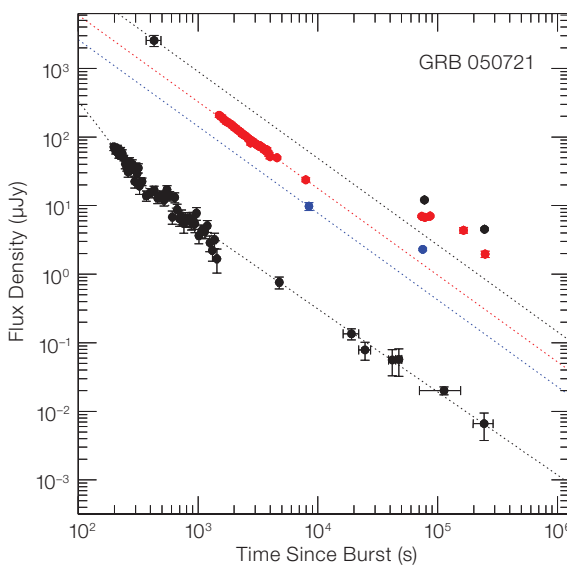
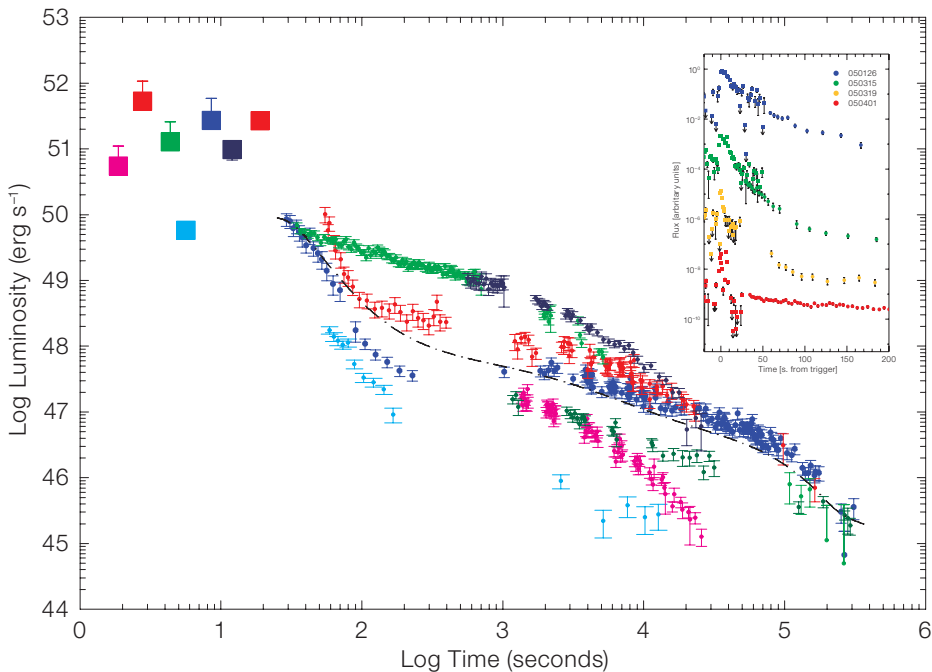


**Figure 2:** On the bottom of the figure the light curve obtained with the XRT in the 0.5–10 keV band. The black filled circle on the top of the figure represents the first optical observation in the *I*-band obtained by a Japanese robotic telescope. The other black filled circles are the *I*-band observations obtained at ESO. Always at ESO we observed in the R pass-band, red filled circles and in the blue pass-band, blue filled circles. The optical re-brightening of  $\Delta R = 1.8$  magnitudes is not present in the XRT observations at the bottom of the figure.

is mainly in the optical and infrared bands. However, depending on the distribution of matter in the ejecta, the emission can be long lasting. The phenomenon is quite complex and depends on the regime of synchrotron emission, the hydrodynamics of the jet and the interaction with the surrounding medium (that could be different in the various shocks) and the behaviour of the energy injection during the evolution of the afterglow. This is why observations in the optical and near infrared are very important and their potential

is to a large extent still to be exploited. There are still a number of unresolved issues: an especially important one is that in some cases an optical/NIR afterglow is not detected.

The observations of GRB 050721 (Figure 2) provide an excellent example of what is needed. The VLT rapid response mode allowed these early observations to be compared with the XRT light curve from the earliest stages, showing that both the X-ray and the R-filter light curves

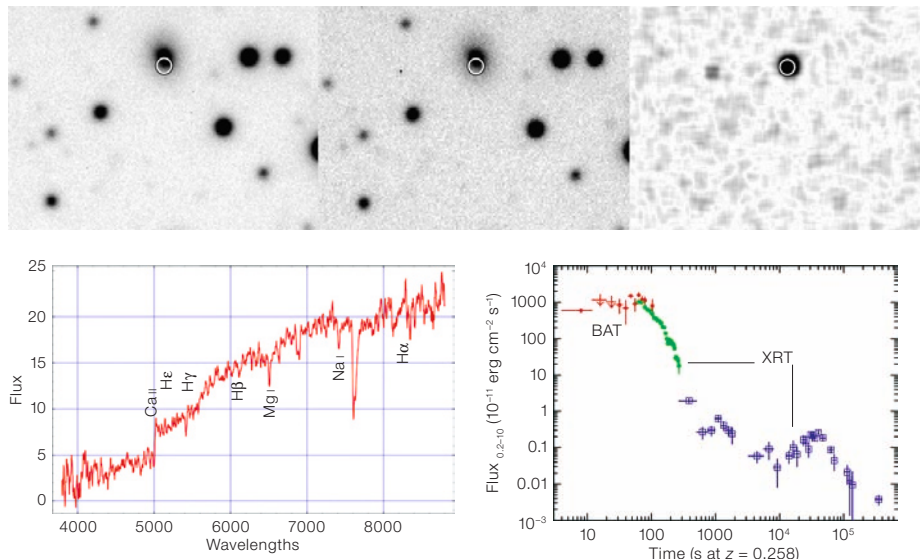
were decaying at a comparable rate. In this case, both the optical and X-ray emissions likely arise from a single component and it is not yet clear whether there is a reverse shock component. On the contrary, when an early rapid X-ray decay phase (e.g. the case of GRB 050713A) is present, the optical and XRT light curves differ significantly, indicating a different origin of the X-ray emission, which perhaps represents the soft tail of the prompt emission. A good coincidence between the optical and X-ray light curves has been observed also in GRB 050525A and GRB 050801. The VLT rapid response mode is a fundamental tool to build the statistics needed to discriminate amongst different models. In addition, detailed monitoring of the light curve might reveal short-timescale variability that may arise from the injection of energy from a highly variable central engine, the newly born black hole.

### Short gamma-ray bursts

The typical duration of a short burst is about 0.2 s. These bursts are spectrally harder than the long ones and comprise about 30 % of the BATSE (25–350 keV) sample, and about 10 % of the Swift sample. The rapid response of the Swift spacecraft yielded the first unambiguous detection of the X-ray emission from a short GRB, GRB 050509, in turn measuring the sky position of the event accurately enough to pinpoint the most likely host galaxy, an elliptical galaxy at  $z = 0.22$ . Excellent images were obtained with VLT, Subaru, HST, and other telescopes. Two months later HETE-II detected GRB 050709 and ESO telescopes were able to discover the optical counterpart and observe the host galaxy at a redshift of  $z = 0.16$ . About two weeks later Swift detected and observed GRB 050724 (Figure 3), and a few other short GRBs in the following months. After many years of chasing, the mystery of the counterparts to short GRB was finally solved.

These observations showed that the host galaxies of short GRBs are either of early type, as in the case of GRB 050509B, or harbour a reasonably old stellar population, as in the case of GRB 050709. This is much at variance with respect to

**Figure 3:** Left top panel: The image of the GRB 050724 plus the host galaxy obtained on the night of 24 July. Top centre panel: The image of the host galaxy plus GRB obtained on 29 July. Right top panel: The image obtained subtracting the two previous images (24 July – 29 July) showing the



long GRBs, which appear to be associated with dwarf galaxies with intense star-forming activity.

The relatively low redshift observed for these objects implies an energy output that is about a factor 100–1000 smaller than that observed for long bursts. For several of the short GRBs with accurate positions detected so far no optical after-glow could be found. In some other cases even the soft X-ray emission was not detected. A continuing programme of fast response observation by ground-based telescopes is essential in order to determine whether short GRBs comprise different subclasses. On the other hand, both long and short bursts are consistent so far with the same general scenario in which the GRB is generated by a newly formed black hole-torus system, resulting however from much different paths in the evolution of massive stars. It should be said that important alternatives exist. In Usov's model, the relativistic flow is mostly Poynting flux and is driven by the magnetic and rotational energies of a rapidly rotating neutron star.

### Flares

Flares were detected superimposed on the 'basic' X-ray light curves (Figure 1) in about 40 % of the bursts, during both the GRB tail (the steep decay phase) and in the early afterglow, in both GRB flavours (long and short), and at small as

detection of the short GRB. Bottom left panel: the VLT FORS spectrum of the host galaxy showing the characteristics of a rather old stellar population. Bottom right panel: the XRT light curve showing the presence of flares and the continuity between the BAT and XRT light curves.

well as high redshift (as in GRB 050724, GRB 050730, and GRB 050904; Figure 4). The energy emitted during a flare is sometimes comparable to the energy emitted during the entire X-ray afterglow, as in the case of GRB 050502B. This is a fundamental discovery made by the Swift mission and provides additional clues about the central engine. Flares might well be due to internal shocks resulting from new energy injection into the jet caused by an active central engine (as opposed to internal shock from the catching-up of shells emitted at different speeds).

No very large flare has been observed yet in the optical band; extensive optical coverage of the light curve during the early stages is essential to address this issue.

### Gamma-ray bursts and supernovae

The first suggestion of a possible connection between SNe and GRBs dates back to Colgate (1968). This prediction was confirmed in recent years, thanks to intensive optical and near-infrared follow-up observations of GRB afterglows discovered by BeppoSAX. These studies firmly established that long-duration GRBs (or at least a large fraction of them) are connected with the death of massive stars. The most persuasive evidence arises from observations of supernova features in the spectra of a few GRB after-

**Figure 4:** The BAT + XRT light curve of the long GRB 050904 at  $z = 6.3$ . The continuity between BAT (after conversion of the emission to the band pass of XRT) and XRT is perfect and the light curve shows the presence of flares. The top-right inset shows the optical observations (mainly from VLT) used to

estimate the photometric redshift. The light curve in various optical and near-infrared bands has been plotted in the inset on the bottom of the figure.

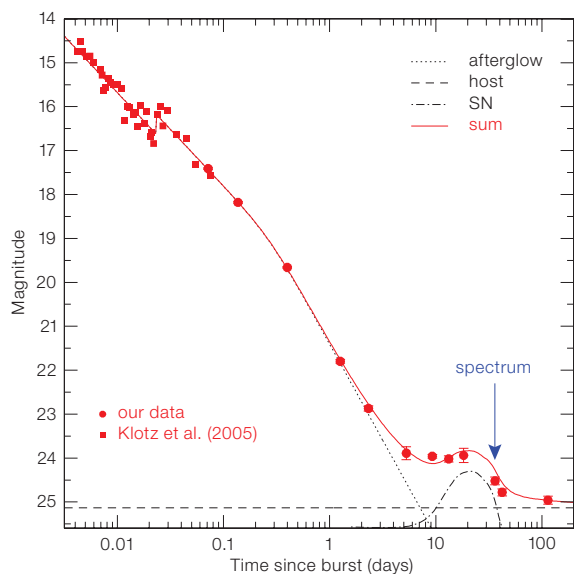
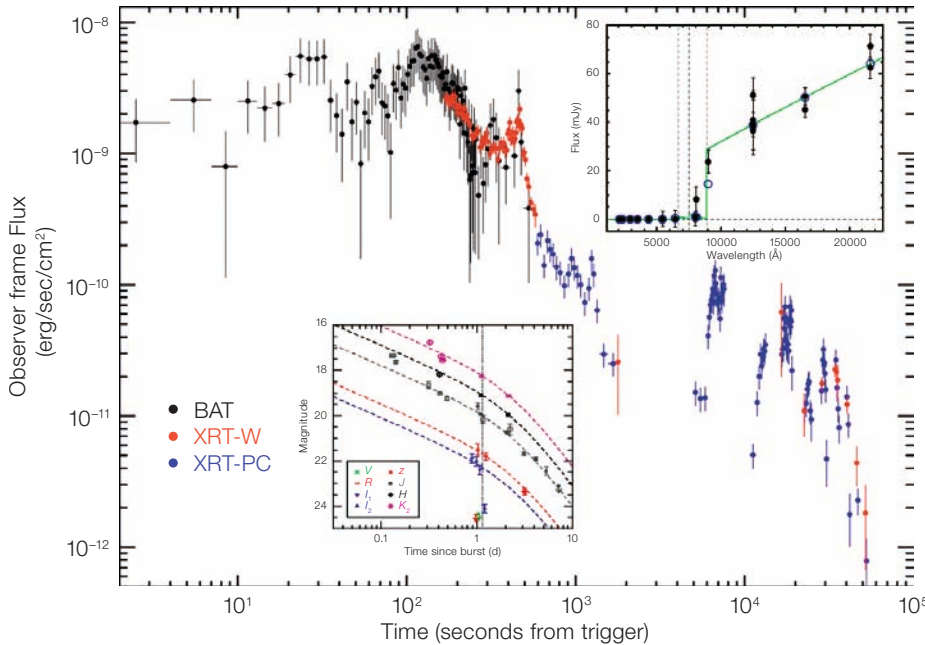


**Figure 5:** The photometric evolution of the afterglow of GRB 050525A, obtained at early stages with TNG and at later epochs with VLT-UT1 + FORS2, shows a flattening in the light curve starting about five days after the gamma event, followed by a sharp dimming. The magnitude and the duration of the flattening suggest the presence of a SN component (dot-dashed line), which is marginally fainter than SN 1998bw (Della Valle et al. 2006, ApJ, submitted).

glows. In a number of other cases, the evidence for a SN is based on a late time photometric hump emerging out of the decaying optical afterglows. Outstanding examples of this SN/GRB connection include SN 1998bw/GRB 980425, SN 2003dh/GRB 030329, and SN 2003lw/GRB 031203. The average redshift of Swift GRBs is quite large ( $\langle z \rangle \sim 2$ ), making the search for an associated SN difficult. GRB 050525A at  $z = 0.606$  is the first supernova detected in a GRB discovered by Swift. The photometric evolution (Figure 5), obtained at early stages

with TNG and NTT, and at later epochs with VLT, allowed us to discover a flattening in the light curve starting about five days after the GRB explosion, followed by a sharp dimming. The magnitude and duration of the flattening suggest the presence of a SN component, marginally fainter than the prototypical SN 1998bw, and characterised by a faster rise to maximum light. An early spectrum obtained by Foley and collaborators with Gemini North and GMOS indicates that GRB 050525A occurred in a star-forming galaxy. A spectrum obtained with

VLT UT1 + FORS2, during the flattening, shows strong similarities with the spectrum exhibited by SN 1998bw at about five days after the maximum. Therefore in this case we have also discovered a connection between a SN and a GRB. With a frequency of about  $4 \cdot 10^{-6}$  GRB per galaxy per year accounting for a jet angle,  $\langle \theta \rangle \sim 10^\circ$ , we have a frequency of  $\sim 4 \cdot 10^{-4}$  GRB per galaxy per year  $\sim 1/30$  the rate of Ibc supernovae.

While the discovery of a clear SN/GRB connection represented a major step in the study of GRBs, it also posed a number of new questions. Whether the association is restricted to bright SNe, as the cases with spectroscopic confirmation seem to indicate so far, or is open also to fainter type-Ibc SNe, remains to be established through forthcoming observations. Based on a reasonably large sample, we may finally track down the physical mechanism of the association and understand how the explosions evolve in time. There is no indication at all in the short GRBs 050709 and 050724 of the signature of a supernova, although they are quite nearby.

### Cosmology and the new frontiers

It is fascinating to consider the possibilities opened in cosmology by GRBs. Indeed, after the detection of GRB 050904 and the measurement of its redshift ( $z = 6.3$ ) by the VLT and the SUBARU telescopes, our wildest hopes became reality. We can now likely trace the star-formation rate and its evolution. Furthermore, since for a few hours after their onset, GRB afterglows are the brightest beacons in the far Universe, they offer a superb opportunity to investigate the environment in which they go off in very young galaxies, determine the properties of the interstellar medium and determine cosmic abundances up to the re-ionisation epoch. The GRACE and MISTICI collaborations achieved milestone discoveries in this field. Here we can only touch upon this fascinating research briefly.

One of the straightforward discoveries of UVES high resolution spectroscopy of GRB afterglows is that the ISM of GRB host galaxies is complex, with many

components resolved down to a width of a few tens of km/s, contributing to each main absorption system, and spanning a total velocity range of up to thousands of km/s. The absorption systems can be divided into three broad categories. First, those associated with the GRB surrounding medium; second, those associated with the ISM of the host galaxy along the line of sight, which is far enough so that it is not affected by the GRB emission; last, the intergalactic matter along the line of sight. Strong ‘fine structure’ lines have been detected in GRB 050922C and in GRB 050730 (previously these were also detected in GRB 020813, GRB 030323 and in GRB 021004). The presence of strong fine structure lines of several ions,  $\text{C II}^*$ ,  $\text{Si II}^*$ ,  $\text{O I}^*$ ,  $\text{O I}^{**}$ ,  $\text{Fe II}^*$ , is at odds with QSO absorption systems, where, despite more than 30 years of investigation, only sparse detections of fine structure lines are available. Strong fine structure lines in GRB sightlines are most likely due to the dense environment of the star-forming regions hosting GRBs. Furthermore, GRB afterglows provide a new, independent tool to study the ISM of high-redshift galaxies. Figure 6 illustrates the UVES spectrum of GRB050922C, but a very similar situation is also present in the spectrum of GRB050730. About six absorption systems of relatively high ionisation are detected, likely associated with the GRB surrounding medium. On the other hand, we also observe a  $\text{Si III}\lambda 1304$  component (marked HG in Figure 6) that is not present in either the  $\text{Si IV}$  or  $\text{Si II}^*$  transitions. This is an indication that the gas of this component is much less dense and ionised than that of the other six components, suggesting that this component is not part of the cloud surrounding the GRB but rather belongs to the ISM of the host galaxy.

Finally, GRB afterglows can be used to probe the  $\text{Ly}\alpha$  forest and the high-redshift intergalactic medium (Figure 7). An accurate determination of the number of absorption systems per unit redshift  $dn/dz$  at high redshift has strong implications for any investigation of the reionisation epoch, since the optical depth due to  $\text{Ly}\alpha$  line blanketing is evaluated by extrapolating the  $\text{Ly}\alpha$   $dn/dz$  measured at lower redshifts. Using GRBs as remote beacons opens up the opportunity of highlighting any deviation from what is already known

from quasar forests. For example the so-called ‘proximity effect’ should be much reduced for GRB. By using GRBs as very remote beacons, carbon, silicon, oxygen and iron ions, as well as  $\text{Ly}\alpha$ , can be studied with UVES up to  $z \sim 6$ –6.5 and with ISAAC up to the reionisation epoch, thus yielding the first metal abundance measurements at epochs when the Universe was less than 1 Gyr old.

### Conclusions

It is by now evident that GRBs provide us with a new fascinating perspective in relativistic astrophysics and Cosmology. The central engine of GRBs must be capable of producing, in a matter of seconds, energies of the order  $10^{49}$ – $10^{52}$  erg, which result in the acceleration of a planetary-mass jet of plasma to ultrarelativistic speed. The energy and duration of the prompt emission and the characteristics of the parent galaxies, including their locations inside them, suggest that both GRB types, long and short, may well end up in the same configuration, consisting of a newborn black hole surrounded by an ultradense torus. However the two GRB types would be the final outcome of two extremely different evolutionary paths: the long bursts may arise in the collapse of the iron nucleus of a very massive star,

while the short bursts might originate from the merging process of a relativistic binary. GRB afterglows can be used to probe the IGM during the reionisation epoch, through the detection of metal systems associated with early starburst winds. High-resolution UVES observations are already giving us precious information on the kinematics, ionisation and metallicity of the interstellar matter of GRB host galaxies up to a redshift of  $z \sim 4$ . Further optical and near-infrared spectroscopy will allow us to extend further the redshift range, possibly up to the reionisation epoch. These were amongst the main motivations for building the REM telescope, a robotic, fast-slewing facility capable of observing the early optical and near-infrared GRB afterglows. However, Swift has shown that most GRB counterparts are fainter than expected in the optical and NIR, so that we must work even more with medium and very large telescopes.

### References

Barthelemy, S. D. et al. 2005, *Nature* 438, 994  
 Chincarini, G. et al. 2003, *The Messenger* 113, 40  
 Woosley, S. E. 1993, *ApJ* 405, 273  
 Cusumano, G. et al. 2006, *Nature* 440, 164  
 Della Valle, M. et al. 2004, *The Messenger* 118, 31  
 Fiore, F. et al. 2005, *ApJ* 624, 853  
 Gehrels, N. et al. 2004, *ApJ* 611, 1005  
 Tagliaferri, G. et al. 2005, *A&A* 443, L1

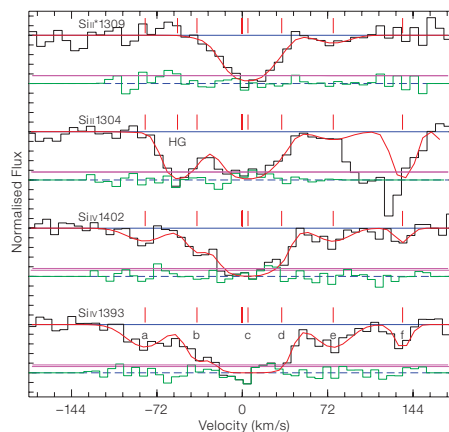


**Figure 6:** The UVES spectrum of GRB 050922C around the the  $\text{Si IV}\lambda 1393$ ,  $\text{Si IV}\lambda 1402$ ,  $\text{Si III}\lambda 1304$  and  $\text{Si II}^*\lambda 1309$  lines. The zero of the velocity scale refers to the redshift of the host galaxy,  $z = 2.199$ . Six components, labelled from ‘a’ to ‘f’, are identified for the  $\text{Si IV}\lambda 1393$  and  $\text{Si IV}\lambda 1402$  lines, spanning a velocity range from  $-75$  to  $+140$  km/s. Each component has a width from 10 to 25 km/s. The main component ‘c’ has nearly zero velocity shift.

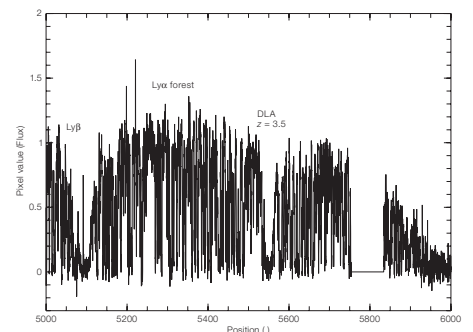


**Figure 7:** UVES spectrum of the  $\text{Ly}\alpha$  forest of GRB 050730. Note the strong  $\text{Ly}\alpha$  absorption at the redshift of the GRB host galaxy ( $\log N_{\text{H}}$  in the range 21.2–22.2). Taken at face value the  $[\text{C}/\text{H}]$ ,  $[\text{O}/\text{H}]$ ,  $[\text{S}/\text{H}]$  and  $[\text{Si}/\text{H}]$  ratios imply a metal abundance between 1/10 and 1/100 of the solar value.

# The ALMA-Herschel Synergies

Paola Andreani<sup>1</sup>  
Tom Wilson<sup>2</sup>

<sup>1</sup> INAF – Osservatorio Astronomico di Trieste, Italy

<sup>2</sup> ESO

One of the ESO-ESA science planning working groups has studied joint opportunities offered by Herschel and ALMA in the infrared and submillimetre bands. A brief summary of the report edited by David Elbaz and Tom Wilson is given here.

The ESA/Herschel Satellite and the Atacama Large Millimeter Array (ALMA) are two large projects in astronomy to investigate the submillimetre and Far Infra-Red (FIR) range. Herschel covers the wavelength range from 60 to 625  $\mu\text{m}$  (480–5000 GHz), while ALMA, an international project in which ESO has the European leadership, covers the range 320  $\mu\text{m}$  to 1 cm (30–950 GHz). Both Herschel and ALMA will come into operation in similar timeframes. ALMA is planned to be completed in 2012, but ‘early science’ operation will begin well before this time. The launch of the Herschel satellite is planned for August 2007 with an expected lifetime longer than three years. Thus there should be an overlap in the time when both are in operation<sup>1</sup>.

Although the two facilities overlap in wavelength range they are ‘complementary’. They will lead to major advances in many fields of astronomy, especially those related to the origins of planets, stars and galaxies. The crucial questions are: (1) How do galaxies form? (2) How do stars form? and (3) What is the life cycle of a dust grain, and how does this depend on environment? The birth of planets, stars and galaxies is hidden by

<sup>1</sup> A description of the bilateral (North America-Europe) ALMA is at <http://www.alma.nrao.edu/projectbk/construction/>. Accounts of ALMA science are in Shaver (1996) and Wootten (2001). The web site for the Herschel project, including all instruments, is <http://www.rssd.esa.int/Herschel/>. Accounts of Herschel and ALMA, some plans for Herschel science, ALMA science and their synergies are to be found in the Proceedings of “The Dusty and Molecular Universe” (ed. A. Wilson 2005).

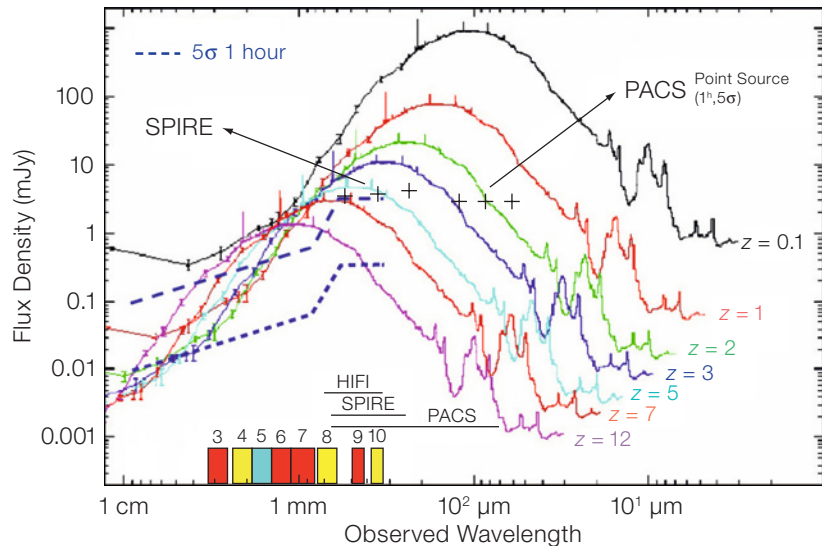


Figure 1: A plot of the emission from the starburst galaxy M82 for different redshifts,  $z$ . The horizontal axis is observed wavelength, the vertical axis is predicted flux density in mJy. The crosses show the sensitivity of the Herschel bolometers. The dashed lines at the left side of this diagram show the  $5\sigma$

sensitivity of ALMA. The lower dashed curve is for the 64-antenna ALMA and the upper dashed curve for a 6-antenna ALMA. PACS, SPIRE and HIFI are Herschel receiver bands. The ALMA bands are shown numbered.

interstellar dust. The cocoons of forming objects are deeply embedded within gaseous dusty clouds where optical extinction can be extremely large and prevents the study of these fundamental processes with traditional optical telescopes. However, cool material emits submm and FIR radiation. By exploring this wavelength range we can directly measure physical phenomena associated with the formation process itself. The third question may seem less fundamental, but since FIR/submm telescopes measure radiation from dust, an accurate characterisation of dust properties is a prerequisite for answering the other two questions.

In the local Universe 30% of the galaxies emit in the FIR/submm because they are dust enshrouded and forming stars. This fraction grows steeply up to redshift  $z = 1-2$  and flattens off at earlier times, to  $z > 6$ , as inferred from the evolution of the cosmic luminosity density. This means that at redshifts larger than 1 the population of galaxies dominating cosmic energetics is that of dusty starburst galaxies, i.e. objects that are rapidly forming stars.

Figure 1 shows the Spectral Energy Distribution (SED) of the starburst galaxy

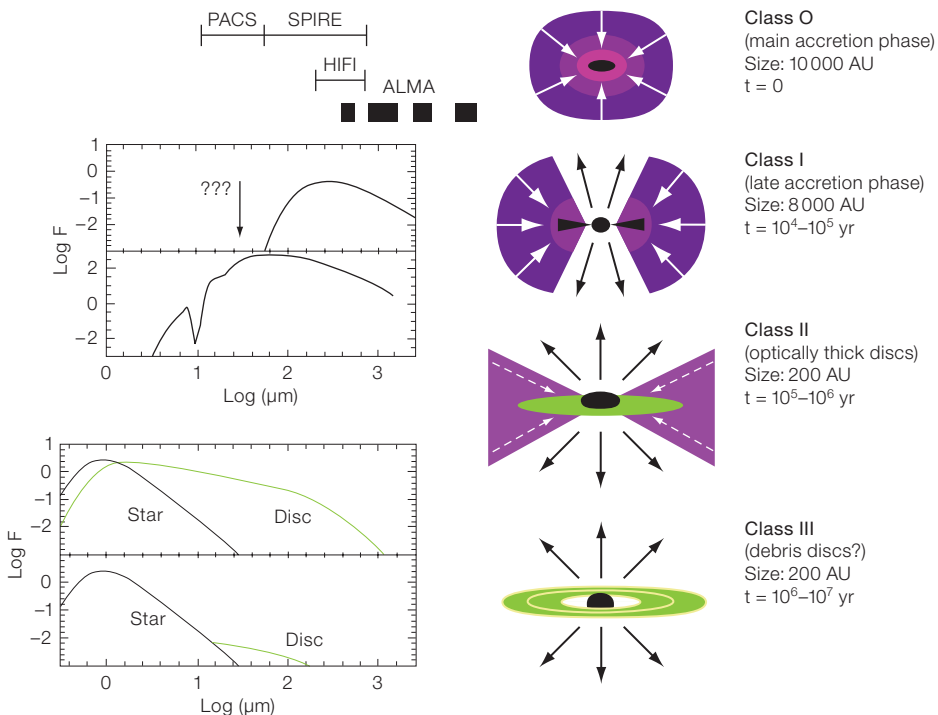
M82, where the broadband radiation peaks in the FIR/submm. This is mostly due to thermal radiation from dust. This continuum radiation is consistent with temperatures in the range 10–100 K. In the FIR/submm/mm there are also spectral lines, mostly from molecular species, although there are prominent atomic fine structure lines of various ionisation stages of oxygen, carbon, silicon and nitrogen. Objects like M82 were much more frequent in the past. With the full ALMA we expect to detect ‘M82-like’ objects even at redshifts up to 12. As Figure 1 shows, if this SED is shifted in redshift, we witness a peculiar effect, called the ‘negative K-correction’, which greatly facilitates the detection of high-redshift objects at FIR/submm wavelength. The thermal spectrum and characteristics of dust emission makes the observed flux density constant at Herschel and ALMA wavelength range over a wide value of redshifts. This Figure shows that the broadband emission of sources such as M82 can be detected with Herschel and the early science ALMA even at high redshifts.

Our knowledge of the star-formation process is still very limited. Figure 2 shows a sketch of the four stages of star formation, from the collapse of a molecular

cloud to the formation of a star surrounded by a disc. Cloud collapse requires high interstellar gas densities and low kinetic temperatures. The starting point is a gravitationally-bound 'pre-stellar core'. For column densities  $N > 10^{18} \text{ cm}^{-2}$  and densities  $n > 10^2 \text{ cm}^{-3}$ , interstellar gas consists mostly of molecular hydrogen,  $\text{H}_2$  and helium. This is a molecular cloud. The  $\text{H}_2$  molecule does not produce emission lines if kinetic temperatures are below  $\sim 100 \text{ K}$  and there are no shock waves. Then the abundances of the  $\text{H}_2$  molecules must be traced indirectly. At high density, in cold clouds, grain properties change and constituents of the gas will condense onto grains. From millimetre-submm maps the mass distribution of pre-stellar cores is remarkably similar to the Initial Mass Function. These pre-stellar cores begin to collapse as the result of processes which may involve ambipolar diffusion, the dissipation of turbulence, or an outside impulse. Once begun, the gravitational collapse is rapid, ending in the formation of a hydrostatically-supported protostar in the centre. During the main accretion phase, the central object plus an accretion disc gradually builds up its mass from a surrounding envelope of matter while progressively warming. The protostar evolves from the Class 0 phase, in which the mass of the envelope is much greater than the mass of the protostar + disc, through the Class I stage, in which the mass of the protostar + disc becomes greater than the mass of the surrounding envelope, to the Class II stage, in which material in the envelope becomes sufficiently rarified that the protostar becomes visible to traditional optical telescopes. These phases can be distinguished by the shape of the FIR/submm SED.

With broadband data from Herschel/SPIRE and Herschel/PACS the SED shortward of the peak of the luminosity curve will be measured, with ALMA the longer wavelength part, so the total luminosity will be measured with accuracy. The Herschel spectrometers will measure the fine structure lines of atomic species and rotational and vibrational transitions of molecular species, without absorption in the Earth's atmosphere. This is especially important for water vapour lines, whose abundance has a strong influence on the energy balance and chem-

Figure 2: A sketch of the development of a low-mass protostar and its disc (after Charles Lada, Figures: Michiel Hogerheijde). Above on the left side are shown the wavelength coverage of the Herschel instruments PACS, SPIRE and HIFI. The ALMA receiver bands from left to right are Band 9, Bands 6 and Band 3 in the bilateral ALMA project. With the addition of Band 5 and Bands 4, 8 and 10, the coverage of ALMA receiver bands provides a solid block in the uppermost part of the figure under 'ALMA'. These will also fill the longer wavelength part of Herschel HIFI coverage, marked 'HIFI'.



istry. The higher angular resolution of ALMA images will help to refine the analysis of models based on Herschel data. The final result will be the distribution of  $\text{H}_2$ , selected atoms, molecules and dust, as well as their dynamics.

The Herschel PACS and SPIRE bolometer systems are well suited to surveying rather large regions of the sky, whereas ALMA can provide high sensitivity, high angular resolution images in spectral line and continuum, but these will usually be limited to a few arc minutes in size, at most. ALMA and Herschel/HIFI are heterodyne instruments, and will be able to resolve even the narrowest lines in velocity. Thus, ALMA is better suited to be a follow-up instrument for Herschel surveys. Such follow-ups could be in CO lines, to determine the redshifts of sources detected in the dust continuum, or in broad-band continuum to provide the component of spectral energy distributions at longer wavelengths. For spectral lines, ALMA will be complementary to Herschel because of different frequency ranges and attenuation in the Earth's atmosphere of most lines of water vapour. The higher angular resolution of ALMA provides high-resolution images of many spectral lines and allows better estimates of source sizes, the variations

of abundances on scales finer than a few arc seconds and thus the true source averaged abundances of species which are those needed for chemistry models.

ALMA data alone and Herschel data alone will be a great step forward. A combined ALMA-Herschel data set will be a tremendous advance. A number of conditions must be fulfilled to combine Herschel and ALMA data sets. First, the calibrations for both instruments and cross calibration must be well determined and consistent. This will require a rather extensive set of Herschel measurements and subsequently, accurate models of the calibration sources. The signal-to-noise ratios must be excellent and the angular sizes of the calibrators well determined. This may restrict calibrators to Solar System objects. Herschel cannot observe sources closer to the Sun than Earth, because of Sun avoidance. Also the detectors will saturate when observing intense sources, so the calibrations may have to be done using the emission from asteroids such as Vesta, Ceres, moons of outer planets, or smaller planets such as Uranus, Neptune or Pluto. PACS and SPIRE cross calibration with ALMA will be more complex because the bandwidths of these instruments are much larger than those possible with ALMA.

For any spectral line surveys with Herschel, follow-up measurements with ALMA will greatly increase the scientific value. However, it must be stressed that this requires Herschel surveys to be as complete as possible.

For an efficient synergy, ESA should devote Herschel time to Legacy projects, i.e. projects of large interest for the community, starting soon after the science verification phase and/or during the very early Herschel lifetime. It should make data available to the community as soon as possible, and provide access to data-reduction tools and calibration. This would be the case for Herschel surveys of Galactic and extragalactic sources, in continuum and spectroscopy.

Most efficient would be a scheme in which ESO reacts quickly to Herschel data. It would be useful to allocate ALMA observ-

ing time as soon as possible to measure variable sources, newly discovered sources, peculiar objects or in general to perform a complete follow-up both in line and continuum of selected fields.

The data sets that will be produced by Herschel and ALMA will be so large that there may have to be special data-reduction procedures to insure the optimal synergy. The analysis and comparisons with models will have to be made on an automatic basis without human intervention. Such computer analysis programs have been developed by Schöier et al. (2005), for example, but these must be further developed to accommodate the very large data sets that will be produced by ALMA and Herschel in the near future.

The contributors to the scientific content of the report are: Paola Andreani (Trieste),

Dominique Bockelée-Morvan (Paris), José Cernicharo (Madrid), Pierre Cox (Grenoble), Carlos De Breuck (ESO), Ewine van Dishoeck (Leiden), David Elbaz, Maryvonne Gerin (Paris), Robert Laing (ESO), Emmanuel Lellouch (Paris), Göran Pilbratt (ESA), Peter Schilke (Bonn), Christoffel Waelkens (Leuven), Tom Wilson and Martin Zwaan (ESO).

#### References

- Schöier F. et al. 2005, A&A 432, 369
- Shaver P. 1996, Science with Large Millimeter Arrays, Springer Verlag.
- Wilson A. 2005, The Dusty and Molecular Universe ESA-SP577, ESTEC, Noordwijk, the Netherlands
- Wootten A. 2001, Science with the Atacama Large Millimeter Array (ALMA), ASP Conference Series, Vol. CS 235

## ESO at AAAS

### Claus Madsen (ESO)

Even casual observers of ESO will have noticed a steady increase in public visibility for our organisation and its projects over the recent years. This increase is the result of a many-sided but focussed effort in public communication about ESO. Entertaining information stands at key fairs and conferences are part of this effort, and ESO's presence at this year's Annual Meeting of the American Association for the Advancement of Science – though a 'first' for us – is therefore no coincidence. This meeting is arguably the largest gathering of its kind worldwide. Indeed, no other event manages to attract more science journalists including a substantial number from Europe, which is certainly one of the reasons why more European organisations have begun to think about participating. Another reason is that the annual AAAS meetings provide plenty of opportunities for exchanges between American and European scientists and science policy makers.

This year's meeting took place on 16–20 February at America's Center in St Louis, Missouri. With an estimated 4000 participants this meeting was one of the 'smaller' AAAS

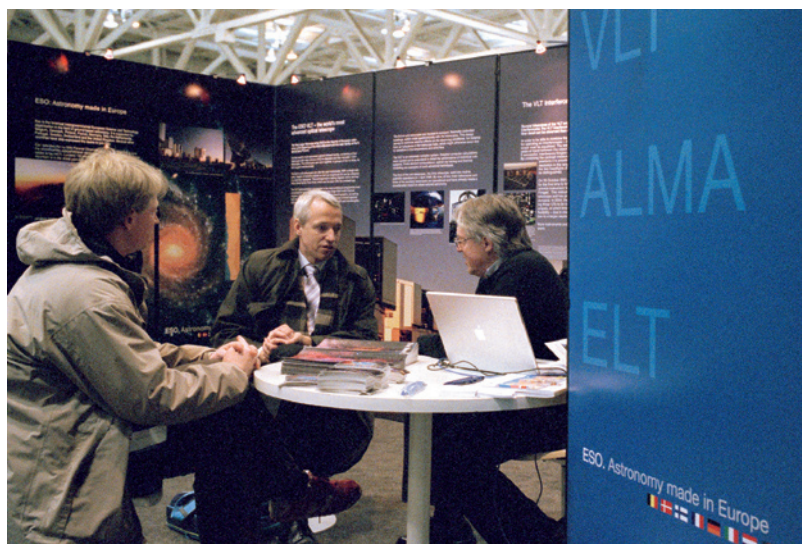


Photo: E. Janssen, ESO

gatherings, but nonetheless it featured nearly 200 symposia, plenary and topical lectures, in-depth seminars, poster presentations, career workshops, etc. in addition to a major exhibition. ESO's 30 sq m information stand was located in the main exhibition hall, located near the stands of the National Science Foundation and the European Commission.

Dr. Herbert Munder (middle), one of the organisers of Euroscience Open Forum 2006, at the ESO stand.

## Latin American Summer School: A Key Event for Future Astronomers

Gonzalo Argandoña, Felix Mirabel (ESO)

More than 200 students gathered in December at ESO-Vitacura for the first multi-thematic Latin American Astronomy Summer School, organised jointly by ESO and the Chilean Astronomical Society (SOCHIAS).

From 8 to 10 December, enthusiastic students and young researchers from 18 different countries had the chance to review important front-line areas of research, presented by major players of those fields.

“Given the large interest in attendance, this summer school could possibly turn out to be one of those meetings of historical significance for the development of astronomy in South America”, commented Bob Williams (STScI, USA), one of the invited speakers, at the opening of the event.

Besides the large number of students from Chile, other countries well represented among the attendees were those from Latin America with longer traditions in astronomical research, such as Argentina, Mexico and Brazil. Even students from countries with incipient departments of astrophysics – such as Honduras or Guatemala – were also present at the conference. Finally, young researchers from Europe attended too, attracted by the series of powerful astronomical facilities operating in northern Chile.

In the first day of the event, Malcolm Longair (Cambridge University, UK) presented an overview of the history of 20th-century cosmology, complemented in the following days by talks on the most luminous radio galaxies, physics of galaxy formation and the cosmic microwave background.

Pat Osmer (Ohio State University, USA) offered a series of talks about quasars, while Dante Minniti (Pontificia Universidad Católica, Chile) described in detail present and future methods for the search for extrasolar planets as well as current models for planetary formation.



Photos: I. Lemus, ESO (2)

Other speakers were Gloria Dubner (IAFE/CONICET, Argentina), Luis Felipe Rodríguez (UNAM, Mexico), Felix Mirabel (ESO, Chile) and Monica Rubio (SOCHIAS, Chile).

This event was the perfect preamble to the 11th Latin American Regional Meeting of the International Astronomical Union (IAU), held just the week after, on 12–16 December in Pucon, Chile.

Given the outstanding success of the summer school and its considerable impact on the education of future astronomers from Latin America, it is now being proposed that such multi-thematic schools should take place associated with the future Regional Meetings of the IAU.

The first multi-thematic Latin American Astronomy Summer School generated large interest among students. At the centre of the picture, some of the speakers (from left to right): Gloria Dubner (IAFE/CONICET, Argentina); Pat Osmer (Ohio State University, USA); Luis Felipe Rodríguez (UNAM, Mexico); Felix Mirabel (ESO); Bob Williams (STScI, USA); Malcolm Longair (Cambridge University, UK) and Dante Minniti (PUC, Chile).

Professor Bob Williams (former director of STScI, USA) stimulated young researchers with the possibilities for research on the distant, early Universe.



# Groups of Galaxies in the Nearby Universe

held in Santiago de Chile, 5–9 December 2006

Ivo Saviane, Valentin D. Ivanov,  
Jura Borissova (ESO)

For every galaxy in the field or in clusters, there are about three galaxies in groups. Therefore, the evolution of most galaxies actually happens in groups. The Milky Way resides in a group, and groups can be found at high redshift. The current generation of 10-m-class telescopes and space facilities allows us to study members of nearby groups with exquisite detail, and their properties can be correlated with the global properties of their host group. Finally, groups are relevant for cosmology, since they trace large-scale structures better than clusters, and the evolution of groups and clusters may be related.

Strangely, there are three times fewer papers on groups of galaxies than on clusters of galaxies, as revealed by an ADS search. Organising this conference was a way to focus the attention of the community on the galaxy groups. We also wanted to offer a venue where people coming from various research fields could meet and discuss groups from different perspectives. All this happened in a friendly atmosphere created by Hotel Torremayor in Santiago.

The discussion was organised in seven sessions, introduced by invited reviews: Eva Grebel (Local Group versus Nearby Groups), Vince Eke (Groups Searches and Surveys), Chris Conselice (The Evolution of Galaxies in Groups – Observations), Gary Mamon (The Evolution of Galaxies in Groups – Theory), Ann Zabludoff (Evolution of Groups as Systems), Trevor Ponman (Interstellar Medium and Intragroup Medium), Stefano Borgani (Groups in a Cosmological context), and finally Ken Freeman (Conference Summary). There were almost 50 contributed talks and 30 posters. Most speakers agreed to share their presentations with the astronomical community at <http://www.sc.eso.org/santiago/science/NGG/finalprogram.html>. Here we give a short summary of the main conference ideas, mostly based on the invited reviews.

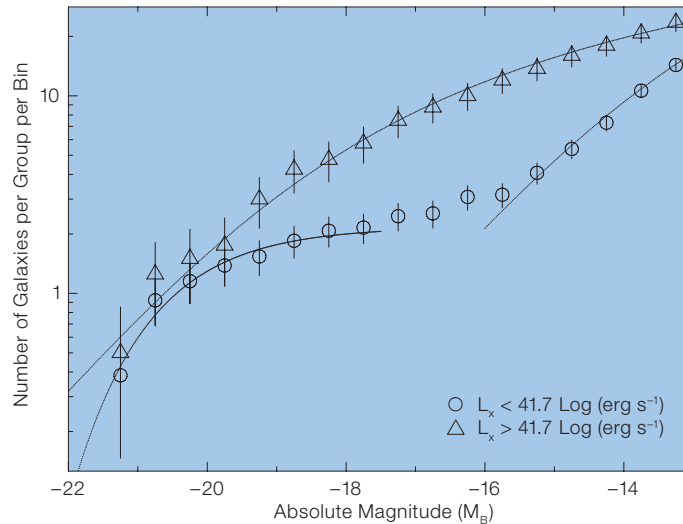


Figure 1: Cumulative  $B$ -band luminosity function of 25 GEMS groups of galaxies grouped into X-ray-bright and X-ray-faint categories, fitted with one or two Schechter functions, respectively (Miles et al. 2004, MNRAS 355, 785; presented by Raychaudhury). Mergers could explain the bimodality of the luminosity function of X-ray-faint groups.

## All you wanted to know about groups (but were afraid to ask)

Groups are bound structures with masses in the range  $M = 10^{12-14} M_{\odot}$  (Eke), containing less than fifty galaxies (Conselice), and with typical sizes of a few Mpc. Groups detected in X-rays have luminosities of  $L_x = 10^{41-43} \text{ erg sec}^{-1}$  and gas temperatures of  $kT = 0.1-3 \text{ keV}$  (Ponman). Most of the stellar mass in the present Universe is in groups similar to the Local Group with masses  $\sim 2 \times 10^{12} M_{\odot}$  and only 2% is in clusters with  $M > 5 \times 10^{14} M_{\odot}$  (Eke). Groups were already present at redshifts  $z > 1$  (Conselice). Cosmological simulations predict a much larger number of galaxy satellites than observed, and  $\text{H I}$  high-velocity clouds cannot fill in this gap (Pisano). Groups follow a fundamental plane (Muriel), and the most massive ones have an X-ray halo with an extended component (Zabludoff).

A special class of groups are the so-called ‘fossil groups’ – isolated ellipticals with properties similar to a group, which could be the final stage of a collapsed group. However, most isolated ellipticals are not collapsed groups (Forbes). There are only 15 fossil groups known to date.

The evolution of low-velocity dispersion groups is dominated by mergers, which could explain the bimodal mass function of the X-ray-faint groups (X-ray-faint groups tend to have low-velocity dispersion, and vice versa), if intermediate-mass members merge to build the largest group members (Raychaudhury). The bimodal mass function (see Figure 1), similar to that of clusters, is confirmed in compact groups (Bomans). Compared to compact groups, the loose ones tend to have fewer low-mass members.

The results presented here were obtained thanks to large observational efforts (Table 1). Historically, the first group catalogues were biased toward compact groups, which are the easiest to identify from imaging surveys. Modern redshift surveys allow selections including recession velocities, and finding algorithms can be tested on mock catalogues generated with dark matter (DM) simulations (Eke).

## Galaxies in groups

Galaxies in groups can be affected by processes like ram pressure stripping, in-

Table 1: Summary of the state-of-the-art group catalogues and surveys discussed at the meeting.

Name	Description	Reference
160 and 400 square-degree ROSAT surveys	14 groups were studied to compute the mass and compare mass-to-light ratios with simulations	Vikhlinin et al. 1998, ApJ 502, 558 (presented by A. Hornstrup)
2PIGG (2dFGRS Percolation-Inferred Galaxy Group) catalogue	The largest available homogeneous sample of galaxy groups, public	Eke et al. 2004, MNRAS 348, 866
ALFALFA (Arecibo Legacy Fast Alfa (= Arecibo L-Band Feed Array)) survey	Large-scale survey of extragalactic HI over 7000 square degrees of sky, up to $cz = 18\,000$ km/s. Spectral resolution is 5 km/s. It can detect HI clouds with more than $10^7 M_{\odot}$ throughout most of the Local Supercluster	Giovanelli 2005, AAS 207, #192.03
AMIGA project (Analysis of the Interstellar Medium of Isolated Galaxies)	Multiwavelength database of isolated galaxies, including optical (B and H $\alpha$ ), infrared (FIR and NIR) and radio (continuum plus HI and CO lines)	Verdes-Montenegro et al. 2005, A&A 436, 443
CNOC2 (Canadian Network for Observational Cosmology) survey	Spectroscopically selected catalogue of 200 groups at intermediate redshift over 1.5 square degrees on the sky	Carlberg et al. 2001, ApJ 552, 427
GEMS (Group Evolution Multiwavelength Study) project	Catalogue of 60 galaxy groups at 15–130 Mpc distance. Plus: X-ray (ROSAT PSPC 10 000 sec, 1.5 degrees), optical imaging (0.5 degrees), Parkes HI mapping (5.5 degrees), ATCA HI follow-up, 6 dFGS spectra, 2 MASS K-band photometry, XMM/Chandra imaging, Mock catalogues	presented by Forbes
HI survey of six loose groups	Observations of six spiral-rich, loose groups between 10.6–13.4 Mpc, over 25–35 square degrees: Parkes Multibeam and ATCA; Mass sensitivity of $5\text{--}8 \times 10^5 M_{\odot}$	presented by Pisano
LVHIS (Local Volume HI Survey)	HI imaging of all nearby (distance less than 10 Mpc), gas-rich galaxies; deep 20-cm radio continuum imaging with ATCA and VLA; deep H-band and H $\alpha$ imaging	presented by Koribalski
Sharc (Serendipitous High-redshift Archival ROSAT Cluster) survey	638 ROSAT PSPC observations with $ b  > 20$ degrees and exposure time greater than 10 000 seconds; total 178.6 square degrees; found the most distant fossil group at $z = 0.59$	Romer et al. 2000, ApJS 126, 209 (presented by F. Durret)

interactions and harassment, mergers, group tidal field, gas loss and suppressed star formation (also known as strangulation or suffocation). Merging is the most important of them because of the low relative velocities of galaxies in groups in comparison with the galaxies in clusters. Simulations show that mergers induce an intense and brief (of the order of a hundred Myrs) surge of star formation before the final coalescence into a spheroid, which evolves passively afterwards. Simultaneously, mergers transfer momentum from the interacting galaxies to the group as a whole, thereby increasing the group velocity dispersion. Indeed, observations show that there are more spheroids in groups with higher velocity dispersion (Zabludoff).

Eventually, the feedback from the residual black-hole and active galactic nucleus (AGN) reduces the star formation by a factor of ten or more. At least 50 % of galaxies in compact groups are low-luminosity AGNs (Martinez), while the field fraction is only 30 %. Moreover, the cores of X-ray groups are often disturbed, which could be additional evidence for AGN feedback (O’Sullivan). The selective suppression of star formation in larger group members could explain the downsizing phenomenon – the decrease of the maximum luminosity of star-forming galaxies

at lower redshifts. Mergers occur mostly at redshifts  $z > 1$ : for example at  $z = 2.5$  about 50 % of bright galaxies are undergoing mergers, while today only 2 % of galaxies merge per Gyr (Conselice). Most of the stars in group members also formed between redshifts  $z = 2.5$  and 1.

Locally, environmental effects can be traced directly by reconstructing star-formation histories of individual galaxies. For example, the fraction of intermediate-age stars of Milky Way dwarf satellites depends on their distance from the Galaxy. On the contrary, this fraction is constant in M81 satellites (Da Costa), probably due to the compactness of the M81 group, where multiple close encounters have homogenised their star-formation histories.

### The evolution of groups

The origin of groups is probably related to large-scale gaseous filaments at high redshift. Before virialisation, smooth accretion, supernovae and AGN activity enhance the entropy, and the metal-enriched gas cannot be retained by the shallow potential of pre-collapse groups (Ponman, Borgani). During the virialisation, the central spheroidals grow via mergers. Early-type stars and enriched

gas become part of the intragroup environment. Eventually, common dark matter and hot (X-ray) gas halos are formed (Zabludoff). The X-ray emission increases, and the X-ray halo becomes more and more regular. Later, the diffuse DM distribution will reduce the merger rate and moderate the evolution of groups. At least a fraction of groups end their lives as fossil groups.

Most low-redshift groups are just detaching from the Hubble flow, as suggested by the time evolution of the virial mass-to-light ratio (Mamon). In particular, the detachment for the Local Group occurred at  $z < 0.7$  (Freeman). The mass-temperature and mass-luminosity distributions in the X-rays for clusters and groups can constrain the cosmological parameters (Borgani).

To summarise, as a group evolves, the dwarf-to-giant ratio, early-type galaxy fraction, intragroup starlight and metallicity, the velocity dispersion, and the mass of the central giant elliptical grow. The metallicity of the intragroup medium also increases thanks to the intragroup stars, whose ejecta do not have to overcome galactic potential wells (Zabludoff).

Observations are consistent with this scenario. As mentioned above, groups with

higher velocity dispersions have higher fractions of early-type galaxies. And the intragroup medium can be responsible for stripping, e.g. of NGC 2276 in the NGC 2300 group (Ponman). In turn, stripping enhances the fraction of passive galaxies in groups. Further observational support for this evolutionary scheme are the constant radial profiles of velocity dispersion, which point to a common DM halo. Next, if the early enrichment history of the intragroup gas is dominated by type II supernovae, and the late history by type Ia supernovae, then this could explain the observed decrease of the overall metallicity toward the outskirts of the group, and the alpha-enhancement in the outer parts of groups (Rasmussen) because the early ejecta had time to spread across the group.

### Groups and clusters of galaxies

It was realised during the conference that groups are important for the evolution of clusters as well. Clusters may grow by accretion of groups, as exemplified by the Eridanus Super-group infalling toward Fornax (Brough). Therefore, some cluster properties might be explained by groups, such as the X-ray medium, high dwarf-to-giant galaxy ratio, brightest cluster galaxies, and the early-type galaxy fraction (especially in more massive groups).

Likewise, the evolution of galaxies in clusters might be dominated by group-scale environment, driving e.g. the morphology-environment relation, the Butcher-Oemler effect, and the brightest cluster galaxies formation. For example, the intraclus-

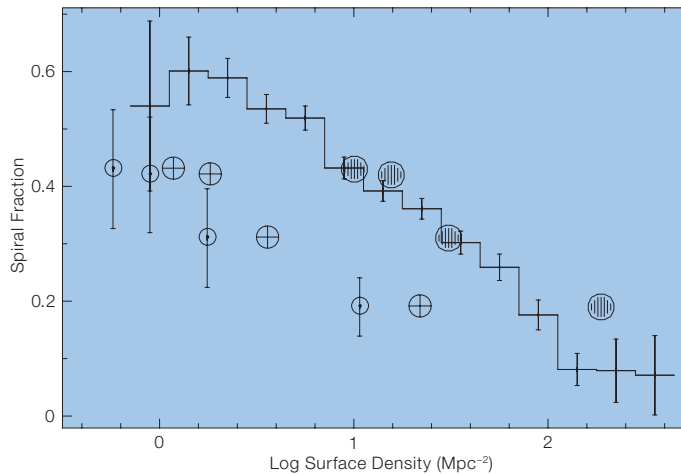


Figure 2: Spiral fraction (including irregulars) as a function of surface density (averaged over radial bins). The histogram represents the local clusters, and the open circles with error bars are the group data. Crossed and shaded circles represent group points after estimated corrections for 3D density and

merging rates, respectively (for clarity the error bars are omitted from these points). Direct type mergers in groups convert late-type galaxies into spheroidal galaxies more efficiently than grazing mergers in clusters (Helsdon and Ponman 2003, MNRAS 339, L29; presented by Mamon).

ter light in Virgo probably originates in tidal interactions inside group-size structures (Mihos), favoured by their low velocity dispersion. Since tidal features are erased as clusters evolve, the presence of such features would indicate that the cluster is dynamically young, still 'fragmented' in groups. Although mergers can happen both in clusters and groups, the high velocity dispersion in clusters leads to less efficient orbital-decay-type mergers, while more efficient, direct head-on mergers are common in groups, especially the evolved, X-ray bright ones (Mamon). This can explain the higher fraction of early-type galaxies in this class of groups compared to the field and clusters (Figure 2).

merging rates, respectively (for clarity the error bars are omitted from these points). Direct type mergers in groups convert late-type galaxies into spheroidal galaxies more efficiently than grazing mergers in clusters (Helsdon and Ponman 2003, MNRAS 339, L29; presented by Mamon).

These few paragraphs can only give a brief sense of the stimulating discussion during the five days of the conference, and we hope that all participants went away with fresh views on the current status of galaxy groups studies. The proceedings will be published later this year in the ESO Astrophysics Symposia series.

### Acknowledgements

We would like to express our gratitude to the members of the SOC, and especially to the SOC chair Duncan Forbes, for their efforts that made it possible to organise this meeting. Last but not least, the success of the conference would have been impossible without the excellent work of Maria Eugenia Gómez, Paulina Jiron and Ismael Martínez, and the financial support of ESO.



Almost all conference participants can be seen in this photograph, taken in the hotel frontyard. The exception is Valentin Ivanov, who's taking the picture!

## Fellows at ESO

### Gaël Chauvin

After studying for five years microelectronics and nuclear physics to become an engineer, I finally changed my mind in fall 1999 to join the small world of Astronomy. With a master of Astrophysics obtained in Grenoble (France), I started a thesis based on a double scientific approach: stellar physics and instrumentation.

A first part of my work was then dedicated to the study of the environment of nearby stars, to search for planetary discs and substellar companions. As this implies searching for very faint objects close to bright stars, I got involved into the development of high-contrast and high-angular-resolution instrumentation. I joined the group integrating and testing the adaptive optics (AO) system of the NACO instrument, now installed at the Paranal Observatory. Later on, with the NACO commissioning and the defense of my thesis, I naturally came to Chile in December 2003 in order to start an ESO fellowship position.

Within the Paranal Science Operation Group, I now work mainly with infrared instruments (coupled to AO). This position offers me the great opportunity to develop constantly an important observing and instrumental experience. This is necessary for my own astrophysical work, now focused on the direct detection of exoplanets and brown dwarf companions and the study of their fundamental physical parameters, the chemical properties of their cool atmosphere, as well as their origin of formation.

This experience also offers me the great chance to fulfill a personal dream, to live abroad, immersing myself in a foreign culture and knowing other people.



Emmanuel Galliano (left) and Gaël Chauvin (right).

### Emmanuel Galliano

Six years have passed since I arrived in Chile. Time flew so quickly and I almost never felt that I had to leave Latin America to return to Europe. It must be because I feel I still have a lot to learn from the people of this side of the world: they probably know better than any other folk how to connect with their emotions.

Thanks to ESO, I could discover the magic of Latin America while fulfilling a professional dream, to be an astronomer. In 1999, I came to Chile for the first time to participate in the Denis Survey, thanks to Pascal Fouqué. I consider it a privilege that I could start learning astronomical observation with a 'small' 1-m telescope, having everything under control. I then started a Ph.D. project with Danielle Alloin at ESO/Santiago. During three years I mainly tried to clarify the distribution of dust and molecules around active galactic nuclei (AGN).

At that time, operations with the interferometer of the VLT were about to start. The communi-

ty was hoping that the VLTI would finally prove the existence of one of the key pieces in the AGN model: the so-called dusty torus. A new exciting field in my research area was about to take off, and this would happen at ESO. This motivated my application for a fellowship in the VLTI team. My duties on Paranal have now been for two years to make starlight interfere, with the most advanced technology available. I broaden my observing skills in the most fascinating way.

In Santiago, I can focus on my favourite research topics: active galactic nuclei and the still mysterious embedded clusters: these bright sources, only visible in the infrared, and thought to be the ancestors of globular clusters. Nothing but the cutting-edge infrared technology offered by the VLT allows studying these objects. I guess this project has a nice future since ESO gives me the opportunity to spend my fourth year at La Universidad de Chile, where I can apply for Chilean VLT observing time.

## Science in School launched

The new quarterly European journal for science education, "Science in School", was launched at the European Molecular Biology Laboratory in Heidelberg, on 28 March 2006. After "Science on Stage" this journal constitutes the second element of the EIROforum European Science Teachers' Initiative (ESTI), which itself is part of a broader effort by the European Commission together with EIROforum and other partners to stimulate innovative science teaching in Europe's primary and secondary schools. The first issue has no less than 92 full-colour pages and covers

a wide range of topics from astronomy and physics to chemistry and biology. It also contains articles on student's perceptions of science and technology, on the teaching of 'process skills', book reviews and other education-related topics.

"Science in School" is available online and in printed form. Visit <http://www.scienceinschool.org/> to find out more and view the first issue which includes an article about 24 hours in the life of the VLT and Paranal.



# The UKIDSS Early Data Release

Steve Warren (Imperial College London),  
Simon Dye (Cardiff University),  
Nigel Hambly (University of Edinburgh),  
on behalf of the UKIDSS consortium

The first release of data from the UKIRT Infrared Deep Sky Survey (UKIDSS) took place on 10 February 2006. The data are proprietary to astronomers in ESO states, for 18 months, before release to the world. This Early Data Release (EDR) comprises mostly data observed in May and June 2005. Although the EDR represents a very small fraction of the complete UKIDSS 7-year plan, it is already large compared to existing surveys, and will be valuable for science exploitation.

UKIDSS has been covered by two previous articles in *The Messenger*. The first (Warren 2002) described the goals and the design of the surveys (depths, areas, fields – which have since changed somewhat). The second (Lawrence and Warren 2005) explained how to obtain data that have been released, from the WFCAM Science Archive (WSA) i.e. the registration process. We briefly review this information, and then give an overview of the contents of the EDR.

UKIDSS is an ESO public survey programme, and comprises five large near-infrared surveys, that together will collect about 100 times as many photons as 2MASS, and survey about 20 times the volume. The UKIDSS programme is set out in detail in Lawrence et al. (2006) (see also <http://www.ukidss.org>). The surveys are currently focused on achieving a set of goals to be reached before the end of 2007, the ‘2-year plan’. The three extragalactic surveys cover complementary combinations of area and depth, running successively deeper from the Large Area Survey (LAS), which is contained within the SDSS footprint, through the Deep Extragalactic Survey (DXS), to the Ultra Deep Survey (UDS). There are two more wide, shallow surveys targeting areas of the Milky Way; the Galactic Plane Survey (GPS) and the Galactic Clusters Survey (GCS). The surveys use the UKIRT Wide Field Camera (WFCAM), the world’s most powerful camera-and-telescope combination for near-infrared surveys. Each survey uses some or all of the broadband filter set ZYJHK. The pho-

tometric system is described by Hewett et al. (2006), who also provide synthetic colours of a wide range of stars, galaxies, and quasars.

UKIDSS data releases are made available at the WSA <http://surveys.roe.ac.uk/wsa>. Any astronomer at an institution in an ESO member state may access the data as soon as it is released. Because ESO astronomers have proprietary access to the data for 18 months, there is a system of registration, which is explained in Lawrence and Warren (2005). Responsibility for the registration process is devolved to volunteers who act as the ‘community contact’ for an institution. A list of institutions with community contacts is maintained at <http://www.ukidss.org/archive/archive.html>. Astronomers who wish to be registered and who have a community contact should ask their contact to provide a username and password. Those without a contact need to find a volunteer, who should then follow the instructions at the above link.

## The contents of the EDR

Details of the contents of the EDR are provided in Dye et al. (2006), including a summary of the results of the quality control (QC) procedures. The paper also includes relevant background information, sufficient to understand the characteristics of the data, including details about WFCAM, and the data-reduction pipeline, as well as a guide to exploiting the WSA.

A bare summary of the contents of the EDR is provided in Table 1 which lists area covered, and mean depth ( $5\sigma$ , Vega), by

Survey	Area (sq degs)	Filter	Depth	Frac. 2-yr plan
LAS	28.2	Y	20.2	0.014
		J	19.5	
		H	18.7	
		K	18.1	
GPS	7.2	J		0.009
		H		
		K		
GCS	15.4	Z	20.3	0.043
		Y	19.9	
		J	19.4	
		H	18.8	
		K	18.1	
DXS	2.4	J	20.9–21.7	0.072
		K	20.2–20.6	
UDS	0.8	J	22.3	0.044
		K	21.1	

filter, for each survey. In good conditions the shallow surveys LAS and GCS, use 40 s integration per band, so the depths are similar, but depend on seeing, sky brightness, and transparency. The GPS uses 40 s in *K* and 80 s in *J* and *H*. We have not attempted to define the depth for the GPS because crowding means that it is difficult to assess, but nominally it is quite similar to that for the LAS and GCS. With the UDS, which covers a single tile (4 WFCAM pointings), 0.8 sq degs, the depth will steadily accumulate, and in any band at any time is defined by a single number (although there are slight variations over the field due to variable q.e. of the detectors). The DXS, on the other hand, is made up of tens of tiles, each accumulating depth at a different rate. A range of depths is therefore quoted for the DXS.

Figure 1 illustrates some of the EDR data. The two plots are the *YJK* and *JHK* two-colour diagrams for all the stellar sources in the LAS, plotting objects detected at  $S/N > 15$ . Overplotted is the sequence of synthetic colours of stars from the BPGS atlas, computed by Hewett et al. (2006).

The progress of the surveys, and a comparison against 2MASS, is made in an interesting way in Figure 2. For sky-limited observations in the *K*-band, the time to reach depth *K* is proportional to  $10^{(0.8K)}$ . One can therefore think of the quantity  $\text{area} \times 10^{(0.8K)}$  as being proportional to the number of photons collected. A related argument, for Euclidian space, leads to the conclusion that the quantity  $\text{area} \times 10^{(0.6K)}$  is proportional to the volume surveyed. By multiplying by the number of filters, and then normalising to the

**Table 1:** Summary of EDR depths and areas for the five surveys, and fractional completeness of the two-year plan. Depths are not quoted for the GPS, as noted in the text. The EDR includes data with seeing  $> 1''$ , whereas most survey-quality (i.e. DR1) data should be better than this. Therefore the depth achieved in DR1 may improve slightly over EDR.

2MASS values, we can compare the size of the EDR against 2MASS in terms of photons and volume. The results are plotted in the figure. Summing over the surveys we see that the EDR is about as large as 2MASS in terms of photons collected. Also shown are the two-year goals, i.e. where UKIDSS aims to be by the end of 2007. The final column in Table 1 shows the fractional completion of the two-year plan in terms of photons, by survey.

Within UKIDSS we consider the EDR to be a small prototype sample, provided to the community as a stepping stone towards the goal of prompt release of survey quality data. The data have passed a set of QC procedures. Some details of the pipeline (including treatment of artefacts) and QC procedures are still being refined, in preparation for the first large release of survey-quality data in the summer of 2006, called Data Release 1 (DR1, we have copied the SDSS nomenclature). We would expect most, but not all, of the EDR to satisfy our final survey QC procedures.

As explained in Dye et al. (2006) the EDR release includes all fields observed, that pass QC, and where the full filter complement exists. There is an additional database included in the release, but in the background, called EDR+. This contains fields that pass QC, but where the filter complement is incomplete. The paper contains an explanation of how to access the EDR+ database as well.

The DR1 release is scheduled to take place this summer, and will be an order of magnitude larger. We will provide a similar paper, and Messenger article, to accompany the release.

#### References

- Dye S. et al. 2006, MNRAS, submitted  
 Hewett P. C. et al. 2006, MNRAS, in press  
 Lawrence A., Warren S. J., Almaini O. 2006, MNRAS, submitted  
 Lawrence A., Warren S. J. 2005, The Messenger 119, 56  
 Warren S. J. 2002, The Messenger 108, 31

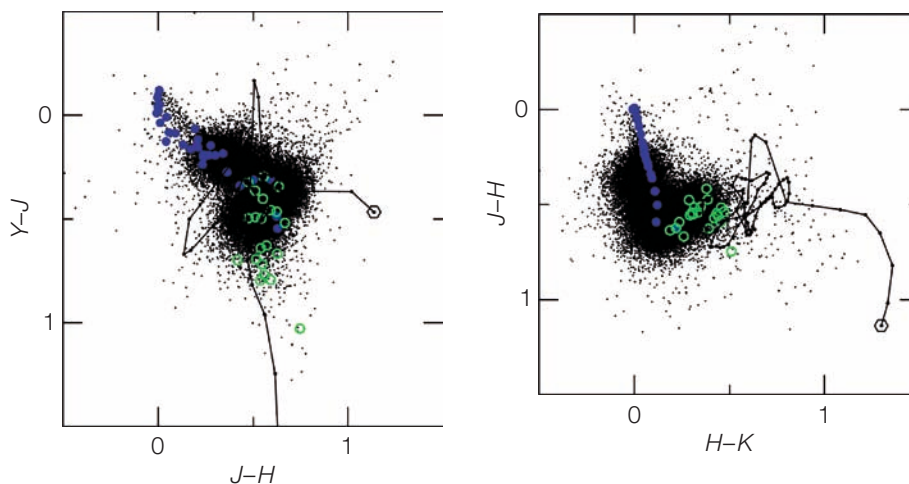


Figure 1: Two-colour diagrams for stellar sources, with colour errors on each axis  $< 0.1$  in the LAS portion of the EDR. The large blue symbols show the synthetic colours computed from the BPGS atlas by Hewett et al. (2006), the large green symbols mark the computed colours of M stars, and the

black track shows the predicted colours of quasars  $0 < z < 8$ , at intervals of  $z$  of 0.1, with  $z = 0$  marked by the hexagon. There are some 80 000 points in each plot. The nature of the small fraction of outliers has not been checked yet in detail, and many may be spurious.

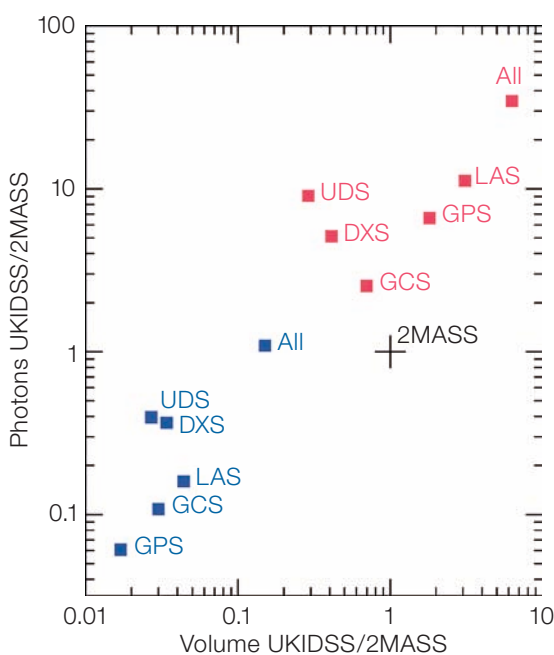


Figure 2: Comparison of the UKIDSS EDR (blue symbols) and two-year plan (cerise symbols) against 2MASS, in terms of number of photons detected, and volume surveyed, computed as described in the text.

# Scisoft VI

Richard Hook (ST-ECF/ESO)  
and the Scisoft Team

Scisoft is a collection of astronomical software intended mostly for ESO users but also distributed to other interested parties. It includes most of the packages needed by working observational astronomers with an emphasis on those widely used for handling optical and infrared data sets. It is installed on all the standard scientific computers running Linux at ESO Garching. More complete details, including a list of software that is included in the bundle, can be found at [www.eso.org/scisoft](http://www.eso.org/scisoft).

We are pleased to announce the availability of Scisoft VI (April 2006). This new version of the collection includes many updates and additional packages and also incorporates some new features.

Scisoft VI was built on, and intended to be used on, Fedora Core 3 Linux, but is likely to run on similar modern Linux systems. We no longer maintain a version of Scisoft for other architectures such as Solaris or HP-UX but an independent version for Mac OS X, maintained outside ESO, is also available.

Scisoft VI can be either downloaded from the ESO ftp site, by following the link on the web page given above, or the entire

collection may be requested on DVD. Requests for DVDs should be made through the request form on the same web page or by email to [scisoft\\_request@eso.org](mailto:scisoft_request@eso.org).

The next release of Scisoft will be Scisoft VII at the end of 2006. This version will include a selection of virtual observatory tools as well as many other new features.

Scisoft is a collaboration between many people at ESO. I would particularly like to thank Alexis Huxley, formerly with Terma at ESO, for his very diligent and thorough help with the technical aspects of the release.

---

Workshop on

## Deep Impact as a World Observatory Event – Synergies in Space, Time, and Wavelength

7–10 August 2006, Palace of the Royal Academy for Science and the Arts (RASAB), Brussels, Belgium

The astronomy group in the physics faculty of the Vrije Universiteit Brussel together with ESO, is organising a workshop on the worldwide observational campaign of the “Deep Impact Experiment” (c.f. Käufel et al. 2005, *The Messenger* 121, 11). In the context of NASA’s Deep Impact space mission Comet 9P/Tempel 1 was at the focus of an unprecedented worldwide long-term multi-wavelength observation campaign. The comet was studied through its perihelion passage by various spacecraft including the Deep Impact mission itself, HST, Spitzer, Rosetta, XMM and all major ground-based observatories in a wavelength band from cm-wave radio astronomy to X-rays.

The objective of this workshop is to make full use of this data set by bringing together observers across the electromagnetic spectrum and from different sites and projects. Synergy between the

different data sets can only be achieved if observers share their data and arrive at a coherent interpretation. Consequently a coherent presentation of all data sets will allow theoreticians to fully appreciate all observational constraints.

Specific topics of this workshop are: General Cometary Topics From Space and Ground; the cometary nucleus; cometary gas; cometary plasma; cometary dust; cometary surface and activity. Deep Impact Specific Questions will include: release of unprocessed primordial material from the formation period of the comet; long-term effects from the impact; understanding of global properties of the nucleus; surface layering of the Comet 9P/Tempel 1 nucleus; impact cratering; understanding of cometary dust after deep impact; understanding the processes in the gas coma; and ground support of space missions (complementarity and needs).

The scientific organising committee is composed of: Chris Sterken (chair), Ulli Käufel (co-chair), Mike A’Hearn, Hermann Bönnhardt, Michael Combi, Yan Fernandez, Marco Fulle, Luisa Lara, Casey Lisse, Jean Manfroid, Karen Meech, Javier Licandro, Heike Rauer, Rita Schulz, Gerhardt Schwehm and Diane Wooden. The proceedings will appear in the ESO/Springer series (eds. Ulli Käufel and Chris Sterken).

The relevant deadlines are: 3 April 2006, final call for papers; 15 June 2006, abstracts due for programme.

For further details, see <http://www.eso.org/~hukaufel/deepimpact.html> or <http://www.vub.ac.be/STER/DI/di-conf2006.htm> or contact Chris Sterken ([csterken@vub.ac.be](mailto:csterken@vub.ac.be)) or Ulli Käufel ([hukaufel@eso.org](mailto:hukaufel@eso.org)).

MPA/ESO/MPE/USM Joint Astronomy Conference on

## Heating versus Cooling in Galaxies and Clusters of Galaxies

6–11 August 2006, Garching, Germany

The aim of the conference is a review of our knowledge of the physical processes controlling the state of the dense, central intracluster medium in galaxy clusters and to discuss their analogy to feedback process in regulated galaxy formation.

Detailed multiwavelength observations suggest that the dense plasma regions at the centres of galaxy clusters, previously thought to harbour cooling flows, are subject to a delicate balance between heating and cooling, which substantially reduces mass condensation and star-formation rates. While these regions are quite complex, the rich observational detail now becoming available can guide understanding and modelling. The aim of this conference is to provide a synthesis of all the observational evidence and to confront it with astrophysical modelling. Analogous issues arise in the models of galaxy formation where the observed properties and the evolution of the galaxy population can only be explained if gas cooling and star formation are assumed to be regulated by feedback heating. The

conference will explore possible connections between these two areas.

In recent years the effort to understand cluster cooling cores has grown both in terms of observation (in particular in X-rays with the Chandra and XMM-Newton satellites) and in terms of detailed numerical hydrodynamical simulations. A review of the state of the subject is thus timely. Also, in recent years it has been much more generally appreciated that the suppression of gas cooling in the centre of galaxy clusters may be a model for the effects of feedback in galaxy and structure formation in general. In our meeting we consequently broaden the view to include feedback and self-regulation during galaxy formation.

The wealth of new observational data and modelling results will provide the basis for the current meeting, which will include the following topics: (i) evidence for cooling, cold material, and star formation in the centres of galaxy clusters and elliptical galaxies with results from observa-

tions in X-rays, optical, IR, radio, and absorption studies), (ii) heating of central cluster regions by the AGN-intracluster medium interaction and by other processes, confrontation of modelling results with observed cooling core structure, (iii) diagnostics of the cooling core regions through the entropy structure of the intracluster medium and chemical enrichment as signatures of feedback heating in the past, (iv) the need for feedback regulation in galaxy formation, detailed comparison of model predictions and observations for the feedback during galaxy formation from both, stars/supernovae and from AGN.

Scientific Organising Committee:  
M. Arnaud, M. Begelman, H. Böhringer, M. Donahue, A. Fabian, G. Hasinger, T. Heckman, C. Jones, B. McNamara, T. Ohashi, F. Owen, M. Pettini, T. Reiprich, A. Renzini, P. Rosati, C. Sarazin, N. Soker, R. Sunyeav, S. White

Visit our webpage: <http://www.mpe.mpg.de/~cool06>

Conference on

## Precision Spectroscopy in Astrophysics

11–15 September 2006, Aveiro, Portugal

In the last decade we have witnessed impressive advancements in the accuracy of Doppler-shift measurements in astronomy and of high-precision spectroscopy in general.

The random measurement uncertainty depends on the inverse of the Signal-to-Noise ratio, therefore high accuracy requires a high photon flux and a large photon-collecting capability. As a consequence, not only the scientific domains using this technique benefit tremendously from the use of 8-m-class telescopes, but, also, they will fully exploit the tremendous gain provided by future Extremely Large Telescopes (ELTs), as clearly shown by the preliminary study of CODEX. Even if most applications so far have been at

optical wavelengths, IR high-resolution spectroscopy should soon approach the same accuracy regime.

The goal of the conference is to gather together scientists to discuss all the scientific topics related to various aspects of high-precision spectroscopy (determination of Doppler shifts, accurate line profiles, isotopic ratios, etc.). In addition to presentations on the state of the art of research in the field, part of the programme will be devoted to future programmes and instruments, including those for ELTs. In addition to presenting their current results, we would like to ask all the speakers to highlight also their limitations and to indicate, when possible, future avenues to progress.

This ESO conference is co-organised with the Centre for Astronomy and Astrophysics (University of Lisbon) and the University of Aveiro.

Scientific Organising Committee: Beatriz Barbuy (Brasil), Jacqueline Bergeron (France), Dainis Dravins (Sweden), Artie Hatzes (Germany), Garik Israelian (Spain), David Lambert (USA), Michel Mayor (Switzerland), Paolo Molaro (Italy), Mario J. Monteiro (Portugal), Luca Pasquini (ESO, co-chair), Max Pettini (UK), Martino Romaniello (ESO, co-chair), Nuno C. Santos (Portugal, co-chair)

Conference webpage:  
<http://www.oal.ul.pt/psa2006>  
Contact: [psa2006@oal.ul.pt](mailto:psa2006@oal.ul.pt)

## Science on Stage 2

National Events: April–October 2006, in 29 participating countries  
International Event: 2–6 April 2007, ATRIA Centre, Grenoble, France

The first Science on Stage festival, held at CERN in Geneva in November 2005, was a great success. As described in the previous issue of *The Messenger*, almost five hundred science educators from across Europe met to share innovative science-teaching techniques.

Now, the countdown has begun for Science on Stage 2. The festival is again being organised by the EIROforum, of which ESO is a member, and co-funded by the European Commission as part of the EIROforum Science Teachers' Initiative (ESTI). The international event will take place in Grenoble at the ATRIA

Centre from 2–6 April 2007. The European Synchrotron Research Facility and the Institut Laue-Langevin are the local organisers from the EIROforum.

If you are a teacher or are interested in innovative teaching methods, and are from one of the 29 countries who will be represented at Science on Stage 2, then now is your chance to get involved! Each country will be running a National Event during 2006, in order to choose the delegates who will go to Grenoble in April 2007.

Visit the Science on Stage website at <http://www.scienceonstage.net/> (or email [eduinfo@eso.org](mailto:eduinfo@eso.org)) to find contact details for your National Steering Committee (NSC). The national websites will be available by the end of April, giving details of how to get involved with Science on Stage at a national level. The National Events will be taking place between April and October of this year, so if you want to join this exciting programme you should contact your NSC as soon as possible.

For further details see <http://www.scienceonstage.net/> or email [eduinfo@eso.org](mailto:eduinfo@eso.org)

---

## Euroscience Open Forum – ESOF2006

15–19 July 2006, Munich, Germany

Following the successful first ESOF2004 event in Stockholm, the second pan-European 'General Science Meeting' ESOF2006 is scheduled to be held in Munich from 15–19 July 2006 at the *Forum am Deutschen Museum* and the *Deutsches Museum*. ESOF constitutes an attempt to create a European version of the famous AAAS meeting and targets scientists, science administrators and policy makers as well as science journalists from across the continent.

ESOF is an initiative by EUROSCIENCE with strong sponsors including the European Commission and major German funders. It is supported by an advisory board, which – among others – includes Enric Banda (former Secretary General of ESF), Phillip Campbell (editor of *Nature*), Helga Nowotny (until recently chairperson of EURAB and a member of the Scientific Advisory Board of the future European Research Council) and the Directors General of ESO, Catherine Cesarsky, and the EPO, Alain Pompidou.

The organisers intend to put a special focus on young scientists, young journalists and students through an extensive Careers Programme with educational workshops and seminars on career development. In this connection, the EIROforum will organise videoconferences to the facilities of the partner organisations, including ESO.

According to the current programme, the meeting comprises over 70 seminars, symposia and workshops.

One of these seminars – on exoplanet research – is organised by ESO. This particular session will take place on 17 July 2006 at the Forum. Another astronomy-related event is the key-note talk by Prof. Gerry Gilmore (Cambridge University) with the title "The history and future of the Universe".

As at the Stockholm meeting, ESO will also be represented as part of the EIROforum partnership that will mount a major information stand at the exhibition area, also at the Forum.

Also as in Stockholm, which featured a wide programme for the general public, ESOF2006 offers an interesting range of outreach activities, comprising hands-on experiments, games and science cafés. These activities will be held together with the German national science week from 15–21 July 2006. The public activities are free and will take place at the *Marienhof* square, behind the historical Munich town hall. The *Wissenschaftssommer* is organised annually by *Wissenschaft im Dialog*, an initiative of the *Stifterverband für die Deutsche Wissenschaft* and other German science-funding organisations.

For further information, see: <http://www.esof2006.org>

Contact: Claus Madsen ([cmadsen@eso.org](mailto:cmadsen@eso.org)), Bruno Leibundgut ([bleibundgut@eso.org](mailto:bleibundgut@eso.org))

## ESO Studentship Programme

The ESO research student programme aims at providing opportunities to enhance the Ph.D. programmes of ESO member-state universities. Its goal is to bring young scientists into close contact with the activities and people at one of the world's foremost observatories. For more information about ESO's astronomical research activities please consult <http://www.eso.org/science/>

The ESO studentship programme is shared between the ESO headquarters in Garching (Germany) and the ESO offices in Santiago (Chile). These positions are open to students enrolled in a Ph.D. programme at a university in an ESO member state or, exceptionally, at an institution outside ESO member states.

Students in the programme work on their doctoral project under the formal supervision of their home university. They come to either Garching or Santiago for a stay of normally between one and two years to conduct part of their studies under the co-supervision of an ESO staff astronomer. Candidates and their home institute supervisors should agree on a research project together with the ESO local supervisor. A list of potential ESO supervisors and their research interests can be found at <http://www.eso.org/science/personnel/index.html> and <http://www.sc.eso.org/santiago/science/person.html>. A list of current Ph.D. projects offered by ESO staff is available at <http://www.eso.org/>

*science/thesis-topics/*. It is highly recommended that the applicants start their Ph.D. studies at their home institute before continuing their Ph.D. work and developing observational expertise at ESO.

In addition, the students in Chile have the opportunity to volunteer for as many as 40 days/night work per year at the La Silla Paranal Observatory. These duties are decided on a trimester by trimester basis, aiming at giving the student insight into the observatory operations and shall not interfere with the research project of the student in Santiago. The outline of the terms of service for students (<http://www.eso.org/gen-fac/adm/pers/student.html>) provides some more details on employment conditions and benefits.

The closing date for applications is **15 June 2006**.

Please apply by:

- (1) filling the form available at <http://www.eso.org/gen-fac/adm/pers/forms/student06-form.pdf>
- (2) and attaching to your application:
  - a Curriculum Vitae (incl. a list of publications, if any), with a copy of the transcript of university certificate(s)/ diploma(s).
  - a summary of the master thesis project (if applicable) and ongoing projects indicating the title and the supervisor (maximum half a page), as well as an outline of the Ph.D. project highlighting

the advantages of coming to ESO (recommended one page, max. two).

- two letters of reference, one from the home institute supervisor/advisor and one from the ESO local supervisor,
- and a letter from the home institution that (i) guarantees the financial support for the remaining Ph.D. period after the termination of the ESO studentship, (ii) indicates whether the requirements to obtain the Ph.D. degree at the home institute are already fulfilled.

All documents should be typed in English (but no translation is required for the certificates and diplomas).

The application material has to be addressed to:

ESO Studentship Programme  
Karl-Schwarzschild-Straße 2  
85748 Garching bei München (Germany)

All material, including the recommendation letters, must reach ESO by the deadline (15 June 2006); applications arriving after the deadline or incomplete applications will not be considered!

Candidates will be notified of the results of the selection process in July 2006. Studentships typically begin between August and December of the year in which they are awarded. In well-justified cases starting dates in the year following the application can be negotiated.

For further information contact Christina Stoffer ([cstoffer@eso.org](mailto:cstoffer@eso.org)).



This photo was obtained with the FORS2 instrument at ESO's Very Large Telescope. It zooms in on the open stellar cluster Haffner 18, perfectly illustrating three different stages of this process of star formation: In the centre of the picture, Haffner 18, a group of mature stars that have already dispersed their birth nebulae, represents the completed product or immediate past of the star-formation process. Located at the bottom left of this cluster, a very young star, just come into existence and, still surrounded by its birth cocoon of gas, provides insight into the very present of star birth. Finally, the dust clouds towards the right corner of the image are active stellar nurseries that will produce more new stars in the future. (ESO PR Photo 42b/05)



ESO

European Organisation  
for Astronomical  
Research in the  
Southern Hemisphere



ESO is opening the following management positions of

## Senior Astronomer Director of the La Silla Paranal Observatory

The Director responsible for the Observatories on La Silla, Paranal and APEX will lead a multidisciplinary team and act as a link between user community, the Director General and the Observatories. She/he will in particular be responsible for:

- the continuation, creation and implementation of scientific and technical policies for the operation of the Observatories in accordance with ESO's overall policy
- the management of the Observatories and their staff members through the definition and implementation of goals and objectives
- the Observatories' budget
- the representation of all Observatories in the science community, public and public relations (e.g. media support, exhibitions, presentations, etc.) in close interaction with ESO's representative in Chile and the Public Affairs Department.

The Director of the Observatories reports directly to the Director General. The staff of the Observatories presently consist of about 70 international and 150 local staff members who work in groups or teams. As a senior astronomer the Director of the Observatories is a member of the ESO science faculty and is expected and encouraged to actively conduct astronomical research. She/he should foster the participation and integration of the scientists of the Observatories in the ESO faculty and in the Office for Science in Santiago.

Basic requirements for the position include a Ph.D. in astronomy, astrophysics or physics, or related fields, substantial and long or equivalent experience in management and leadership preferably gained within multinational scientific organisations. A proven record in astronomical systems such as instruments, large optical telescopes or systems of equivalent complexity as well as an outstanding record of astronomical research and international scientific collaborations are required. Initiative, ability to judge, to decide and to work with people of different nationalities as well as excellent communication skills are essential. The position requires a very good knowledge of English and a working knowledge of Spanish or willingness to learn it.

## Associate Director

The primary purpose of this position is to support and assist the Director General in the discharge of his/her duties. The Associate Director reports directly to the Director General and is required to work closely with division heads and other senior staff in the Organisation. She/he shall carry out such tasks as requested or delegated by the Director General which shall include, but not be limited to, responsibility for:

- providing the Director General with briefing material and appropriate analysis on any matter which could have implications for the operation of ESO
- the management of the Council secretariat
- the management of the ALMA board and European ALMA board business, and specifically acting as ALMA board secretary when the chair is nominated by ESO.

An appropriate professional qualification as well as substantial management and leadership experience within a scientific organisation, preferably international, are required. Excellent communication skills and a very good knowledge of English are essential.

As members of the ESO management both job holders contribute directly to the development of the overall policy, the strategic planning, and maintain professional contacts at highest level outside the Organisation.

For details and to download an application form, please consult our homepage: <http://www.eso.org>. If you are interested in working in areas of frontline technology and in a stimulating international environment please send your application in English to:

ESO Personnel Department, Karl-Schwarzschild-Straße 2  
85748 Garching near Munich, Germany  
e-mail: [vacancy@eso.org](mailto:vacancy@eso.org)

*ESO is an equal opportunity employer. Qualified female candidates are invited to apply.*

ESO. Astronomy made in Europe





ESO

European Organisation  
for Astronomical  
Research in the  
Southern Hemisphere



ESO is opening the following positions of

## Instrument Scientist

This position is in the Instrumentation Division which is responsible for the design and development of advanced optical and infrared instruments for the Very Large Telescope and other telescopes at ESO's La Silla Paranal Observatory and, in the future, for a possible Extremely Large (30–60 m diameter) Telescope (see <http://www.eso.org/instruments/>).

The successful candidate will initially work in the Optical Instrumentation Department as Instrument Scientist of the X-shooter, a medium-resolution, echelle spectrograph for the VLT, covering in one exposure the spectral region from the UV to the K-band and expected to go to the telescope in 2008. She/he will directly be in charge or collaborate with the P.I. and project manager of the project in various tasks related to the documentation for the instrument (e.g. calibration plan, commissioning plan, user manual), the development of the exposure time calculator, of the data-reduction pipeline, the testing of the instrument in Europe and the commissioning in Chile. She/he will be responsible for verifying that the overall performance of the instrument at the telescope matches the specified values, and support the operation during the first year. In parallel, she/he will be involved in the definition studies of other instrument projects for the VLT and possibly the ELT.

Basic requirements for the position include qualified experience in observational astronomy at optical or IR wavelengths at large telescopes. A proven, strong record of scientific research in areas which are related to the functional work and good experience with spectroscopic data-reduction packages in IDL, IRAF or MIDAS are a requirement.

This is an astronomer position in the ESO faculty. The successful candidate is expected to carry out a vigorous research programme in the field of observational astronomy. He/she is entitled to work up to 50 % on scientific research and will receive financial and technical support by the ESO faculty for this purpose.

## Front End Production Engineer Software Engineers

Within the European ALMA team, the selected candidate will take up responsibilities in the production engineering, integration and monitoring of contracts for the receivers of the ALMA radio telescope.

The position will include the following tasks:

- management, both technical and programmatic, of individual production work packages for the ALMA Front End (FE) subsystem and the related production contracts
- developing front end integration and test plans, and assist in the development of an operations and maintenance plan in close collaboration with ALMA system engineers
- quality management: definition of applicable processes, mainly in the areas of production, integration and validation. Participation in and organisation of product reviews
- assisting in developing and maintaining the FE subsystem specifications and interfaces. Assuring that subsystem designs comply with defined specifications.
- keeping track of detailed subsystem performance of the front end technical budgets.
- contributing to the ALMA configuration and change-control processes.
- reporting directly to the European ALMA Front End IPT manager.

We seek a professional with a university degree in engineering, in one or more of the following fields: electronics, technical physics or other relevant fields and at least five years of working experience in an engineering position on multidisciplinary, high-technology, and complex electronics project(s).

The successful candidates will work within the Data Flow Systems (DFS) Department, which is responsible for designing, implementing, testing and maintaining the Data Flow System used to operate ESO's Very Large Telescope (VLT) array.

Two positions are opened in the area of detailed design, development and documentation of components of the back-end DFS, that is the collection of client server applications used on-line at the Observatory and off-line in Garching to collect, archive and organise the raw data, schedule and parallelise their processing. Sound experience in Java, C++ and a solid understanding of data archives are required.

An additional position is opened to the verification and validation of a subset of the DFS, starting with the back-end applications used at the Observatory and in Garching. She/he will be responsible for defining, implementing and executing manually or automatically test cases to ensure that users' requirements have been met and that the behaviour under abnormal or extreme conditions is acceptable. Test data will have to be defined and maintained, test plans and reports produced and discussed with development teams, according to DFS Software Quality Assurance standards. A first level support to DFS users should be provided. Finally, she/he will contribute to the DFS installation activities and software configuration management. A minimum of three years of experience in testing and integration of complex distributed software applications running on UNIX platforms is required.

For details and to download an application form, please consult our homepage: <http://www.eso.org>.

If you are interested in working in a stimulating international research environment and in areas of frontline science and technology, please send us your application in English to:

ESO Personnel Department  
Karl-Schwarzschild-Straße 2  
85748 Garching near Munich, Germany  
e-mail: [vacancy@eso.org](mailto:vacancy@eso.org)

*ESO is an equal opportunity employer. Qualified female candidates are invited to apply.*

ESO. Astronomy made in Europe



# Personnel Movements

1 January–31 March 2006

## Arrivals

### Europe

Abuter, Roberto (RCH)	Software Engineer
Botticella, Maria Teresa (I)	Student
Caproni, Alessandro (I)	Software Engineer
Di Dio, Tommaso (I)	Accounting Clerk
Guidolin, Ivan Maria (I)	Electronics Engineer
Jahreiss, Hans (D)	Head of Administration
Patkós, Enikő (H)	European Affairs Officer
Suc, Vincent (F)	Student
Taylor, Luke (GB)	Laser Specialist
Turolla, Stefano (I)	Software Engineer
Vasisht, Gautam (IND)	Software Engineer
Yaitskova, Nataliya (RUS)	Applied Scientist

### Chile

Choque Cortez, Christian (BOL)	Student
Francois, Patrick (F)	Operations Staff Astronomer
Haguenauer, Pierre (F)	Optical Engineer
Kubas, Daniel (D)	Fellow
Mellado, Angel (RCH)	Mechanical Technician
Pizarro, Andres (RCH)	Safety Officer
Rahoui, Farid (F)	Student
Somboli, Fabio (I)	System Engineer

## Departures

### Europe

Alves, João (P)	Astronomer
Boneva, Kristina (BG)	Student
Dell'Erba, Anna Maria (I)	Administrative Assistant
Larsen, Søren (DK)	Instrument Scientist
Leoni, Marco (I)	Software Engineer
Nees, Walter (D)	Head of Electronic Systems
Pott, Jörg-Uwe (D)	Student
Rettura, Alessandro (I)	Student

### Chile

Badel, Arnaud (F)	Student
Brancacho, Jorge (RCH)	Software Engineer
Coppolani, Franck (F)	Student
Inzunza, Lorena (RCH)	Telescope Instruments Operator
Schemrl, Anton (RCH)	Data Handling Administrator
Torres, Danilo (RCH)	Electronics Engineer

# List of Proceedings from the ESO Astrophysics Symposia

Volume	Title	Editors
(foreseen for July) 2006	Chemical Abundances and Mixing in Stars in the Milky Way and its Satellites	Sofia Randich, Luca Pasquini
(foreseen for April) 2006	Planetary Nebulae Beyond the Milky Way	Letizia Stanghellini, Jeremy R. Walsh, Nigel G. Douglas
2005	Growing Black Holes: Accretion in a Cosmological Context	Andrea Merloni, Sergei Nayakshin, Rashid A. Sunyaev
2005	High Resolution Infrared Spectroscopy in Astronomy	Hans-Ulrich Käufl, Ralf Siebenmorgen, Alan F. M. Moorwood
2005	Multiwavelength Mapping of Galaxy Formation and Evolution	Alvio Renzini, Ralf Bender
2005	Science with Adaptive Optics	Wolfgang Brandner, Markus Kasper
16/2003	Astronomy, Cosmology and Fundamental Physics	Peter A. Shaver, Luigi DiLella, Alvaro Giménez
15/2004	Toward an International Virtual Observatory	Peter J. Quinn, Krzysztof M. Górski
14/2003	Extragalactic Globular Cluster Systems	Markus Kissler-Patig
13/2003	From Twilight to Highlight: The Physics of Supernovae	Wolfgang Hillebrandt, Bruno Leibundgut
12/2003	The Mass of Galaxies at Low and High Redshift	Ralf Bender, Alvio Renzini
11/2003	Lighthouses of the Universe: The Most Luminous Celestial Objects and Their Use for Cosmology	Marat Gilfanov, Rashid A. Sunyaev, Eugene Churazov
10/2003	Scientific Drivers for ESO Future VLT/VLTI Instrumentation	Jacqueline Bergeron, Guy Monnet
9/2003	The Origin of Stars and Planets: The VLT View	João F. Alves, Mark J. McCaughrean
8/2003	Gamma-Ray Bursts in the Afterglow Era	Enrico Costa, Filippo Frontera, Jens Hjorth
7/2003	Deep Fields	Stefano Cristiani, Alvio Renzini, Robert E. Williams
6/2003	Mining the Sky	Anthony J. Banday, Saleem Zaroubi, Matthias Bartelmann

# Annual Index 2005 (Nos. 119–122)

## Subject Index

Scientific Strategy Planning at ESO; 119, 2

Science with Extremely Large Telescopes; Hook I. and the OPTICON ELT Science Working Group; 121, 2

## Telescopes and Instrumentation

Wide Field Infrared Imaging on the VLT with HAWK-I; Casali, M.; Pirard, J.-F.; Kissler-Patig, M.; Moorwood, A.; Bedin, R.; Biereichel, P.; Delabre, B.; Dorn, R.; Finger, G.; Gojak, D.; Hubin, N.; Huster, G.; Jung, Y.; Koch, F.; Le Louarn, M.; Lizon, J.-L.; Mehrgan, L.; Pozna, E.; Silber, A.; Sokar, B.; Stegmeier, J.; 119, 6

ESO's Two Observatories Merge (based on ESO Press Release 03/05); 119, 8

New observing modes of NACO; Kasper, M.; Ageorges, N.; Boccaletti, A.; Brandner, W.; Close, L. M.; Davies, R.; Finger, G.; Genzel, R.; Hartung, M.; Kaufer, A.; Kellner, S.; Hubin, N.; Lenzen, R.; Lidman, C.; Monnet, G.; Moorwood, A.; Ott, T.; Riaud, P.; Röser, H.-J.; Rouan, D.; Spyromilio, J.; 119, 9

Observing with the ESO VLT Interferometer; Wittkowski, M.; Comerón, F.; Glindemann, A.; Hummel, C.; Morel, S.; Percheron, I.; Petrotzgens, M.; Schöller, M.; 119, 14

Improvements at the 3.6-m Telescope; Gilliotte, A.; Ihle, G.; Lo Curto, G.; 119, 18

Telescope Time Allocation Tool; Alves, J.; 119, 20

ALMA News; Wilson, T.; 119, 24

Progress Report on X-shooter, the first second-generation VLT Instrument; Dekker, H.; D'Odorico, S.; 120, 2

VLT First Fringes with Two Auxiliary Telescopes at Paranal; Koehler, B. and the AT Assembly and Commissioning Team; 120, 5

The OPTICON FP6 Programme and ESO; Monnet, G.; 120, 7

The VLT Survey Telescope: A Status Report; Capaccioli, M.; Mancini, D.; Sedmak, G.; 120, 10

OmegaCAM: The VST Camera; Cappellaro, E.; 120, 13

ALMA News; Wilson, T.; 120, 15

The Sampo Project; Hook, R.; Møller, P.; Ignatius, J.; Vasko, K.; Peron, M.; Quinn, P.; 120, 17

ALMA News; Wilson, T.; 121, 48

ALMA Site Development; Eschwey, J.; 121, 50

Technology Transfer at ESO; Cullum, M.; 121, 52

Surveying the High-Redshift Universe with KMOS; Sharples, R.; Bender, R.; Bennet, R.; Burch, K.; Carter, P.; Casali, M.; Clark, P.; Content, R.; Davies, R.; Dubbeldam, M.; Finger, G.; Genzel, R.; Häfner, R.; Hess, A.; Kissler-Patig, M.; Laidlaw, K.; Lehnert, M.; Lewis, I.; Moorwood, A.; Muschiello, B.; Förster Schreiber, N.; Pirard, J.; Ramsay Howat, S.; Rees, P.; Richter, J.; Robertson, D.; Robson, I.; Saglia, R.; Tecza, M.; Thatte, N.; Todd, S.; Wegner, M.; 122, 2

Instrument Concepts for the OWL Telescope; D'Odorico, S.; 122, 6

The Centre of the Active Galaxy NGC 1097 (ESO Press Photo 33/0); 122, 9

CODEX: Measuring the Expansion of the Universe (and beyond); Pasquini, L.; Christiani, S.; Dekker, H.; Haehnelt, M.; Molaro, P.; Pepe, F.; Avila, G.; Delabre, B.; D'Odorico, S.; Liske, J.; Shaver, P.; Bonifacio, P.; D'Odorico, V.; Vanzella, E.; Bouchy, F.; Dessauges-Lavadsky, M.; Lovis, C.; Mayor, M.; Queloz, D.; Udry, S.; Murphy, M.; Viel, M.; Grazian, A.; Levshakov, S.; Moscardini, L.; Wiklind, T.; Zucker, S.; 122, 10

Afterglows of Elusive Short Gamma-Ray Bursts (based on ESO Press Release 26/05); 122, 14

ALMA News; Wilson, T.; 122, 15

ALMA Antenna Contract Signed (based on ESO Press Release 31/05); 122, 17

Inauguration of the APEX Telescope; Argandoña, G.; Mirabel, F.; 122, 18

Towards an Automatic Reduction of FORS2-MXU Spectroscopy; Kuntschner, H.; Kümmel, M.; Larsen, S.; Walsh, J.; 122, 19

The Virtual Observatory in Europe and at ESO; Padovani, P.; Quinn, P.; 122, 22

## Reports from Observers

VISIR, a Taste of Scientific Potential; Pantin, E.; Lagage, P.-O.; Claret, A.; Doucet, C.; Kaufer, A.; Käufel, H.-U.; Pel, J.-W.; Peletier, R. F.; Siebenmorgen, R.; Smette, A.; Sterzik, M.; 119, 25

The VIMOS-VLT Deep Survey First Epoch Observations: Evolution of Galaxies, Large Scale Structures and AGNs over 90% of the Current Age of the Universe; Le Fèvre, O.; Vettolani, G.; Bottini, D.; Garilli, B.; Le Brun, V.; Maccagni, D.; Picat, J.-P.; Scaramella, R.; Scodreggio, M.; Tresse, L.; Zanichelli, A.; Adami, C.; Arnaboldi, M.; Arnouts, S.; Bardelli, S.; Bolzonella, M.; Cappi, A.; Charlot, S.; Ciliegi, P.; Contini, T.; Franzetti, P.; Foucaud, S.; Gavignaud, I.; Guzzo, L.; Ilbert, O.; Iovino, A.; McCracken, H.-J.; Marano, B.; Marinoni, C.; Mazure, A.; Meneux, B.; Merighi, R.; Paltini, S.; Pellò, R.; Pollo, A.; Pozzetti, L.; Radovich, M.; Zamorani, G.; Zucca, E.; Bondi, M.; Bongiorno, A.; Busarello, G.; Lamareille, F.; Mathez, G.; Mellier, Y.; Merluzzi, P.; Ripepi, V.; Rizzo, D.; 119, 30

Recent Astrophysical Results from the VLTI; Wittkowski, M.; Paresce, F.; Chesneau, O.; Kervella, P.; Meilland, A.; Meisenheimer, K.; Ohnaka, K.; 119, 36

VLTI Observation of IRS 3: The brightest compact MIR source at the Galactic Centre; Pott, J.-U.; Eckart, A.; Glindemann, A.; Viehmann, T.; Schödel, R.; Straubmeier, C.; Leinert, C.; Feldt, M.; Genzel, R.; Robberto, M.; 119, 43

Transiting Extra-solar Planets, follow the FLAMES ...; Pont, F.; Bouchy, F.; Queloz, D.; Melo, C.; Santos, N.; Udry, S.; Mayor, M.; Moutou, C.; 120, 19

On the Track of very low-mass Planets with HARPS; Pepe, F.; Mayor, M.; Queloz, D.; Benz, W.; Bertaux, J.-L.; Bouchy, F.; Lovis, C.; Mordasini, C.; Santos, N.; Sivan, J.-P.; Udry, S.; 120, 22

Confirmation of the First Image of an Extra-Solar Planet (based on ESO Press Release 12/06); 120, 25

First Science with SINFONI; Gillissen, S.; Davies, R.; Kissler-Patig, M.; Lehnert, M.; van der Werf, P.; Nowak, N.; Eisenhauer, F.; Abuter, R.; Horrobin, M.; Gilbert, A.; Genzel, R.; Bender, R.; Saglia, R.; Lemoine-Busserolle, M.; Reunanen, J.; Kjær, K.; Messineo, M.; Nürnberg, D.; Dumas, C.; 120, 26

Galaxy Cluster Archaeology; Böhringer, H.; Mullis, C.; Rosati, P.; Lamer, G.; Fassbender, R.; Schwope, A.; Schuecker, P.; 120, 33

The Horsehead Nebula: A Beautiful Case; Habart, E.; Walmsley, M.; Abergel, A.; 120, 37

Resolving the Host Galaxies of Quasars at  $z = 2.5$  with VLT + NACO; Scarpa, R.; Falomo, R.; Kotilainen, J. K.; Treves, A.; 120, 40

A New Isotopic Abundance Anomaly in Chemically Peculiar Stars; Cowley, C. R.; Castelli, F.; Hubrig, S.; 120, 42

Deep Impact at ESO Telescopes; Käufel, H.-U.; Ageorges, N.; Bagnulo, S.; Barrera, L.; Bönnhardt, H.; Bonev, T.; Hainaut, O.; Jehin, E.; Kerber, F.; Lo Curto, G.; Manfroid, J.; Marco, O.; Pantin, E.; Pompei, E.; Saviane, I.; Selman, F.; Sterken, C.; Rauer, H.; Tozzi, G. P.; Weiler, M.; 121, 11

A Triple Asteroid System (based on ESO Press Release 21/05); 121, 17

FLAMES Observations of Old Open Clusters: Constraints on the Evolution of the Galactic Disc and Mixing Processes in Stars; Randich, S.; Bragaglia, A.; Pastori, L.; Prisinzano, L.; Sestito, P.; Spanò, P.; Villanova, S.; Carraro, G.; Carretta, E.; Romano, D.; Zaggia, S.; Pallavicini, R.; Pasquini, L.; Primas, F.; Tagliaferri, G.; Tosi, M.; 121, 18

Measuring Improved Distances to Nearby Galaxies: The Araucaria Project; Gieren, W.; Pietrzynski, G.; Bresolin, F.; Kudritzki, R.-P.; Minniti, D.; Urbaneja, M.; Soszynski, I.; Storm, J.; Fouqué, P.; Bono, G.; Walker, A.; García, J.; 121, 23

Early Galaxy Evolution: Report on UVES Studies of a New Class of Quasar Absorbers; Péroux, C.; Dessauges-Zavadsky, M.; D'Odorico, S.; Kim, T. S.; McMahon, R. G.; 121, 29

A New Einstein Ring (ESO Press Photo 20b+c/05); 121, 32

Resolved Spectroscopy of a  $z = 5$  Gravitationally Lensed Galaxy with the VIMOS IFU; Swinbank, M.; Bower, R.; Smail, I.; Morris, S.; Smith, G.; 121, 33

Farthest Known Gamma-Ray Burst (based on ESO Press Release 22/05); 121, 35

Surveying the High-Redshift Universe with the VIMOS IFU; Jarvis, M. J.; van Breukelen, C.; Venemans, B. P.; Wilman, R. J.; 121, 38

The zCOSMOS Redshift Survey; Lilly, S. and the zCOSMOS team; 121, 42

Observing with the New High-Speed Camera ULTRACAM on Melipal (based on ESO Press Release 17/05); 121, 46

GOODS' Look at Galaxies in the Young Universe; Vanzella, E.; Christiani, S.; Dickinson, M.; Kuntschner, H.; Rettura, A.; Moustakas, L. A.; Nonino, M.; Popesso, P.; Rosati, P.; Stern, D.; Cesarsky, C.; Ferguson, H. C.; Fosbury, R. A. E.; Giavalisco, M.; Haase, J.; Renzini, A. and the GOODS Team; 122, 25

The Dynamics and Evolution of Luminous Galaxy Mergers: ISAAC Spectroscopy of ULIRGs; Tacconi, L. J.; Dasyra, K.; Davies, R.; Genzel, R.; Lutz, D.; Burkert, A.; Naab, T.; Sturm, E.; Veilleux, S.; Baker, A. J.; Sanders, D. B.; 122, 28

Supernova in NGC 1559 (ESO Press Photo 26/05); 122, 31

Lithium Isotopic Abundances in Metal-Poor Stars: A Problem for Standard Big Bang Nucleosynthesis?; Nissen, E. P.; Asplund, M.; Lambert, D. L.; Primas, F.; Smith, V. V.; 122, 32

The VLT-FLAMES Survey of Massive Stars; Evans, C.; Smartt, S.; Lennon, D.; Dufton, P.; Hunter, I.; Mokiemi, R.; de Koter, A.; Irwin, M.; 122, 36

Why are G and K Giants Radial Velocity Variables?; Döllinger, M. P.; Pasquini, L.; Hatzes, A. P.; Setiawan, J.; da Silva, L.; de Medeiros, J. R.; von der Lühe, O.; Girardi, L.; Di Mauro, M. P.; Weiss, A.; Roth, M.; 122, 39

#### Other Astronomical News

Comparison of Science Metrics of Observatories; Grothkopf, U.; Leibundgut, B.; Maccchetto, D.; Madrid, J. P.; Leitherer, C.; 119, 45  
The ESO Telescope Bibliography Web Interface – Linking Publications and Observations; Delmotte, N.; Treumann, A.; Grothkopf, U.; Micol, A.; Accomazzi, A.; 119, 50  
ESO Exhibitions in Granada and Naples; Janssen, E.; 119, 52  
EAAE Meeting at ESO Headquarters; West, R.; 119, 53  
Public Affairs Highlights in Chile: Achievements of 2004; Rodríguez, V.; Mirabel, F.; 119, 54  
Fellows at ESO: Nicolas Bouché, Eric Depagne, Markus Hartung, Jochen Liske; 119, 55  
ESO Studentships: PhD opportunities in Garching and Santiago; Kissler-Patig, M.; Kaufer, A.; Leibundgut, B.; Mirabel, F.; 120, 44  
"Towards a Europe of Knowledge and Innovation" – EIROforum presents a major science policy paper; Madsen, C.; 120, 46  
Report on the Workshop on The Power of Optical/IR Interferometry: Recent Scientific Results and Second-Generation VLTI Instrumentation; Richichi, A.; Glindemann, A.; 120, 48  
Dutch Minister of Science Visits ESO Facilities in Chile (based on ESO Press Release 14/05); 120, 51  
ESO Receives Computerworld Honors Program 21st Century Achievement Award in Science Category (based on ESO Press Release 16/05); 120, 52  
ESO at the European Research and Innovation Salon in Paris; Janssen, E.; 120, 53  
Fellows at ESO: Martin Vannier, Martin Zwaan; 120, 53  
The ESA-ESO Topical Science Working Groups; Fosbury, R. A. E.; 121, 56  
ESA-ESO Working Group on Extra-Solar Planets; Kerber, F.; Hainaut, O.; 121, 56  
Report on the ESO-ESA-IAU Conference Communicating Astronomy with the Public 2005; Robson, I.; Christensen, L. L.; 121, 59  
Report on the ESO Workshop on Virtual Observatory Standards and Systems for Data Centres and Large Projects; Padovani, P.; Dolensky, M.; 121, 60  
Report on the EPS-ESA-ESO-CERN Conference on Relativity, Matter and Cosmology; Shaver, P.; Leibundgut, B.; Liske, J.; 121, 62  
ESO Public Activities in July 2005; Janssen, E.; 121, 63  
Public Information and Education in Chile; Argandoña, G.; Mirabel, F.; 121, 64  
Universe Awareness for Young Children; Miley, G.; Madsen, C.; Scorza de Appl, C.; 121, 66  
Catherine Cesarsky Elected Member of Academies of Sciences; 121, 68  
Fellows at ESO: Cédric Foellmi, Margrethe Wold; 121, 69  
ASTRONET: Towards a Strategic Plan for European Astronomy; Lagrange, A.-M.; 122, 42  
The Current and Future ST-ECF; Fosbury, R. A. E.; 122, 44

PPARC Council at ESO; 122, 45  
Open House at ESO Garching; Boffin, H.; 122, 46  
Danish Minister visits ESO Chile; Argandoña, G.; Mirabel, F.; 122, 47  
Science on Stage 2005; Pierce-Price, D.; Boffin, H.; Madsen, C.; 122, 47  
ESO at CER 2005; Madsen, C.; 122, 48  
Report on the Conference on Science Perspectives for 3D Spectroscopy; Walsh, J.; Kissler-Patig, M.; 122, 49  
Report on the Science Day in Honour of Alvio Renzini; Cesarsky, C.; Leibundgut, B.; 122, 52

#### Announcements

The UKIRT Infrared Deep Sky Survey (UKIDSS): Data Access; Lawrence, A.; Warren, S.; 119, 56  
Symposium on Relativity, Matter and Cosmology; 119, 57  
ESO Workshop on Multiple Stars across the H-R Diagram; 119, 57  
MPA/ESO/MPE/USM Joint Astronomy Conference on Open Questions in Cosmology: The First Billion Years; 119, 58  
ESO Conference on Science Perspectives for 3D Spectroscopy; 119, 58  
Felix Mirabel becomes ESO Representative in Chile; 119, 59  
ESO Studentship Programme; 119, 59  
ESO Vacancy: Head of Administration; 119, 60  
ESO Vacancy: Operations Staff Astronomer; 119, 60  
ESO Vacancy: ALMA Back-end Integration and Data Communication Engineer; 119, 61  
ESO Vacancy: Senior Engineer – Head of Paranal Engineering Department; 119, 61  
ESO Vacancy: ALMA Project Planner/Scheduler; 119, 62  
Personnel Movements; 119, 63  
Recent Proceedings from the ESO Astrophysics Symposia; 119, 63  
ESO/MPA Workshop on Carbon-Rich Ultra Metal-Poor Stars in the Galactic Halo; 120, 54  
ESO Conference on Groups of Galaxies in the nearby Universe; 120, 54  
High Honour for Daniel Hofstadter; Argandoña, G.; Mirabel, F.; 120, 55  
Richard West retires; Madsen, C.; 120, 56  
Fizeau Exchange Visitors Programme, Optical Interferometry in Europe; 120, 57  
Personnel Movements; 120, 57  
ESO Fellowship Programme 2005/2006; 120, 58  
ESO Vacancy: ALMA Project Planner/Scheduler; 120, 59  
International Conference on Relativistic Astrophysics and Cosmology – Einstein's Legacy; 121, 70  
Latin American Astronomy Summer School; 121, 70  
Personnel Movements; 121, 71  
ESO Vacancy: European Affairs Officer; 121, 70  
Conference on Globular Clusters – Guides to Galaxies; 122, 54  
NEON Observing Schools; 122, 54  
Personnel Movements; 122, 55  
List of Proceedings from the ESO Astrophysics Symposia; 122, 55

#### Author Index

##### A

Alves, J.; Telescope Time Allocation Tool; 119, 20  
Argandoña, G.; Mirabel, F.; High Honour for Daniel Hofstadter; 120, 55  
Argandoña, G.; Mirabel, F.; Public Information and Education in Chile; 121, 64  
Argandoña, G.; Mirabel, F.; Inauguration of the APEX Telescope; 122, 18  
Argandoña, G.; Mirabel, F.; Danish Minister visits ESO Chile; 122, 47

##### B

Böhringer, H.; Mullis, C.; Rosati, P.; Lamer, G.; Fassbender, R.; Schwobe, A.; Schuecker, P.; Galaxy Cluster Archaeology; 120, 33  
Boffin, H.; Open House at ESO Garching; 122, 46

##### C

Capaccioli, M.; Mancini, D.; Sedmak, G.; The VLT Survey Telescope: A Status Report; 120, 10  
Cappellaro, E.; OmegaCAM: The VST Camera; 120, 13  
Casali, M.; Pirard, J.-F.; Kissler-Patig, M.; Moorwood, A.; Bedin, R.; Biereichel, P.; Delabre, B.; Dorn, R.; Finger, G.; Gojak, D.; Hubin, N.; Huster, G.; Jung, Y.; Koch, F.; Le Louarn, M.; Lizon, J.-L.; Mehrgan, L.; Pozna, E.; Silber, A.; Sokar, B.; Stegmeier, J.; Wide Field Infrared Imaging on the VLT with HAWK-I; 119, 6  
Cesarsky, C.; Leibundgut, B.; Report on the Science Day in Honour of Alvio Renzini; 122, 52  
Cowley, C. R.; Castelli, F.; Hubrig, S.; A New Isotopic Abundance Anomaly in Chemically Peculiar Stars; 120, 42  
Cullum, M.; Technology Transfer at ESO; 121, 52

##### D

D'Odorico, S.; Instrument Concepts for the OWL Telescope; 122, 6  
Dekker, H.; D'Odorico, S.; Progress Report on X-shooter, the first second-generation VLT Instrument; 120, 2  
Delmotte, N.; Treumann, A.; Grothkopf, U.; Micol, A.; Accomazzi, A.; The ESO Telescope Bibliography Web Interface – Linking Publications and Observations; 119, 50  
Döllinger, M. P.; Pasquini, L.; Hatzes, A. P.; Setiawan, J.; da Silva, L.; de Medeiros, J. R.; von der Lühe, O.; Girardi, L.; Di Mauro, M. P.; Weiss, A.; Roth, M.; Why are G and K Giants Radial Velocity Variables?; 122, 39

##### E

Eschwey, J.; ALMA Site Development; 121, 50  
Evans, C.; Smartt, S.; Lennon, D.; Dufton, P.; Hunter, I.; Mokiem, R.; de Koter, A.; Irwin, M.; The VLT-FLAMES Survey of Massive Stars; 122, 36

## F

- Fosbury, R. A. E.; The ESA-ESO Topical Science Working Groups; 121, 56  
 Fosbury, R. A. E.; The Current and Future ST-ECF; 122, 44

## G

- Gieren, W.; Pietrzynski, G.; Bresolin, F.; Kudritzki, R.-P.; Minniti, D.; Urbaneja, M.; Soszynski, I.; Storm, J.; Fouqué, P.; Bono, G.; Walker, A.; García, J.; Measuring Improved Distances to Nearby Galaxies: The Araucaria Project; 121, 23  
 Gillissen, S.; Davies, R.; Kissler-Patig, M.; Lehnert, M.; van der Werf, P.; Nowak, N.; Eisenhauer, F.; Abuter, R.; Horrobin, M.; Gilbert, A.; Genzel, R.; Bender, R.; Saglia, R.; Lemoine-Busserolle, M.; Reunanen, J.; Kjær, K.; Messineo, M.; Nürnberger, D.; Dumas, C.; First Science with SINFONI; 120, 26  
 Gilliotte, A.; Ihle, G.; Lo Curto, G.; Improvements at the 3.6-m Telescope; 119, 18  
 Grothkopf, U.; Leibundgut, B.; Macchetto, D.; Madrid, J. P.; Leitherer, C.; Comparison of Science Metrics of Observatories; 119, 45

## H

- Habart, E.; Walmsley, M.; Abergel, A.; The Horsehead Nebula: A Beautiful Case; 120, 37  
 Hook I. and the OPTICON ELT Science Working Group; Science with Extremely Large Telescopes; 121, 2  
 Hook, R.; Möller, P.; Ignatius, J.; Vasko, K.; Peron, M.; Quinn, P.; The Sampo Project; 120, 17

## J

- Janssen, E.; ESO Exhibitions in Granada and Naples; 119, 52  
 Janssen, E.; ESO at the European Research and Innovation Salon in Paris; 120, 53  
 Janssen, E.; ESO Public Activities in July 2005; 121, 63  
 Jarvis, M. J.; van Breukelen, C.; Venemans, B. P.; Wilman, R. J.; Surveying the High-Redshift Universe with the VIMOS IFU; 121, 38

## K

- Kasper, M.; Ageorges, N.; Boccaletti, A.; Brandner, W.; Close, L. M.; Davies, R.; Finger, G.; Genzel, R.; Hartung, M.; Kaufer, A.; Kellner, S.; Hubin, N.; Lenzen, R.; Lidman, C.; Monnet, G.; Moorwood, A.; Ott, T.; Riaud, P.; Röser, H.-J.; Rouan, D.; Spyromilio, J.; New observing modes of NACO; 119, 9  
 Käufel, H.-U.; Ageorges, N.; Bagnulo, S.; Barrera, L.; Böhnhardt, H.; Bonev, T.; Hainaut, O.; Jehin, E.; Kerber, F.; Lo Curto, G.; Manfroid, J.; Marco, O.; Pantin, E.; Pompei, E.; Saviane, I.; Selman, F.; Sterken, C.; Rauer, H.; Tozzi, G. P.; Weiler, M.; Deep Impact at ESO Telescopes; 121, 11  
 Kerber, F.; Hainaut, O.; ESA-ESO Working Group on Extra-Solar Planets; 121, 56  
 Kissler-Patig, M.; Kaufer, A.; Leibundgut, B.; Mirabel, F.; ESO Studentships: PhD opportunities in Garching and Santiago; 120, 44

- Koehler, B. and the AT Assembly and Commissioning Team; VLT First Fringes with Two Auxiliary Telescopes at Paranal; 120, 5  
 Kuntschner, H.; Kümmel, M.; Larsen, S.; Walsh, J.; Towards an Automatic Reduction of FORS2-MXU Spectroscopy; 122, 19

## L

- Lagrange, A.-M.; ASTRONET: Towards a Strategic Plan for European Astronomy; 122, 42  
 Lawrence, A.; Warren, S.; The UKIRT Infrared Deep Sky Survey (UKIDSS): Data Access; 119, 56  
 Le Fèvre, O.; Vettolani, G.; Bottini, D.; Garilli, B.; Le Brun, V.; Maccagni, D.; Picat, J.-P.; Scaramella, R.; Scoddeggio, M.; Tresse, L.; Zanichelli, A.; Adami, C.; Arnaboldi, M.; Arnouts, S.; Bardelli, S.; Bolzonella, M.; Cappi, A.; Charlot, S.; Ciliegi, P.; Contini, T.; Franzetti, P.; Foucaud, S.; Gavignaud, I.; Guzzo, L.; Ilbert, O.; Iovino, A.; McCracken, H.-J.; Marano, B.; Marinoni, C.; Mazure, A.; Meneux, B.; Merighi, R.; Paltini, S.; Pellò, R.; Pollo, A.; Pozzetti, L.; Radovich, M.; Zamorani, G.; Zucca, E.; Bondi, M.; Bongiorno, A.; Busarello, G.; Lamareille, F.; Mathez, G.; Mellier, Y.; Merluzzi, P.; Ripepi, V.; Rizzo, D.; The VIMOS-VLT Deep Survey First Epoch Observations: Evolution of Galaxies, Large Scale Structures and AGNs over 90 % of the Current Age of the Universe; 119, 30  
 Lilly, S. and the zCOSMOS team; The zCOSMOS Redshift Survey; 121, 42

## M

- Madsen, C.; "Towards a Europe of Knowledge and Innovation" – EIROforum presents a major science policy paper; 120, 46  
 Madsen, C.; Richard West retires; 120, 56  
 Madsen, C.; ESO at CER 200,5; 122, 48  
 Miley, G.; Madsen, C.; Scorza de Appl. C.; Universe Awareness for Young Children; 121, 66  
 Monnet, G.; The OPTICON FP6 Programme and ESO; 120, 7

## N

- Nissen, E. P.; Asplund, M.; Lambert, D. L.; Primas, F.; Smith, V. V.; Lithium Isotopic Abundances in Metal-Poor Stars: A Problem for Standard Big Bang Nucleosynthesis?; 122, 32

## P

- Padovani, P.; Dolensky, M.; Report on the ESO Workshop on Virtual Observatory Standards and Systems for Data Centres and Large Projects; 121, 60  
 Padovani, P.; Quinn, P.; The Virtual Observatory in Europe and at ESO; 122, 22  
 Pantin, E.; Lagage, P.-O.; Claret, A.; Doucet, C.; Kaufer, A.; Käufel, H.-U.; Pel, J.-W.; Peletier, R. F.; Siebenmorgen, R.; Smette, A.; Sterzik, M.; VISIR, a Taste of Scientific Potential; 119, 25

- Pasquini, L.; Christiani, S.; Dekker, H.; Haehnelt, M.; Molaro, P.; Pepe, F.; Avila, G.; Delabre, B.; D'Odorico, S.; Liske, J.; Shaver, P.; Bonifacio, P.; D'Odorico, V.; Vanzella, E.; Bouchy, F.; Desauges-Lavadsky, M.; Lovis, C.; Mayor, M.; Queloz, D.; Udry, S.; Murphy, M.; Viel, M.; Grazian, A.; Levshakov, S.; Moscardini, L.; Wiklind, T.; Zucker, S.; CODEX: Measuring the Expansion of the Universe (and beyond); 122, 10  
 Pepe, F.; Mayor, M.; Queloz, D.; Benz, W.; Bertaux, J.-L.; Bouchy, F.; Lovis, C.; Mordasini, C.; Santos, N.; Sivan, J.-P.; Udry, S.; On the track of very low-mass planets with HARPS; 120, 22  
 Péroux, C.; Dessauges-Zavadsky, M.; D'Odorico, S.; Kim, T. S.; McMahon, R. G.; Early Galaxy Evolution: Report on UVES Studies of a New Class of Quasar Absorbers; 121, 29  
 Pierce-Price, D.; Boffin, H.; Madsen, C.; Science on Stage 200,5; 122, 47  
 Pont, F.; Bouchy, F.; Queloz, D.; Melo, C.; Santos, N.; Udry, S.; Mayor, M.; Moutou, C.; Transiting Extrasolar Planets, follow the FLAMES ...; 120, 19  
 Pott, J.-U.; Eckart, A.; Glindemann, A.; Viehmann, T.; Schödel, R.; Straubmeier, C.; Leinert, C.; Feldt, M.; Genzel, R.; Robberto, M.; VLT Observation of IRS 3: The brightest compact MIR source at the Galactic Centre; 119, 43

## R

- Randich, S.; Bragaglia, A.; Pastori, L.; Prisinzano, L.; Sestito, P.; Spanò, P.; Villanova, S.; Carraro, G.; Carretta, E.; Romano, D.; Zaggia, S.; Pallavicini, R.; Pasquini, L.; Primas, F.; Tagliaferri, G.; Tosi, M.; FLAMES Observations of Old Open Clusters: Constraints on the Evolution of the Galactic Disc and Mixing Processes in Stars; 121, 18  
 Richichi, A.; Glindemann, A.; Report on the Workshop on The Power of Optical/IR Interferometry: Recent Scientific Results and Second-Generation VLT Instrumentation; 120, 48  
 Robson, I.; Christensen, L. L.; Report on the ESO-ESA-IAU Conference Communicating Astronomy with the Public 200,5; 121, 59  
 Rodríguez, V.; Mirabel, F.; Public Affairs Highlights in Chile: Achievements of 200,4; 119, 54

## S

- Scarpa, R.; Falomo, R.; Kotilainen, J. K.; Treves, A.; Resolving the Host Galaxies of Quasars at  $z = 2.5$  with VLT + NACO; 120, 40  
 Sharples, R.; Bender, R.; Bennet, R.; Burch, K.; Carter, P.; Casali, M.; Clark, P.; Content, R.; Davies, R.; Dubbeldam, M.; Finger, G.; Genzel, R.; Häfner, R.; Hess, A.; Kissler-Patig, M.; Laidlaw, K.; Lehnert, M.; Lewis, I.; Moorwood, A.; Muschiello, B.; Förster Schreiber, N.; Pirard, J.; Ramsay Howat, S.; Rees, P.; Richter, J.; Robertson, D.; Robson, I.; Saglia, R.; Tecza, M.; Thatte, N.; Todd, S.; Wegner, M.; Surveying the High-Redshift Universe with KMOS; 122, 2  
 Shaver, P.; Leibundgut, B.; Liske, J.; Report on the EPS-ESA-ESO-CERN Conference on Relativity, Matter and Cosmology; 121, 62  
 Swinbank, M.; Bower, R.; Smail, I.; Morris, S.; Smith, G.; Resolved Spectroscopy of a  $z = 5$  Gravitationally Lensed Galaxy with the VIMOS IFU; 121, 33

## T

Tacconi, L. J.; Dasyra, K.; Davies, R.; Genzel, R.; Lutz, D.; Burkert, A.; Naab, T.; Sturm, E.; Veilleux, S.; Baker, A. J.; Sanders, D. B.; The Dynamics and Evolution of Luminous Galaxy Mergers: ISAAC Spectroscopy of ULIRGs; 122, 28

## V

Vanzella, E.; Christiani, S.; Dickinson, M.; Kuntschner, H.; Rettura, A.; Moustakas, L. A.; Nonino, M.; Popesso, P.; Rosati, P.; Stern, D.; Cesarsky, C.; Ferguson, H. C.; Fosbury, R. A. E.; Giavalisco, M.; Haase, J.; Renzini, A. and the GOODS Team; GOODS' Look at Galaxies in the Young Universe; 122, 25

## W

Walsh, J.; Kissler-Patig, M.; Report on the Conference on Science Perspectives for 3D Spectroscopy; 122, 49

West, R.; EAAE Meeting at ESO Headquarters; 119, 53

Wilson, T.; ALMA News; 119, 24

Wilson, T.; ALMA News; 120, 15

Wilson, T.; ALMA News; 121, 48

Wilson, T.; ALMA News; 122, 15

Wittkowski, M.; Comerón, F.; Glindemann, A.; Hummel, C.; Morel, S.; Percheron, I.; Petrotzgens, M.; Schöller, M.; Observing with the ESO VLT Interferometer; 119, 14

Wittkowski, M.; Paresce, F.; Chesneau, O.; Kervella, P.; Meilland, A.; Meisenheimer, K.; Ohnaka, K.; Recent Astrophysical Results from the VLTI; 119, 36



---

**Left:** A comparison between two images of Messier 100, taken in March 2002 with the VIMOS instrument on Melipal (VLT) and in February 2006 with FORS1 on Kueyen (VLT). The difference in colours comes from the different filters used. The supernova SN 2006X is clearly present in the FORS1 image as the bright object in the middle, just above the lower main spiral arm. It is not seen in the VIMOS image. (ESO PR Photo 08b/06)



---

**Front Cover Picture:** Spiral galaxy NGC 1350. This colour-composite image was taken with FORS2 on the VLT unit telescope Kueyen. See ESO Press Photo 31a/05 for details.

ESO is the European Organisation for Astronomical Research in the Southern Hemisphere. Whilst the Headquarters (comprising the scientific, technical and administrative centre of the organisation) are located in Garching near Munich, Germany, ESO operates three observational sites in the Chilean Atacama desert. The Very Large Telescope (VLT), is located on Paranal, a 2 600 m high mountain south of Antofagasta. At La Silla, 600 km north of Santiago de Chile at 2 400 m altitude, ESO operates several medium-sized optical telescopes. The third site is the 5 000 m high Llano de Chajnantor, near San Pedro de Atacama. Here a new submillimetre telescope (APEX) is in operation, and a giant array of 12-m submillimetre antennas (ALMA) is under development. Over 1600 proposals are made each year for the use of the ESO telescopes.

The ESO MESSENGER is published four times a year: normally in March, June, September and December. ESO also publishes Conference Proceedings and other material connected to its activities. Press Releases inform the media about particular events. For further information, contact the ESO Public Affairs Department at the following address:

ESO Headquarters  
Karl-Schwarzschild-Straße 2  
85748 Garching bei München  
Germany  
Phone +49 89 320 06-0  
Fax +49 89 320 23 62  
information@eso.org  
www.eso.org

The ESO Messenger:  
Editor: Peter Shaver  
Technical editor: Jutta Boxheimer  
www.eso.org/messenger/

Printed by  
Peschke Druck  
Schatzbogen 35  
81805 München  
Germany

© ESO 2006  
ISSN 0722-6691

## Contents

Spain to Join ESO	3
<b>Telescopes and Instrumentation</b>	
G. Monnet, R. Gilmozzi – Status of the European ELT	4
R. Arsenault et al. – The VLT Adaptive Optics Facility Project: Telescope Systems	6
R. Arsenault et al. – The VLT Adaptive Optics Facility Project: Adaptive Optics Modules	11
First Light for the VLT Laser Guide Star Facility	16
S. Hubrig et al. – VLT-UVES Long-Slit Spectroscopy	17
T. Wilson – ALMA News	19
M. Hogerheijde – The ALMA Design Reference Science Plan	20
<b>Reports from Observers</b>	
M. Kürster, M. Endl, F. Rodler – In Search of Terrestrial Planets in the Habitable Zone of M Dwarfs	21
Low-Mass Exoplanet Found Using Microlensing	24
R. Neuhauser, M. Mugrauer, E. Guenther – Direct Imaging of Sub-Stellar Companions around Young Stars	25
T. Henning et al. – The Formation and Early Evolution of Massive Stars	28
E. Tolstoy et al. – The Dwarf galaxy Abundances and Radial-velocities Team (DART) Large Programme – A Close Look at Nearby Galaxies	33
A. Koch et al. – The Age-Metallicity Degeneracy in the Dwarf Spheroidal Carina as Seen by FLAMES	38
F. Hammer et al. – The Formation of Intermediate-Mass Galaxies over the Last 8 Gyrs	41
A. van der Wel et al. – Masses and Mass-to-Light Ratios of Early-Type Galaxies at High Redshift – The Impact of Ultradeep FORS2 Spectroscopy	45
H. Böhringer et al. – Unveiling the Structure of Galaxy Clusters with Combined ESO-VLT, WFI, and XMM-Newton Observations	49
G. Chincarini et al. – Gamma-Ray Bursts: Learning about the Birth of Black Holes and Opening new Frontiers for Cosmology	54
<b>Other Astronomical News</b>	
P. Andreani, T. Wilson – The ALMA-Herschel Synergies	59
C. Madsen – ESO at AAAS	61
G. Argandoña, F. Mirabel – Latin American Summer School	62
I. Saviane, V. D. Ivanov, J. Borissova – Report on the Conference on Groups of Galaxies in the Nearby Universe	63
Fellows at ESO – G. Chauvin, E. Galliano	66
Science in School launched	66
<b>Announcements</b>	
S. Warren et al. – The UKIDSS Early Data Release	67
R. Hook et al. – Scisoft VI	69
Workshop on Deep Impact as a World Observatory Event	69
MPA/ESO/MPE/USM Joint Astronomy Conference on Heating versus Cooling in Galaxies and Clusters of Galaxies	70
Conference on Precision Spectroscopy in Astrophysics	70
Science on Stage 2	71
Euroscience Open Forum – ESOF2006	71
ESO Studentship Programme	72
Vacancies	73
Personnel Movements	75
List of Proceedings from the ESO Astrophysics Symposia	75
Annual Index 2005	76